

**e-ISSN 2667-9973**  
**p-ISSN 1512-1127**

**საქართველოს გეოფიზიკური საზოგადოების  
ჟურნალი**

**მყარი დედამიწის, ატმოსფეროს, ოკეანისა და კოსმოსური პლაზმის  
ფიზიკა**

*ტომი 28, № 1*

**JOURNAL  
OF THE GEORGIAN GEOPHYSICAL SOCIETY**

*Physics of Solid Earth, Atmosphere, Ocean and Space Plasma*

*Vol. 28, № 1*

**Tbilisi**  
**2025**

**e-ISSN 2667-9973**  
**p-ISSN 1512-1127**

**საქართველოს გეოფიზიკური საზოგადოების  
ჟურნალი**

**მყარი დედამიწის, ატმოსფეროს, ოკეანისა და კოსმოსური პლაზმის  
ფიზიკა**

*ტომი 28, № 1*

**JOURNAL  
OF THE GEORGIAN GEOPHYSICAL SOCIETY**

*Physics of Solid Earth, Atmosphere, Ocean and Space Plasma*

*Vol. 28, № 1*

**Tbilisi  
2025**

საქართველოს გეოფიზიკური საზოგადოების ჟურნალი  
მყარი დედამიწის, ატმოსფეროს, ოკეანისა და კოსმოსური პლაზმის ფიზიკა  
მთავარი რედაქტორი: თ. ჭელიძე  
მთ. რედაქტორის მოადგილე: ჯ. ქირია; მდივანი: ა. ამირანაშვილი

**სარედაქციო კოლეგია**

ვ. ალიევი (აზერბაიჯანი), თ. ბიბილაშვილი (აშშ), ე. ბოლოპოულოსი (საბერძნეთი), გ. ჩაგელიშვილი, თ. ჭელიძე, ლ. დარახველიძე, დ. დემეტრაშვილი, კ. ეფტაქსიასი (საბერძნეთი), ვ. ერემეევი (უკრაინა), ნ. ლლონტი, ა. გოგიჩაიშვილი (მექსიკა), ი. გეგენი (საფრანგეთი), თ. გვენცაძე, ო. ხარშილაძე, თ. ქირია, გ. კოროტაევი (უკრაინა), თ. მაჭარაშვილი, გ. მეტრეველი, ვ. სტაროსტენკო (უკრაინა), კ. თავართქილაძე, ნ. ვარამაშვილი, ვ. ზაალიშვილი (რესპუბლიკა ჩრდილოეთ ოსეთი-ალანია, რუსეთი), ვ. ზალესნი (რუსეთი), ი. ჩშაუ (გერმანია).

**ჟურნალის შინაარსი:**

ჟურნალი მოიცავს მყარი დედამიწის, ატმოსფეროს, ოკეანისა და კოსმოსური პლაზმის ფიზიკის ყველა მიმართულებას. ჟურნალში ქვეყნდება: კვლევითი წერილები, მიმოხილვები, მოკლე ინფორმაციები, დისკუსიები, წიგნების მიმოხილვები, განცხადებები, კონფერენციების მოხსენებები.

**JOURNAL OF THE GEORGIAN GEOPHYSICAL SOCIETY**

*Physics of Solid Earth, Atmosphere, Ocean and Space Plasma*

**Editor-in-chief: T. Chelidze**

**Vice-Editor: J. Kiria; Secretary: A. Amiranashvili**

**Editorial board:**

V. Aliyev (Azerbaijan), T. Bibilashvili (USA), E. Bolopoulos (Greece), G. Chagelishvili, T. Chelidze, L. Darakhvelidze, D. Demetrashvili, K. Eftaxias (Greece), V. N. Eremeev (Ukraine), N. Ghlonti, A. Gogichaishvili (Mexico), Y. Gueguen (France), T. Gventsadze, Z. Kereselidze, O. Kharshiladze, T. Kiria, G. K. Korotaev (Ukraine), T. Matcharashvili, G. Metreveli, V. Starostenko (Ukraine), K. Tavartkiladze, N. Varamashvili, V.B. Zaalishvili (Republic of North Ossetia-Alania, Russia), V. B. Zalesny (Russia), J. Zschau (Germany).

**Scope of the Journal:**

The Journal is devoted to all branches of the Physics of Solid Earth, Atmosphere, Ocean and Space Plasma. Types of contributions are: research papers, reviews, short communications, discussions, book reviews, announcements, conference reports.

**ЖУРНАЛ ГРУЗИНСКОГО ГЕОФИЗИЧЕСКОГО ОБЩЕСТВА**

**Физика Твердой Земли, Атмосферы, Океана и Космической Плазмы**

**Главный редактор: Т. Челидзе**

**Зам. гл. редактора: Дж. Кирия; Секретарь: А. Амиранашвили**

**Редакционная коллегия:**

В. Алиев (Азербайджан), Т. Бибилашвили (США), Е. Болополоус (Греция), Г. Чагелишвили, Т.Л. Челидзе, Л. Дарахвелидзе, Д. Деметрашвили, К. Эфтаксиас (Греция), В. Н. Еремеев (Украина), Н. Глонти, А. Гогичайшвили (Мексика), И. Геген (Франция), Т. Гвенцадзе, З. Кереселидзе, О. Харшиладзе, Т. Кирия, Г. К. Коротаев (Украина), Т. Мачарашвили, Г. Метревели, В. Старостенко (Украина), К. Таварткиладзе, Н. Варамашвили, В.Б. Заалишвили (Республика Северная Осетия-Алания, Россия), В. Б. Залесный (Россия), И. Чшау (Германия).

**Содержание журнала:**

Журнал Грузинского геофизического общества охватывает все направления физики твердой Земли, Атмосферы, Океана и Космической Плазмы. В журнале публикуются научные статьи, обзоры, краткие информации, дискуссии, обзоры книг, объявления, доклады конференций.

### **მისამართი:**

საქართველო, 0160, თბილისი, ალექსიძის ქ. 1, მ. ნოდის სახ. გეოფიზიკის ინსტიტუტი  
ტელ.: 233-28-67; ფაქსი; (995 32 2332867); ელ. ფოტა: [tamaz.chelidze@gmail.com](mailto:tamaz.chelidze@gmail.com);  
[avtandilamiranashvili@gmail.com](mailto:avtandilamiranashvili@gmail.com);  
[geophysics.journal@tsu.ge](mailto:geophysics.journal@tsu.ge)

### **გამოქვეყნების განრიგი და ხელმოწერა:**

გამოიცემა წელიწადში ორჯერ. მყარი ვერსიის წლიური ხელმოწერის ფასია: უცხოელი ხელმომწერისათვის - 30 დოლარი, საქართველოში - 10 ლარი. ხელმოწერის მოთხოვნა უნდა გაიგზავნოს რედაქციის მისამართით. შესაძლებელია უფასო ონლაინ წვდომა:

<http://openjournals.gela.org.ge/index.php/GGS>

ჟურნალი ინდექსირებულია Google Scholar-ში:

<https://scholar.google.com/citations?hl=en&user=pdG-bMAAAAAAJ>

### **Address:**

M. Nodia Institute of Geophysics, 1 Alexidze Str., 0160 Tbilisi, Georgia  
Tel.: 233-28-67; Fax: (99532) 2332867; e-mail: [tamaz.chelidze@gmail.com](mailto:tamaz.chelidze@gmail.com);  
[avtandilamiranashvili@gmail.com](mailto:avtandilamiranashvili@gmail.com);  
[geophysics.journal@tsu.ge](mailto:geophysics.journal@tsu.ge)

### **Publication schedule and subscription information:**

The journal is issued twice a year. The subscription price for print version is 30 \$ in year. Subscription orders should be sent to editor's address. Free online access is possible:

<http://openjournals.gela.org.ge/index.php/GGS>

The journal is indexed in the Google Scholar:

<https://scholar.google.com/citations?hl=en&user=pdG-bMAAAAAAJ>

### **Адрес:**

Грузия, 0160, Тбилиси, ул. Алексидзе, 1. Институт геофизики им. М. З. Нодиа  
Тел: 233-28-67; 294-35-91; Fax: (99532)2332867; e-mail: [tamaz.chelidze@gmail.com](mailto:tamaz.chelidze@gmail.com);  
[avtandilamiranashvili@gmail.com](mailto:avtandilamiranashvili@gmail.com);  
[geophysics.journal@tsu.ge](mailto:geophysics.journal@tsu.ge)

### **Порядок издания и условия подписки:**

Журнал издается дважды в год. Годовая подписная цена для печатной версии - 30 долларов США. Заявка о подписке высылается в адрес редакции. Имеется бесплатный онлайн доступ

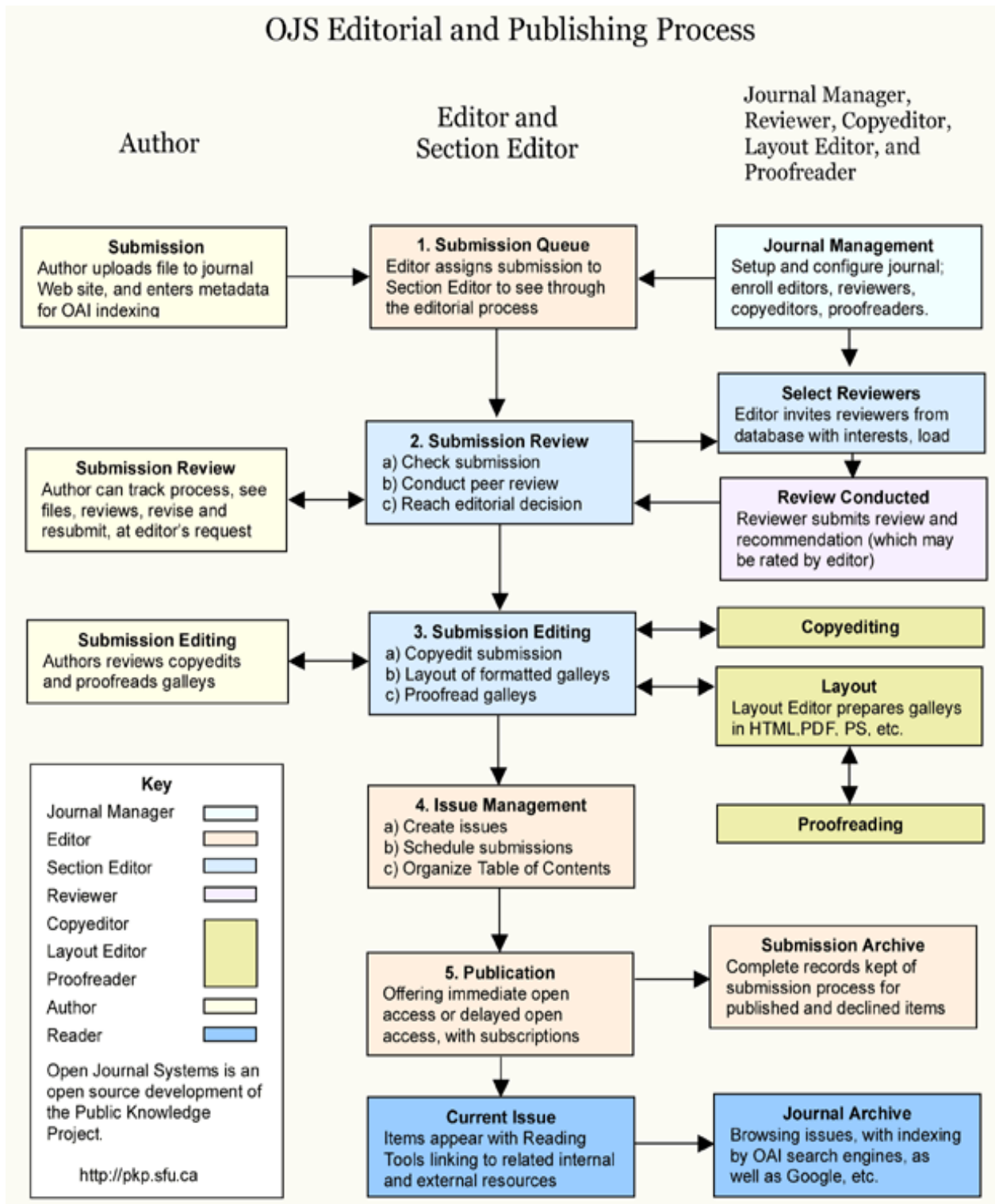
<http://openjournals.gela.org.ge/index.php/GGS>

Журнал индексируется в Google Scholar:

<https://scholar.google.com/citations?hl=en&user=pdG-bMAAAAAAJ>

This journal uses Open Journal Systems 2.4.8.3, which is open source journal management and publishing software developed, supported, and freely distributed by the Public Knowledge Project under the GNU General Public License.

(<http://openjournals.gela.org.ge/index.php?journal=GGS&page=about&op=aboutThisPublishingSystem>)



# Temporal Evolution of Microseismicity in Response to Reservoir Operation at the Enguri Dam (Georgia)

Nino S. Tsereteli, Luka N. Ghomidze, Nazi E. Tugushi

*M. Nodia Institute of Geophysics of the I. Javakhishvili Tbilisi State University, Georgia*

*e-mail: [nino\\_tsereteli@tsu.ge](mailto:nino_tsereteli@tsu.ge)*

## ABSTRACT

*In this study, we analyze the temporal evolution of microseismicity near the Enguri Dam (Georgia) using over four years of data from a local seismic network installed under the DAMAST project. A detailed completeness analysis identifies a conservative threshold of  $M_c = 0.6$  within 17 km of the dam, enabling robust estimation of Gutenberg–Richter parameters. Elevated  $b$ -values in the local catalog—compared to national  $M_w$ -based data—suggest a significant reservoir-induced component. Extending the analysis to a 30 km radius, we find that the completeness threshold increases to  $M_c = 1.0$ ; however, the  $b$ -value remains high ( $\geq 1$ ) when estimated using the Maximum Likelihood method. This spatial consistency in elevated  $b$ -values indicates that reservoir operations influence seismicity up to at least 30 km from the dam. Seismicity correlates with water level changes, especially during filling and drawdown phases, while meteorological variables show no consistent relationship. Our findings highlight the influence of reservoir operations on microseismic activity and underscore the value of integrated hydrological and seismological monitoring in dam regions.*

**Key words:** *microseismicity, Inguri reservoir, seismic catalog analysis,  $b$ -parameter assessment.*

## Introduction

In this study, we analyze over four years of continuous seismic monitoring around the Enguri Hydropower Plant (HPP) using the DAMAST seismic network. The Enguri arch dam, standing 271.5 m high, is among the tallest dams in the world. Its reservoir, Jvari—approximately 30 km long and reaching depths of up to 226 m—is located in the Samegrelo region of Georgia. The underground powerhouse is situated in the Gali District of the Abkhazia region and is connected to the reservoir via a 15 km long headrace tunnel. The entire Enguri HPP system represents one of the most complex and strategically important hydropower infrastructures in the South Caucasus. Despite the political conflict, the plant has continued to operate as a shared energy facility, supplying electricity to both Abkhazia and other region of Georgia through ongoing technical cooperation and joint operation agreements. This region, approximately 50 km east of the Black Sea in the west part of Georgia, lies within an active seismotectonic zone associated with the southern margin of the Greater Caucasus. The seismotectonic setting of the area has been described in detail in our previous publications [1-2]. Accordingly, we omit a detailed discussion here and briefly note that the Enguri high dam is located within an active tectonic zone along the southern margin of the Greater Caucasus. The associated seismogenic source is defined based on national earthquake catalog data ( $M_w \geq 3.0$ ), and its Gutenberg–Richter (GR) parameters  $a$ -value and  $b$ -value [3] have been estimated using various statistical methods. Importantly, these parameters were derived from cataloged tectonic earthquakes only; reservoir-induced events were not included in the analysis. The estimated values are presented in Table 1.

With the improved detection capabilities of the DAMAST seismic network, it is now possible to estimate Gutenberg–Richter parameters, based on a more complete catalog that includes low-magnitude events ( $M_w < 3.0$ ). This allows, for the first time, a direct comparison between the statistical properties of microseismicity and those derived from the national catalog, which only includes moderate to large tectonic events. Such a comparison provides a basis to investigate whether the microearthquake population reflects the same seismotectonic regime as larger tectonic earthquakes, or whether it reveals distinct characteristics potentially linked to reservoir-induced processes. The outcome of this comparison has important implications for understanding the nature of small-magnitude seismicity near large dams and its relation to regional tectonic stress fields. In this paper, we focus in particular on the b-value of the Gutenberg-Richter relation. The b-value of the Gutenberg-Richter law not only reflects the relative proportion of small to large earthquakes but also serves as an indicator of the mechanical state of the crust. Higher b-values are generally associated with heterogeneous, fractured, and fluid-influenced rock masses, often implying the presence of stress perturbations, increased pore pressure, or weaker fault structures. In contrast, lower b-values typically indicate a more homogeneous and competent lithology subjected to higher differential stress. Therefore, the elevated b-values observed near the Enguri Dam may suggest that the surrounding rock volume is extensively fractured and potentially weakened by repeated hydrological loading, making it more susceptible to microseismic activity triggered by minor stress changes due to reservoir operation.

## Seismic Networks and Data

To capture low-magnitude seismicity in the vicinity of the Enguri Dam, a dedicated local seismic network comprising ten stations was established under the DAMAST project. (Fig. 1). The network consists of both surface (KETI, BRID, GULB equipped with MBB-2 sensors and HPP, OKM, GAL equipped with 4.5 Hz Geophone PE-6/B) and borehole (KIT1, BUFF, NIKA, DOG equipped with Trillium Compact Posthole 20s sensors) installations.

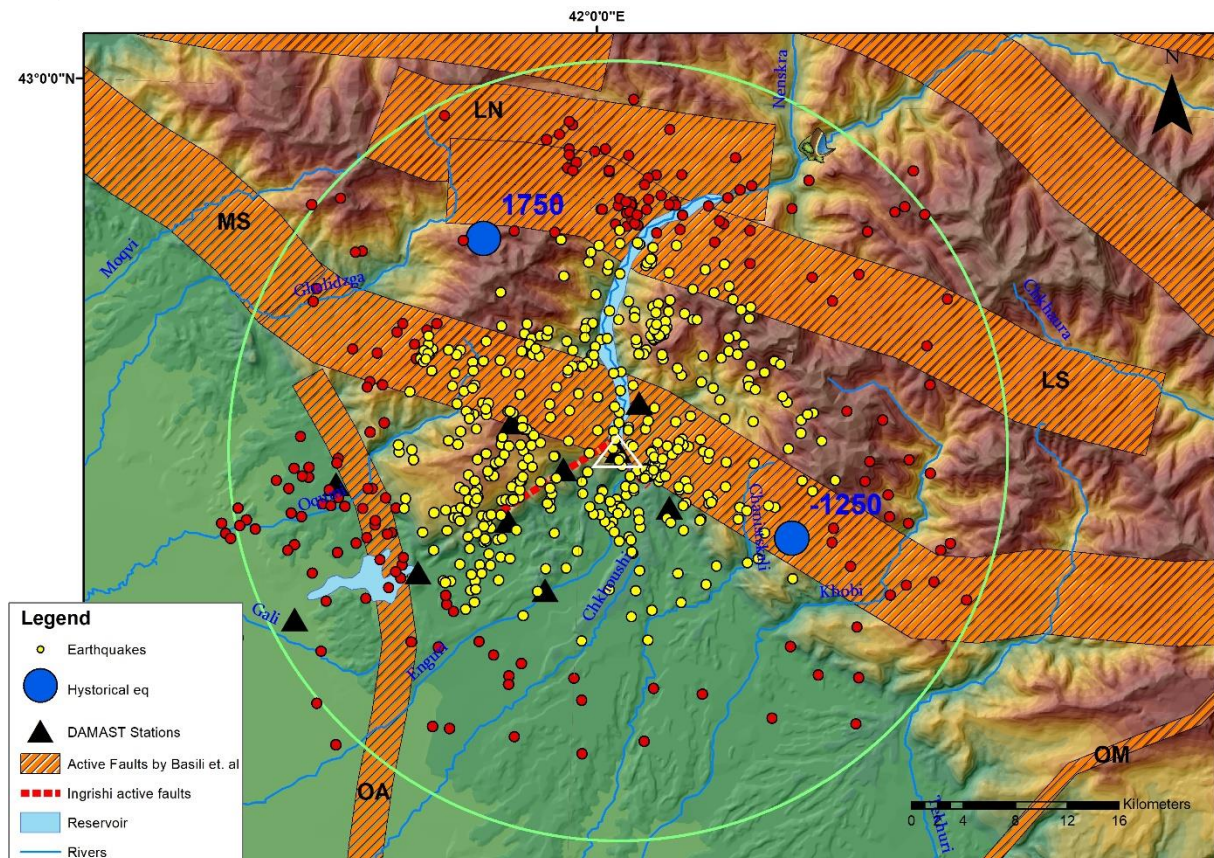


Fig. 1. Damast seismic network, seismicity and active fault structures in the Enguri Dam region. Yellow circles indicate microearthquakes recorded between 2020 and 2024 within 17 km radius.

Fig. 2 presented a normalized comparison plot showing the amplitude response of all three sensor types. A -3 dB reference line is included to indicate the effective bandwidth for each sensor. The comparison confirms that the Trillium 20s sensor provides the broadest usable frequency range, followed by the MBB-2, with the 4.5 Hz geophone effective in the high-frequency band only.

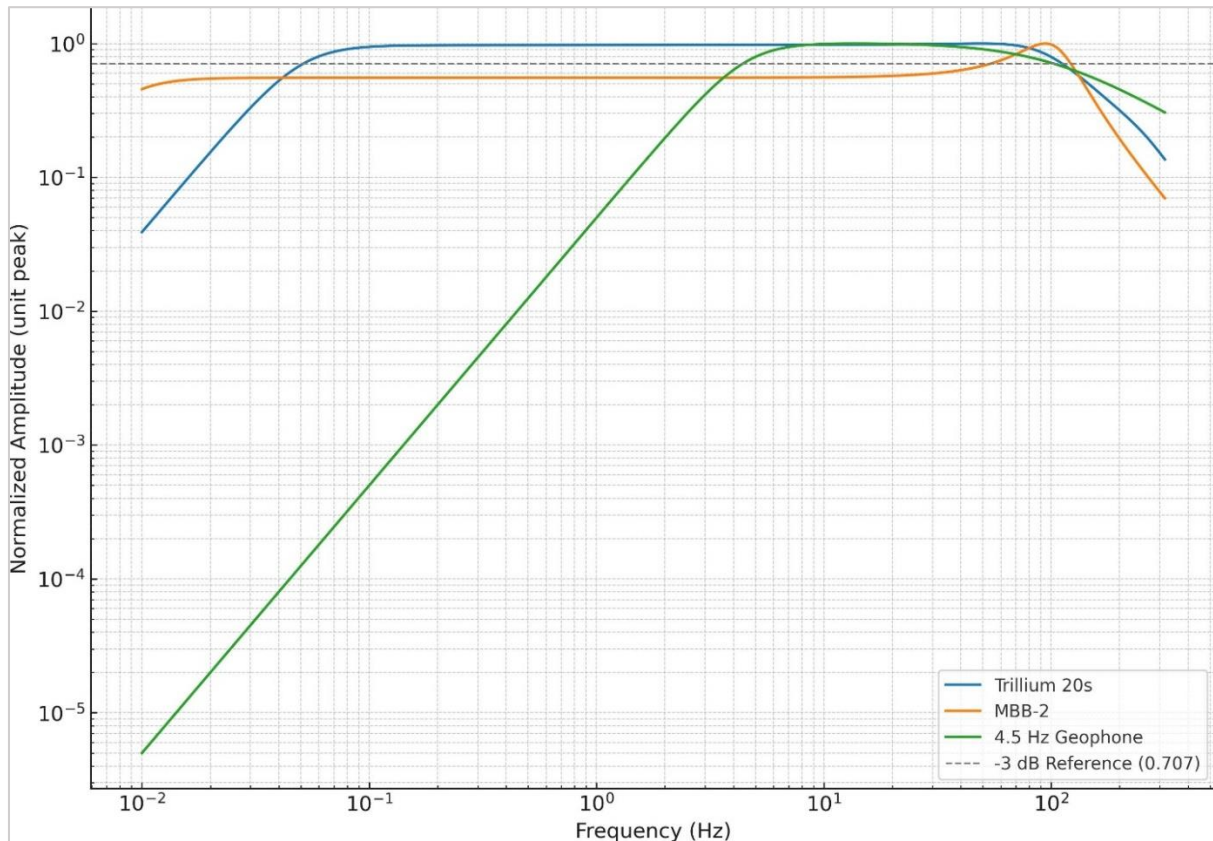


Fig. 2. Normalized Frequency Response of Trillium 20s, MBB-2, and 4.5 Hz Geophone Sensors.

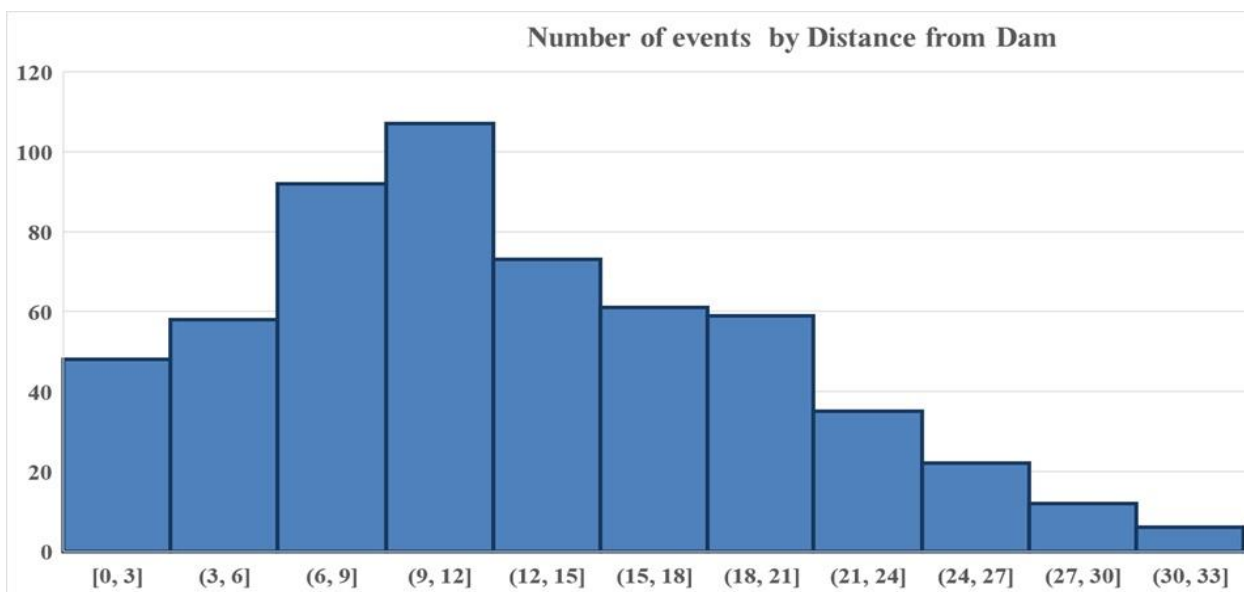
Background seismic noise conditions were evaluated through vertical-component power spectral density (PPSD) analysis for each station, using the ObsPy package. Median acceleration-referenced spectra were computed and compared against Peterson’s New High and Low Noise Models (NHNM and NLNM; [4]) to characterize site-specific noise levels. The borehole installations (KIT1, BUFF, NIKA, DOG) and the remote station GULB consistently demonstrated low ambient noise, with spectral levels closely tracking the NLNM across a broad frequency range. In contrast, surface stations (GAL, KETI, OKM, HPP), subject to greater environmental influence, exhibited elevated noise levels; however, these remained below the NHNM thresholds. These results confirm that the network achieves sufficiently low noise conditions to support reliable microseismic monitoring [1].

### Analysis of Local Seismicity and Network Performance

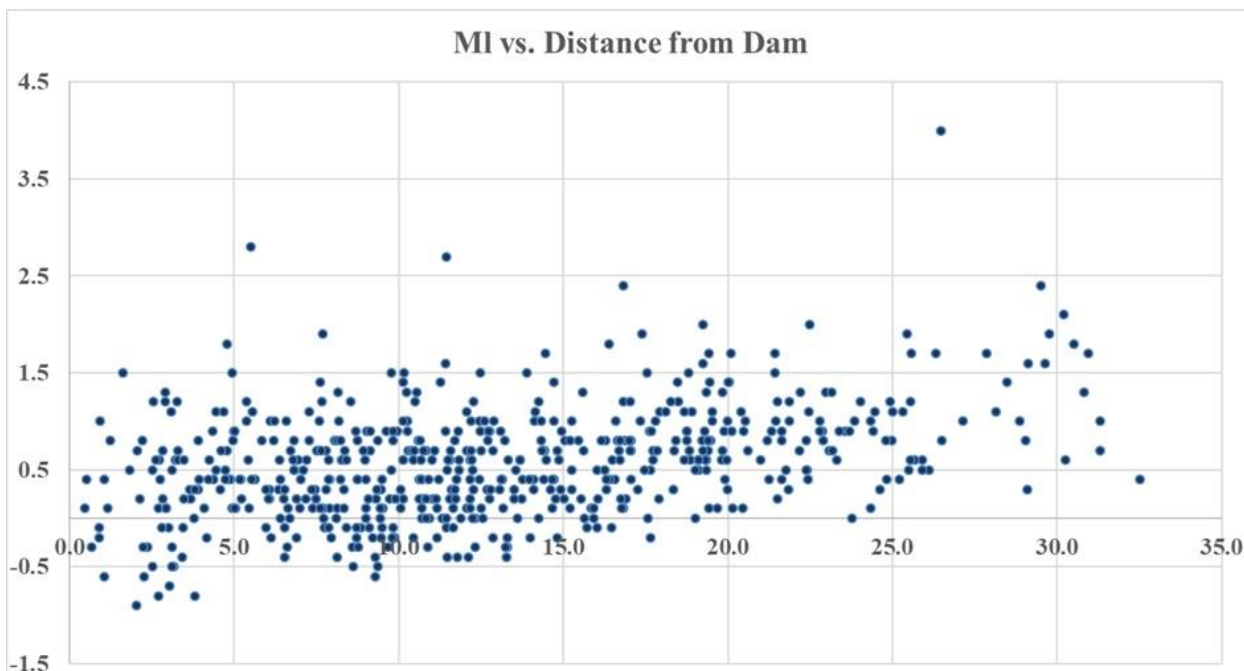
The procedures for earthquake detection, location, and magnitude determination using the DAMAST network have been previously detailed in [1] and are not repeated here. In this study, we focus on the analysis of the resulting seismic dataset, with particular attention to the spatial distribution of events around the dam, magnitude distribution, and catalog completeness. Additionally, we examine statistical relationships among key earthquake parameters to better characterize the nature of the observed seismicity. These analyses aim to evaluate whether the recorded events are consistent with regional tectonic processes or exhibit anomalies potentially related to reservoir-induced effects.

Fig. 3(a,b,c,d) present an overview of the key statistical characteristics of the seismic catalog. Specifically, they show: (a) the distribution of earthquake epicenters as a function of distance from the dam (DFD), (b) the relationship between local magnitude (MI) and DFD, (c) the number of events as a function of focal depth, and (d) the distribution of events by magnitude. From the distributions we observe that the DAMAST network is capable of detecting microearthquakes with local magnitudes (MI) as low as  $-1$  within approximately 5 km of the dam. Detection of events with  $MI < 0$  remains possible up to a distance of 17.7 km. Beyond this range, and up to  $\sim 30$  km from the dam, only events with  $MI > 0$  are consistently recorded. The depth distribution indicates that the majority of events occur between 4 and 6 km, while the magnitude histogram shows a peak near  $MI = 0.3$ , with an estimated uncertainty of approximately  $\pm 0.23$ . These distributions provide important constraints on the sensitivity limits of the network and the spatial characteristics of the local seismicity.

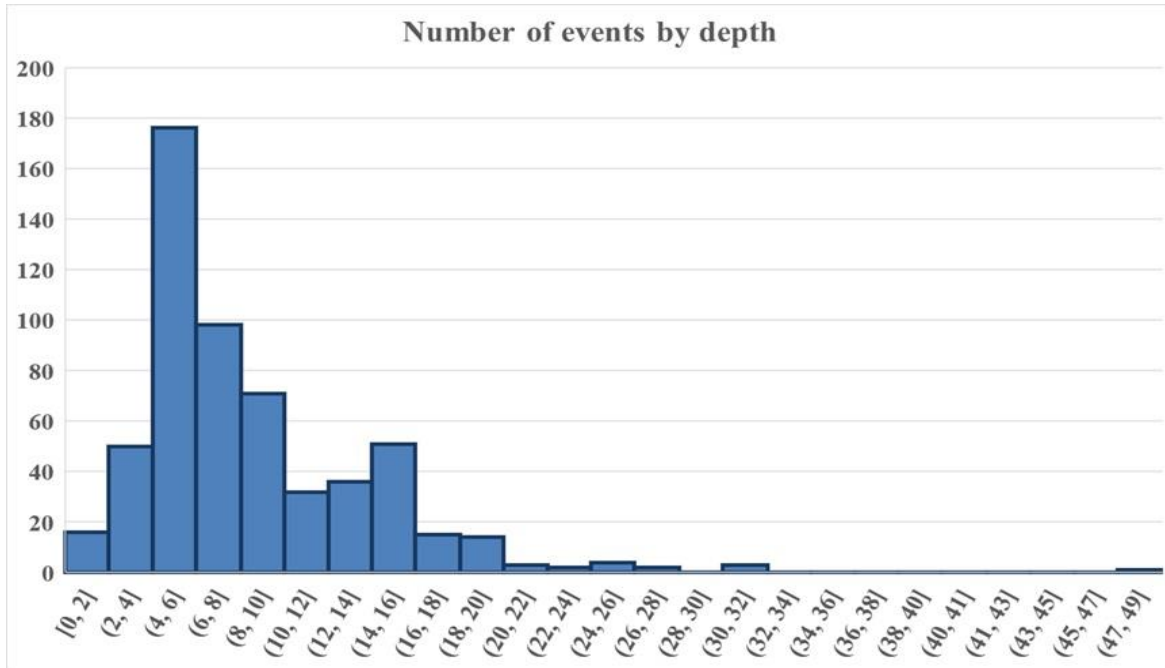
a)



b)



c)



d)

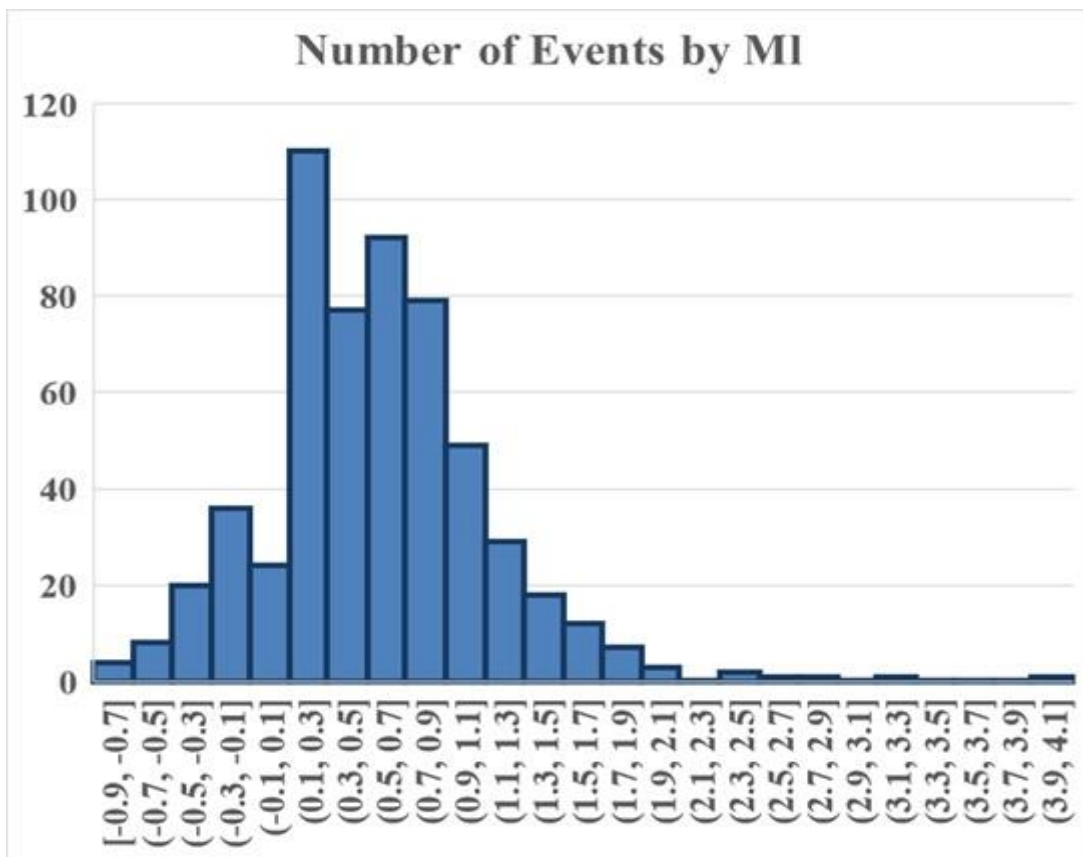
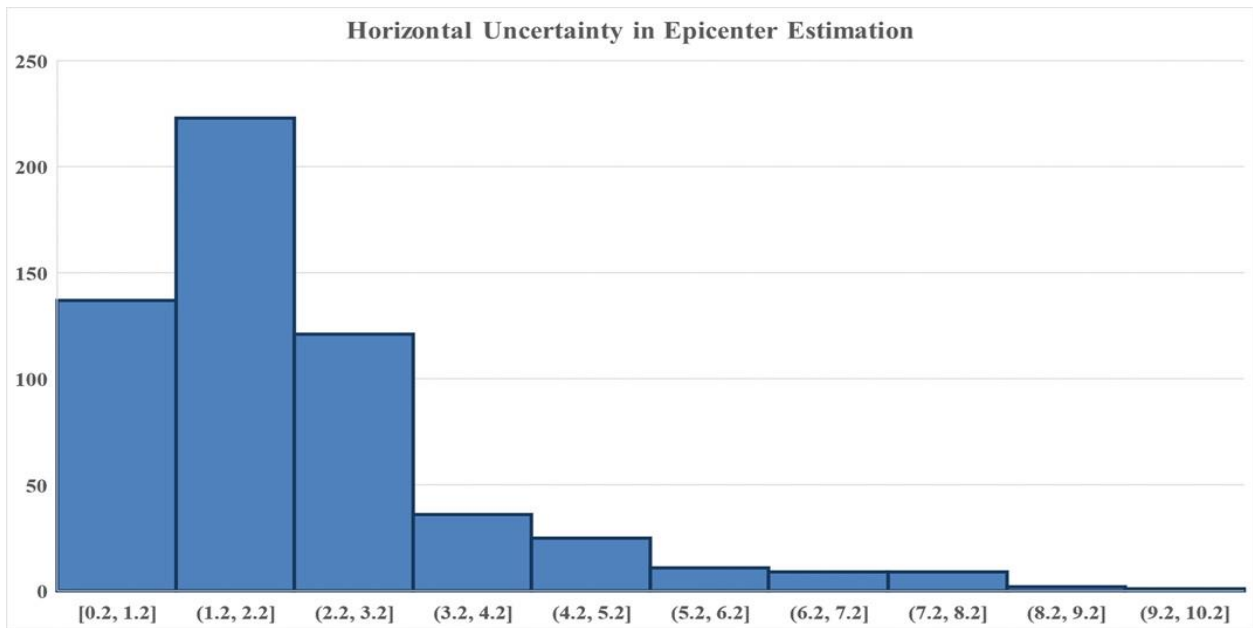


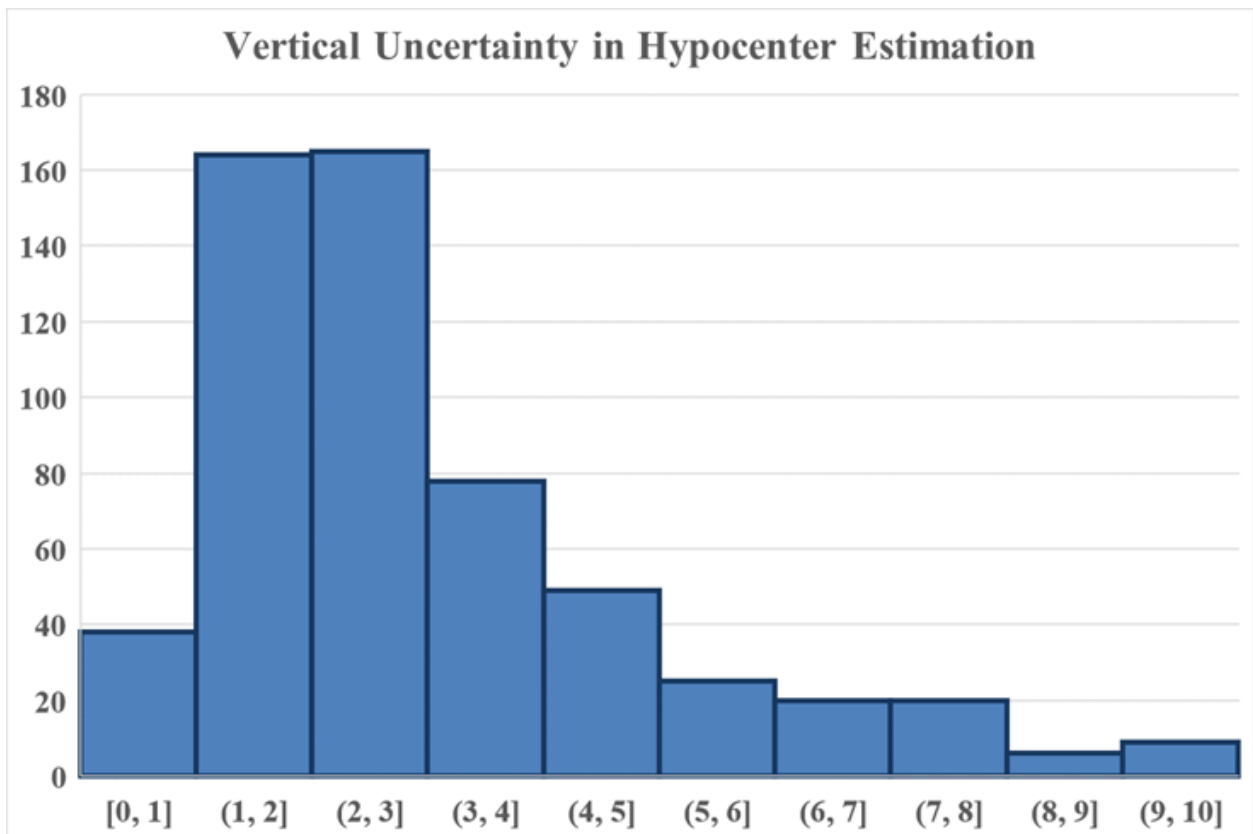
Fig. 3 a) Number of events by distance from Dam; b) Local magnitude (MI) by distance from the dam (DFD);c) The number of events by focal depth; d) Number of events by magnitude.

In addition, we examined the horizontal and vertical location uncertainties of the recorded events, along with the azimuthal gap distribution. These parameters were analyzed with respect to event magnitude and are summarized in Figure 4 (a,b,c,d).

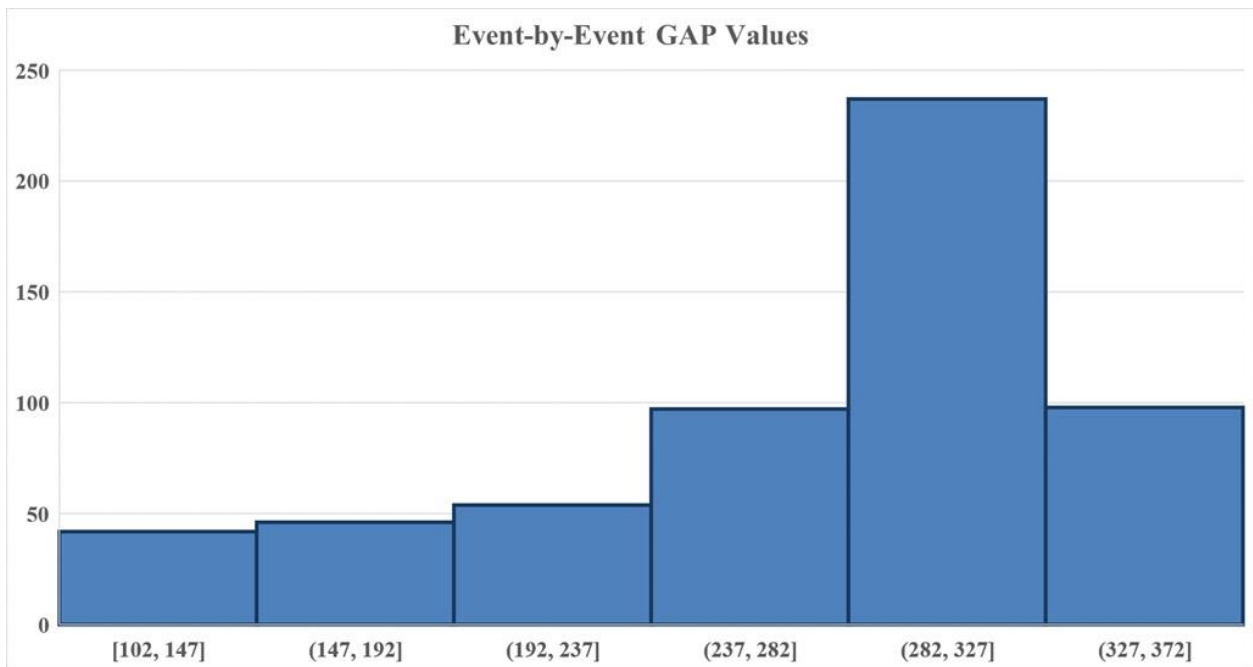
a)



b)



c)



d)

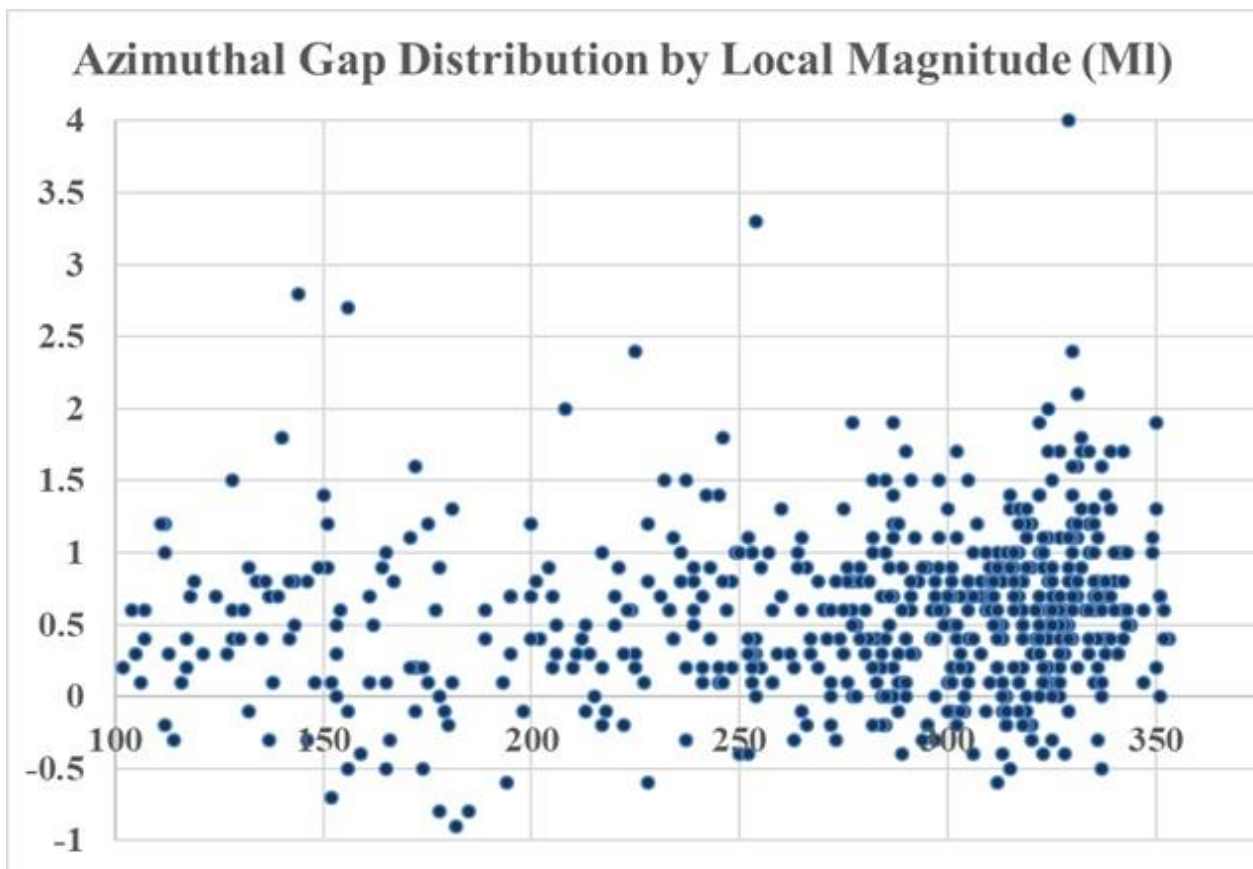


Fig. 4 a) The horizontal location uncertainties of the recorded events; b) The vertical location uncertainties of the recorded events; c) Azimuthal GAP of the recorded events; d) Azimuthal GAP distribution by MI

The results show that horizontal and vertical estimation errors are below 5 km for the majority of events, indicating generally reliable hypocentral locations. However, azimuthal gaps are relatively high, often exceeding  $222^\circ$ , due to the spatial configuration of the network and the presence of inaccessible regions.

Despite this, events with  $M_I < 0$  are still detected within these conditions, highlighting the network’s sensitivity to low-magnitude seismicity even under suboptimal geometric coverage.

### Completeness Magnitude and Gutenberg–Richter Analysis

To assess temporal variations in seismic monitoring performance and investigate possible hydrologically modulated seismicity, we analyzed the cumulative number of earthquakes over time. To determine an appropriate temporal resolution for estimating completeness magnitude ( $M_c$ ) and tracking the evolution of microseismicity, we first estimated recurrence intervals for small-magnitude earthquakes using the Gutenberg–Richter (GR) relationship derived from the broader tectonic zone encompassing the Enguri Dam (Tab1).

Based on the national seismic catalog and applying the GR relation to events with  $M_I \geq 3$ , we extrapolated the expected recurrence rates for lower-magnitude events. This analysis suggests that, according to the least-squares (LS) method:

- Earthquakes with  $M_I \geq 2$  occur approximately every 2.4 months,
- Events with  $M_I \geq 1$  occur in less than one month.

Estimates obtained from the maximum likelihood (ML) method suggest even shorter recurrence intervals. Considering these results and the typical 4-month duration of hydrological transitions (filling and drawdown) at the reservoir, we adopted a 3-month window for  $M_c$  estimation. This window size ensures statistical robustness while remaining sensitive to possible seasonal changes in detectability or seismic response associated with reservoir level fluctuations. In other words These recurrence intervals justify the chosen window size, which is sufficiently long to include multiple low-magnitude events yet short enough to resolve temporal changes in detection capability and seismic response.

To evaluate the detection threshold and temporal consistency of the local seismic catalog, we examined the cumulative number of earthquakes within a 0–17 km distance from the dam, using several magnitude bins and discrete time intervals. Preliminary analysis of the full dataset, aggregated in 3-month windows, revealed a noticeable change in the slope of the cumulative trend around April 2022 (Figure 5).

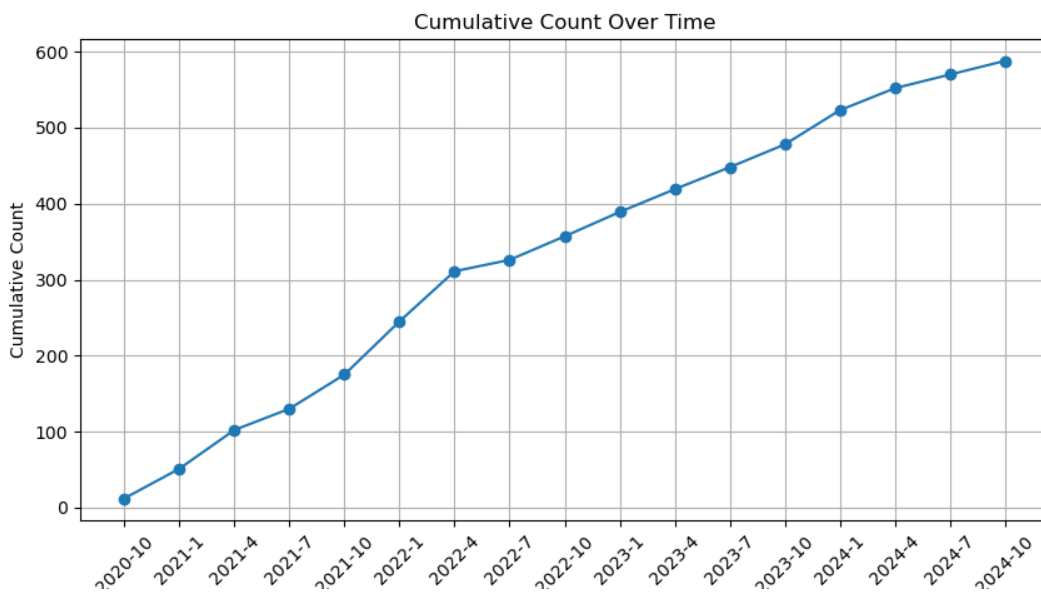


Fig. 5. The cumulative number of earthquakes within a 0–17 km distance from the dam aggregated in 3-month windows.

This feature is apparent for events with magnitudes up to  $M_I = 0$ ; for  $M_I \geq 0$ , the trend becomes linear and consistent, with only a minor deviation near April 2022, likely attributable to transient clustering rather than

a systematic decline in detectability. The timing of this shift coincides with a transition in data processing responsibility—from German collaborators to a local student—raising concerns about possible inconsistencies in the detection or cataloging of low-magnitude events. Based on these findings, we conclude that the catalog can be complete for  $M_I > 0.0$ , while detection reliability decreases for magnitudes below this threshold, particularly after April 2022.

To investigate whether the seismicity rate for these low-magnitude events has remained constant, we repeated the analysis using 12-month bins. This revealed a distinct flattening of the cumulative event curve after late 2023, despite the absence of any change in network operation or data processing methods. Since this trend is not observed in higher-magnitude bins (e.g.,  $M_I \geq 0.4$ ), we interpret it as a real decline in the occurrence rate of smaller microearthquakes ( $M_I \approx 0.0–0.3$ ) since November of 2023 (Fig.6). This reduction may reflect stress relaxation following a previously more active phase, potentially driven by pore pressure diffusion or changes in reservoir-induced stress. Alternatively, it may signal progressive stress accumulation, in which small asperities have already ruptured and stress is increasingly focused on larger fault segments. This type of seismic quiescence has been reported prior to larger events in other tectonic and reservoir settings. Although additional analysis (e.g., clustering behavior, focal mechanism trends, or geomechanical modeling) would be required to test these scenarios, the current observations point to a genuine physical change in the system, rather than an artifact of detection or processing.

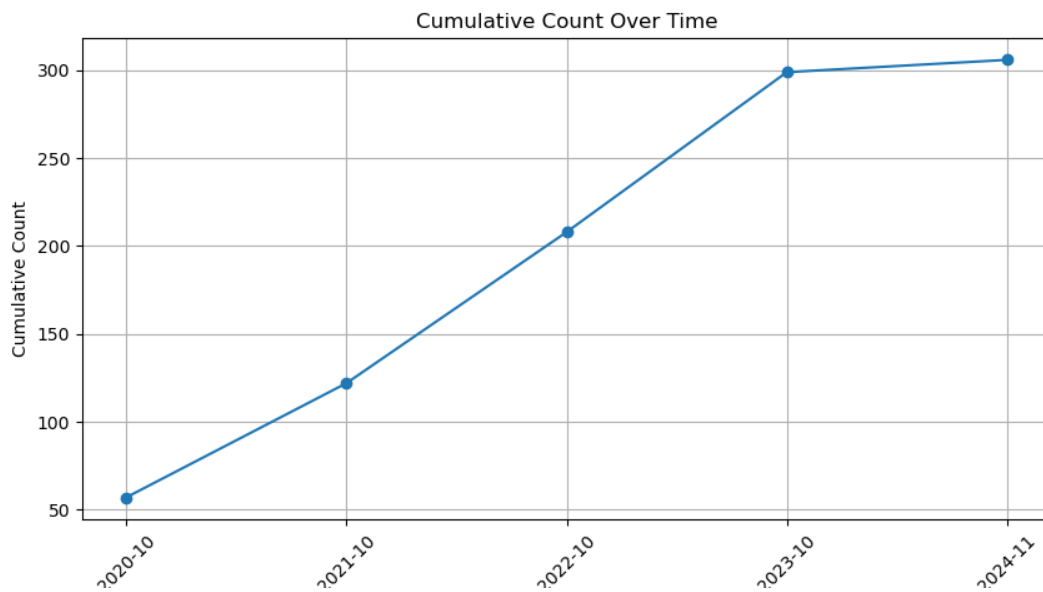


Fig. 6. The cumulative number of earthquakes within a 0–17 km distance from the dam aggregated in 12-month windows.

Catalog completeness was carefully assessed using both cumulative number analysis by magnitude and time and the MAXC method. Based on this analysis and on the discussion above, we adopt  $M_c = 0.6$  as a conservative completeness threshold in the range 0–17 km.

To assess the spatial characteristics of seismicity around the Enguri Dam, we analyzed Gutenberg–Richter parameters within two distance ranges: 0–17 km, 0–30 km, using both least squares (LS) and maximum likelihood (ML) estimation methods. The results are summarized in Table 1. In particular, induced seismicity—often characterized by elevated  $b$ -values due to transient stress perturbations from reservoir fluctuations—may affect the observed distribution. In the 0–17 km range, the ML and the LS method gives  $b$  value  $\geq 1$ . Completeness analysis for the broader 0–30 km region indicates a reliable threshold of  $M_c = 1.0$ , reflecting decreased sensitivity at larger distances. For this zone, LS yields  $b = 0.77$ , while ML gives  $b = 1.04$ .

The Gutenberg–Richter law [3] describes a cumulative distribution of discrete earthquake magnitudes and is commonly expressed as:

$$\log_{10}N(M)=a-bM$$

where  $N(M)$  is the number of earthquakes with magnitude  $\geq M$ , and  $a$  and  $b$  are constants characterizing the seismic productivity and the relative proportion of small to large events, respectively [2;5]. Accurate estimation of the  $b$ -value is essential for understanding the stress regime and failure characteristics of a given seismotectonic or anthropogenically influenced region.

The Maximum Likelihood Estimation (MLE) method provides an efficient, unbiased estimator for the exponential distribution of magnitudes above the completeness threshold  $M_c$  [6-7]. The MLE approach avoids the pitfalls of the Least Squares (LS) method, which assumes linearity in the log-transformed cumulative frequency–magnitude distribution and is highly sensitive to data binning, magnitude rounding, and departures from ideal power-law behavior [8-9]. This distinction is particularly relevant for the Enguri Dam region, where seismic catalog completeness may vary due to changes in network configuration, processing protocols, and temporal variations in ambient noise. In such environments, LS regression can significantly underestimate or overestimate the  $b$ -value, especially near the magnitude of completeness. The MLE method, by contrast, operates directly on the individual magnitudes and remains robust against these catalog limitations [8-9].

Furthermore, MLE allows for the derivation of analytical confidence intervals, enabling statistically rigorous comparisons across different spatial or temporal windows. This capability is critical in high-resolution microseismic studies, such as those conducted around large hydropower reservoirs, where subtle changes in seismicity may reflect stress perturbations or hydrologically induced pore pressure diffusion [11-13].

For comparison, the Gutenberg-Richter  $b$ -values derived from the national seismic catalog-homogenized to moment magnitude ( $M_w$ )-are notably lower than those obtained from the local catalog within both the 0–17 km and 0-30 km distance ranges around the Enguri Dam. While differences in magnitude scales can affect  $b$ -value estimation, particularly for low-magnitude events where  $M_l$  and  $M_w$  diverge, the consistently high  $b$ -values ( $\geq 1$ ) obtained using  $M_l$  suggest that this discrepancy cannot be explained solely by the choice of magnitude type. Instead, the results likely reflect genuine local conditions, including the occurrence of a larger proportion of small-magnitude events and the influence of reservoir-induced processes. The similarity of  $b$ -values across both spatial ranges implies that the effects of reservoir operations-most notably water level fluctuations-may extend at least 30 km from the dam, supporting the interpretation that the observed seismicity is induced or significantly modulated by anthropogenic activity.

Table 1. The Gutenberg–Richter parameters for the seismogenic source were estimated from the national earthquake catalog using two approaches: the least squares (LS) method and the maximum likelihood method.

Mc	bin	Method	b-value	a-value	Range km	network
0.6( $M_l$ )	0.2	LS	1.02	2.26	0-17	DAMAST
0.6( $M_l$ )	0.2	ML	1.00	2.85	0-17	DAMAST
1.0( $M_l$ )	0.2	LS	0.77	2.13	0-30	DAMAST
1.0( $M_l$ )	0.2	ML	1.04	3.23	0-30	DAMAST
3.5( $M_w$ )	0.2	LS	0.7	2.1		National
3.5( $M_w$ )	0.2	ML	0.88	3.08		National

## Hydro-Meteorological Controls on Monthly Seismic Activity

To evaluate the influence of short-term hydrological and meteorological processes on local seismicity, we analyzed monthly earthquake counts in relation to three key parameters: reservoir water level, water inflow, and the rate of water level change (velocity) (Fig.7-8). From early 2021 to mid-2022, the reservoir followed a regular seasonal cycle with gradual filling and drawdown phases and extended high- and low-water plateaus. During this period, elevated seismicity systematically coincided with the transition phases, consistent with

classical models of hydro-mechanical triggering. Earthquake counts peaked at the end of drawdown in early 2021, again during reservoir filling in mid-2021, and most notably during and after drawdown in early 2022. These periods also coincide with significant water inflow peaks and positive or negative extremes in water level velocity, highlighting a coupled response to both volumetric and stress-rate changes in the system.

After July 2022, the dam's operational regime changed-high-water plateaus disappeared, and the reservoir exhibited faster and less symmetric cycling. The corresponding seismicity became less periodic and more scattered. Although seismic activity continued to respond at times to hydrological transitions, the relationship weakened, likely due to shortened stress-loading intervals, more abrupt pressure changes, and altered diffusion pathways within the crust.

Interestingly, a notable seismicity peak in January 2023 occurred without a sharp change in water level velocity. This suggests that not all triggering is driven by high stress rates; instead, it may reflect delayed rupture following earlier stress accumulation or unloading. In contrast, a period of high negative velocity around November 2023-indicative of rapid drawdown-was not accompanied by increased seismicity. This implies that the crustal system had either already released accumulated strain or was in a post-rupture relaxation phase. These observations emphasize that the triggering process depends not only on instantaneous stress changes but also on the temporal evolution of the stress field and fault memory effects.

Overall, the results point to a complex and evolving relationship between seismicity and hydrological forcing. While water level, inflow, and rate of change all appear to influence the timing and amplitude of microseismic activity, the underlying mechanism is ultimately rooted in stress perturbations caused by water level variations. However, the presence of both responsive and unresponsive phases, as well as asymmetries between loading and unloading, suggests that the system's behavior is modulated by additional factors such as preexisting stress state, fault maturity, and potential fatigue or healing processes. Rather than supporting a single deterministic model, the observations imply a dynamic interplay between reservoir-induced stress changes and local fault stability conditions, with the seismic response being highly context dependent.

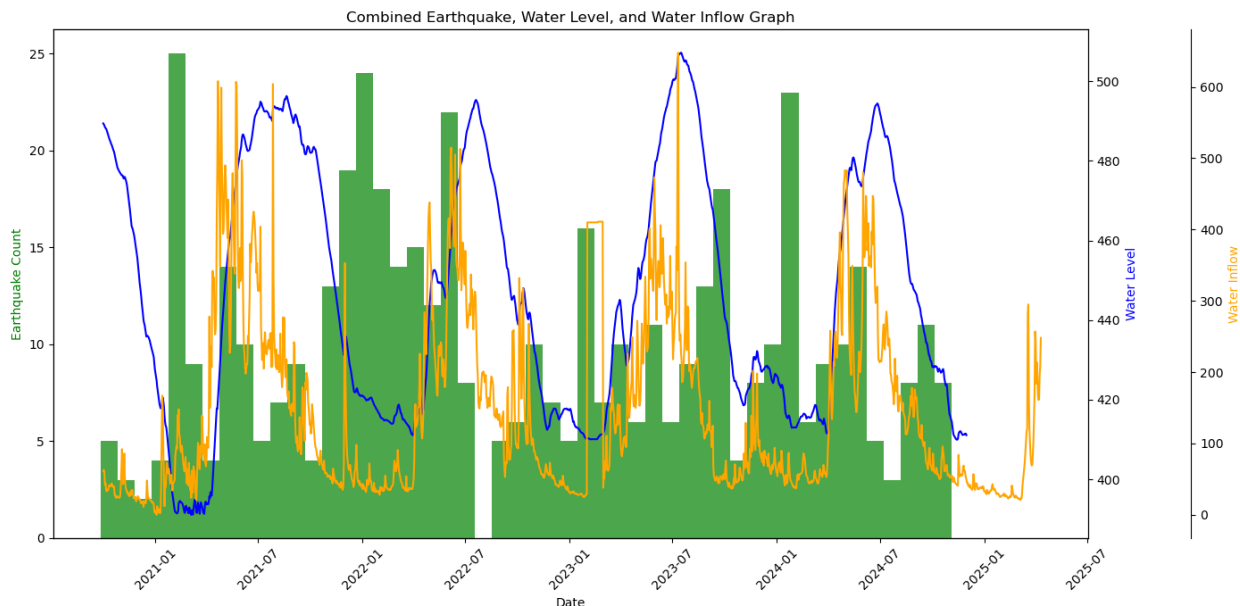


Fig. 7. Monthly Seismicity, Reservoir Water Level Changes, and Inflow at Enguri Dam.

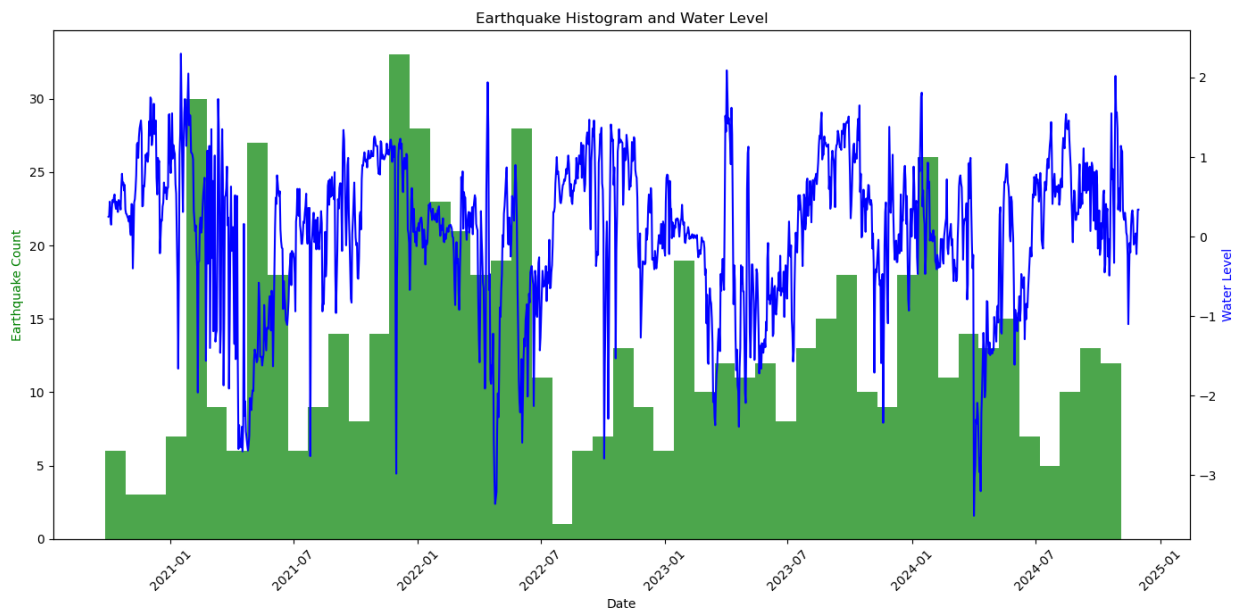


Fig. 8. Monthly Seismicity and Water Level Change Rate at Enguri Reservoir.

While hydrological controls exhibit a clear relationship with microseismicity, meteorological parameters-namely air temperature, humidity, and rainfall-show no consistent correlation with monthly earthquake rates (Fig 9-11). Although isolated coincidences exist, seasonal temperature cycles and short-lived rainfall or humidity fluctuations do not align systematically with seismicity peaks. This suggests that atmospheric variables are not primary drivers of stress changes at seismogenic depths. Their influence, if any, is likely indirect-manifesting through surface runoff and infiltration processes already reflected in inflow and reservoir level dynamics.

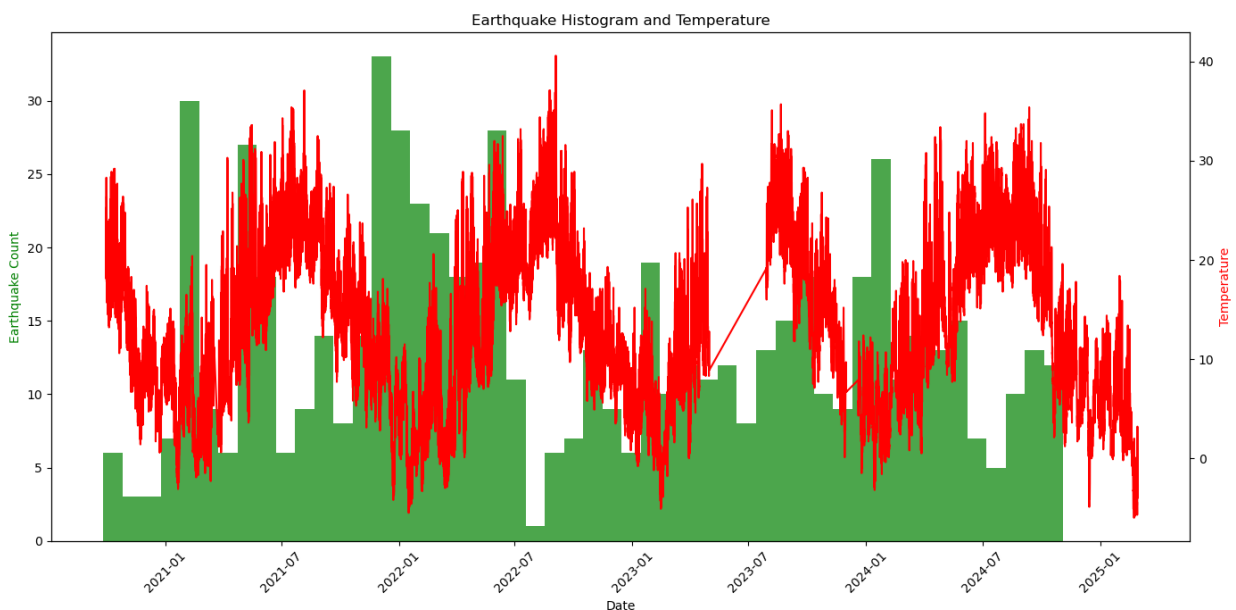


Fig. 9. Monthly Seismicity and Temperature Changes.

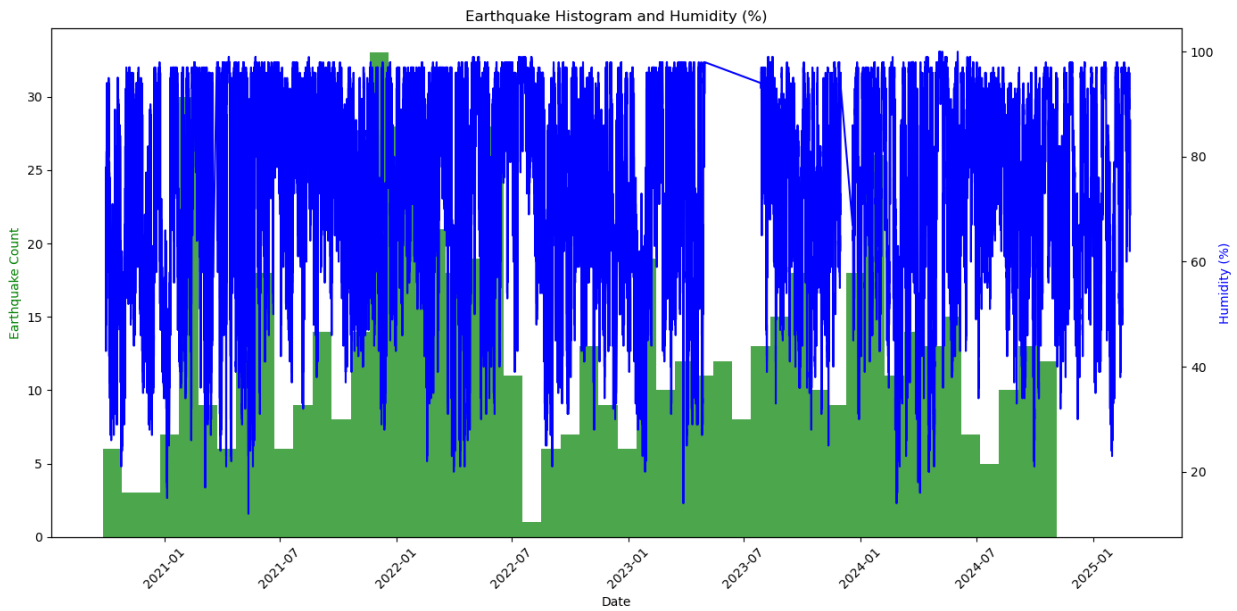


Fig. 10. Monthly Seismicity and Humidity Variations.

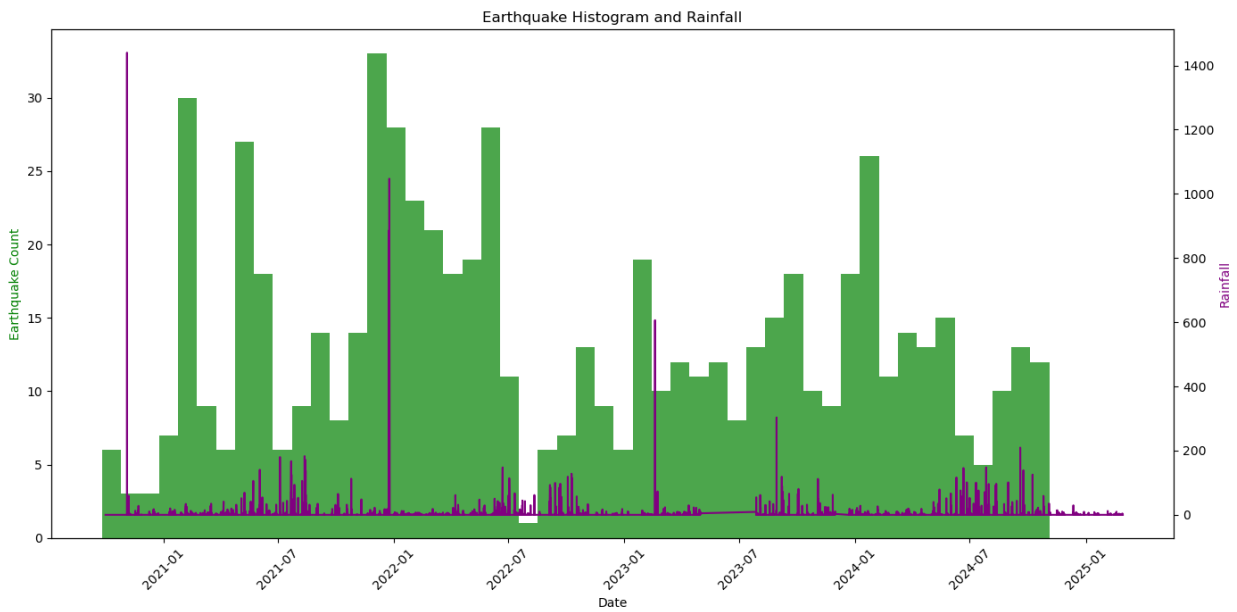


Fig. 11. Monthly Seismicity and Precipitation.

## Conclusion

The DAMAST microseismic catalog [14] provides a unique opportunity to study reservoir-induced seismicity near the Enguri Dam with high resolution. Catalog completeness was carefully assessed using both cumulative number analysis by magnitude and the MAXC method, leading to a conservative completeness magnitude of  $M_c = 0.6$  within a 17 km radius of the dam. This threshold enabled robust estimation of Gutenberg–Richter parameters, revealing elevated b-values, indicative of a relatively high proportion of low-magnitude events. These findings contrast with lower b-values derived from the national  $M_w$ -based catalog for the same tectonic zone, suggesting that local processes—including reservoir operations—may be influencing the microseismic population. The similarity of b-values across both spatial ranges implies that the effects of

reservoir operations—most notably water level fluctuations—may extend at least 30 km from the dam, supporting the interpretation that the observed seismicity is induced or significantly modulated by anthropogenic activity

The temporal evolution of seismicity further supports this interpretation. During periods of regular reservoir operation (2021–mid-2022), seismicity rates increased during both water level rise and drawdown phases, consistent with expected stress changes due to volumetric loading and unloading. This behavior aligns with the elevated *b*-values, often associated with induced seismicity in response to transient stress perturbations.

Following a shift in reservoir management after mid-2022, the seismic response became less periodic and more irregular, yet still showed isolated peaks temporally correlated with rapid water level transitions. This pattern supports a continued, though more complex, hydro-seismic interaction. In contrast, meteorological parameters such as temperature, humidity, and rainfall showed no meaningful correlation with seismicity, reinforcing the conclusion that stress changes from water level variation are the primary modulating factor.

Overall, the integration of statistical seismological analysis with hydrological and meteorological records reveals that microseismicity near the Enguri Dam is closely linked to reservoir-induced stress changes. The combination of elevated *b*-values, spatiotemporal clustering, and correlation with water level dynamics points to induced processes operating alongside regional tectonic background activity.

**Acknowledgments.** The authors would like to thank the Federal Ministry of Education and Research of Germany (BMBF, now BMFTR) for funding the DAMAST and DAMAST-Transfer projects as part of ‘CLIENT II - International Partnership for Sustainable Innovations’, a funding programme within the framework of ‘Research for Sustainable Development (FONA<sup>3</sup>)’, BMBF project 03G0882A - DAMAST and DAMAST transfer. This enabled to establish the new station network. We would like to express our sincere gratitude to Birgit Müller for her excellent coordination and management of the project, as well as for her scientific contributions to the broader research activities. Special thanks are due to Andreas Rietbrock, who served as the main academic supervisor and played a central role in organizing the teaching activities associated with the project. We also thank Michael Frietsch for his support in setting up the online data transmission and for providing related training to our students. We are grateful to Nasim Karamzadeh for her contribution to the data processing training. Finally, we acknowledge Emmanuel Gaucher, Felix Bögelspacher, and Hans Agurto Detzel for their assistance during the installation of the seismic stations. Their collective support was vital to the successful implementation and educational impact of this work.

## References

- [1] Karamzadeh N., Tsereteli N., Gaucher E., et al. Seismological study around the Enguri dam reservoir (Georgia) based on old catalogs and ongoing monitoring. *Journal of Seismology* 27, 2023, pp. 953–977. <https://doi.org/10.1007/s10950-023-10173-5>.
- [2] Telesca L., Tsereteli N., Chelidze T., Lapenna V. Spectral investigation of the relationship between seismicity and water level in the Enguri high dam area (Georgia). *Geosciences* 2024, 14. <https://doi.org/10.3390/geosciences14010022>.
- [3] Gutenberg R., Richter C.F. Frequency of earthquakes in California. *Bull. Seismol. Soc. Am.* 1944, 34, pp. 185–188.
- [4] Peterson J. Observations and modeling of seismic background noise (U.S. Geological Survey Open-File Report 93-322), 1993. <https://doi.org/10.3133/ofr93322>
- [5] Utsu T. A method for determining the value of *b* in a formula  $\log N = a - bM$  showing the magnitude-frequency relation for earthquakes. *Geophysical Bulletin of Hokkaido University*, 13, 1965, pp. 99–103.
- [6] Aki K. Maximum likelihood estimate of *b* in the formula  $\log N = a - bM$  and its confidence limits. *Bulletin of the Earthquake Research Institute*, 43, 1965, pp. 237–239.
- [7] Bender B. Maximum likelihood estimation of *b*-values for magnitude grouped data. *Bulletin of the Seismological Society of America*, 73(3), 1983, pp. 831–851.
- [8] Wiemer S., Wyss M. Minimum magnitude of completeness in earthquake catalogs: Examples from Alaska, the western United States, and Japan. *Bulletin of the Seismological Society of America*, 90(4), 2000, pp. 859–869.

- [9] Marzocchi W., Sandri L. A review and new insights on the estimation of the b-value and its uncertainty. *Annals of Geophysics*, 46(6), 2003, pp. 1271–1282.
- [10] Woessner J., Wiemer S. Assessing the quality of earthquake catalogs: Estimating the magnitude of completeness and its uncertainty. *Bulletin of the Seismological Society of America*, 95(2), 2005, pp. 684–698.
- [11] Tormann T., Wiemer S., Enescu B. Mapping and validating the frequency–magnitude distribution of earthquakes in subduction zones. *Journal of Geophysical Research: Solid Earth*, 119(6), 2014, pp. 4270–4287.
- [12] Shapiro S. A., Dinske C., Langenbruch C., Wenzel F. Seismogenic index and magnitude probability of earthquakes induced during reservoir fluid stimulations. *Leading Edge*, 26(6), 2007, pp. 648–651.
- [13] Mignan A., Woessner J. Estimating the magnitude of completeness for earthquake catalogs. *Community Online Resource for Statistical Seismicity Analysis*, 2012. doi:10.5078/corssa-00180805
- [14] Frietsch M., Tugushi N., Karamzadeh N., Tsereteli N., Gaucher E., Rietbrock A. *Zeitschrift für Wasserwirtschaft*, in preparation 2025.

## ენგურის კაშხლის (საქართველო) მიმდებარე ტერიტორიაზე მიკროსეისმური აქტივობის დროითი ცვლილება წყალსაცავის ექსპლუატაციის გავლენის ფონზე

ნ. წერეთელი, ლ. ლომიძე, ნ. ტულუში

### რეზიუმე

წარმოდგენილ ნაშრომში განიხილება მიკროსეისმურობის დროით-სივრცული ანალიზი ენგურის კაშხლის (საქართველო) მახლობლად, DAMAST პროექტის ფარგლებში დამონტაჟებული ადგილობრივი სეისმური ქსელის ოთხ წელზე მეტი ხნის მონაცემების საფუძველზე. კატალოგის სისრულის ანალიზის საფუძველზე, წარმომადგენელი მიწისძვრის მაგნიტუდა განისაზღვრა, როგორც  $M_c = 0.6$  კაშხლიდან 17 კმ რადიუსში, რაც შესაძლებელს ხდის გუტენბერგ–რიხტერის პარამეტრების სანდო შეფასებას. DAMAST-ის კატალოგის მიხედვით მიღებული მაღალი  $b$ -მნიშვნელობა, ეროვნულ კატალოგზე მიღებულ  $b$ -მნიშვნელობაზე, მიუთითებს, რომ სეისმურობის მნიშვნელოვანი ნაწილი შესაძლოა კაშხლის ექსპლუატაციით იყოს გამოწვეული. მსგავსი ანალიზის შედეგად, 30 კმ რადიუსში გამოვლინდა, რომ კატალოგის სისრულის ზღვარი შეესაბამება  $M_c = 1.0$ -ს, თუმცა მაქსიმალური მსგავსების მეთოდით შეფასებული  $b$ -ის მნიშვნელობა კვლავ მაღალია ( $\geq 1$ ).  $b$ -ს ამგვარი მაღალი მნიშვნელობის სივრცული ერთგვაროვნება მიუთითებს, რომ რეზერვუარის ექსპლუატაციას აქვს გავლენა სეისმურობაზე მინიმუმ 30 კმ რადიუსში კაშხლისგან. კვლევამ აჩვენა, რომ სეისმური აქტივობის ზრდა ძირითადად ემთხვევა წყალსაცავის შევსებისა და დაცლის პერიოდებს, მაშინ როდესაც მეტეოროლოგიურ პარამეტრებთან სტატისტიკურად მნიშვნელოვანი კავშირი არ აღინიშნება. ჩვენი შედეგები ხაზს უსვამს კაშხლის მუშაობით გამოწვეული დამაბულობის ცვლილებების როლს მიკროსეისმურობაზე და აჩვენებს, რამდენად მნიშვნელოვანია უწყვეტი ჰიდროლოგიური და სეისმოლოგიური მონიტორინგის ინტეგრაცია მსგავსი სახის ინფრასტრუქტურის სეისმური რისკების შეფასებისთვის.

**საკვანძო სიტყვები:** მიკროსეისმურობა, ენგურის კაშხალი, სეისმური კატალოგის ანალიზი,  $b$ -ფაქტორის შეფასება

# Эволюция микросейсмичности во времени в ответ на эксплуатацию водохранилища у плотины Ингури (Грузия)

Н. Церетели, Л. Гомидзе, Н. Тугуши

## Резюме

В настоящем исследовании анализируется временная эволюция микросейсмичности в районе плотины Ингури (Грузия) на основе более чем четырехлетних данных, собранных локальной сейсмической сетью, установленной в рамках проекта DAMAST. Подробный анализ полноты каталога позволил определить консервативный порог  $M_c = 0.6$  в радиусе 17 км от плотины, что обеспечило надежную оценку параметров Гутенберга–Рихтера. Повышенные значения параметра  $b$  в локальном каталоге - по сравнению с данными национального каталога, приведённого к шкале моментной магнитуды ( $M_w$ ) - указывают на возможное влияние процессов, вызванных эксплуатацией водохранилища. При расширении анализа до радиуса 30 км установлено, что порог полноты увеличивается до  $M_c = 1.0$ ; однако значение  $b$  остаётся высоким ( $\geq 1$ ) при использовании метода максимального правдоподобия. Такое пространственное постоянство повышенных значений  $b$  свидетельствует о том, что эксплуатация водохранилища оказывает влияние на сейсмичность на расстоянии как минимум 30 км от плотины. Сейсмичность коррелирует с изменениями уровня воды, особенно в фазах наполнения и спуска, тогда как метеорологические параметры не демонстрируют устойчивой связи. Полученные результаты подчеркивают влияние работы водохранилища на микросейсмическую активность и важность комплексного мониторинга гидрологических и сейсмических процессов в районах крупных гидротехнических сооружений.

**Ключевые слова:** микросейсмичность, Ингурское водохранилище, анализ сейсмического каталога, оценка  $b$ -параметра

## **A Three-Dimensional Representation of the Piles Radio Image on the Radargram for the Completed Construction**

**Davit T. Odilavadze, Tamaz L. Chelidze, Olga V. Yavolovskaya**

*M. Nodia Institute of Geophysics of I. Javakishvili Tbilisi State University, Tbilisi, Georgia*

[odildavit@gmail.com](mailto:odildavit@gmail.com)

### **ABSTRACT**

*One of the important issues in urban geolocation is the determination of the depth of piles within the scope of geolocation activity. The peculiarity of the complexity of the issue lies in the heterogeneity of the work environment, which can be found both in an open space, such as a construction site, and in a closed, i.e. completed and put into operation building. Conducting geolocation profiles under operational building conditions is also limited due to existing partitions and architectural elements of non-conductive placement. In some cases, we are forced to limit ourselves by taking partial profiles and use a complicated interpretation for such a radargram. In particular, we additionally use the three-dimensional spatial representation for the intersections of geolocation profiles to determine the depth of the target pile. For the interpretation of the depth limit of pile, it is recommended to fix the location of the hyperbola of the pile radio image on the axis of intersection of the intersecting profiles for both profiles, to imagine and interpret the 3D radio image of the target pile for the intersection axis of the profiles.*

**Key words:** urban geolocation, radio image, depth of piles, radargram.

### **Introduction**

One of the important issues in urban georadiolocation is the determination of the depth of piles within the georadiolocation activity [1, 2, 3, 4]. The peculiarity of the complexity of the issue lies in the heterogeneity of the working environment, which can be found both in an open space, such as a construction site and in a closed, i.e. completed and put into operation, building. Conducting geolocation profiles under operational building conditions is also limited due to existing partitions and architectural elements of non-conductive placement. In some cases, we are forced to limit ourselves by taking partial profiles and use a complicated interpretation for such a radargram. In particular, we additionally use the three-dimensional spatial representation for the intersections of geolocation profiles to determine the depth of the target pile.

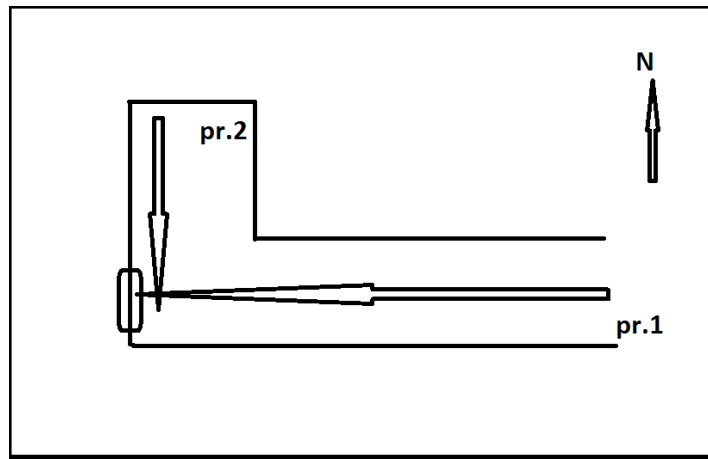
### **Task**

For the completed and operational medical building, it was necessary to determine the crossing of one of the corners of pile. The problem was the presence of limited space because a complete geolocation profile could not be conducted. It was decided to perform two mutually directed georadar profiles, at the intersection of which the target pile was placed in the corner of the walls.

### **Method and instrumental part**

On the first floor of the completed building, the deepening of the load-bearing pile was to be investigated in the internal area. The survey was carried out using georadiolocation method georadar Zond12e, with official software "Prizm-6.0", for further, three-dimensional interpretation, compatible software - "Voxler 4" was used.

Two intersecting profiles were conducted, the schematic representation of which is given in the schematic drawing (Scheme 1).



Scheme 1. The diagram shows the conditional location of geolocation profiles 1-2 and shows the probable location of pile.

### Data and reasoning

It follows from the interpretation of Prof. 1 presented on the radargram (Fig. 1) that the pile radio image was marked at distances of 15-16m and at a depth of 9m on average. The radio image is marked with white lines.

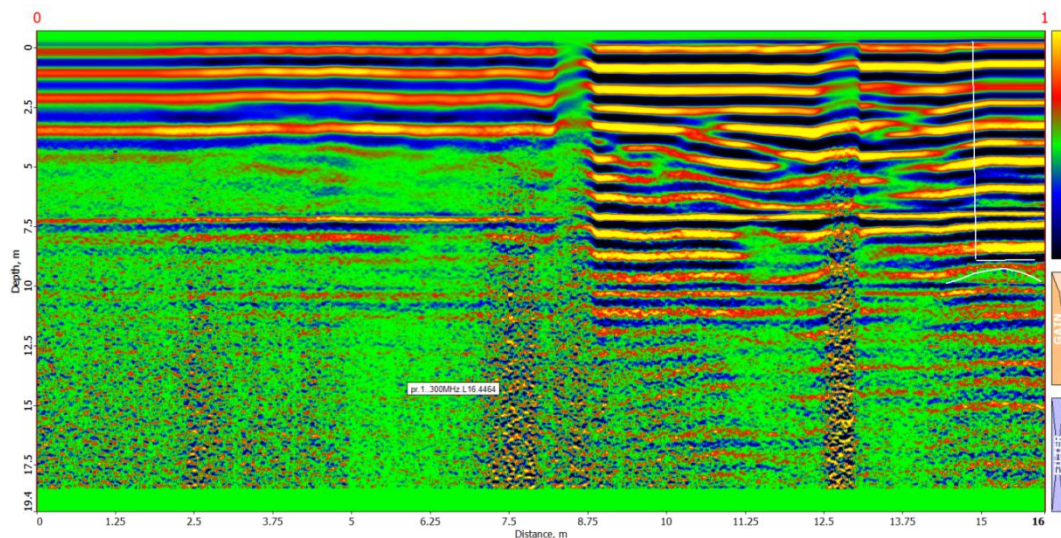


Fig. 1. Radargram Prof. 1, length - 16 m, is presented Zond-12e with standard shielded antenna 300MHz.

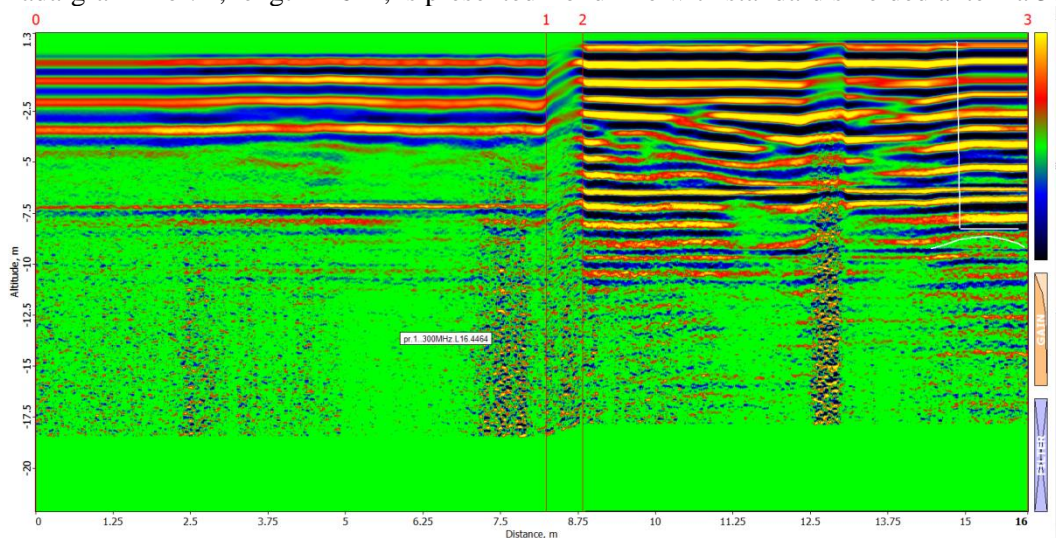


Fig. 2. Radargram Prof. 1 is presented, length - 16 m. It is made with a standard shielded radar antenna of 300MHz. The topographic effect is taken into account.

For visualization, Prof. 1 (Fig. 2) has been added to the radar chart, the pile radio image has been marked at a distance 15-16 m and at a depth of 9m. Since the base of the borehole is naturally uneven, the lateral placement of the poured concrete is also uneven, thus the plane of the base of pile changes within the limits of 8.9-9.2m. The radar profile passed through one side of pile; the other sides are covered by the wall construction.

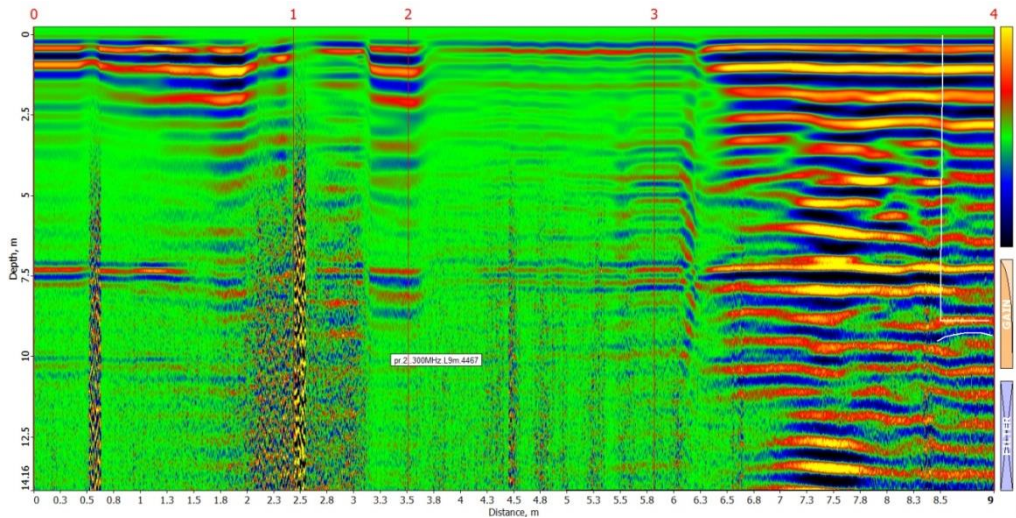


Fig. 3. Presents radargram Prof. 2, length -9m. It is made with a standard radar shielded antenna of 300MHz.

From the Prof. 2 (Fig. 3) interpretation presented on the radar chart, it follows that the pile radio image was marked at a distance 8.5-9m and at a depth 9m.

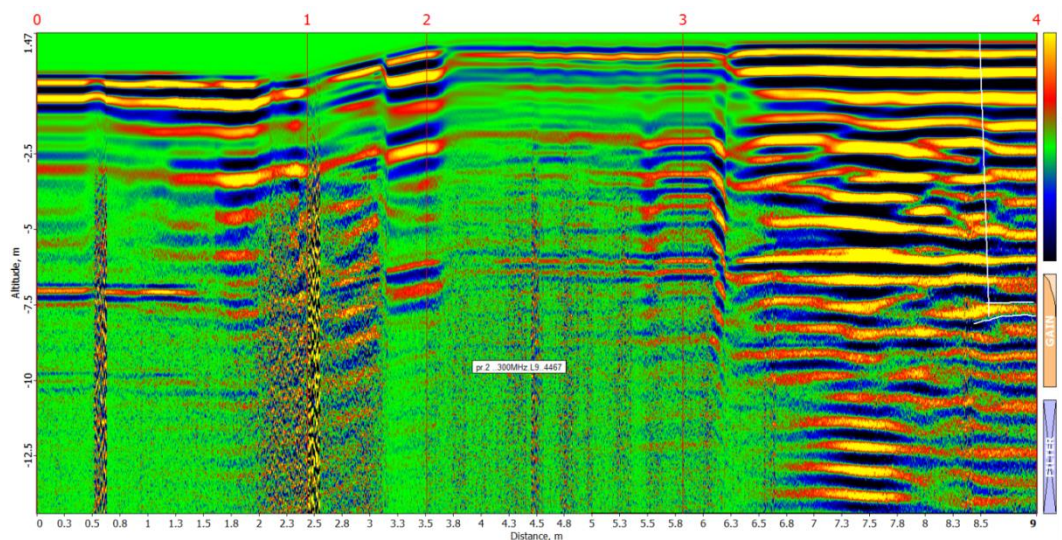


Fig. 4. Radargram Prof. 2, length -9m is presented. It is made with a standard radar shielded antenna of 300MHz. The topographical effect is taken into account.

From the Prof. 2 interpretation on the radar chart, it follows that the pile radio image was marked at a distance 8.5-9m and at a depth of 9m. Since the base of the borehole is naturally uneven, the lateral placement of the poured concrete is also uneven, thus the sections of the pile base vary within the limits of 8.9-9.2m, the results of profile-2 coincide with the results of profile-1 within the location of the hyperbola indicator.

The radio view of the object of vertical placement recorded by Prof. 1 and Prof. 2 corresponds to the pile with a depth of 9-9.2 m.

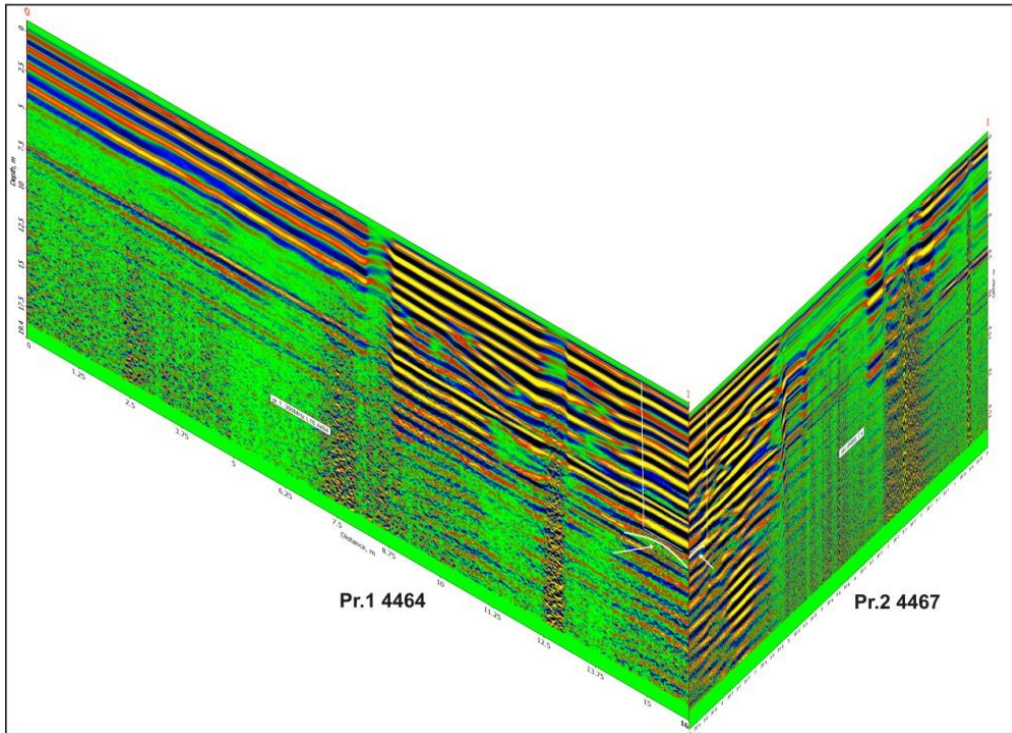


Fig. 5. Radargram Prof. 1 and Prof. 2 are presented, the target pile is located at the intersection, it is made with the radar staff screened antenna 300MHz.

At the intersection of Profiles-1, 2 (Fig. 5) the location of the hyperbola indicating the pile radio image was identified. Shown by a white circle adjacent to the synphasic axis.

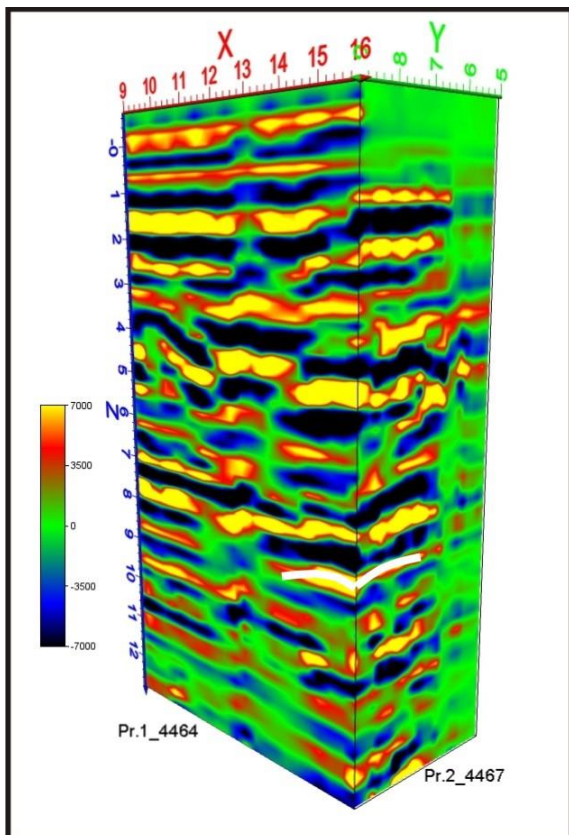


Fig. 6. An excerpt from the spatial representation of the intersection of profiles-1, 2 is provided. The 3D radio image is built using Voxler 4 software.

The radargram presented in Fig. 6 clearly defines the hyperbola marked with white circles for the target, the carrier pile 3D radio image, which uniquely characterizes the deepening of pile as a physical object and its location.

## Conclusion

For the interpretation of the depth limit of pile, it is recommended to fix the location of the hyperbola of the pile radio face in the cross section of the intersecting profiles for both profiles, to imagine and interpret the 3D radio face for the target pile for the axis of the intersection of the profiles.

## References

- [1] Odilavadze D., Chelidze T., Yavolovskaya O. The radio image of an object with an elongated, face-fragmented, dielectrically complex structure was studied using the method of georadar physical modeling. Journal of the Georgian Geophysical Society, ISSN 1512-1127, E-ISSN 2667-9973, v. 27(2), 2024.
- [2] Odilavadze D., Chelidze T., Yavolovskaya O. Radio images investigated by the method of physical modeling of an archaeogeoradiolocationally complex building object. International Scientific Conference “Complex Geophysical Monitoring in Georgia: History, Modern Problems, Promoting Sustainable Development of the Country”, Tbilisi, Georgia, October 17-19, 2024. Transactions of Mikheil Nodia Institute of Geophysics, 2024. <http://openlibrary.ge/handle/123456789/10610> (in Georgian).
- [3] Odilavadze D., Yavolovskaya O. On the possibility of determining the depth of hidden parts of cylindrical building structures by georadar method. Transactions of Mikheil Nodia Institute of Geophysics, ISSN 1512-1135, T.LXXVI, ISSN1512-1135, 2023, (in Georgian)
- [4] Odilavadze D., Chelidze T., Ghlonti N., Yavolovskaya O. Determining the presence and structure of a subsurface radioactive burial when interpreting the results of the GPR method by analyzing a three-dimensional rotating radio image. Journal of the Georgian Geophysical Society, E-ISSN: 2667-9973, p-ISSN: 1512-1127, Physics of Solid Earth, Atmosphere, Ocean and Space Plasma, v. 25(1), 2022, pp.21-28.

# რადაროგრამაზე ხიმინჯის რადიოსახის სამგანზომილებიანი წარმოდგენა დასრულებული ნაგებობისთვის

დ. ოდილავაძე, თ. ჭელიძე, ო. იავოლოვსკაია

## რეზიუმე

ურბანულ გეორადიოლოკაციაში ერთერთი მნიშვნელოვანი საკითხია ხიმინჯების დაღრმავების განსაზღვრა გეორადიოლოკაციური აქტივობის ფარგლებში. საკითხის სირთულის თავისებურება მდგომარეობს სამუშაო გარემოს არაერთგვაროვნებაში, რომელიც შეიძლება აღმოჩნდეს როგორც ღია სივრცეში (მაგალითად, სამშენებლო მოედანი), ასევე დახურულ, ანუ დასრულებულ და ექსპლუატაციაში შესული შენობის პირობებში. ექსპლუატაციაში მყოფი შენობის პირობებში გეორადიოლოკაციური პროფილების გატარება ერთობ შეზღუდულია არსებული ტიხრებისა და არა ხელშემწყობი განთავსების არქიტექტურული ელემენტების გამო. ზოგ შემთხვევაში იძულებული ვხვდებით შემოვისაზღვროთ ნაწილობრივი პროფილების გატარებითა და ასეთი რადაროგრამისთვის გართულებული ინტერპრეტაცია გამოვიყენოთ. კერძოდ, დამატებით ვიყენებთ სამგანზომილებიან სივრცულ წარმოდგენას გეორადიოლოკაციური პროფილების გადაკვეთებისთვის სამიზნე ხიმინჯის დაღრმავების განსაზღვრისთვის. ხიმინჯის დაღრმავების განსაზღვრის ინტერპრეტაციისათვის რეკომენდებულია დაფიქსირდეს ხიმინჯის რადიოსახის ჰიპერბოლის მდებარეობა გადამკვეთი

პროფილების გადაკვეთის ღერძზე ორივე პროფილისთვის, აიგოს და ინტერპრეტირდეს პროფილთა გადაკვეთის ღერძისთვის 3D რადიოსახე სამიზნე ხიმინჯისთვის.

**საკვანძო სიტყვები:** ურბანულ გეორადიოლოკაცია, ხიმინჯის დაღრმავების ინტერპრეტაცია, რადიოსახე, რადაროგრამა.

## **Трехмерное изображение радиообраза свай на радарограмме для завершенного строения**

**Д. Одилавадзе, Т. Челидзе, О. Яволовская**

### **Резюме**

Одним из важных вопросов городской геолокации является определение глубины свай в рамках геолокационной деятельности. Особенность и сложность вопроса заключается в неоднородности рабочей среды, которую можно встретить как на открытом пространстве, например, на строительной площадке, так и в закрытом, т.е. завершенном и введенном в эксплуатацию здании. Проведение геолокационных профилей в условиях эксплуатации здания также ограничено из-за существующих перегородок и архитектурных элементов неблагоприятного размещения. В некоторых случаях мы вынуждены ограничиться получением частичных профилей и использовать сложную интерпретацию такой радарограммы. В частности, мы дополнительно используем трехмерное пространственное представление пересечений профилей геолокации для определения глубины целевой сваи. Для интерпретации границы глубины сваи рекомендуется зафиксировать расположение гиперболы радиообраза сваи на оси пересечения пересекающихся профилей для обоих профилей, представить и интерпретировать 3D радиообраз целевой сваи для оси пересечения профилей.

**Ключевые слова:** радиообраз, глубинные сваи, радарограмма, городская геолокация.

## **Preliminary Archaeogeophysical Survey of the Construction Site in the Vicinity of the Narikala Citadel**

**Davit T. Odilavadze, Tamaz L. Chelidze, Olga V. Yavolovskaya**

*M. Nodia Institute of Geophysics of the I. Javakhishvili Tbilisi State University, Tbilisi, Georgia*

[odildavit@gmail.com](mailto:odildavit@gmail.com)

### **ABSTRACT**

*Due to the construction and rehabilitation works in the territory of “Old Tbilisi”, one of the historically ancient and archaeologically very important places in the capital of Georgia, Tbilisi, there was a need to carry out a preliminary reconnaissance archaeogeoradiolocation survey. The pre-marked area for the archaeogeoradiolocation survey was intended as a place for the operation of construction equipment. During the construction process, it was possible to damage multi-ton construction equipment and cause accidents as a result of underground voids, as well as destroy possible archaeological monuments.*

*The archaeogeoradiolocation survey revealed a number of voids, signs of the presence of possible archaeological sites, and mapped their locations. The archaeogeoradiolocation work was performed using a Zond 12e georadar, the data was collected, processed and interpreted using the Prizm 2.6 software. The aim of the task was to conduct a georadiolocation survey to identify voids in the subsurface and near-surface areas.*

*It turned out that the study area is loaded with objects containing cavities of various shapes and contents. The continentality of the soil is disturbed by numerous cavities. Their depth ranges from 0.5 m to 5 m and their length is 1-5 m. A boundary between geological layers has been identified, on which a radio image of a man-made object could be located, such as: a foundation, tunnel, culvert or other cylindrical object located above the foundation and with a width of 1–1.5 m. The presence of a geological object is not excluded.*

*From an archaeological-geological point of view, the study requires further continuation of detailed archaeogeoradiolocation works.*

**Keywords:** *archaeogeoradiolocation survey, georadar works, radio image*

### **Introduction**

Due to the construction and rehabilitation works in the territory of “Old Tbilisi”, one of the historically ancient and archaeologically very important places in the capital of Georgia, Tbilisi, there was a need to conduct a preliminary reconnaissance archaeogeoradiolocation survey. The pre-marked area for the archaeogeoradiolocation [1, 2, 3] survey was intended as a place for the operation of construction equipment. During the construction process, it was possible to damage multi-ton construction equipment and cause accidents as a result of underground voids, as well as destroy possible archaeological monuments.

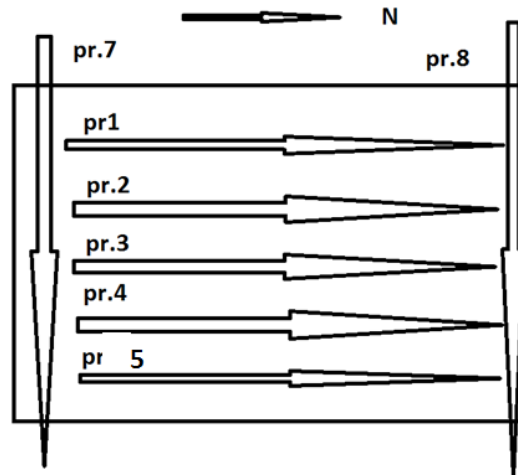
The archaeogeoradiolocation survey revealed a number of voids, signs of the existence of possible archaeological monuments, and mapped their locations.

Archaeological georadar works were performed using the Zond 12e georadar, data were collected, processed and interpreted using the software - Prizm 2.6.

### **Task/Objective**

The purpose of the task was to conduct a georadiolocation survey to identify voids in the subsurface [4, 5, 6, 7] of the underground.

## Environment and Instrumentation



Scheme 1.

In the vicinity of the "Old Tbilisi" citadel, "Nariakala", in geographically difficult terrain, in a pre-marked area, a georadar Zond-12e, with its standard 150MHz dipole antenna, and software Prizm-2.6, was used to conduct a georadiolocation survey to identify voids in the underground near-surface layout.

The schematic drawing (Scheme 1) shows the conditional placement of geo-radiolocation profiles and their directions.

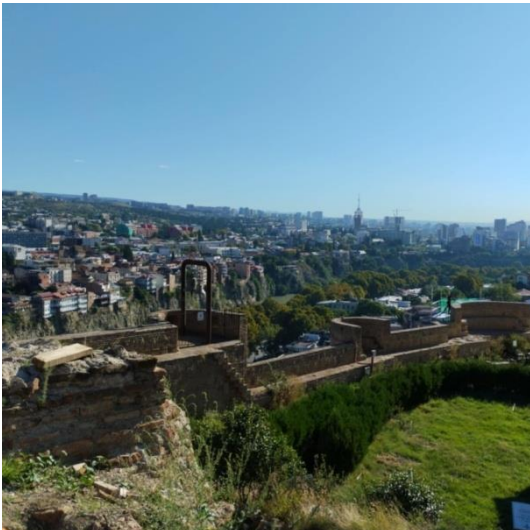


Photo 1.  
View from Narikala Citadel



Photo 2.  
Environment for placing geo-radiolocation profiles.



Photo 3. The location of one of the geo-radiolocation profiles.

## Results and Discussion

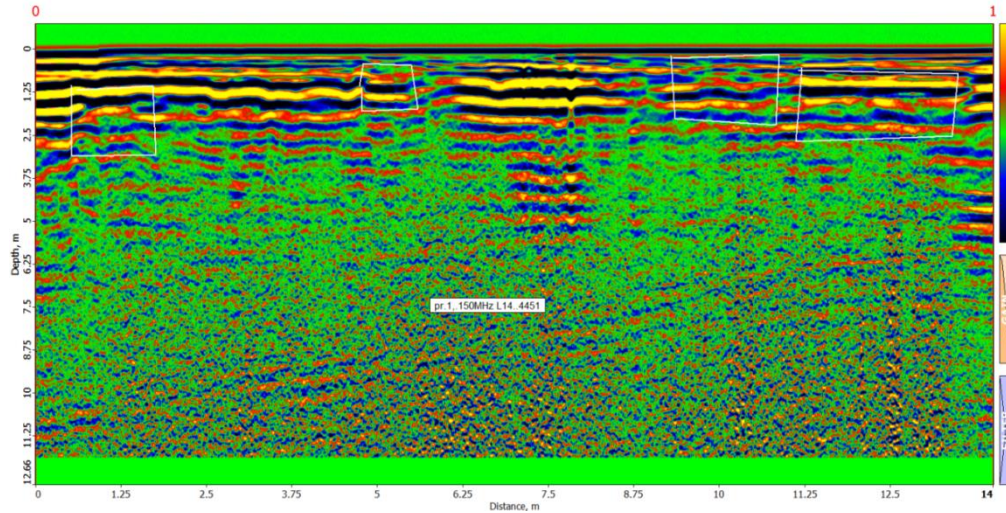


Fig. 1. Georadiolocation profile 1 was made with a 150 MHz georadar antenna. The length of the profile is 14 m.

Georadiolocation profiles are presented, with anomaly locations marked and separated by white lines. Anomalies were separated according to their radio features/amagine [7].

Georadiolocation profile 1 (Fig. 1) shows pit-type cavities at distances of 1.25 m with a size of 1-1.5m, as well as at a distance of 5m, in addition, at a distance of 10m and a distance of 12.5m there are radio images of pit-type cavities filled with waste material, their depths are from 1m to 2m.

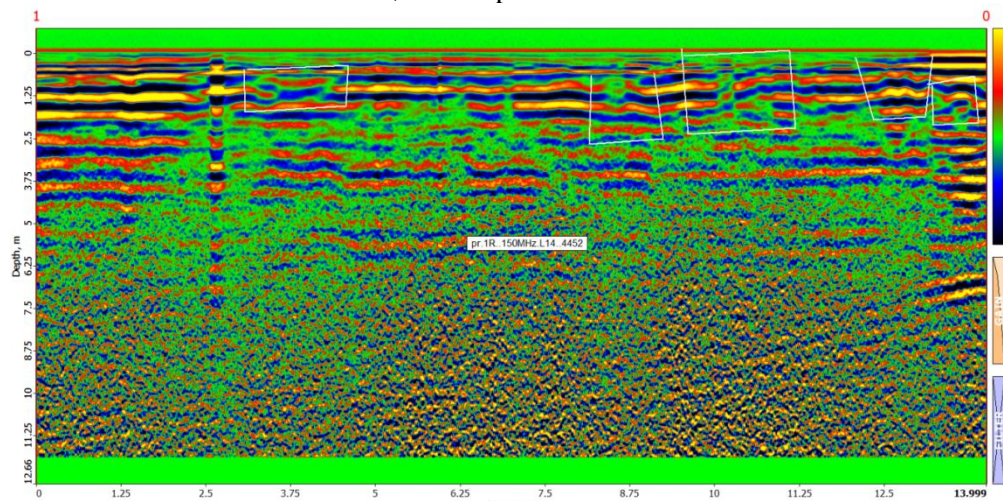


Fig. 2. Georadiolocation reverse profile-1R is made with a 150 MHz georadar antenna. The length of the profile is 14 m. Parallel and separated from profile 1 by 0.5-1 m.

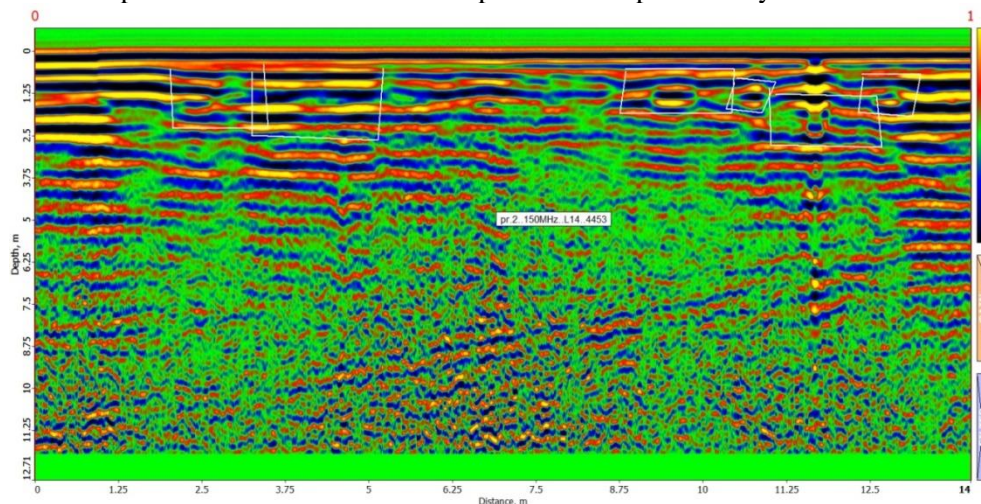


Fig. 3. Georadar profile-2 was performed with a 150MHz georadar antenna. The length of the profile is 14m.

On profile 1R (Fig. 2) at distances of 3.75, 8, 12, 13m, radio features corresponding to the depth of the depression were marked with depressions of 2-2.5m. The radio features of the marked objects continue on profile 1, therefore they are of a volumetric type and their length is not less than 1m.

On profile 2 (Fig. 3), characteristic radio features of the pit and cylindrical cavity were marked at distances of 2.5, 10, 12.5m with a depth of 2.5m.

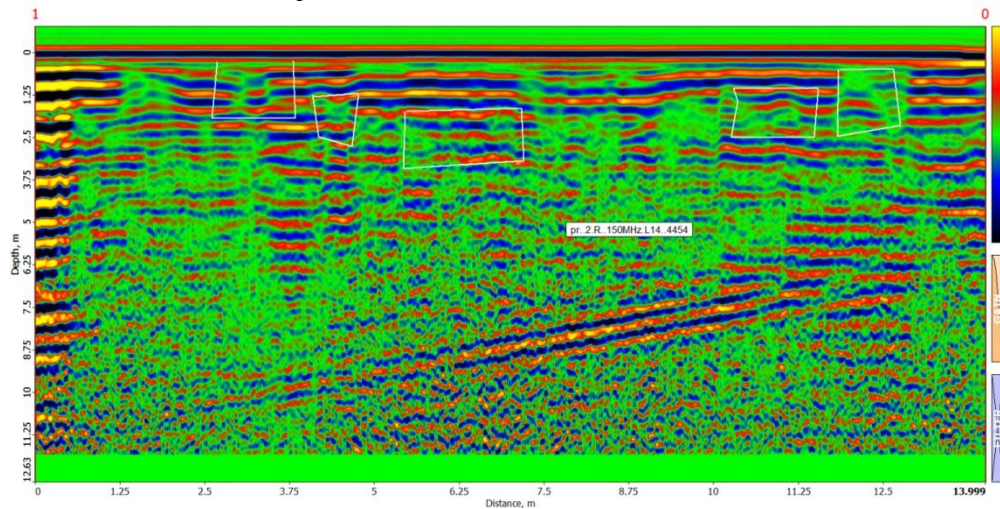


Fig. 4. Georadiolocation reverse profile-2R was performed with a 150MHz georadar antenna. The length of the profile is -14m. Parallel and separated from profile-2 by 0.5-1m.

On profile 2R (Fig. 4), characteristic radio features of the pit and cylindrical cavity were marked at distances of 2.8, 10, 12.5m with a depth of 2.5m. They extend continuously on profile 2. Thus, they are dimensionally up to 1m wide.

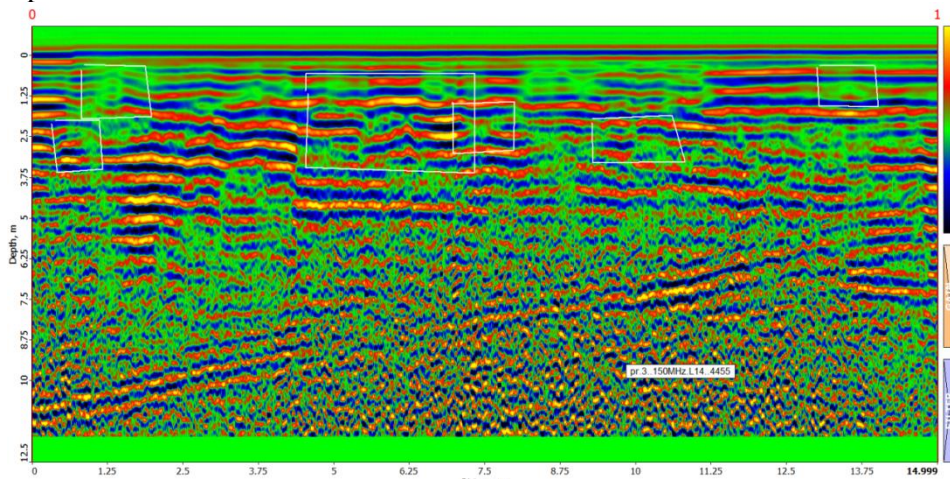


Fig. 5. Georadar profile -3 was performed with a 150 MHz georadar antenna. The length is 15m.

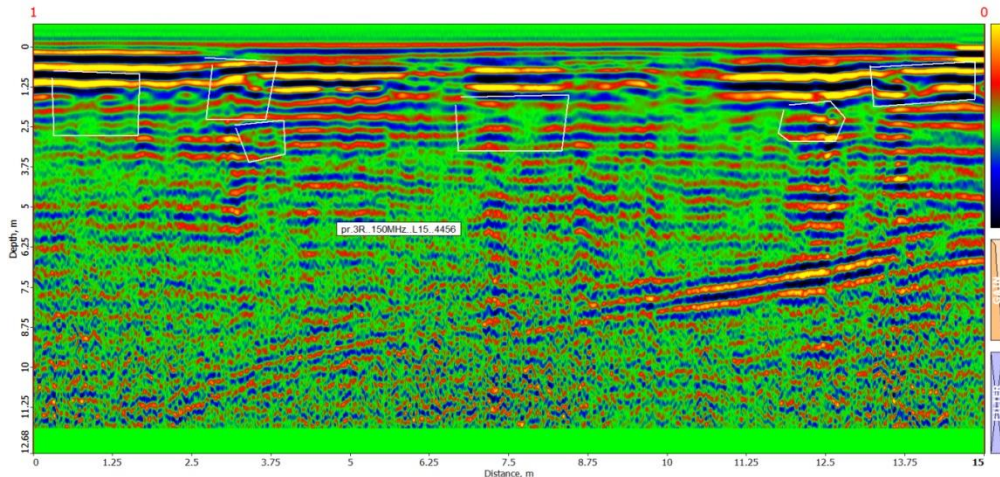


Fig. 6. Georadiolocation reverse profile-3R is performed with a 150Hz georadar antenna. The profile length is 15m. Parallel and is separated from profile 3 by 0.5-1m.

On profile 3 (Fig. 5) the radio images of pit-like objects were marked at distances of 1.25, 6, 10, 13.75m. In addition, they represent radio images of continuous objects and extend to profiles 2-2R.

On profile 3R (Fig. 6) dimensional cavities 1, 3, 3.75, 7.5, 12.5, 13.75m were marked. In addition, the radio image of a cylindrical object and at a distance of 7.5m continues on the previous profiles.

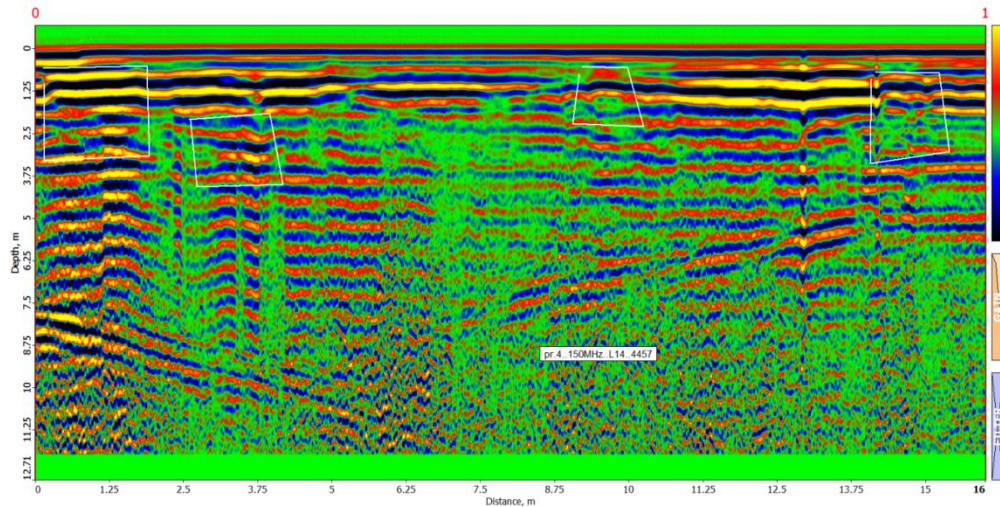


Fig. 7. Georadar profile-4 was performed with a 150 MHz georadar antenna. The length is 16m.

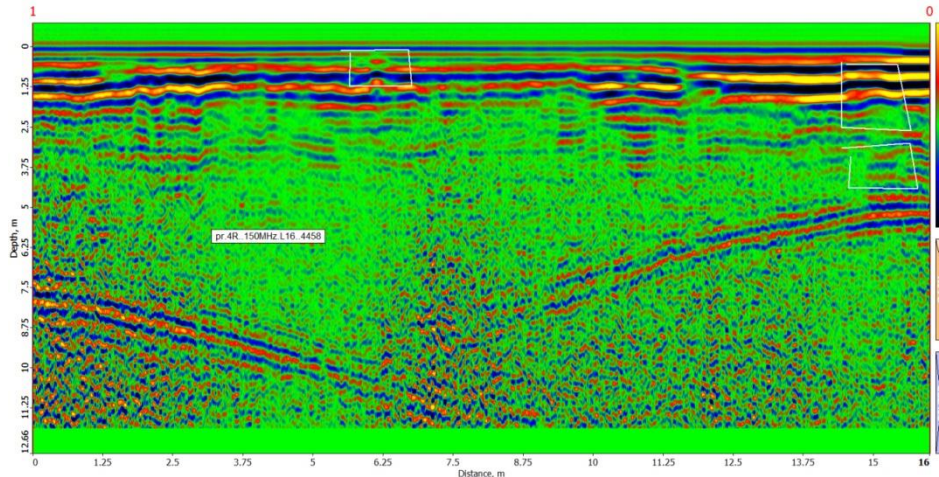


Fig. 8. Georadar reverse profile-4R is made with a 150Hz georadar antenna. The length of the profile is 15m. Parallel and separated from profile 4 by 0.5-1m.

On profile 4 (Fig. 7), radio features of pit-like objects were marked at distances of 1.25, 3.75 m, and cylinder-type at 10 m. At distances of 13-15 m, radio features of partially collapsed sided cavities. Their depth is up to 4 m.

Profile 4R (Fig. 8) shows the radio faces of the objects recorded in profile 4, as well as the radio faces of partially collapsed pit-type objects at distances of 2.5, 6, 11.25, 15 m.

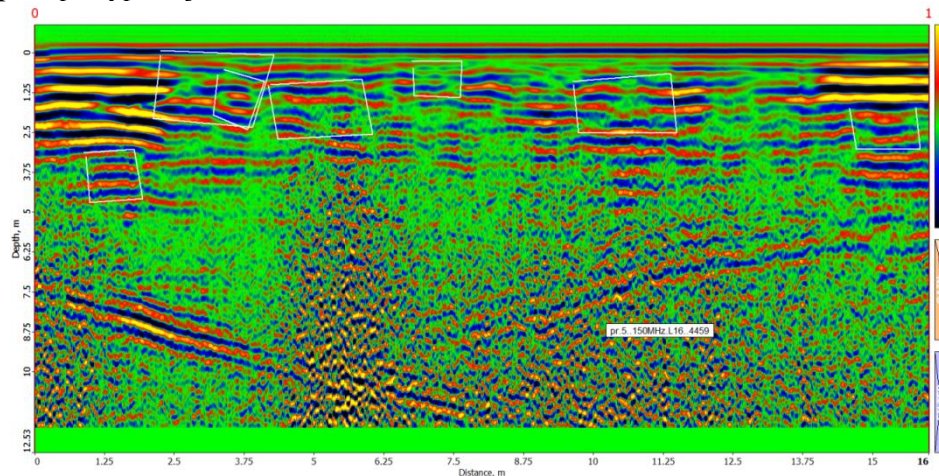


Fig. 9. Georadiolocation profile-5 was made with a 150MHz georadar antenna. The length is 16m.

On profile 5 (Fig. 9), at distances of 1.25, 3.75, 7.5, 11, 15m, radio images of objects containing cavities were marked, possibly of anthropogenic origin. They continue continuously on profile 4. Their depth is 5 m.

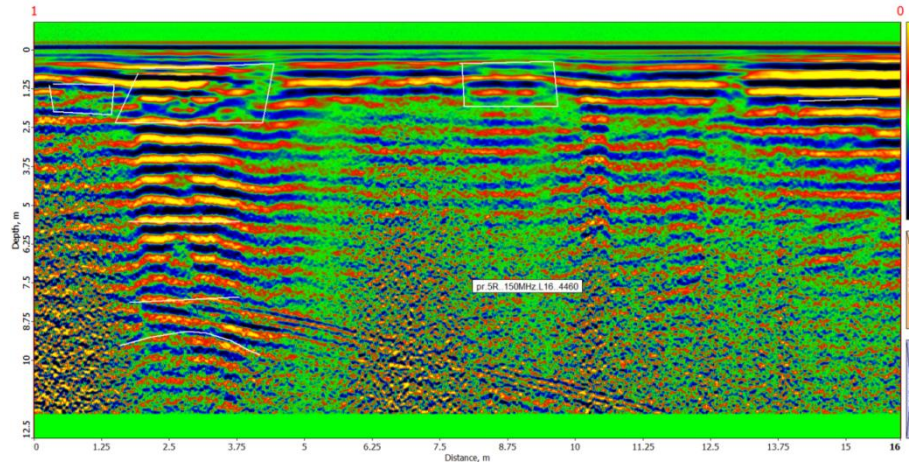


Fig. 10. Georadiolocation reverse profile-5R is made with a 150Hz georadar antenna. The length of the profile is 16m. Parallel and separated from profile 5 by 0.8-1.5m.

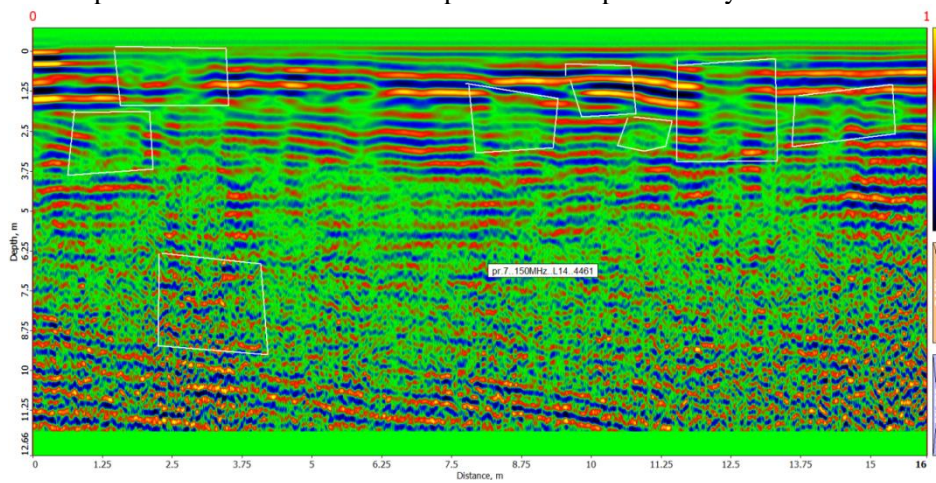


Fig. 11. Georadar profile-7 was made with a 150 MHz georadar antenna. The length of the profile is 16 m.

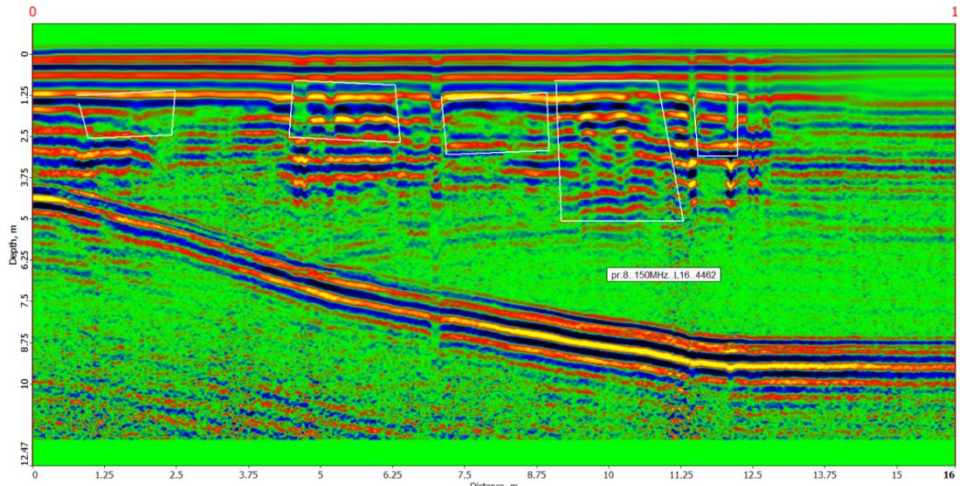


Fig. 12. Georadiolocation profile-8 was performed with a 150MHz georadar antenna. The length of the profile is 16 m.

Profile 5R (Fig. 10) marks hollows at distances of 1.25, 3, 4, 9, 12.5, 15m, their deepening is 2.5 m.

On profile 7 (Fig. 11), radio features with depth signs were marked at distances of 1.25, 3, 8.75, 10, 11.25, 12.5, 15m. Their depth is mainly 4m, and the depth of the object of the type that was destroyed at a distance of 3 m is 9m.

On profile 8 (Fig. 12) cavities were marked at distances of 2, 6, 8, 10, 12.5m, their deepening is 5 m.

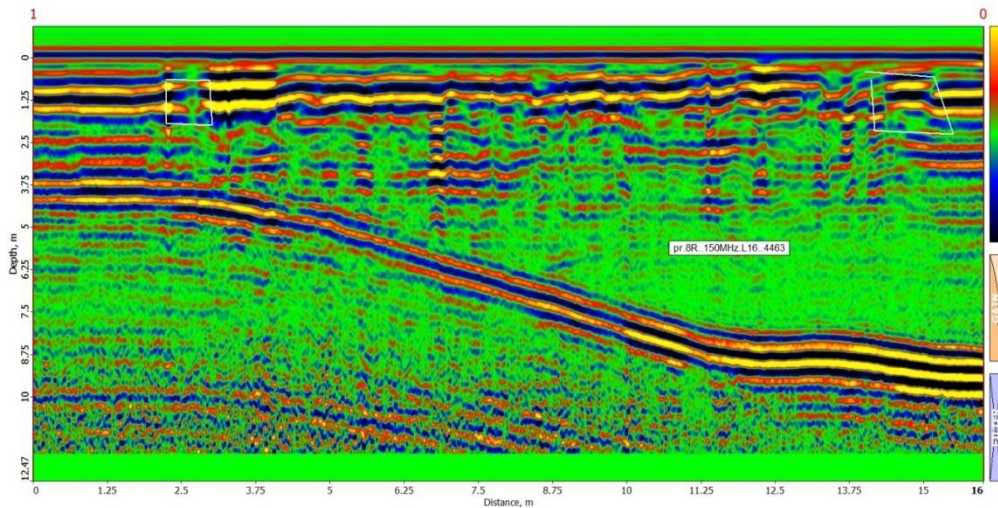


Fig. 13. Georadiolocation reverse profile-8R performed with a 150MHz georadar antenna. The profile length is 16m. Parallel and separated from profile 8 by 0.8-1.5 m.

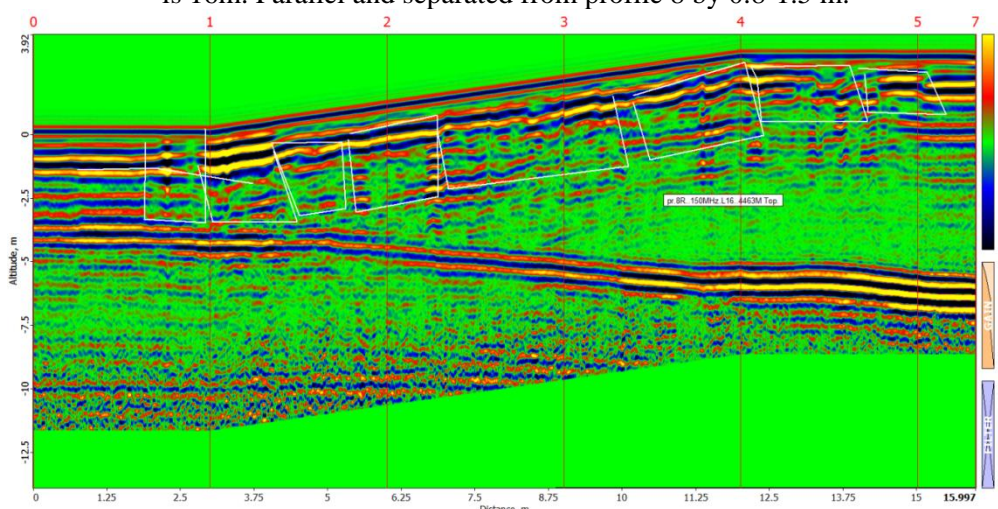


Fig. 14. Georadiolocation reverse profile-8R performed with a 150MHz georadar antenna. The length of the profile is 16 m. Parallel and separated from profile 8 by 0.8-1.5 m. Topographic representation.

Profile 8R (Fig. 13) revealed radio features of cavity-type objects at distances of 2.5, 3, 6, 12, 13, 15m, the maximum depth is 4m.

Fig. 14 shows profile 8R with topographic content, marked with radio images of cavities.

Profile 8 and profile 8R revealed the geological structure, the boundary between geological layers was distinguished, on which there may be a radio feature of an anthropogenic object, e.g. a watercourse or other cylindrical object with a width of 1-1.5m.

Prof-8 and Prof-8R have identified a continuous anomalous structure, a boundary between geological layers, on which a radio image of a man-made object can be located, for example: a foundation, tunnel, culvert or other massive cylindrical object located above the foundation and with a width of 1–1.5m. The presence of a geological object cannot be ruled out.

## Conclusion

The study area is loaded with objects containing cavities of many shapes and contents, marked with white lines. The continuity of the soil is disturbed by multiple cavities. Their depth ranges from 0.5 m to 5 m and their length is 1-5 m.

Prof-8 and Prof-8R A geological structure has been identified, a boundary between geological layers has been identified, on which a radio image of a man-made object can be placed, for example: a foundation, tunnel, culvert or other cylindrical object located above the foundation and with a width of 1–1.5 m. The presence of a geological object is not excluded.

From an archaeological-geological point of view, the study requires further continuation of detailed archaeogeoradiolocation works.

## References

- [1] Odilavadze D., Kiria J., Ghlonti N., Yavolovskaya O. The Results of archaeogeoradiolocation investigations of the territory inside the Rampart of St. Sophia Church of Khobi. „Moambe”, Bulletin of the Georgian National Academy of Sciences, V.14, n.4, 2020, pp. 51-56.
- [2] Chelidze T., Odilavadze D., Pitskhelauri K. Archaeogeophysics in Georgia-New Results, New Prospects. Proceedings of the Georgian National Academy of Sciences, Series of History, Archeology, Ethnology and Art History, N 1, 2012.
- [3] Odilavadze D., Chelidze T. A preliminary GPR investigation of Metekhi Cathedral and the surrounding area. Journal of the Georgian Geophysical Society, № 14, 2011.
- [4] Kofman L., Ronen A., Frydman S. Detection of model voids by identifying reverberation phenomena in GPR records. Journal of Applied Geophysics, (59), 2006, pp. 284-299.
- [5] Odilavadze D., Chelidze T., Yavolovskaya O. Some georadiolocation images of cylindrical bodies built with different dielectric fillers, placed in a dielectric environment. International Scientific Conference "Geophysical Processes in the Earth and its Envelopes", Proceedings, ISBN 978-9941-36-147-0, Tbilisi, Georgia, November 16-17, 2023, pp.217-220.
- [6] Odilavadze D., Chelidze T., Ghlonti N., Yavolovskaya O. Determining the presence and structure of a subsurface radioactive burial when interpreting the results of the GPR method by analyzing a three-dimensional rotating radio image. Journal of the Georgian Geophysical Society, e-ISSN: 2667-9973, p-ISSN: 1512-1127, Physics of Solid Earth, Atmosphere, Ocean and Space Plasma, v. 25(1), 2022, pp.21-28.
- [7] Odilavadze D., Chelidze T., Yavolovskaya O. THE radio image of an object with an elongated, face-fragmented, dielectrically complex structure was studied using the method of georadar physical modeling. Journal of the Georgian Geophysical Society, e-ISSN: 2667-9973, p-ISSN: 1512-1127, Physics of Solid Earth, Atmosphere, Ocean and Space Plasma, v. 27(2), 2024, pp.15-28.

## ნარიყალას ციტადელის მიმდებარე ტერიტორიაზე სამშენებლო მოედნის წინასწარი არქეოგეოფიზიკური კვლევა

დ. ოდილავაძე, თ. ჭელიძე, ო. იავოლოვსკაია

### რეზიუმე

საქართველოს დედაქალაქ თბილისის ერთერთი, ისტორიულად ძველი და არქეოლოგიურად მეტად მნიშვნელოვანი ადგილის, „ძველი თბილისის“ ტერიტორიაზე სამშენებლო-სარეაბილიტაციო სამუშაოების ჩატარების გამო გაჩნდა საჭიროება შესრულებულიყო დაზვერვითი არქეოგეორადიოლოკაციური წინასწარი კვლევა. არქეოგეორადიოლოკაციური გამოკვლევის წინასწარ მონიშნული ტერიტორია გათვალისწინებული იყო სამშენებლო ტექნიკის ოპერირების ადგილად. სამშენებლო პროცესის მიმდინარეობისას შესაძლებელი შეიძლება ყოფილიყო როგორც მიწისქვეშა სივრცეების შედეგად მრავალტონიანი სამშენებლო ტექნიკის დაზიანება და უბედური შემთხვევების გამოწვევა, ასევე შესაძლო არქეოლოგიური ძეგლების განადგურება.

არქეოგეორადიოლოკაციურმა კვლევამ გამოავლინა რიგი სივრცეები, შესაძლო არქეოლოგიური ძეგლების არსებობის ნიშნები, მოახდინა მათი ლოკაციების კარტირება.

არქეოგეორადიოლოკაციური სამუშაოები შესრულდა გეორადარ Zond 12e, მონაცემები მოიკრიბა, დამუშავდა და ინტერპრეტირდა პროგრამული უზრუნველყოფით - Prizm 2.6.

ამოცანის მიზანს წარმოადგენდა გეორადიოლოკაციური კვლევა მიწისქვეშა ახლოქვეყნაპირული განლაგების სივრცეების გამოსავლენად.

აღმოჩნდა, რომ საკვლევი ფართობი დატვირთულია მრავალი ფორმისა და შინაარსის სიღრუის შემცველი ობიექტებით. ნიადაგის კონტინენტალურობა დარღვეულია მრავლობითი სიღრუეებით. მათი სიღრმეთა განთავსება მერყობს 0.5მ-დან 5მ-დე და განგრძობითობით 1-5მ.

იდენტიფიცირებულია საზღვარი გეოლოგიურ ფენებს შორის, რომელზედაც შეიძლება განთავსებულიყო ადამიანის მიერ შექმნილი ობიექტის რადიო გამოსახულება, ასეთებია: საძირკველი, გვირაბი, წყალგამტარი ან სხვა ცილინდრული ობიექტი, რომელიც მდებარეობს საძირკველის ზემოთ და სიგანით 1–1.5 მ არ არის გამორიცხული გეოლოგიური ობიექტის არსებობა.

არქეოლოგიურ-გეოლოგიური თვალსაზრისით, კვლევა მოითხოვს დაწვრილებითი არქეოგეორადიოლოკაციური სამუშაოების შემდგომ გაგრძელებას.

**საკვანძო სიტყვები:** არქეოგეორადიოლოკაციური სამუშაოები, გეორადარი, რადიოსახე, რადაროგრამა.

## **Предварительное археогеофизическое исследование строительной площадки в районе цитадели Нарикала**

**Д. Одилавадзе, Т. Челидзе, О. Яволовская**

### **Резюме**

В связи с проведением строительно-восстановительных работ на территории «Старого Тбилиси», одного из исторически древних и археологически важнейших мест столицы Грузии города Тбилиси, возникла необходимость проведения предварительной рекогносцировочной археогеорадиолокационной съемки. Предварительно размеченная территория для археогеорадиолокационной съемки предназначалась для работы строительной техники. В процессе строительства существовала вероятность повреждения многотонной строительной техники и возникновения аварий из-за подземных пустот, а также уничтожения возможных археологических памятников.

Археогеорадиолокационное исследование выявило ряд пустот, признаков существования возможных археологических памятников, а также нанесло на карту их местоположение. Археологические георадарные работы выполнялись с использованием георадара «Zond 12e». Сбор, обработка и интерпретация данных осуществлялись с использованием программного обеспечения Prizm 2.6.

Целью задания было проведение георадиолокационной съемки для выявления пустот в подземной приповерхностной структуре. Оказалось, что исследуемая зона заполнена полыми предметами разнообразной формы и содержания. Континентальность почвы нарушена многочисленными понижениями. Их глубина колеблется от 0.5 до 5 м, а длина — от 1 до 5 м.

Выявлена граница между геологическими слоями, на которой может располагаться радио изображение искусственного объекта, например: фундамента, тоннеля, водопропускной трубы или другого цилиндрического объекта, расположенного выше фундамента и шириной 1–1.5 м. Наличие геологического объекта исключить нельзя.

С археолого-геологической точки зрения исследование требует дальнейшего продолжения детальных археогеорадиолокационных работ.

**Ключевые слова:** археогеорадиолокационные работы, георадар, радио образ, радарограмма.

## Water Level Phase Shift Relative to Gravity into Georgian Wells

**Genadi N. Kobzev, Tamaz L. Chelidze, George G. Melikadze,  
Tamar J. Jimsheladze, Tengiz V. Kiria, Aleksandre Sh. Tchankvetadze,  
Zviad I. Maghradze, Nino T. Gogvadze**

*M. Nodia Institute of Geophysics of the I. Javakhishvili Tbilisi State University, Georgia,  
e-mail: [kobzev47@gmail.com](mailto:kobzev47@gmail.com)*

### ABSTRACT

*The baytap08 program is used to study the phase shift of the water level relative to gravity in wells in Georgia. In the extreme east of Georgia (Lagodekhi) and in the west (Kobuleti, Black Sea), the phase shift is  $<0$  (from  $-25^\circ$  to  $-60^\circ$ ). In the central part of the country, the phase shift is  $\geq 0$ : Marneuli (center, south) about  $0^\circ$ ; Nakalakevi (center, south, west of Marneuli) from  $+0.8^\circ$  to  $+1.6^\circ$ ; Gori (center)  $+10^\circ$ ; Oni (center, northwest of Gori) from  $+15^\circ$  to  $+26^\circ$ . Note that among the specified wells, those with a positive phase shift turned out to be sensitive to remote earthquakes.*

**Key words:** phase shift, tidal, water level, Georgia

### Introduction

The water level (WL) in the well reacts to gravity force (GF) variation, especially the Z-component. The phase shift between WL and GF can have positive and negative values. If the phase shift value is  $>0$ , then the water is ahead of gravity; if the phase shift value is  $<0$ , then the water is behind it. Usually, the delay is observed for confined water layers. An advance is typical for shallow unconfined layers.

### Results

Using long-term observations, the phase shift between the water level and gravity was calculated for different wells in Georgia (Fig.1). The phase shift was calculated using the baytap08 program. Baytap08 is a modification of the baytap-G program (suggested by D.C. Agnew), developed by M. Ishiguro, Y. Tamura, T. Sato and M. Ooe [1].

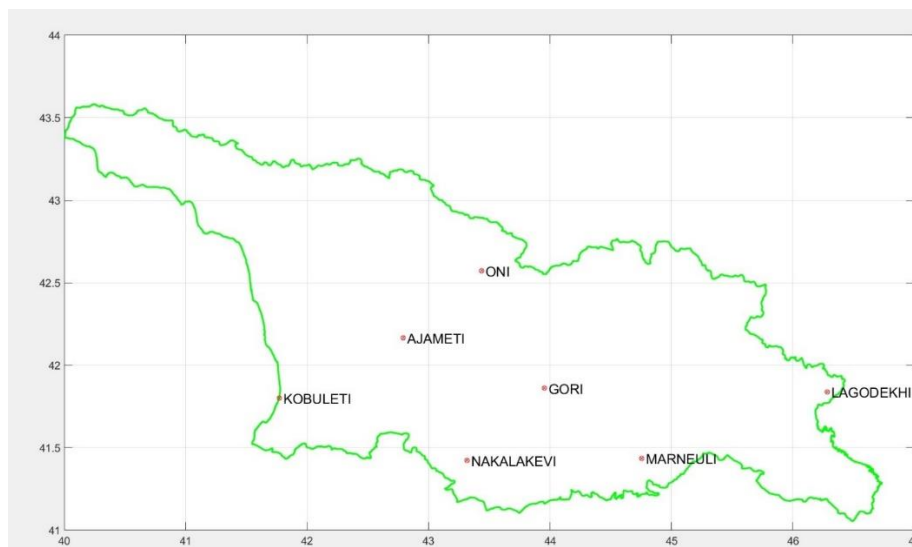


Fig.1. Boreholes in Georgia.

The baytap08 program allows one to estimate the impact of different gravity oscillations, including  $M_2$  and  $O_1$ . Recall that  $M_2$  is a semi-diurnal lunar wave and  $O_1$  is the principal lunar declination. For  $M_2$ , the period length is 12.42 hours, and speed is 28.98550725 degrees/hour. For  $O_1$ , the period length is 25.82 hours, and speed is 13.94268009 degrees/hour.

The initial data in the baytap08 program are: water level in the well, atmospheric values, well coordinates and height. The data frequency is 1 hour.

Phase shift can be converted to a delay or advance in hours using the formula:

$$\text{Time Shift} = \text{Phase Shift} / \text{Speed},$$

where phase shift is measured in degrees and speed in degrees/hour.

Table. Phase shift of water level in wells of Georgia

Name	Time	Phase shift, degrees, $M_2$	Phase shift, degrees, $O_1$
Lagodekhi 41.839N, 46.282E H=538; Depth=800	2012:	-46.343	-23.746
	2013:	-45.102	-26.147
	2014:	-47.171	-29.938
	2018:	-55.612	-35.736
	2019:	-61.940	-41.673
	2020:	-62.940	-42.013
	2022:	-65.318	-42.013
	2023:	<b>-50.638</b>	<b>-26.443</b>
	2024:	-57.227	-35.832
	2025:	-57.981	-39.171
Marneuli 41.436N, 44.755E H=382; Depth=3505  Turkey, Feb 2023, earthquake M=7.8	2020, 1 Jan – 1 Jul	3.089	2.051
	2021, 1 Jan – 1 Apr	3.662	2.373
	1 Apr – 1 Jul	2.946	1.899
	2022, 1 Apr – 1 Jul	0.488	1.380
	1 Jul – 1 Oct	0.780	0.018
	1 Oct – 31 Dec	0.131	-0.011
	2023, 1 Jan – 1 Apr	<b>-0.430</b>	0.093
	1 Apr – 1 Jul	1.641	0.485
	1 Jul – 1 Oct	-0.681	2.077
	2024, 1 Jan – 1 Apr	0.443	0.770
	1 Apr – 1 Jul	-0.145	-0.055
	1 Jul – 1 Oct	-0.995	-0.430
	1 Oct – 31 Dec	-1.269	0.063
2025, 1 Jan – 1 Apr	-0.117	-0.759	
Kobuleti 41.802N, 41.772E H=12; Depth=2000	2019, 1 Jan – 1 Oct	-28.157	-1.358
	2020, 1 Jan -1 Apr	-27.096	-10.276
	1 Apr – 1 Jul	-26.347	-2.377
	1 Jul – 1 Oct	-28.837	2.382
	1 Oct -31 Dec	-29.004	-4.637
	2020, all year	-27.613	-3.220
	2021, 1 Jan -1 Apr	-28.164	-3.808
	2025, 1 Jan – 1 May	-28.052	-6.143
Nakalakevi 41.424N, 43.317E H=1175; Depth=600	2019, 1 Jan -1 Aug	1.613	4.630
	2023, 1 Jun -15 Nov	0.868	6.114
	2024, 15 Feb – 31 Dec	0.859	5.469
	2025, 1 Jan – 1 May	1.052	6.726
Gori	2018, 1 Apr – 29 Sep	9.327	11.034

Name	Time	Phase shift, degrees, M2	Phase shift, degrees, O1
41.862N, 43.9536E H=1103; D=1500	2021, all year	7.354	5.926
	2025, 9 Mar- 4 May	10.74	1.188
Oni 42.573N, 43.437E H=798; Depth=255	2020, 1 Jan – 1 Apr	62.043	-33.075
	1 Apr – 1 Jul	15.627	18.318
	1 Jul – 1 Oct	23.597	34.922
	1 Oct – 31 Dec	26.317	-6.333
	2020, all year	22.313	0.71
	2021, 1 Jan – 1 Apr	24.726	17.619
	1 Apr – 1 Jul	17.661	19.188
	1 Oct – 31 Dec	20.342	49.512
	2022, 1 Jan – 30 Apr	18.796	9.393
	atmos not used ->	2023, 1 Jan – 1 Apr	3.404
Ajameti 42.187N, 42.791E H=102;Depth=1339	2011, 15 May – 1 Oct	-16.648	-8.755
	2012, 5 May – 25 Oct	-20.782	-9.944
	2024, 15 Sep – 1 Nov	-17.98	-7.314

## Conclusions

A significant delay of WL relative to GF is observed for Lagodekhi and Kobuleti ( $\varphi < 0$ ). For Marneuli, the phase shift is approximately 0, with a transition from positive to negative values of the shift. For Nakalakevi, Gori, Oni stations, the phase shift is  $> 0$ , i.e. water is ahead of gravity.

It may be a coincidence, but at the same time Nakalakevi, Gori, Oni have the property of responding to distant earthquakes. The most sensitive is the Oni well, which has the largest positive phase shift value.

It should be noted that the search for sensitive wells remains a pressing task.

The peculiarity of calculations using the baytap08 program is the duration of the initial data – several months and the frequency of the survey is 1 hour. The result is a single number characterizing the phase shift over an interval of several months.

For a more rapid assessment of the phase shift, another method can be used: the ellipse method. In this case, the amount of data for one day with a polling period of 1 minute may be sufficient to obtain one value of the phase shift [2].

## Acknowledgement

This work was supported by Shota Rustaveli National Science Foundation of Georgia (SRNSFG), Grant number FR24-17839.

## References

- [1] Tamura Y., Sato T., Ooe M., Ishiguro M. A procedure for tidal analysis with a Bayesian information criterion. *Geophys. J. Internat.*, 104, 1991, pp. 507–516.
- [2] Vinogradov E., Gorbunova E., Besedina A., Kabychenko N. *Earth tide analysis specifics in case of unstable aquifer regime*. Pure Appl. Geophys., Springer International Publishing AG, 2017. DOI 10.1007/s00024-017- 1585-z.

# საქართველოს ჭაბურღილებში წყლის დონის ფაზური წანაცვლება გრავიტაციასთან მიმართებაში

გ. კობზევი, თ. ჭელიძე, გ. მელიქაძე, თ. ჯიმშელაძე, თ. ქირია,  
ა. ჭანკვეტაძე, ზ. მაღრაძე, ნ. გოგუაძე

## რეზიუმე

პროგრამა baytap08-ის საშუალებით ხდება გრავიტაციასთან მიმართებით წყლის დონის ფაზური წანაცვლების შესწავლა საქართველოს ჭაბურღილებში. შედეგი: საქართველოს უკიდურეს აღმოსავლეთში (ლაგოდეხი) და დასავლეთში (ქობულეთი, შავი ზღვა) ფაზური წანაცვლება  $<0$  (მერყეობს  $-25^{\circ}$ -დან  $-60^{\circ}$ -მდე). ქვეყნის ცენტრალურ ნაწილში ფაზური წანაცვლება  $\geq 0$ : მარნეული (ცენტრი, სამხრეთი) დაახლოებით  $0^{\circ}$ ; ნაქალაქევი (ცენტრ. სამხრეთი, მარნეულიდან დასავლეთით) —  $+0.8^{\circ}$ -დან  $+1.6^{\circ}$ -მდე; გორი (ცენტრი) —  $+10^{\circ}$ ; ონი (ცენტრი, გორიდან ჩრდილო-დასავლეთით) —  $+15^{\circ}$ -დან  $+26^{\circ}$ -მდე.

საკვანძო სიტყვები: ფაზური წანაცვლება, გრავიტაცია, წყლის დონე, საქართველო.

## Фазовый сдвиг уровня воды относительно гравитации в скважинах Грузии

Г. Кобзев, Т. Челидзе, Г. Меликадзе, Т. Джимшеладзе, Т. Кирия,  
А. Чанкветадзе, З. Маградзе, Н. Гогуадзе

### Резюме

С помощью программы baytap08 изучается фазовый сдвиг уровня воды по отношению к гравитации в скважинах Грузии. Результат. На крайнем востоке Грузии (Лагодехи) и на западе (Кобулети, Черное море) фазовый сдвиг  $<0$  (от  $-25^{\circ}$  до  $-60^{\circ}$ ). В центральной части страны фазовый сдвиг  $\geq 0$ : Марнеули (центр, юг) около  $0^{\circ}$ ; Накалакеви (центр, юг, на запад от Марнеули) от  $+0.8^{\circ}$  до  $+1.6^{\circ}$ ; Гори (центр)  $+10^{\circ}$ ; Они (центр, северо-запад от Гори) от  $+15^{\circ}$  до  $+26^{\circ}$ .

**Ключевые слова:** фазовый сдвиг, гравитация, уровень воды, Грузия.

## Numerical Modeling of Kutaisi City Atmospheric Air Pollution with PM<sub>2.5</sub> Particles in Winter During Ground Level Calm and Background Eastern Wind in the Free Atmosphere

<sup>1,2</sup>Aleksandre A. Surmava, <sup>2</sup>Vepkhia G. Kukhalashvili, <sup>1</sup>Natia G. Gigauri,  
<sup>1</sup>Liana N. Intskirveli, <sup>3</sup>Leila V. Gverdtsiteli

<sup>1</sup> Institute of Hydrometeorology of the Georgian Technical University, Georgia

<sup>2</sup> M. Nodia Institute of Geophysics of the I. Javakishvili Tbilisi State University, Georgia

<sup>3</sup> Georgian Technical University, Georgia

e-mail: l.inwkirveli@gtu.ge

### ABSTRACT

*Spatial distribution and time change of PM<sub>2.5</sub> particles dissipated in the atmosphere as a result of motor transport traffic in Kutaisi city has been studied using computer modeling. This modeling has been made through combined integration of equations of time evolution of meso-scale atmospheric processes and admixtures' transfer-diffusion, using the relevant initial and boundary conditions. Such meteorological situation has been considered, during which wind velocity in surface layer of the atmosphere equal to 0, while there is background eastern wind in the free atmosphere. Atmospheric pollution is caused by microparticles dissipated in the air during motor transport traffic. The wind fields formed in boundary layer of the atmosphere resulting from interaction of terrain and background flows in winter and fields of concentrations of microparticles transferred by wind and dissipated in the air at different heights from the earth ground have been plotted using numerical modeling data. Areas of relatively severe and mild contamination have been determined, peculiarities of vertical distribution of concentrations have been analyzed. It has been showed that the shapes of vertical distribution of concentrations in surface layer of the atmosphere are similar of temperature distributions in to dry thermals.*

**Key words:** PM<sub>2.5</sub>, microparticles, concentration field, atmosphere, numerical modeling, calm.

### Introduction

It has been showed by numerous studies that solid and liquid microparticles – PM<sub>2.5</sub> and PM<sub>10</sub>, which hit the atmosphere as a result of emissions from industrial facilities, agricultural activities and motor transport operation are ranked among atmosphere polluting substances with high risk-factor extremely hazardous for health [1-5]. Due to very small sizes (diameters are  $\leq 2.5 \mu$  and  $\leq 10 \mu$ ) they easily penetrate human organism, cause various illnesses and frequently even a death [6-7]. The ecological problems caused with atmospheric pollution with PM has been thoroughly studied in the fundamental work [8].

As a result of practical air-protecting measures carried out in the XXI century, number of microparticles emitted in the air has been significantly decreased. As a consequence, PM<sub>2.5</sub> concentrations have been reduced in the air and atmosphere purity degree has been improved. Though, the air contamination level in number of large and small cities still exceeds the European Union standards [9-14].

Kutaisi, the second largest city of Georgia, with 147 thousand habitants is ranked among the small cities. Despite the small size it has a great international medicinal-health promoting and touristic importance. Resort Tskaltubo, historical monuments: Gelati monastery complex – a monument of UNESCO cultural heritage, Bagrati Cathedral, Palace of Geguti, Martvili and Motsameta monasteries, touristic attractions – Sataplia and Prometheus caves, Kinchkhi, Martvili, Balda canyons etc. are located in the city suburbs. Hundreds of thousands of people visit it every year. Based on this fact, study and assessment of environmental state, diagnostic forecast of pollution level, maintenance of high degree of air purity have of paramount ecologic

importance. It should be noted that a monitoring carried out in two air quality observation points existing as of today is unable to estimate real picture air of purity in the city.

In order to cope with the above-mentioned problem, the pattern of propagation and time change of PM<sub>2.5</sub> particles generated by the motor transport and emitted in the air in Kutaisi city and at the adjacent territories has been simulated and analyzed in the presented article by means of field measurements and computer modeling of admixture propagation in the atmosphere.

## Research method

Propagation of dust and PM microparticles discharged by the motor transport to the air of Georgian cities has been numerically simulated through combined integration of 3D equations of meso-scale atmospheric processes and equation of a passive polluting admixture propagation in Caucasus [15-24].

## Numerical modeling results

PM<sub>2.5</sub> propagation has been modeled in 13.4×13.4×9 km<sup>3</sup> space domain of complex terrain (Fig. 1), with city of Kutaisi located in its center. Orography height of the modeling area varies from 80 to 400 m. Numerical modeling of the mathematical model equations [17, 18] has been made using relevant initial and boundary conditions. Numerical grid steps in horizontal direction equal to 200 m, while in vertical direction in the free atmosphere – 300 m. Vertical steps in 100 m thick surface layer of the atmosphere vary from 0.3 to 15 m. Time step is 1 sec. Calculations have been made for 3-day period.



Fig. 1. Administrative units and urban development scheme of city of Kutaisi.

A case of Kutaisi atmosphere pollution with PM<sub>2.5</sub> in December has been modeled. There is a calm at 100 m height in surface layer of the atmosphere – background wind velocity is 0 m/sec. There is an eastern wind above the surface layer and its velocity linearly increases with height and reaches 21 m/sec at 9 km height. Atmospheric relative humidity equals to 50%.

It has been obtained via calculations that microaerosol pollution of atmospheric air occurs due to motor transport traffic from underlying surface at 0.3 m height. PM<sub>2.5</sub> particles are emitted in the atmosphere at 5 types of areas: at highways, city central streets, residential, industrial zones, and unpopulated territories of surrounding villages. Emission rate is periodical with 24-hour period and proportional to motor transport traffic intensity. Emission rate is maximum and constant in time interval from 10 to 18 h, minimal in the interval of 0-4 h, linearly increases from 4 to 10 h, linearly decreases within time period from 18 to 24 h and by 0 h becomes equal to existing emission rate. Maximum emission rate is 12.5 µg/s.

Fig. 2 shows graphs of PM<sub>2.5</sub> concentration time change obtained via calculations for 5 basic types of pollution points. It is seen from Fig. 2 that time change of concentration is similar for all types of observation

points and is featured by 2 intervals of large values and 2 ones of small values. Large concentration values are obtained approximately within time intervals from 11 to 13 h and 16 to 19 h, while small ones – in the intervals from 0 to 5 h and from 13 to 16 h. It should be noted that time change of concentrations in case of identical meteorological and contamination pollutions is qualitatively similar and quantitatively different for summer [18] and winter seasons (Fig. 2).

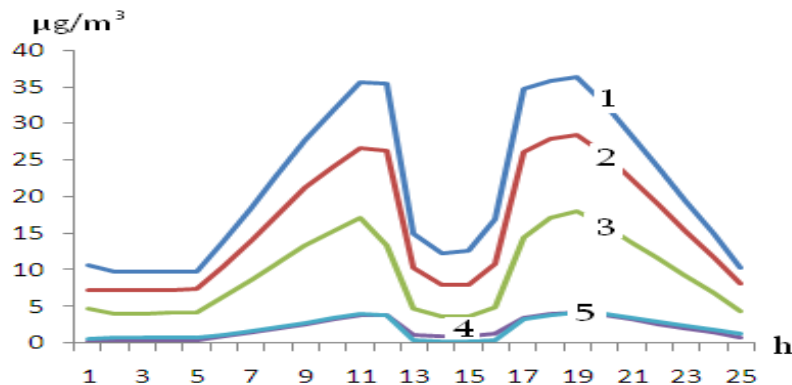


Fig. 2. Time change of PM2.5 concentrations obtained via calculations at highway (1), city central streets (2), industrial (3), rural (4) zones and unpopulated points (5) at the 2m height from earth surface.

The difference lies in the period of high pollution onset. In summer [17], compared to winter, the maximal pollution level is obtained approximately 2-3 hours earlier in the first half of the day, and 2-3 hours later in the second half. The mentioned effect is associated with time change of thermal stability of the atmosphere. In summer, soil surface and adjacent surface layer of the atmosphere are rapidly cooled early in the morning, so vertical temperature gradient  $\gamma = \partial T / \partial z$  ( $T$  is temperature,  $z$  – vertical coordinate) is reduced, while thermal stability coefficient  $S = \gamma_a - \gamma$  ( $\gamma_a$  - dry adiabatic gradient) is increased respectively. As a consequence, ground-level air layer becomes more dynamically stable and less turbulized. Reduction of turbulence is accompanied by intense accumulation of emitted aerosols in the lower part of the surface layer and rise of pollution level. The similar process takes place in summer in the second half of the day, approx. within interval of 19-20 h. Despite the fact that quantity of substances emitted in the atmosphere is identical in the same types of points located in different parts of the city, their concentrations in these points obtained via calculation differ from each other (Fig. 3). In the lower part of surface layer, it equals to 2-10 mkg/m<sup>3</sup> at highways and industrial zones of the city, while at unpopulated rural territories it is 0.2-4 mkg/m<sup>3</sup>. The similar dependence is obtained for other types of observation points as well.

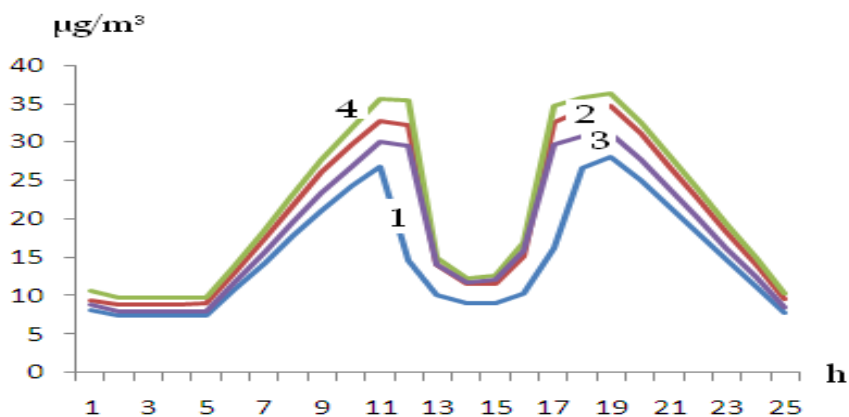


Fig. 3. Time change of PM2.5 concentration in the eastern, western, northern and southern parts of the city, in four points located at highway, at 2 m height from earth surface

Vertical distribution of concentration differs from each other in different types of points. Concentration value is maximal at the highway and in the vicinity of city central streets in the close proximity to surface layer of the atmosphere and hyperbolically reduces with height increase (Fig. 4). In this case, concentration value in the close proximity to the surface layer varies within  $13\text{-}48\mu\text{g}/\text{m}^3$ , while at 100 m height – within  $0.1\text{-}7\mu\text{g}/\text{m}^3$ .

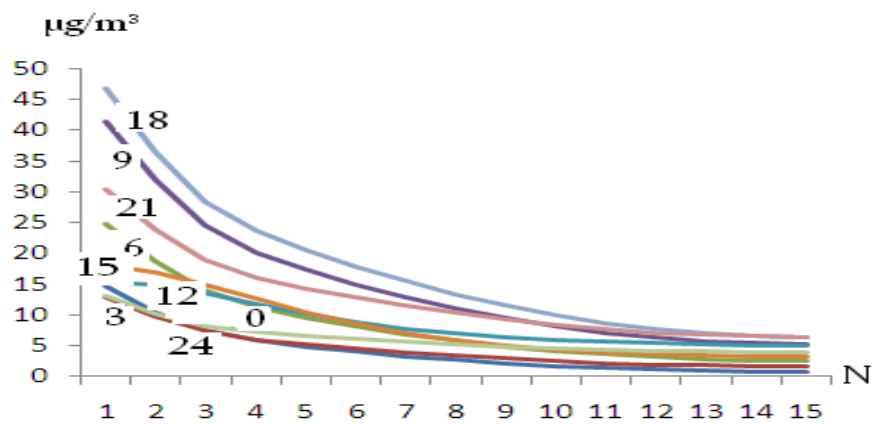


Fig. 4. Vertical distribution of PM2.5 concentration ( $\mu\text{g}/\text{m}^3$ ) in points located at the highway in surface layer of the atmosphere, when  $t = 0, 3, 6, \dots, 24$  h. (N is a number of vertical numerical grid)

In points placed at the territory of industrial area, vertical distribution of concentration is of parabolic shape (Fig. 5). Its vertex is located at  $N = 4\text{-}6$  levels (at 5-15 m height from earth surface), while branches are down-directed. Concentration maximum values in these points vary within  $4\text{-}20\mu\text{g}/\text{m}^3$ . At 100 m height concentrations approximately equal to  $1\text{-}7\mu\text{g}/\text{m}^3$ .

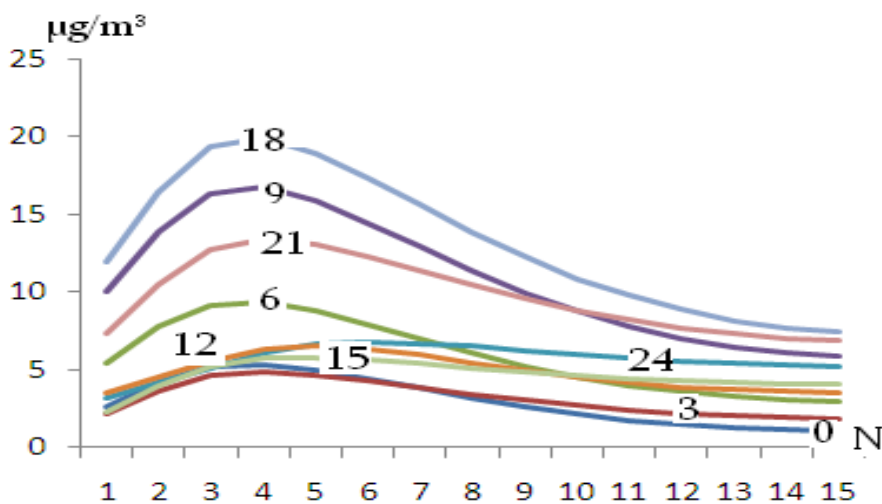


Fig. 5. Vertical distribution of PM2.5 concentration ( $\mu\text{g}/\text{m}^3$ ) in points located at the territory of industrial purpose in surface layer of the atmosphere, when  $t = 0, 3, 6, \dots, 24$  h. (N is a number of vertical numerical grid)

As for observation points placed at the territory of agricultural purpose, the concentration here is small at 2 m height, then increases with height and reaches maximum values at 10-15 m heights ( $N = 5\text{-}6$ ). At high altitudes, small decrease of concentration is obtained. At 100 m height, concentration value is minimal, when  $t = 0$ h, and maximal when  $t = 18$  and  $21$ h. By  $t = 24$ h, concentration value at 100 m height is approx  $4\mu\text{g}/\text{m}^3$ .

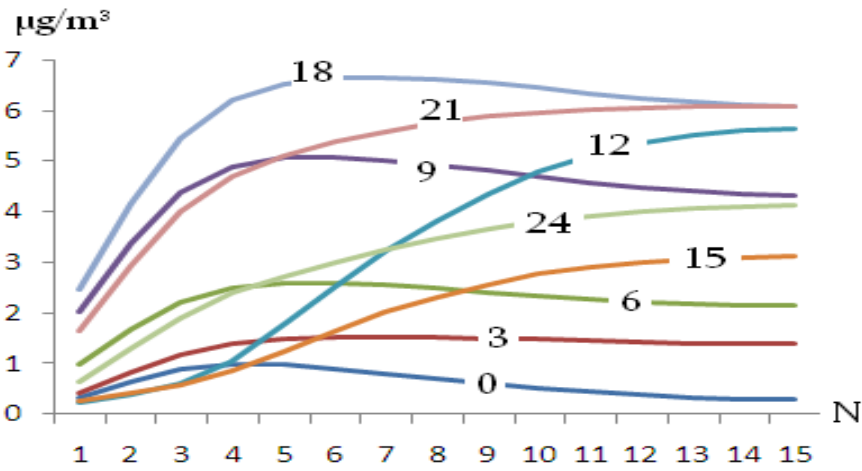


Fig. 6. Vertical distribution of PM2.5 concentration ( $\mu\text{g}/\text{m}^3$ ) in points located at the territory of agricultural purpose in surface layer of the atmosphere, when  $t = 0, 3, 6, \dots, 24$  h. (N is a number of vertical numerical grid)

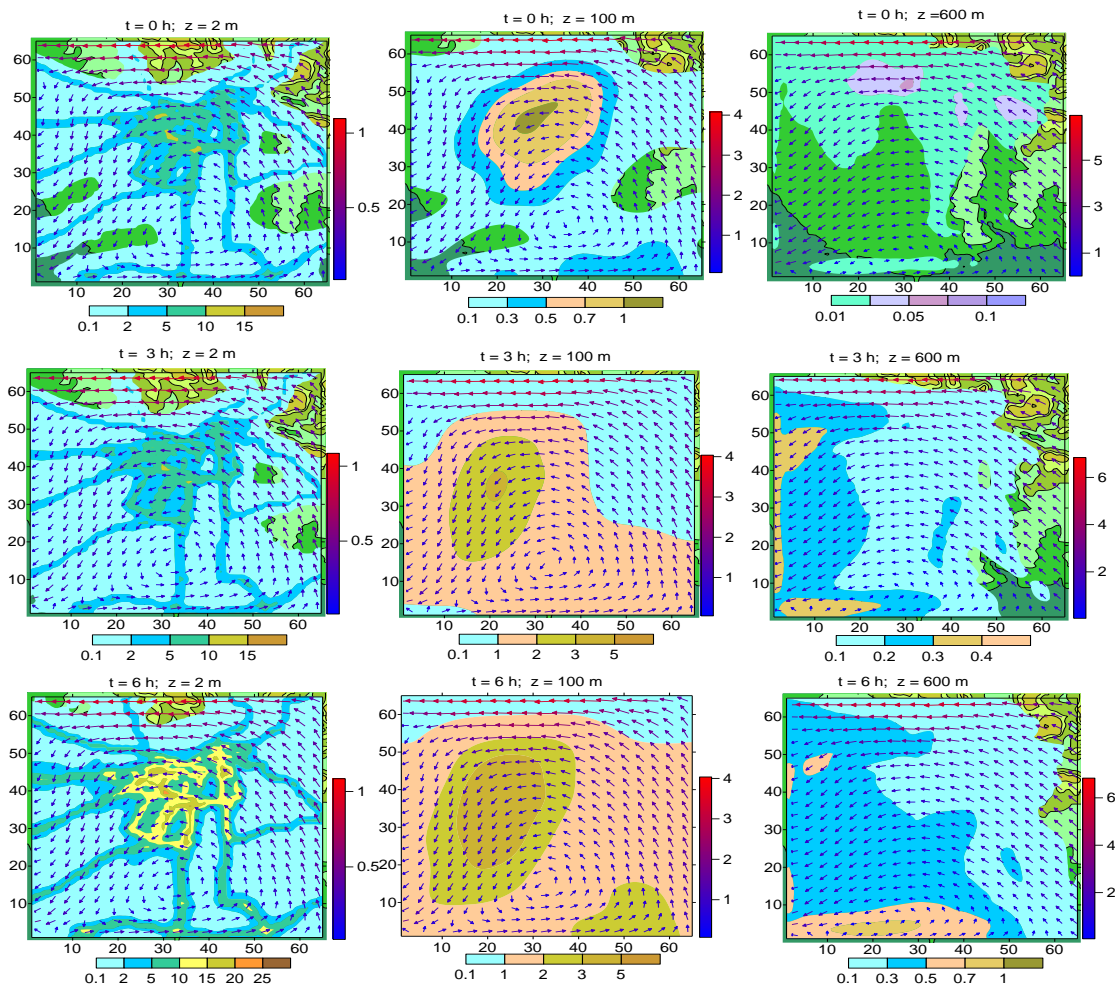


Fig. 7. Distribution of PM2.5 concentration ( $\mu\text{g}/\text{m}^3$ ) and wind velocity (m/sec) fields at 2, 100 and 600 m heights from earth ground, when  $t = 0, 3$  and 6 h.

In Fig. 7-9 there is shown spatial distribution of wind velocity and PM2.5 concentrations fields, obtained via numerical modeling within 1 day. It is seen from the figures that in case of constant background eastern

wind, interaction of terrain and underlying surface with background flow in free atmosphere generates quasi-stationary cyclonic vortex of local scale. This vortex is formed in the center of southern part of the region. The vortex is clearly manifested in 100 m thick surface sub-layer of the atmosphere and gradually weakens at higher levels of boundary layer of the atmosphere.

PM2.5 concentration within interval of 0-3 h, at 2 m height in surface layer of the atmosphere exceeds  $0.1 \mu\text{g}/\text{m}^3$  in the major part of area (Fig. 7). Concentration values at urbanized territories of the city and in the vicinity of motoring highways vary within  $2\text{-}10 \mu\text{g}/\text{m}^3$ . At small territories of Dzelkviani and Vake administrative units (AU), concentrations reach  $10\text{-}14 \mu\text{g}/\text{m}^3$ . From  $t = 3\text{h}$  concentration begins to increase at the substantial areas of the city center. By  $t = 6\text{h}$  concentration value in the central areas of the city and in the vicinity of highways is  $10\text{-}15 \mu\text{g}/\text{m}^3$ , and even exceeds these figures in some observation points. At 100 m height from earth surface, concentration of polluting microaerosols propagated to the south-eastern part of the modeling area mainly varies within interval of  $1\text{-}5 \mu\text{g}/\text{m}^3$ . At higher levels (600 m), concentration doesn't exceed  $1 \mu\text{g}/\text{m}^3$ .

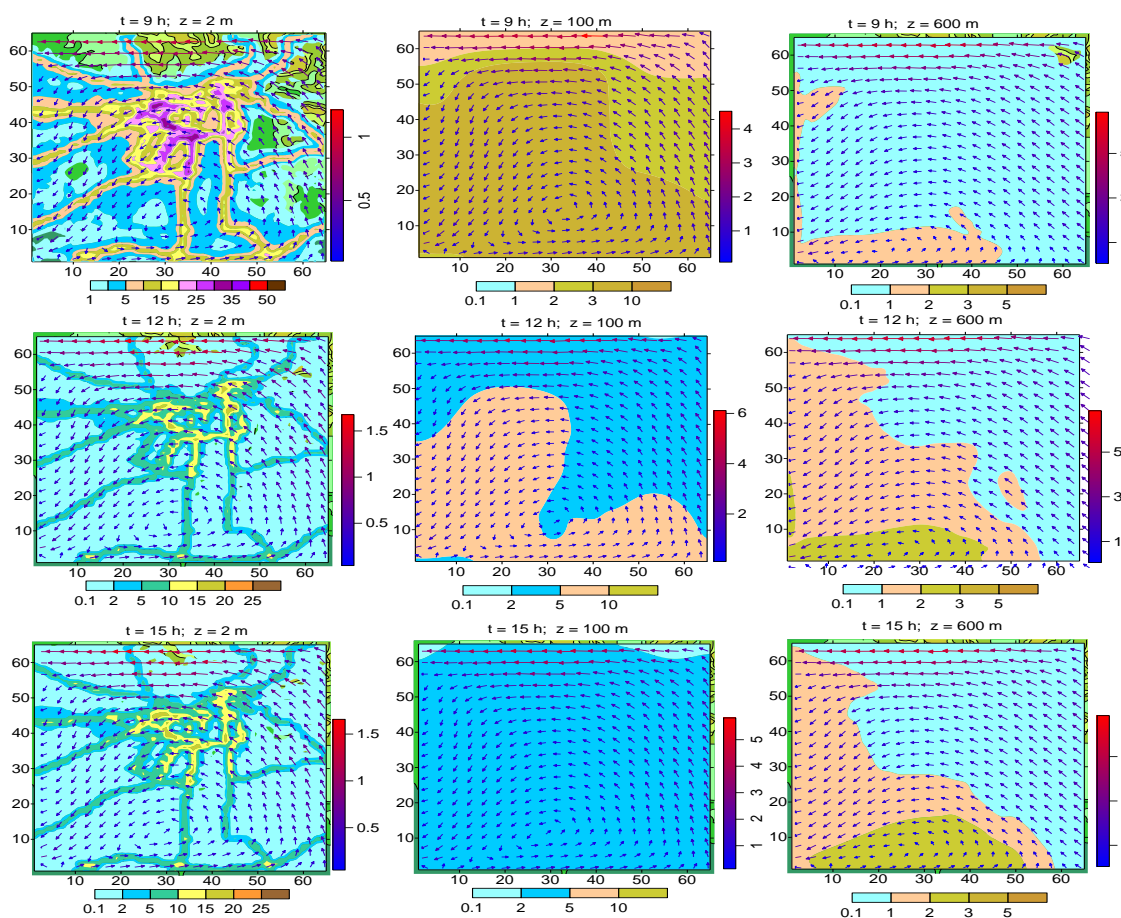


Fig. 8. Distribution of PM2.5 concentration ( $\mu\text{g}/\text{m}^3$ ) and wind velocity (m/sec) fields at 2, 100 and 600 m heights from earth ground, when  $t = 9, 12$  and  $15 \text{ h}$ .

After 6 AM, ground-level concentrations of PM2.5 begin to increase with motor traffic intensity. Concentration build-up is especially high at the central avenues passing through the territory of Avtokarkhana, Gamarjveba, Sul Khan-Saba, City-Museum and Sapichkhia AUs (Fig. 8). Concentration values at the mentioned territories at 2 m height from the earth surface reach  $25\text{-}30 \mu\text{g}/\text{m}^3$ . At their adjacent territories, concentrations gradually decrease with distance from the emission source and become equal  $10\text{-}20 \mu\text{g}/\text{m}^3$  first, and afterwards,  $1\text{-}5 \mu\text{g}/\text{m}^3$  at larger distances.

Intense air pollution takes place in the upper parts of surface layer of the atmosphere. Convective and vertical diffusive motions take place here, due to which concentration synchronically increases with ground-

level concentration. As a result, by 9AM, concentration value at the upper limit of surface layer of the atmosphere (100 m) equals to 3-10  $\mu\text{g}/\text{m}^3$  at quite large territory.

After 9AM, especially within interval of 9-15 h, vertical turbulent diffusion and convective transfer are strengthened and, as a consequence, maximum concentration of microaerosols reduces to 10-15  $\mu\text{g}/\text{m}^3$  at urbanized territories of the city. At 100 and 600 m heights, pollution level reduces, as well – to 2-5 and 2-3  $\mu\text{g}/\text{m}^3$ , respectively.

After 3PM, intensive build-up of concentration begins in the eastern and western parts of the central district of the city: at the territories of City-Museum, Kakhianouri, Gamarjveba, Sul Khan-Saba and Nikea AUs (Fig. 5). Concentration build-up is associated with thermal stability increase. At large territories of the central parts of the city concentration values are 25-35, while in populated and industrial areas of suburbs – 10-25  $\mu\text{g}/\text{m}^3$ . High values of concentration are not maintained over a long period of time. It starts to intensively decrease from  $t = 20\text{h}$  and this process lasts until 3AM. The mentioned decrease is caused by quantity reduction of emitted microaerosols caused by vehicle traffic intensity.

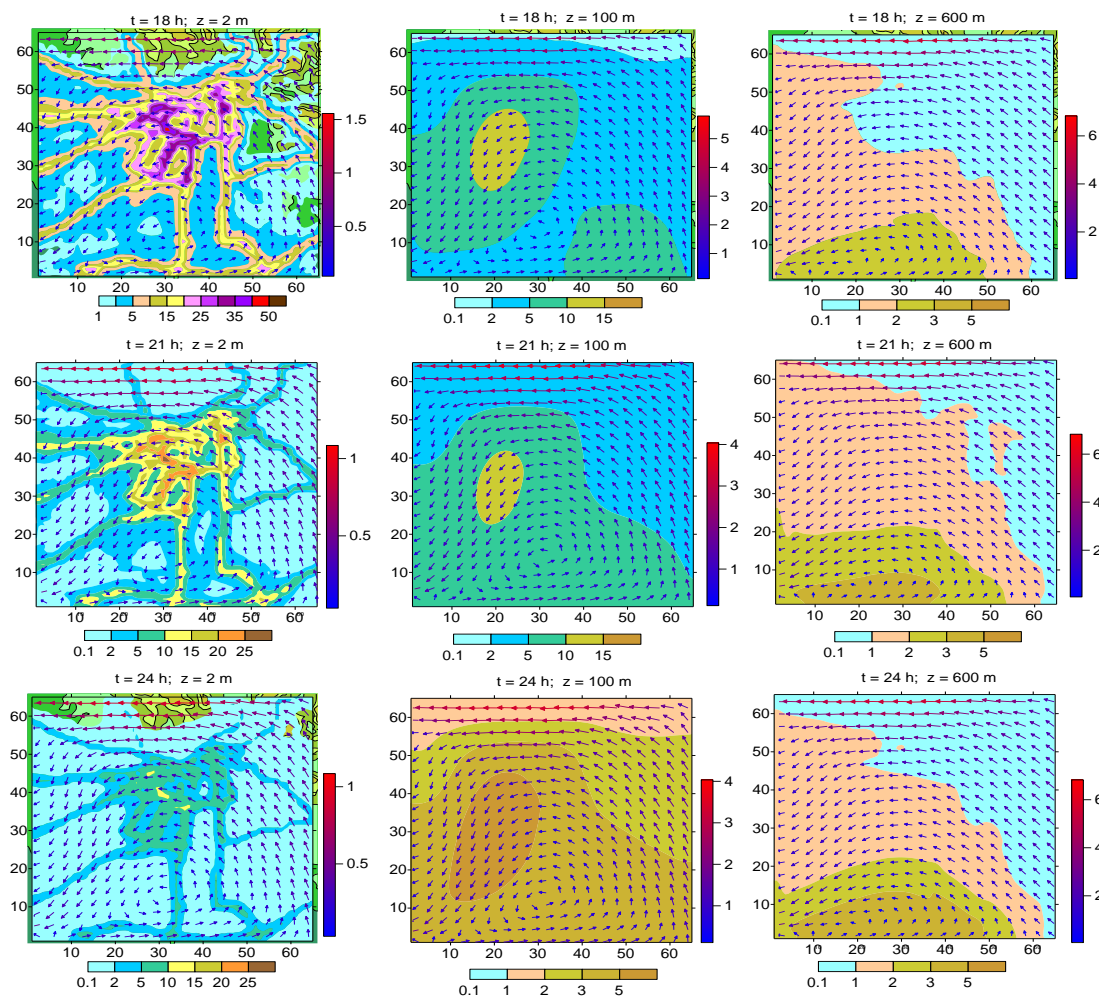


Fig. 9. Distribution of PM2.5 concentration ( $\mu\text{g}/\text{m}^3$ ) and wind velocity (m/sec) fields at 2, 100 and 600 m heights from earth ground, when  $t = 18, 21$  and  $24$  h.

## Conclusion

Features of spatial distribution and time change of PM2.5 particles formed by motor transport at the territory of Kutaisi in winter during ground-level background calm and western wind in the free atmosphere has been studied. It has been obtained via calculations that in winter season, interaction of regional terrain with

background western wind generates meso-scale cyclonic vortex of wind velocity. Formed dynamic and thermobaric fields have an influence on spatial distribution of aerosols emitted in the atmosphere due to motor transport traffic. Patterns of spatial distribution of PM<sub>2.5</sub> concentration has been obtained resulting from modeling, time behavior of concentrations has been established both in surface and boundary layers of the atmosphere. It has been shown that vertical distribution and time change of concentration depends on both aerosol emission rate and motor transport traffic intensity, as well as on kinematics of surface layer of the atmosphere and local circulation system formed due to diurnal variation of thermal regime on the underlying surface. High and average pollution levels in the city and at adjacent territories and change in their position within a day have been established.

**Acknowledgements.** The scientific research has been funded and performed with financial support of the Shota Rustaveli National Science Foundation within the grant project FR-22-4765.

## References

- [1] Pope C.A., Burnett R.T., Thun M.J., Calle E.E., Krewski D. et al. Lung cancer, cardiopulmonary mortality, and long-term exposure to fine particulate air pollution. *J. Am. Med. Assoc.*, 287, 2022, pp. 1132–1141.
- [2] World Health Organization. Regional Office for Europe. Review of evidence on health aspects of air–REVIHAAP Project. First result, 2022. <https://media.xpair.com › pdf › REVIHAAP>
- [3] Mortality and burden of disease from ambient air pollution-WHO, 2020. [https://www.who.int/gho/phe/outdoor\\_air\\_pollution/burden/en/](https://www.who.int/gho/phe/outdoor_air_pollution/burden/en/)
- [4] World's most polluted cities (historical data 2017-2022). <https://www.iqair.com/world-most-polluted-cities>.
- [5] Agrawal G., Mohan D., Rahman H. Ambient air pollution in selected small cities in India: observed trends and future challenges. *IATSS Research*, 45(1), 2021, pp. 19-30. <https://doi.org/10.1016/j.iatssr.2021.03.004>
- [6] Kobza J., Geremek M., Dul L. Characteristics of air quality and sources affecting high levels of PM<sub>10</sub> and PM<sub>2.5</sub> in Poland in Upper Silesia urban area *Environmental Monitoring and Assessment* 190, 515, 2018.
- [7] Integrated Science for Particulate Matter. EPA. United States Environmental Protection Agency, 2019, p. 1967. EPA/600/R-19/188. [www.epa.gov](http://www.epa.gov).
- [8] Hong H., Choi H., Jeon H., Kim Y., Jae-Bum Lee, Park C.H., Kim H.S. An air pollutants prediction method integrating numerical models and artificial intelligence models targeting the area around Busan port in Korea. *1462, Atmosphere*, 13(9), 1462, 2022. <https://doi.org/10.3390/atmos13091462>.
- [9] Udristioiu M., Mghouchi Y., Yildizhan H. Prediction, modelling, and forecasting of PM and AQI using hybrid machine learning. *Journal of Cleaner Production*, Vol. 421, 2023. <https://doi.org/10.1016/j.jclepro.2023.138496> Get rights and content.
- [10] Draper E., Whyatt J., Taylor R., Metcalfe S. Estimating background concentrations of PM<sub>2.5</sub> for urban air quality modelling in a data poor environment. *Atmospheric Environment*, Vol. 314, 120107, 2023. <https://doi.org/10.1016/j.atmosenv.2023.120107> Get rights and content.
- [11] Chae S., Shin J., Kwon S., Lee S., Kang S., Lee D. PM<sub>10</sub> and PM<sub>2.5</sub> real-time prediction models using an interpolated convolutional neural network. *Scientific Reports*, vol. 11, 11952, 2021. <https://www.nature.com/articles/s41598-021-91253-9>.
- [12] Deters J., Zalakeviciute R., Gonzalez M., Rybarczyk Y. Modeling PM<sub>2.5</sub> urban pollution using machine learning and selected meteorological parameters. *Machine intelligence in signal sensing. Processing and Recognition*, 2017. <https://doi.org/10.1155/2017/5106045>.
- [13] World Health Organization. Regional office for Europe. Review of evidence on health aspects of air–REVIHAAP Project. First result, 2022. <https://media.xpair.com › pdf › REVIHAAP> 7. Mortality and burden of disease from ambient air pollution-WHO, 2020. [https://www.who.int/gho/phe/outdoor\\_air\\_pollution/burden/en/](https://www.who.int/gho/phe/outdoor_air_pollution/burden/en/).
- [14] Integrated science for particulate matter. EPA. United States Environmental Protection Agency, 2019, p. 1967. EPA/600/R-19/188. [www.epa.gov](http://www.epa.gov).
- [15] Agrawal G., Mohan D., Rahman H. Ambient air pollution in selected small cities in India: observed trends and future challenges. *IATSS Research*, 45, Iss. 1, 2021, pp. 19-30. <https://doi.org/10.1016/j.iatssr.2021.03.004>.

- [16] Kobza J., Geremek M., Dul L. Characteristics of air quality and sources affecting high levels of PM10 and PM2.5 in Poland. Upper Silesia urban area environmental monitoring and assessment, 190, Article number: 515, 2018.
- [17] Environmental pollution, 2021. [https://air.gov.ge/reports\\_page](https://air.gov.ge/reports_page)
- [18] World's most polluted cities (historical data 2017-2022). <https://www.iqair.com/world-most-polluted-cities>.
- [19] Amiranashvili A.G., Kirkitadze D.D., Kekenadze E.N. Pandemic of coronavirus COVID - 19 and air pollution in Tbilisi in spring 2020. Journals of Georgian Geophysical Society, 23(1), 2020. <https://doi.org/10.48614/ggs2320202654>.
- [20] Gigauri N., Surmava A., Kukhalashvili V., Intskirveli L., Beglarashvili N. Investigation of the distribution of PM2.5 and PM10 in the atmosphere of Kutaisi through experimental observations. Collection of Scientific Refereed Works of the Institute of Hydrometeorology of the Tbilisi State University, Vol. 135, 2024, pp. 82-87. [Doi.org/10.36073/1512-0902-2024-135-82-87](https://doi.org/10.36073/1512-0902-2024-135-82-87).
- [21] Surmava A., Intskirveli L., Kordzakhia G. Numerical modeling of dust propagation in the atmosphere of a city with complex terrain. The case of background eastern light air. Journal of Applied Mathematics and Physics, 38.7, 2020, pp. 1222-1228. <https://doi.org/10.4236/jamp.2020.87092>.
- [22] Surmava A., Intskirveli L., Kukhalashvili V. Numerical Modeling of the transborder, regional and local diffusion of the dust in Georgian Atmosphere. Publishing House, Technical University, Tbilisi, Georgia. ISBN 978-9941-28-810-4, 2021, 139 p. <http://www.gtu.ge> (in Georgian).
- [23] Surmava A., Intskirveli L., Gigauri N. PM2.5 and PM10 microaerosols in the atmosphere of Tbilisi. Tbilisi, Publishing House of the Institute of Hydrometeorology, 2021, 94 p.
- [24] Gigauri N., Intskirveli L., Surmava A., Kukhalashvili V. The results of Kutaisi city atmospheric air pollution with PM particles. Bulletin of the Georgian National Academy of Sciences, vol. 18, no. 3, 2024, pp. 90-96.

## **ქ. ქუთაისის ატმოსფერული ჰაერის PM2.5 -ნაწილაკებით დაბინძურების რიცხვითი მოდელირება ზამთარში მიწისპირა შტილისა და თავისუფალ ატმოსფეროში ფონური აღმოსავლეთის ქარის დროს**

**ა. სურმავა, ნ. გიგაური, ვ. კუხალაშვილი, ლ. ინჭკირველი,  
ლ. გვერდწითელი**

### **რეზიუმე**

რიცხვითი მოდელირებით გამოკვლეულია ქ. ქუთაისის ტერიტორიაზე ავტოტრანსპორტის მიერ წარმოქმნილი PM2.5-ის სივრცული განაწილებისა და დროში ცვლილების თავისებურება ზამთარში მიწისპირა ფონური შტილის და თავისუფალ ატმოსფეროში დასავლეთის ქარის დროს. გამოთვლებით მიღებულია, რომ ზამთრის სეზონში მეზომასშტაბის რეგიონის რელიეფის ურთიერთქმედება ფონურ დასავლეთის ქართან წარმოშობს მეზომასშტაბის ქარის სიჩქარის ციკლონურ ცირკულაციას. ფორმირებული დინამიკური და თერმობარული ველები ახდენენ გავლენას ატმოსფეროში ავტოტრანსპორტის მოძრაობის შედეგად გაფრქვეული აეროზოლის სივრცულ განაწილებაზე. მოდელირების შედეგად მიღებულია PM2.5 – ის კონცენტრაციის სივრცული განაწილების სურათები, განსაზღვრულია კონცენტრაციების დროში ცვლილების ხასიათი, როგორც ატმოსფეროს მიწისპირა ფენაში ასევე სასაზღვრო ფენაში. ნაჩვენებია, რომ კონცენტრაციის ვერტიკალური განაწილება და დროში ცვლილება დამოკიდებულია როგორც აეროზოლის გაფრქვევის სიჩქარეზე და ავტოტრანსპორტის მოძრაობის ინტენსივობაზე, ასევე ატმოსფეროს მიწისპირა ფენის კინემატიკაზე და ქვეფენილ ზედაპირზე თერმული რეჟიმის დღეღამური ცვლილებით ფორმირებულ ლოკალურ

ცირკულაციურ სისტემაზე. განსაზღვრულია ქალაქის და მიმდებარე ტერიტორიებზე მაღალი და საშუალო დაბინძურების დონეები და მათი მდებარეობის ცვლილება დღეღამის განმავლობაში.

**საკვანძო სიტყვები:** PM2.5, მიკრო ნაწილაკები, კონცენტრაციის ველი, ატმოსფერო, რიცხვითი მოდელირება, შტილი.

## **Численное моделирование загрязнения атмосферного воздуха г. Кутаиси частицами PM2.5 в зимний период при штиле на суше и фоновом восточном ветре в свободной атмосфере**

**А. Сурмава, Н. Гигаури, В. Кухалашвили, Л. Инцкирвели, Л. Гвердцители**

### **Резюме**

С помощью численного моделирования на территории г. Кутаиси исследованы особенности пространственного распределения и временных изменений микрочастиц PM2.5, генерируемых зимой автотранспортом в районе города во время приземного фоновое штиля и западных ветров в свободной атмосфере. Расчеты показали, что в зимний сезон взаимодействие рельефа мезомасштабного региона с фоновым западным ветром формирует циклоническую циркуляцию мезомасштабных скоростей ветра. Формирующиеся динамические и термобарические поля оказывают влияние на пространственное распределение аэрозолей, выбрасываемых в атмосферу транспортными средствами. В результате моделирования получены графические изображения пространственного распределения концентраций PM2.5, а также определен характер изменения концентраций во времени как в приземном слое атмосферы, так и в пограничном слое. Показано, что вертикальное распределение концентрации и ее изменение во времени зависят как от скорости рассеивания аэрозоля, так и от интенсивности дорожного движения, а также от кинематики приземного слоя атмосферы и местной циркуляционной системы, формируемой суточными изменениями термического режима. Определены высокие и средние уровни загрязнения в городе и прилегающих территориях, а также их изменение в течение суток.

**Ключевые слова:** PM2.5, микрочастицы, поле концентрации, атмосфера, численное моделирование, штиль.

# Statistical Analysis of Annual and Semi-Annual Sum of Atmospheric Precipitation Data for 59 Municipalities (11 Regions) of Georgia with Landslide Hazard Zones from 2015 to 2024

<sup>1</sup>Avtandil G. Amiranashvili, <sup>2</sup>Luca Brocca, <sup>1</sup>Tamaz L. Chelidze,  
<sup>1</sup>David T. Svanadze, <sup>3</sup>Tamar N. Tsamalashvili, <sup>1</sup>Nodar D. Varamashvili

<sup>1</sup>M. Nodia Institute of Geophysics of I. Javakishvili Tbilisi State University, Tbilisi, Georgia  
[avtandilamiranashvili@gmail.com](mailto:avtandilamiranashvili@gmail.com)

<sup>2</sup>Research Institute for Geo-Hydrological Protection, Perugia, Italy

<sup>3</sup>A. Janelidze Geological Institute of I. Javakishvili Tbilisi State University, Tbilisi, Georgia

## ABSTRACT

*The article presents the results of statistical analysis of data from 62 meteorological stations of Georgia located in the territories of 59 municipalities (11 regions) of Georgia with dangerous landslide zones on semi-annual and annual sum of atmospheric precipitation. The observation period is from 2015 to 2024. In particular, empirical (map) and calculated model of distribution of annual sum of atmospheric precipitation averaged over the territories of municipalities were obtained; the relationships of semi-annual and annual sum of atmospheric precipitation averaged over the territories of municipalities and regions with the altitude and longitude of the area, etc. were studied. In the future, it is planned to use the results of this work for a more detailed study of the relationship between precipitation and the activation of landslide processes on a climatic time scale.*

**Key words:** atmospheric precipitations, correlation and regression analysis, natural catastrophe, landslides.

## Introduction

Atmospheric precipitation, as one of the most important climate-forming factors, has long been the subject of research in various countries of the world [1-13], including Georgia [14-17]. Considering that the territory of Georgia is known for its diversity of climatic zones, increased attention is paid to the study of the variability of the precipitation regime here, especially against the background of observed and expected changes in the global climate [18].

For example, a large number of studies have been conducted on the climatology of annual, seasonal, monthly and daily precipitation amounts [19-24]; the role of precipitation in the formation of bioclimatic conditions of territories [25,26]; the influence of precipitation deficit and excess on the provocation of droughts [27-29], floods [30,31], landslides, mudflows [32], other negative phenomena [33,34], etc. The representativeness of the data of meteorological stations of Georgia on the annual, semi-annual and monthly amount of atmospheric precipitation around these stations was studied [35,36]. The study of the relationships between ground-based and satellite data on atmospheric precipitation has begun [37-40]. In recent years, an analysis of the applicability of various precipitation forecasting models [41,42], as well as the use of an integrated hybrid approach to forecasting various events associated with natural disasters [43] has been carried out.

In particular, as a result of the analysis of data from 39 meteorological stations of Georgia on atmospheric precipitation from 1936 to 2015, it was established that, in general, for the year, the data of meteorological stations on precipitation are representative around these stations at a distance of 19 km (Mta-Sabuetti, Kobuleti) to 46 km (Gori); in the cold period of the year - from 13 km (Mta-Sabuetti) to 49 km (Zugdidi); in the warm period of the year - from 20 km (Chokhatauri) to 43 km (Pasanauri); for monthly precipitation amounts - from 14 km (Akhalkalaki, January) to 90 km (Akhhaltsikhe, October). The paper [38] presents information on the

linear regression coefficients between satellite and ground-based data on annual and semi-annual precipitation sum for 26 points in Georgia for 2001–2020.

It is known that the time scale of the influence of atmospheric precipitation on the provocation of various natural disasters (including landslides and mudflows) has a wide range - from several tens of minutes to several days, months and years (climatic time scale). A whole series of studies were carried out by us in [44-51].

For example, in [45] preliminary results of the study of the relationship between the variability of the mean annual sum of atmospheric precipitation and landslide processes in Georgia for 32 years are presented. In particular, it was found that with an increase in the annual sum of atmospheric precipitation, the tendency of increase in the number of landslides is observed in accordance with a second power of polynomial.

Some results of statistical analysis of long-term variations of annual amount of atmospheric precipitation for 21 meteorological stations of Georgia (P) located in areas with landslides, average annual amount of precipitation for these stations ( $P_a$ ), relationship between the  $P_a$  and number of re-activated and new cases of landslides (LS), and the estimated values of LS up to 2045 using predictive data on  $P_a$  are presented in [47]. Data from the Environmental Agency of Georgia on the P in period 1936 - 2020 and data on LS in period 1996 – 2018 are used.

The forecast of  $P_a$  using the AAA version of the Exponential Smoothing (ETS) algorithm was carried out.

In particular, the following results are obtained.

The correlations between the annual amounts of P at each of the meteorological stations with averaged data for all 21 stations  $P_a$  are established.

In 1981-2020, compared with 1936-1975, no significant variability of the mean P values is observed at 11 stations, an increase - at 6 stations, and a decrease - at 4 stations. The  $P_a$  value do not change during the indicated time periods.

The forecast of the  $P_a$  value up to 2040 were estimated taking into account the periodicity of precipitation variability, which is 11 years.

A cross-correlation analysis of the time series of the  $P_a$  and LS values showed that the best correlation between the indicated parameters is observed with a five-year advance of precipitation data. With this in mind, a linear regression equation was obtained between the five-year moving average of the  $P_a$  and the five-year moving average of the LS values.

Using this equation and predictive  $P_a$  data, five-year moving averages of re-activated and new landslides cases up to 2045 were estimated.

The accumulation of new and systematization of existing information on various natural disasters in Georgia (storm winds, floods, landslides, mudflows, hail, etc.) [52,53] allows for a more qualitative scientific analysis of these events, as well as for clarifying the degree and scale of their impact on the environment [54-59].

In particular, a series of geological bulletins [53] presents detailed data on precipitation patterns and various geological processes (including landslides) for almost all municipalities of Georgia from 2015 to 2024.

This work is a continuation of previous studies related to the study of the relationship between precipitation and the activation of landslide processes on a climatic time scale. Below is the first part of the work, concerning the statistical analysis of data on annual and semi-annual precipitation amounts for 59 municipalities of Georgia for which there are data on landslides causing damage to the environment [53], from 2015 to 2024.

## Study area, material and methods

Study area – 11 region of Georgia including 59 municipalities with registered landslide hazard zones: Autonomous Republic of Adjara (Keda, Khelvachauri, Khulo, Kobuleti, Shuakhevi), Guria (Chokhatauri, Lanchkhuti, Ozurgeti), Imereti (Baghdati, Chiatura, Kharagauli, Khoni, Kutaisi, Sachkhere, Samtredia, Terjola, Tkibuli, Tskaltubo, Vani, Zestaphoni), Kakheti (Akhmeta, Dedoplistskaro, Gurjaani, Kvareli, Lagodekhi, Sagarejo, Signagi, Telavi), Kvemo Kartli (Bolnisi, Dmanisi, Gardabani, Marneuli, Tetritskaro, Tsalka), Mtskheta-Mtianeti (Dusheti, Kazbegi, Mtskheta, Tianeti), Samegrelo-Zemo Svaneti (Chkhorotsku, Khobi, Martvili, Mestia, Senaki, Tsalenjikha, Zugdidi), Racha-Lechkhumi and Kvemo Svaneti

(Ambrolauri, Lentekhi, Oni, Tsageri), Samtskhe-Javakheti (Adigeni, Akhalkalaki, Akhaltsikhe, Aspindza, Borjomi), Shida Kartli (Gori, Kareli, Kaspi, Khashuri), Tbilisi.

The data of Department of Geology at Georgian National Environmental Agency about monthly sum of atmospheric precipitations for 62 meteorological stations are used [53]. Period of observation: 2015-2024 (10 years). Locations of meteorological stations in Fig. 1 is presented.

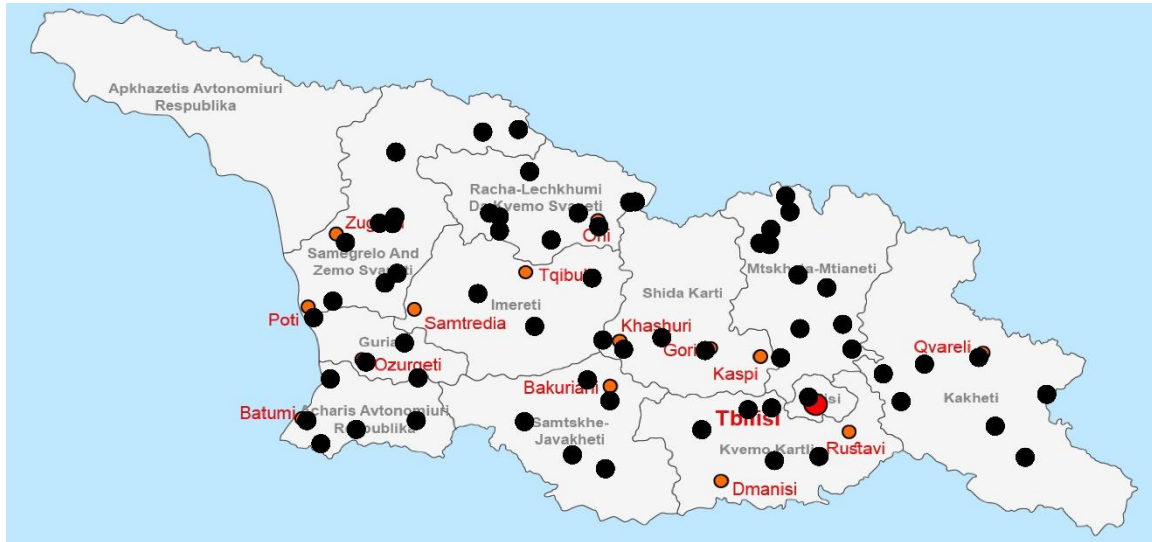


Fig. 1. Locations of meteorological stations.

Precipitation data from missing weather stations for some municipalities were compensated by data from the nearest weather stations, taking into account their representativeness [35].

In the proposed work the analysis of data is carried out with the use of the standard statistical analysis methods [60].

The following designations will be used below: Max - maximal values; Min - minimal values; Mean - average values; St Dev - standard deviation;  $R^2$  – coefficient of determination; R – coefficient of linear correlation;  $R'$  - correlation index for nonlinear regression;  $\alpha$  - the level of significance; Lat - north latitude, °N; Lon - east longitude, °E; H – altitude above sea level, m; P – precipitation, mm;  $P_{cold}$  – sum precipitation in cold period from October to March;  $P_{warm}$  – sum precipitation in warm period from April to September;  $P_{year}$  – annual sum of precipitation from January to December. In the text below, the dimensions of precipitation (mm) are often omitted.

The degree of correlation was determined in accordance with [60]: very high correlation ( $0.9 \leq R \leq 1.0$ ); high correlation ( $0.7 \leq R < 0.9$ ); moderate correlation ( $0.5 \leq R < 0.7$ ); low correlation ( $0.3 \leq R < 0.5$ ); negligible correlation ( $0 \leq R < 0.3$ ).

## Results and discussion

Results in Table 1-4 and Fig. 2-8 are presented.

In Table 1 statistical characteristics of semi-annual and annual sum of atmospheric precipitation by 59 municipalities of Georgia in 2015-2024 is presented.

As follows from Table 1  $P_{cold}$  values change from 139 (Gardabani) to 1589 (Kobuleti),  $P_{warm}$  – from 236 (Marneuli) to 1072 (Kobuleti) and  $P_{year}$  – from 383 (Gardabani) to 2662 (Kobuleti). In Fig. 2 as an example distribution of mean annual sum of atmospheric precipitation by municipalities of Georgia in 2015-2024 is presented.

Table 1. Statistical characteristics of semi-annual and annual sum of atmospheric precipitation by municipalities of Georgia in 2015-2024.  $R_{\min} = 0.25$ ,  $\alpha = 0.05$

Variable	Lat	Lon	H, m	Cold	Warm	Year
Max	43.04	46.24	1747	1589	1072	2662
Min	41.36	41.67	7	139	236	383
Mean	42.01	43.50	556	569	523	1092
St Dev	0.39	1.30	439	397	200	577
Correlation Matrix						
Lat	1	-0.39	-0.19	0.27	0.38	0.32
Lon	-0.39	1	0.39	-0.79	-0.66	-0.77
H	-0.19	0.39	1	-0.68	-0.56	-0.66
Cold	0.27	-0.79	-0.68	1	0.85	0.98
Warm	0.38	-0.66	-0.56	0.85	1	0.93
Year	0.32	-0.77	-0.66	0.98	0.93	1

There is a very high linear correlation between the values of  $P_{\text{year}}$ ,  $P_{\text{cold}}$  and  $P_{\text{warm}}$  (Table 1, Fig. 3). The degree of correlation between the values of  $P_{\text{warm}}$  and  $P_{\text{cold}}$  is high. With increasing altitude in a linear approximation, there is a tendency for the average semi-annual and annual precipitation to decrease (moderate correlation). The values of the parameters under study in a linear approximation either do not depend ( $P_{\text{cold}}$ , negligible correlation) or depend weakly ( $P_{\text{warm}}$  and  $P_{\text{year}}$ , low positive correlation) on the latitude of the area. At the same time, there is a moderate negative correlation of  $P_{\text{warm}}$  and a high negative correlation of  $P_{\text{year}}$ , and  $P_{\text{cold}}$  with the longitude of the area (decreasing to the east).

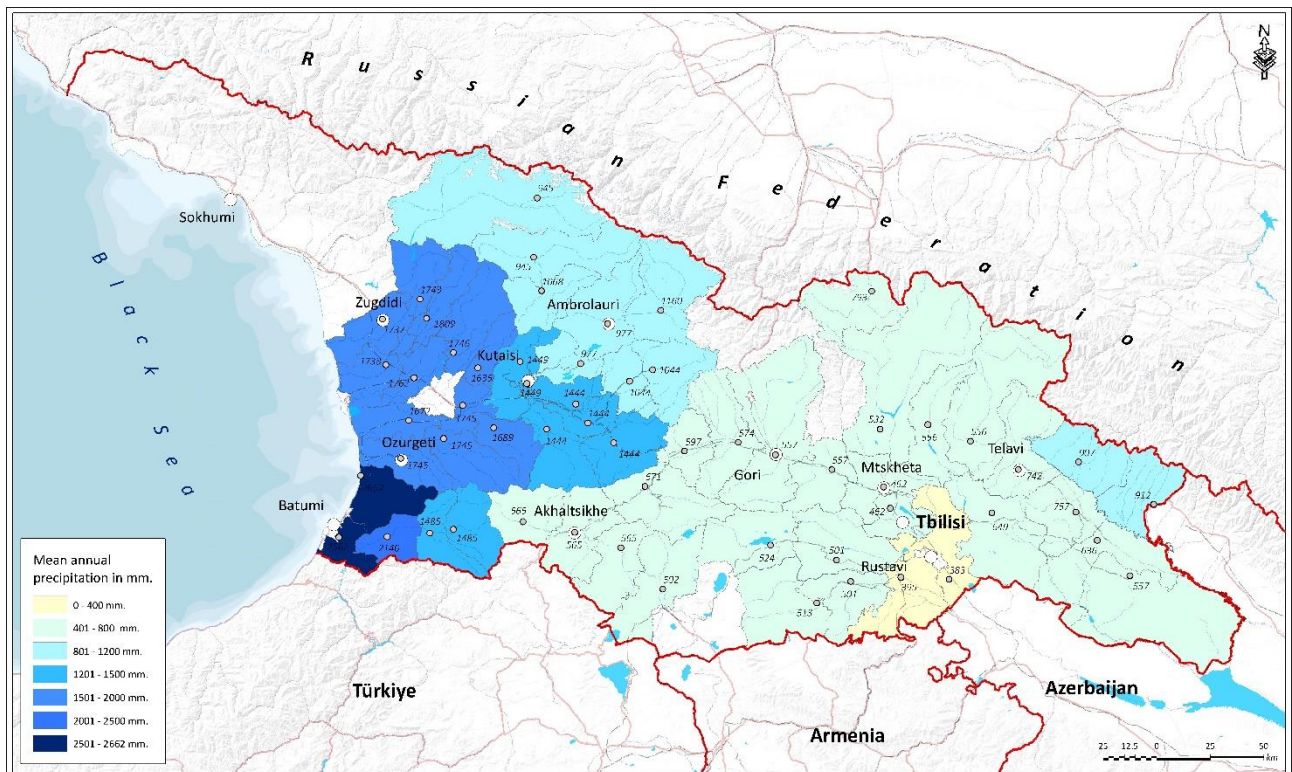


Fig. 2. Distribution of mean annual sum of atmospheric precipitation by municipalities of Georgia in 2015-2024.

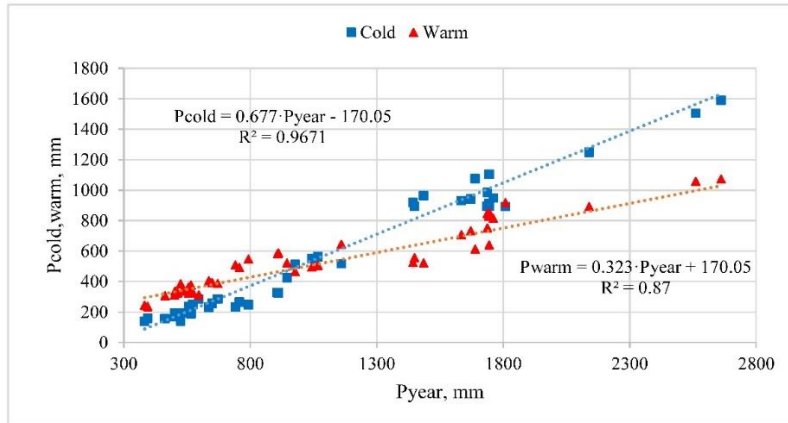


Fig. 3. Linear correlation and regression between semi-annual and annual sum of atmospheric precipitation by municipalities of Georgia in 2015-2024.  $R \geq 0.93$ , very high correlation.

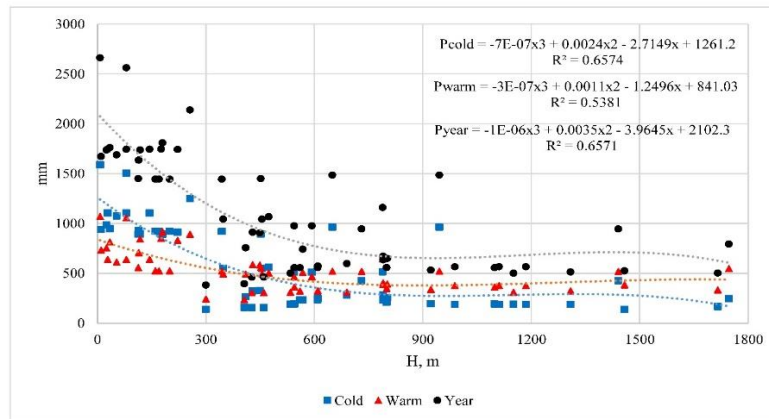


Fig. 4. Vertical distribution of semi-annual and annual atmospheric precipitation in Georgia, averaged over its municipalities in 2015-2024.  $0.73 \leq R' \leq 0.81$ , high correlation.

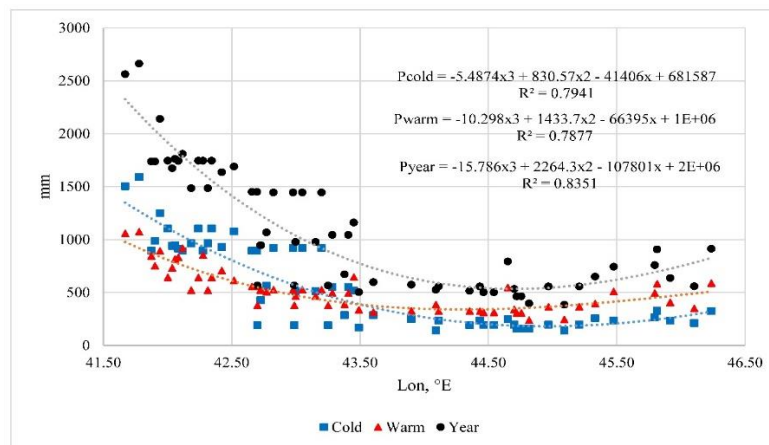


Fig. 5. Distribution by longitude of semi-annual and annual atmospheric precipitation in Georgia, averaged over its municipalities in 2015-2024. For  $P_{cold}$  and  $P_{warm}$  value of  $R' = 0.89$ , high correlation; for  $P_{year}$  value of  $R' = 0.91$ , very high correlation.

In reality, the dependence of the studied parameters on the altitude and longitude of the area is better described by third-degree polynomials (Fig. 4 and 5). In the first case, the correlation index R' is high, in the second – very high.

With a high level of reliability, relationship between the annual sum of atmospheric precipitation averaged by municipalities and the latitude and longitude of the area in Georgia can be represented by the following regression equation (the corresponding regression coefficients are presented in Table 2):

$$P_{\text{year}} = a + b/x_1 + c/x_2 + d/x_1^2 + e/x_2^2 + f/(x_1 * x_2) + g/x_1^3 + h/x_2^3 + i/(x_1 * x_2^2) + j/(x_1^2 * x_2)$$

$x_1 - \text{Lon } ^\circ\text{E}, x_2 - \text{Lat } ^\circ\text{N}, R^2 = 0.8936, R' = 0.95, \text{ very high correlation.}$

Table 2. Coefficients of the equation for the relationship between the annual sum of atmospheric precipitation averaged by municipalities and the latitude and longitude of the area in Georgia in 2015-2024.

Coefficient	a	b	c	d	e	f	g	h	i	j
Value	-3.79· E+07	9.69· E+08	3.85· E+09	-3.72· E+10	-1.55· E+11	-1.14· E+10	1.79· E+11	2.41· E+12	-7.86· E+11	1.07· E+12

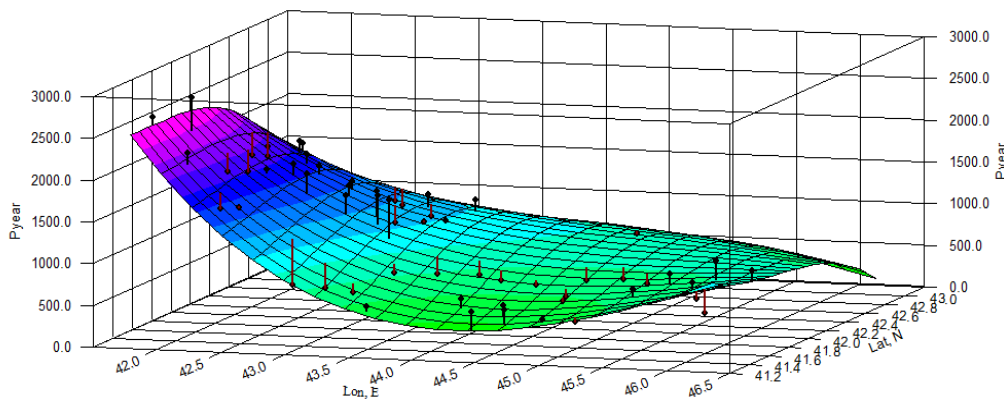


Fig. 6. Calculation model of distribution of annual sum of atmospheric precipitation in Georgia, averaged across its municipalities in 2015-2024.

In Fig. 6 calculation model of distribution of annual sum of atmospheric precipitation in Georgia, averaged across its municipalities, is presented, the actual data of which are given in Fig. 2.

In separated regions of Georgia changeability of semi-annual and annual sum of atmospheric precipitation is as follows (Table 3).

Table 3. Statistical characteristics of semi-annual and annual sum of atmospheric precipitation by separated region of Georgia in 2015-2024.

Variable	Lat	Lon	H, m	Cold	Warm	Year
Region	Autonomous Republic of Adjara (Adj)					
Max	41.85	42.31	946	1589	1072	2662
Min	41.59	41.67	7	963	522	1485
Mean	41.66	41.976	388	1254	813	2067
St Dev	0.11	0.27	399	293	275	566
Region	Guria (Gur)					
Max	42.09	42.24	144	1105	732	1745
Min	41.93	42	10	941	640	1672
Mean	42.01	42.09	78	1050	671	1721
St Dev	0.08	0.13	67	95	53	42
Region	Imereti (Im)					
Max	42.35	43.41	593	1105	706	1745
Min	42.02	42.34	28	512	465	977

Mean	42.21	42.87	253	849	552	1401
St Dev	0.12	0.35	181	200	69	253
Region	Kakheti (Kakh)					
Max	42.04	46.24	802	326	587	912
Min	41.47	45.21	410	194	348	556
Mean	41.78	45.74	599	255	460	715
St Dev	0.19	0.37	173	49	96	141
Region	Kvemo Kartli (KK)					
Max	41.6	45.09	1458	191	384	524
Min	41.36	44.09	300	139	236	383
Mean	41.48	44.56	860	168	302	470
St Dev	0.08	0.35	504	25	55	63
Region	Mtskheta-Mtianeti (MM)					
Max	42.67	44.97	1747	246	546	793
Min	41.85	44.65	460	156	306	462
Mean	42.18	44.76	1057	198	388	586
St Dev	0.35	0.14	533	37	108	144
Region	Samegrelo-Zemo Svaneti (S-ZS)					
Max	43.04	42.73	1441	986	917	1809
Min	42.27	41.87	25	425	520	945
Mean	42.52	42.15	314	850	790	1640
St Dev	0.26	0.29	503	191	129	307
Region	Racha-Lechkhumi and Kvemo Svaneti (R-L KS)					
Max	42.79	43.45	789	562	645	1160
Min	42.52	42.72	474	425	465	945
Mean	42.64	43.02	635	504	534	1038
St Dev	0.12	0.34	150	57	78	97
Region	Samtskhe-Javakheti (S-J)					
Max	41.84	43.49	1716	285	386	671
Min	41.41	42.7	790	167	335	502
Mean	41.63	43.16	1158	204	370	574
St Dev	0.16	0.32	346	46	20	61
Region	Shida Kartli (Sh K)					
Max	42.03	44.43	690	284	325	597
Min	41.92	43.6	560	234	312	557
Mean	41.98	44.01	617	250	321	571
St Dev	0.05	0.35	54	24	6	19
Region	Tbilisi (Tb)					
Mean	41.76	44.76	427	156	306	462

Adj: Cold period – from 963 (Khulo, Shuakhevi) to 1589 (Kobuleti), average value – 1254. Warm period – from 522 (Khulo, Shuakhevi) to 1072 (Kobuleti), average value – 1072. Year – from 1485 (Khulo, Shuakhevi) to 2262 (Kobuleti), average value – 2067.

Gur: Cold period – from 941 (Lanchkhuti) to 1105 (Chokhatauri, Ozurgeti), average value – 1050. Warm period – from 640 (Chokhatauri, Ozurgeti) to 732 (Lanchkhuti), average value – 671. Year – from 1672 (Lanchkhuti) to 1745 (Chokhatauri, Ozurgeti), average value – 1721.

Im: Cold period – from 512 (Tkibuli) to 1105 (Samtredia), average value – 849. Warm period – from 465 (Tkibuli) to 706 (Khoni), average value – 552. Year – from 977 (Tkibuli) to 1745 (Samtredia), average value – 1401.

Kakh: Cold period – from 194 (Akhmeta) to 326 (Kvareli), average value – 255. Warm period – from 348 (Dedoplistskaro) to 587 (Lagodekhi), average value – 460. Year – from 556 (Akhmeta) to 912 (Lagodekhi), average value – 715.

KK: Cold period – from 139 (Gardabani) to 191 (Bolnisi, Tetrtskaro), average value – 168. Warm period – from 236 (Marneuli) to 384 (Tsalka), average value – 302. Year – from 383 (Gardabani) to 524 (Tsalka), average value – 470.

MM: Cold period – from 156 (Mtskheta) to 246 (Kazbegi), average value – 198. Warm period – from 306 (Mtskheta) to 546 (Kazbegi), average value – 388. Year – from 462 (Mtskheta) to 793 (Kazbegi), average value – 586.

(S-ZS: Cold period – from 425 (Mestia) to 986 (Khobi), average value – 850. Warm period – from 520 (Mestia) to 917 (Chkhorotsku), average value – 790. Year – from 945 (Mestia) to 1809 (Chkhorotsku), average value – 1640.

R-L KS: Cold period – from 425 (Lentekhi) to 562 (Tsageri), average value – 504. Warm period – from 465 (Ambrolauri) to 645 (Oni), average value – 534. Year – from 945 (Lentekhi) to 1160 (Oni), average value – 1038.

S-J: Cold period – from 167 (Akhalkalaki) to 285 (Borjomi), average value – 204. Warm period – from 335 (Akhalkalaki) to 386 (Borjomi), average value – 370. Year – from 502 (Akhalkalaki) to 671 (Borjomi), average value – 574.

Sh K: Cold period – from 234 (Gori, Kaspi) to 284 (Khashuri), average value – 250. Warm period – from 312 (Khashuri) to 325 (Kareli), average value – 321. Year – from 557 (Gori, Kaspi) to 597 (Khashuri), average value – 571.

Tb: Cold period, average value – 156. Warm period, average value – 306. Year, average value – 462.

Table 4. Statistical characteristics of semi-annual and annual sum of atmospheric precipitation averaged by regions of Georgia in 2015-2024.  $R_{\min} = 0.60$ ,  $\alpha = 0.05$

Variable	Lat	Lon	H, m	Cold	Warm	Year
Max	42.64	45.74	1158	1254	813	2067
Min	41.48	41.98	78	156	306	462
Mean	41.99	43.55	581	522	501	1022
St Dev	0.37	1.28	337	405	188	584
Correlation Matrix						
Lat	1	-0.34	-0.28	0.25	0.38	0.30
Lon	-0.34	1	0.49	-0.84	-0.78	-0.84
H, m	-0.28	0.49	1	-0.73	-0.63	-0.71
Cold	0.25	-0.84	-0.73	1	0.93	0.99
Warm	0.38	-0.78	-0.63	0.93	1	0.97
Year	0.30	-0.84	-0.71	0.99	0.97	1

Changeability of semi-annual and annual sum of atmospheric precipitation averaged by regions of Georgia is as follows (Table 4).

Cold period – from 156 (Tb) to 1254 (Adj), average value – 522. Warm period – from 306 (Tb) to 813 (Adj), average value – 501. Year – from 462 (Tb) to 2067 (Adj), average value – 1022.

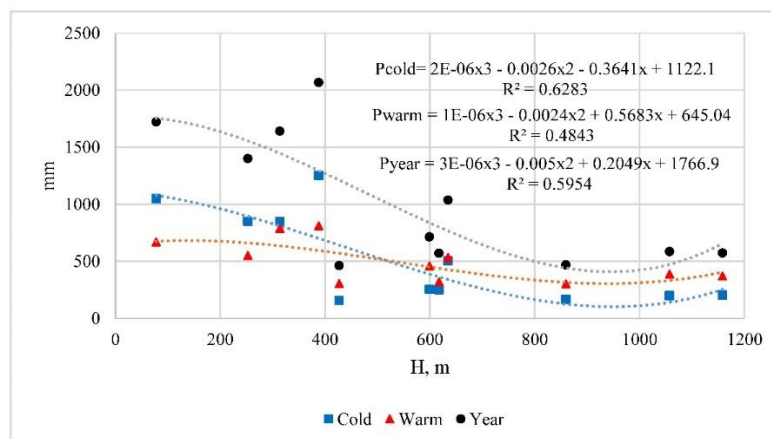


Fig. 7. Vertical distribution of semi-annual and annual atmospheric precipitation in Georgia, averaged over its regions in 2015-2024.  $0.70 \leq R' \leq 0.79$ , high correlation.

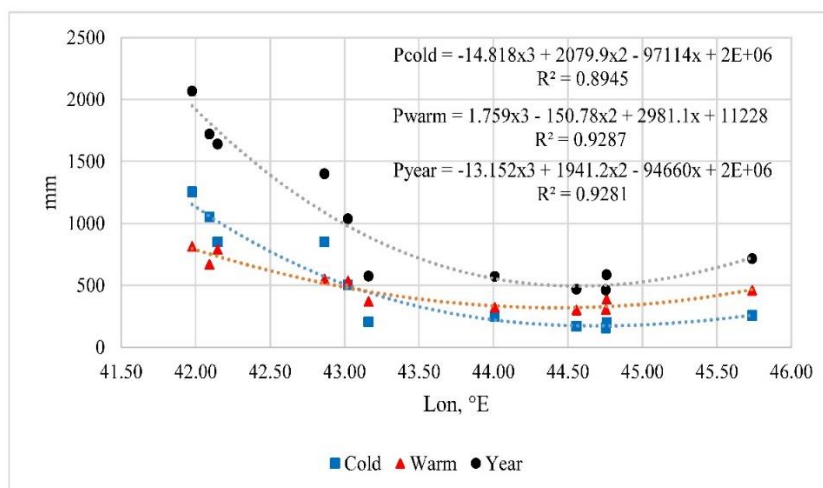


Fig. 8. Distribution by longitude of semi-annual and annual atmospheric precipitation in Georgia, averaged over its regions in 2015-2024.  $R' \geq 0.95$ , very high correlation.

Both in the cases with municipalities (Fig. 4 and 5) and according to the data for the regions of Georgia (Fig. 7 and 8, data from Table 3), the dependence of the average values of semi-annual and annual precipitation sum on the altitude and longitude of the area has the form of third-degree polynomials. As in the previous cases the correlation index  $R'$  is high for connection of parameters under study with  $H$ , and very high - or connection with  $E$ .

## Conclusion

A detailed statistical analysis of data from 62 meteorological stations in Georgia, located in 59 municipalities (11 regions) of Georgia with dangerous landslide zones, on semi-annual and annual sum of atmospheric precipitation was conducted.

In the near future, it is planned to use the results of this work for a more detailed study of the connections between precipitation and the activation of landslide processes on a climatic time scale.

## Acknowledgments

This work was supported by Shota Rustaveli National Science Foundation of Georgia (SRNSFG), Grant number FR-23-5466, "Machine Learning Approach to the Landslide Activation Prediction in Georgia".

## References

- [1] Brocca L. et al. Soil as a natural rain gauge: Estimating global rainfall from satellite soil moisture data. *Journal of Geophysical Research: Atmospheres*, 119, 2014, pp. 5128–5141.
- [2] Massari C., Crow, W., Brocca, L. An assessment of the performance of global rainfall estimates without ground-based observations. *Hydrology and earth system sciences*, 21, 2017, pp. 4347–4361.
- [3] Sun Q. et al. A review of global precipitation data sets: Data sources, estimation, and intercomparisons. *Reviews of Geophysics*, 56, 2018, pp. 79–107.
- [4] Brocca L. et al. SM2RAIN–ASCAT (2007–2018): global daily satellite rainfall data from ASCAT soil moisture observations. *Earth System Science Data*, 11, 2019, pp. 1583–1601.
- [5] Bartolini G., Grifoni D., Magno R., Torrigiani T., Gozzini B. Changes in temporal distribution of precipitation in a Mediterranean area (Tuscany, Italy) 1955–2013. *Int. Journal of Climatology*, 38, 2018, pp. 1366–1374. <https://doi.org/10.1002/joc.5251>
- [6] Yaman B., Ertugrul M. Change-point detection and trend analysis in monthly, seasonal and annual air temperature and precipitation series in Bartın province in the western Black Sea region of Turkey. *Geology, Geophysics and Environment*, 46, 223, 2020. <https://doi.org/10.7494/geol.2020.46.3.223>

- [7] Bouklikha A., Habi M., Elouissi A., Hamoudi, S. Annual, seasonal and monthly rainfall trend analysis in the Tafna watershed, Algeria. *Applied Water Science*, 11, 77, 2021. <https://doi.org/10.1007/s13201-021-01404-6>
- [8] Kharyutkina E, Loginov S, Martynova Y, Sudakov I. Time series analysis of atmospheric precipitation characteristics in Western Siberia for 1979–2018 across different datasets. *Atmosphere*, 13(2), 2022 Jan 24, 189.
- [9] Mosaffa H., Filippucci P., Massari C., Ciabatta, Brocca L. SM2RAIN-Climate, a monthly global long-term rainfall dataset for climatological studies. *Sci Data*, 10, 2023, 749. <https://doi.org/10.1038/s41597-023-02654-6>
- [10] Gonzalez-Hidalgo J.C., Beguería S., Peña-Angulo D., Trullenque-Blanco V. MOPREDAS\_century database and precipitation trends in mainland Spain, 1916–2020. *Int. Journal of Climatology*, 43, 2023, pp. 3828–3840. <https://doi.org/10.1002/joc.8060>
- [11] Benziane S. Survey: Rainfall prediction precipitation, review of statistical methods. *WSEAS Transactions on Systems*, 23, 2024, pp. 47-59.
- [12] Gonzalez-Hidalgo J.C., Trullenque-Blanco V., Beguería S., Peña-Angulo D. Seasonal precipitation changes in the western Mediterranean Basin: The case of the Spanish mainland, 1916–2015. *Int. Journal of Climatology*, 44(5), 2024, pp. 1800-1815.
- [13] Syam N. S. S., Sunil A., Pichuka, S., Mandal A. Assessment of climate change impacts on the precipitation and temperature: A case study on Krishna River Basin, India. *Russian Meteorology and Hydrology*, 49(1), 2024, pp. 62-70.
- [14] Alibegova D., Elizbarashvili E. *Statisticheskaya struktura atmosfernih osadkov v gornikh raionakh*. Leningrad, 1980, 136 p., (in Russian).
- [15] *Opasnyye gidrometeorologicheskiye yavleniya na Kavkaze*. Pod red. Svanidze G.G. i Tsutskiridze Ya.A., L., Gidrometeoizdat, 1980, 288 s., (in Russian).
- [16] Tavartkiladze K. Saqartveloshi naleqebis ganacilebis statistikuri struktura. *Hidrometeorologiis institutis Sromebi*, “Mecniereba”, N 105, 2002, 117 p., (in Georgian).
- [17] Tavartkiladze K., Begalishvili N., Kharchilava J., Mumladze D., Amiranashvili A., Vachnadze J., Shengelia I., Amiranashvili V. Contemporary climate change in Georgia. Regime of Some Climate Parameters and their Variability. Monograph, ISBN 99928-885-4-7, Tbilisi, 2006, 177 p., (in Georgian).
- [18] Kartvelishvili L., Tatishvili M., Amiranashvili A., Megrelidze L., Kutaladze N. Weather, Climate and their Change Regularities for the Conditions of Georgia. Monograph, publishing house “UNIVERSAL”, ISBN: 978-9941-33-465-8, Tbilisi 2023, 406 p., <https://doi.org/10.52340/mng.9789941334658>
- [19] Khvedelidze Z., Amiranashvili A., Dolidze J., Chitaladze D., Pavlenishvili N. Statistical structure of diurnal precipitation distribution on the territory of Eastern Georgia. *Proc. of I. Javakhishvili Tbilisi State University, Physics*, N 357, ISSN 1512-1461, Tbilisi University Press, Tbilisi, 2004, pp. 79-87.
- [20] Amiranashvili A.G. Special features of changeability of daily sum of precipitation in Tbilisi in 1957-2006. *Journal of the Georgian Geophysical Society, Issue B. Physics of Atmosphere, Ocean and Space Plasma*, v.18B, Tbilisi, 2015, pp.81-91.
- [21] Amiranashvili A., Bliadze T., Kartvelishvili L. Statistical characteristics of monthly sums of atmospheric precipitations in Tianeti (Georgia) in 1956-2015. *Trans. of Mikheil Nodia institute of Geophysics*, ISSN 1512-1135, vol. 70, Tb., 2019, pp. 112-118, (in Russian), <http://dspace.gela.org.ge/handle/123456789/254>;
- [22] Bliadze T., Gvasalia G., Kirkitadze D., Mekoshkishvili N. Changeability of the atmospheric precipitations regime in Kakheti in 1956-2015. *Int. Sc. Conf. “Natural Disasters in Georgia: Monitoring, Prevention, Mitigation”*. Proceedings, ISBN 978-9941-13-899-7, Publish House of Iv. Javakhishvili Tbilisi State University, December 12-14, Tbilisi, 2019, pp. 74-77.
- [23] Amiranashvili A. Changeability of air temperature and atmospheric precipitations in Tbilisi for 175 Years. *Int. Sc. Conf. “Natural Disasters in Georgia: Monitoring, Prevention, Mitigation”*. Proceedings, ISBN 978-9941-13-899-7, Publish House of Iv. Javakhishvili Tbilisi State University, December 12-14, Tbilisi, 2019, pp. 86-90.

- [24] Bolashvili N., Chikhladze V., Kartvelishvili L., Tatishvili M. Variability of atmospheric precipitation in Tbilisi in 1844-2023. Int. Sc. Conf. "Complex Geophysical Monitoring in Georgia: History, Modern Problems, Promoting Sustainable Development of the Country", Proceedings, ISBN 978-9941-36-272-9, publish house of Iv. Javakhishvili Tbilisi State University, Tbilisi, Georgia, October 17-19, 2024, pp. 150 – 154. [http://dspace.gela.org.ge/bitstream/123456789/10620/1/38\\_MM-180.pdf](http://dspace.gela.org.ge/bitstream/123456789/10620/1/38_MM-180.pdf)
- [25] Amiranashvili A.G., Revishvili A.A., Khazaradze K.R., Japaridze N.D. Connection of Holiday Climate Index with public health (on example of Tbilisi and Kakheti region, Georgia). Journal of the Georgian Geophysical Society, e-ISSN: 2667-9973, p-ISSN: 1512-1127, Physics of Solid Earth, Atmosphere, Ocean and Space Plasma, v. 24(1), 2021, pp. 63-76.
- [26] Amiranashvili A.G., Kartvelishvili L.G., Kutaladze N.B., Megrelidze L.D., Tatishvili M.R. Changeability of the meteorological parameters associated with Holiday Climate Index in different mountainous regions of Georgia in 1956-2015. Journal of the Georgian Geophysical Society, e-ISSN: 2667-9973, p-ISSN: 1512-1127, Physics of Solid Earth, Atmosphere, Ocean and Space Plasma, v. 24(2), 2021, pp. 78-91. DOI: <https://doi.org/10.48614/ggs2420213326>
- [27] Tatishvili M., Palavandishvili A., Tsitsagi M., Gulashvili Z., Suknidze N. Drought evaluation based on SPEI, SPI Indices for Georgian territory. Int. Conf. of young scientists "Modern Problems of Earth Sciences", Proceedings, ISBN 978-9941-36-044-2, Publish House of Iv. Javakhishvili Tbilisi State University, Tbilisi, November 21-22, 2022, pp. 119-121
- [28] Tsitsagi M., Gulashvili Z., Bolashvili N., Tatishvili M., Suknidze N. Relationship between Normalized Difference Vegetation Index, precipitation and Drought Indices (Case of Kakheti, Georgia). 22nd International Multidisciplinary Scientific GeoConference SGEM 2022. <https://doi.org/10.5593/sgem2022/4.1/s19.46>
- [29] Tatishvili M., Kapanadze N., Mkurnalidze I., Palavandishvili A. Drought evaluation in Georgia using SPI and SPEI Indices. Int. Sc. Conf. "Complex Geophysical Monitoring in Georgia: History, Modern Problems, Promoting Sustainable Development of the Country", Proceedings, ISBN 978-9941-36-272-9, Publish House of Iv. Javakhishvili Tbilisi State University, Tbilisi, Georgia, October 17-19, 2024, pp. 96 – 100.
- [30] Beglarashvili N., Janelidze I., Pipia M., Varamashvili N. Heavy rainfall, floods and floodings in Kakheti (Georgia) in 2014-2018. Int. Sc. Conf. „Modern Problems of Ecology“, Proc., ISSN 1512-1976, v. 7, Tbilisi-Telavi, Georgia, 26-28 September, 2020, pp. 180-184.
- [31] Beglarashvili N., Jamrlishvili N., Janelidze I., Pipia M., Tavidashvili Kh. Analysis of strong precipitation in Tbilisi on August 29, 2023. Int. Sc. Conf. "Geophysical Processes in the Earth and its Envelopes". Proceedings, ISBN 978-9941-36-147-0, Publish House of Iv. Javakhishvili Tbilisi State University, November 16-17, 2023, pp. 143-146. <http://www.dspace.gela.org.ge/handle/123456789/10421>
- [32] Varazanashvili O., Tsereteli N., Amiranashvili A., Tsereteli E., Elizbarashvili E., Dolidze J., Qaldani L., Saluqvadze M., Adamia Sh., Arevadze N., Gventcadze A. Vulnerability, hazards and multiple risk assessment for Georgia. Natural Hazards, Vol. 64, Number 3, 2012, pp. 2021-2056. DOI: 10.1007/s11069-012-0374-3, <http://www.springerlink.com/content/9311p18582143662/fulltext.pdf>.
- [33] Elizbarashvili E.Sh., Elizbarashvili M.E. Stikhiynnye meteorologicheskkiye yavleniya na territorii Gruzii. Tbilisi, Zeon, 2012, 104 s., (in Russian).
- [34] Tatishvili M., Elizbarashvili E., Meskhia R., Elizbarashvili Sh. Natural hydrometeorological disasters, their causes and prevention measures. The Macrotheme Review. A Multidisciplinary Journal of Global Macro Trends. A Macrotheme Capital Management. LLC Academic Publication, ISSN 1848-4735, v. 2, iss.1, Winter 2013 (January), France, pp. 148-154.
- [35] Amiranashvili A., Chelidze T., Svanadze D., Tsamalashvili T., Tvauri G. On the representativeness of data from meteorological stations in Georgia for annual and semi-annual sum of atmospheric precipitation around of these stations. Int. Sc. Conf. „Natural Disasters in the 21st Century: Monitoring, Prevention, Mitigation“. Proceedings, ISBN 978-9941-491-52-8, Tbilisi, Georgia, December 20-22, 2021. Publish house of Iv. Javakhishvili Tbilisi State University, Tbilisi, 2021, pp. 79 - 83. [http://openlibrary.ge/bitstream/123456789/9566/1/20\\_Conf\\_ND\\_2021.pdf](http://openlibrary.ge/bitstream/123456789/9566/1/20_Conf_ND_2021.pdf)

- [36] Amiranashvili A., Chelidze T., Svanadze D., Tsamalashvili T., Varamashvili N. About the representativeness of data from meteorological stations in Georgia for monthly sum of atmospheric precipitation around of these stations. *Journal of the Georgian Geophysical Society*, e-ISSN: 2667-9973, p-ISSN: 1512-1127, *Physics of Solid Earth, Atmosphere, Ocean and Space Plasma*, v. 27(1), 2024, pp. 52–57. <https://ggs.openjournals.ge/index.php/GGS/article/view/7983>
- [37] Amiranashvili A., Chelidze T., Svanadze D., Tsamalashvili T., Tvauri G. Comparison of data from ground-based and satellite measurements of the monthly sum of atmospheric precipitation on the example of Tbilisi city in 2001-2020. *Int. Conf. of young scientists “Modern Problems of Earth Sciences”*. Proceedings, ISBN 978-9941-36-044-2, Publish House of Iv. Javakhishvili Tbilisi State University, Tbilisi, November 21-22, 2022, pp. 154-158. [http://openlibrary.ge/bitstream/123456789/10251/1/37\\_YSC\\_2022.pdf](http://openlibrary.ge/bitstream/123456789/10251/1/37_YSC_2022.pdf)
- [38] Amiranashvili A., Chelidze T., Svanadze D., Tsamalashvili T., Varamashvili N. Comparison of satellite and ground-based data on semi-annual and annual sum of atmospheric precipitation for 26 points in Georgia in 2001-2020. *Int. Sc. Conf. “Complex Geophysical Monitoring in Georgia: History, Modern Problems, Promoting Sustainable Development of the Country”*, Proceedings, ISBN 978-9941-36-272-9, Publish House of Iv. Javakhishvili Tbilisi State University, Tbilisi, Georgia, October 17-19, 2024, pp. 159 – 163. [http://www.openlibrary.ge/bitstream/123456789/10618/1/40\\_MM-180.pdf](http://www.openlibrary.ge/bitstream/123456789/10618/1/40_MM-180.pdf)
- [39] Beglarashvili N., Jamrlishvili N., Janelidze I., Pipia M., Tavidashvili Kh. Some results of analysis of heavy precipitation in Tbilisi on July 7, 2024 based on ground-level and satellite measurements. *Int. Sc. Conf. “Complex Geophysical Monitoring in Georgia: History, Modern Problems, Promoting Sustainable Development of the Country”*, Proceedings, ISBN 978-9941-36-272-9, Publish house of Iv. Javakhishvili Tbilisi State University, Tbilisi, Georgia, October 17-19, 2024, pp. 164 – 167. [http://dspace.gela.org.ge/bitstream/123456789/10617/1/41\\_MM-180.pdf](http://dspace.gela.org.ge/bitstream/123456789/10617/1/41_MM-180.pdf)
- [40] Tselashvili N., Biggs T., Ye Mu, Trapaidze V. Regional precipitation regimes and evaluation of national precipitation datasets against satellite-based precipitation estimates, Republic of Georgia. *Journal of Hydrometeorology*, Vol. 25, Iss. 4, 2024, pp. 591–600. <https://doi.org/10.1175/JHM-D-23-0116.1>
- [41] Elizbarashvili M., Amiranashvili A., Elizbarashvili E., Mikuchadze G., Khuntselia T., Chikhradze N. Comparison of RegCM4.7.1 Simulation with the station observation data of Georgia, 1985–2008. *Atmosphere*, ISSN: 2073-4433, 15, 369, 2024, 19 pp. <https://doi.org/10.3390/atmos15030369>
- [42] Elizbarashvili M., Elizbarashvili E., Kalmár T., Khuntselia T., Chikhradze N. Assessing regional climate model RegCM4.7.1: Insights from simulations in Georgia. *Geomate Journal*, 27(121), 2024 Sep 30, pp. 41-55.
- [43] Aliyev V., Pkhovelishvili M., Archvadze N., Gasitashvili Z. Hybrid risk review. *Int. Journal of Sustainability and Risk Control*, Baku, Azerbaijan, Vol.1, No 1(1), June 2025, pp. 12-23.
- [44] Amiranashvili A., Chelidze T., Dalakishvili L., Svanadze D., Tsamalashvili T., Tvauri G. Preliminary results of a study of the relationship between the monthly mean sum of atmospheric precipitation and landslide cases in Georgia. *Journal of the Georgian Geophysical Society*, ISSN: 1512-1127, *Physics of Solid Earth, Atmosphere, Ocean and Space Plasma*, v. 23(2), 2020, pp. 37 – 41.
- [45] Amiranashvili A., Chelidze T., Dalakishvili L., Svanadze D., Tsamalashvili T., Tvauri G. Preliminary results of a study of the relationship between the variability of the mean annual sum of atmospheric precipitation and landslide processes in Georgia. *Int. Sc. Conf. „Modern Problems of Ecology“*, Proc., ISSN 1512-1976, v. 7, Tbilisi-Telavi, Georgia, 26-28 September, 2020, pp. 202-206.
- [46] Chelidze, T., Tsamalashvili, T., Fandoeva, M. Mass-movement stationary hazard maps of Georgia including precipitation triggering effect: fuzzy logic approach. *Bull. Georg. Nat. Acad. Sci.*, vol. 16, no. 2, 56-63, 2022, [http://science.org.ge/bnas/t16-n2/07\\_Chelidze\\_Geophysics.pdf](http://science.org.ge/bnas/t16-n2/07_Chelidze_Geophysics.pdf)
- [47] Amiranashvili A., Chelidze T., Svanadze D., Tsamalashvili T., Tvauri G. Some results of a study of the relationship between the mean annual sum of atmospheric precipitation and re-activated and new landslide cases in Georgia taking into account of climate change. *Journal of the Georgian Geophysical Society*, e-ISSN: 2667-9973, p-ISSN: 1512-1127, *Physics of Solid Earth, Atmosphere, Ocean and Space Plasma*, v. 25(2), 2022, pp. 38–48. <https://openjournals.ge/index.php/GGS/article/view/5959>, DOI: <https://doi.org/10.48614/ggs2520225959>

- [48] Chelidze T., Amiranashvili A., Svanadze D., Tsamalashvili T., Tvauri G. Terrestrial and satellite-based assessment of rainfall triggered landslides activity in Georgia, Caucasus. *Bull. Georg. Nat. Acad. Sci.*, vol. 17, no. 2, 71-77, 2023, <http://science.org.ge/bnas/vol-17-2.html>
- [49] Amiranashvili A., Chelidze T., Svanadze D., Tsamalashvili T., Tvauri G. Study of the relationship between the mean annual sum of atmospheric precipitation and re-activated and new mudflow cases in Georgia. *Journal of the Georgian Geophysical Society*, e-ISSN: 2667-9973, p-ISSN: 1512-1127, *Physics of Solid Earth, Atmosphere, Ocean and Space Plasma*, v. 26(1), 2023, pp. 19–29. <https://ggs.openjournals.ge/index.php/GGS/article/view/6958>; DOI: <https://doi.org/10.48614/ggs2620236958>
- [50] Amiranashvili A., Chelidze T., Svanadze D., Tsamalashvili T., Tvauri G. Abnormal precipitation before the landslide in Akhaldaba (A Suburb of Tbilisi, Georgia) on June 13, 2015 according to radar measurements. *Journal of the Georgian Geophysical Society*, e-ISSN: 2667-9973, p-ISSN: 1512-1127, *Physics of Solid Earth, Atmosphere, Ocean and Space Plasma*, v. 26(1), 2023, pp. 30–41.
- [51] Amiranashvili A., Brocca L., Chelidze T., Svanadze D., Tsamalashvili T., Varamashvili N. Analysis of the precipitation regime that triggered the landslide in Nergeeti (Imereti, Georgia) on February 7, 2024. *Int. Sc. Conf. “Complex Geophysical Monitoring in Georgia: History, Modern Problems, Promoting Sustainable Development of the Country”*, Proceedings, ISBN 978-9941-36-272-9, Publish house of Iv. Javakhishvili Tbilisi State University, Tbilisi, Georgia, October 17-19, 2024, pp. 155 – 158. [http://dSPACE.gela.org.ge/bitstream/123456789/10619/1/39\\_MM-180.pdf](http://dSPACE.gela.org.ge/bitstream/123456789/10619/1/39_MM-180.pdf)
- [52] Varazanashvili O., Gaprindashvili G., Elizbarashvili E., Basilashvili, Ts., Amiranashvili A., Fuchs S. The First Natural Hazard Event Database for the Republic of Georgia (GeNHs). *Catalog*, 2023, 270 p. <http://dSPACE.gela.org.ge/handle/123456789/10369>; DOI: 10.13140/RG.2.2.12474.57286
- [53] Geological bulletins. 2016–2025, (in Georgian). <https://nea.gov.ge/c/Departments/Geology>
- [54] Amiranashvili A., Basilashvili Ts., Elizbarashvili E., Varazanashvili O. Catastrophic floods in the vicinity of Tbilisi. *Transactions IHM, GTU*, ISSN: 1512-0902, vol.133, 2023, pp. 56-61, (in Georgian), <doi.org/10.36073/1512-0902-2023-133-56-61>; <http://openlibrary.ge/bitstream/123456789/10337/1/133-11.pdf>; <doi.org/10.36073/1512-0902-2023-133-56-61>
- [55] Amiranashvili A., Elizbarashvili E., Gaprindashvili G., Varazanashvili O., Fuchs S. Assessment of the long-term risk of dangerous hurricanes on the territory of Georgia using data from 1961 to 2022. *Reliability: Theory and Applications*, ISSN 1932-2321, Special Issue № 6 (81), Part-2, Vol. 19, 2024, pp. 508 - 514. <https://doi.org/10.24412/1932-2321-2024-681-508-514>
- [56] Amiranashvili A., Elizbarashvili E., Gaprindashvili G., Varazanashvili O., Fuchs S. Statistical analysis of parameterized landslide data in Georgia from 1900 to 2022. *Reliability: Theory and Applications*, ISSN 1932-2321, Special Issue № 6 (81), Part-2, Vol. 19, 2024, pp. 812 - 818. <https://doi.org/10.24412/1932-2321-2024-681-812-818>
- [57] Pipia M., Amiranashvili A., Elizbarashvili E., Varazanashvili O., Beglarashvili N., Jamrshvili N. Variability in the number of days with hail in the warm half of the year on the territory of Georgia in 1941-2021. *Reliability: Theory and Applications*, ISSN 1932-2321, Special Issue № 6 (81), Part-2, Vol. 19, 2024, pp. 552 - 559. <https://doi.org/10.24412/1932-2321-2024-681-552-559>
- [58] Pipia M.G., Amiranashvili A.G., Elizbarashvili E. Sh., Beglarashvili N.G., Pipia G.G., Jamrshvili N.K., Varazanashvili O. Sh. Degree and areas of damage caused by hail in the territory of Kakheti region (Georgia). *Journal of International Scientific Publications: Agriculture & Food*, ISSN 1314-8591, vol. 12, 2024, pp. 54-60. <https://doi.org/10.62991/AF1996546926>
- [59] Pipia M.G., Amiranashvili A.G., Chikhladze V.A., Elizbarashvili E. Sh., Pipia G.G., Beglarashvili N.G., Varazanashvili O.Sh. Distribution of hailstorm areas in Kakheti region (Georgia) According to the diameter of hailstones in the clouds. *Journal of International Scientific Publications: Ecology & Safety*, ISSN 1314-7234, vol. 18, 2024, pp.103-108. <https://doi.org/10.62991/ES1996566836>
- [60] Hinkle D. E., Wiersma W., Jurs S. G. *Applied statistics for the behavioral sciences*. Boston, MA, Houghton Mifflin Company, ISBN: 0618124055; 9780618124053, 2003, 756 p.

**ატმოსფერული ნალექების წლიური და ნახევარწლიური ჯამის  
სტატისტიკური ანალიზი საქართველოს 59 მეწყრული  
საშიშროების ზონების მქონე მუნიციპალიტეტისთვის (11  
რეგიონი) 2015 - 2024 წწ.**

**ა. ამირანაშვილი, ლ. ბროკა, თ. ჭელიძე,  
დ. სვანაძე, თ. წამალაშვილი, ნ. ვარამაშვილი**

**რეზიუმე**

სტატიაში წარმოდგენილია საქართველოს იმ 62 მეტეოროლოგიური სადგურიდან ატმოსფერული ნალექების ჯამური წლიური და ნახევარწლიური მონაცემების სტატისტიკური ანალიზის შედეგები, რომლებიც განლაგებულია 59 მუნიციპალიტეტის (11 რეგიონის) ტერიტორიებზე, სადაც საშიში მეწყრული ზონები არსებობს. დაკვირვების პერიოდია 2015 წლიდან 2024 წლამდე. კერძოდ, მიღებული იქნა მუნიციპალიტეტების ტერიტორიებზე საშუალოდ გათვლილი ატმოსფერული ნალექების წლიური რაოდენობების განაწილების ემპირიული (რუკა) და გამოთვლითი მოდელები; შესწავლილი იქნა მუნიციპალიტეტებისა და რეგიონების ტერიტორიებზე საშუალოდ გათვლილი ატმოსფერული ნალექების ნახევარწლიური და წლიური რაოდენობების დამოკიდებულებები ტერიტორიის სიმაღლესთან, გრძედთან და ა.შ. მომავალში იგეგმება ამ ნაშრომის შედეგების გამოყენება ნალექებსა და მეწყრული პროცესების გააქტიურებას შორის კავშირის უფრო დეტალური შესწავლისთვის კლიმატური დროის მასშტაბში.

**საკვანძო სიტყვები:** ნალექი, კორელაციური და რეგრესიული ანალიზი, სტიქიური უბედურებები, მეწყრები.

**Статистический анализ данных о годовых и полугодовых суммах  
атмосферных осадков для 59 муниципалитетов (11 регионов)  
Грузии с опасными оползневыми зонами с 2015 по 2024 гг.**

**А. Амиранашвили, Л. Брокка, Т. Челидзе,  
Д. Сванадзе, Т. Цамалашвили, Н. Варамашвили**

**Резюме**

Представлены результаты статистического анализа данных 62 метеорологических станций Грузии, расположенных на территориях 59 муниципалитетов (11 регионов) Грузии с опасными оползневыми зонами о полугодовых и годовых суммах атмосферных осадков. Период наблюдений – с 2015 по 2024 годы. В частности, получены эмпирическая (карта) и расчетная модели распределения осредненных по территориям муниципалитетов годовых сумм атмосферных осадков; изучены связи осредненных по территориям муниципалитетов и регионов значений полугодовых и годовых сумм атмосферных осадков с высотой и долготой местности и др.

В дальнейшем предусмотрено использовать результаты данной работы для более детального изучения связи между осадками и активизацией оползневых процессов в климатическом масштабе времени.

**Ключевые слова:** атмосферные осадки, корреляционно-регрессионный анализ, природные катастрофы, оползни.

# Forest Cover – the Primary Guardian Against Climate Change and Biosphere Security

<sup>1</sup>Tsisana Z. Basilashvili, <sup>2</sup>Magda G. Janelidze, <sup>2</sup>Khatuna G. Basilashvili

<sup>1</sup>Institute of Hydrometeorology at the Georgian Technical University, Tbilisi, Georgia,

<sup>2</sup>Caucasus University, Tbilisi, Georgia

<sup>1</sup>e-mail: [jarjino@mail.ru](mailto:jarjino@mail.ru)

## ABSTRACT

*Due to ongoing global warming on our planet, the frequency of catastrophic natural disasters has increased, resulting in significant destruction and loss of life. In the 21st century, a further rise in temperature is expected, which will accelerate glacial melting, cause a sharp rise in sea levels, and lead to coastal flooding. Freshwater resources and agricultural productivity will decline. Desertification and other negative processes will intensify. Forest cover plays a critical role in climate regulation, oxygen balance stabilization, and biodiversity conservation. However, at present, widespread deforestation and forest fires are reducing forest areas worldwide, decreasing the process of photosynthesis. As a result, the excess thermal energy of solar radiation becomes a cause of global warming, reduced oxygen levels, and the emergence of new viral, bacterial, and chronic diseases. Today, to mitigate climate change and ensure the safety of the biosphere and the environment, all countries must pay special attention to the protection and expansion of forest cover. Everyone must contribute to forest restoration and afforestation. In agricultural fields, protective forest belts should be planted to help increase crop yields.*

**Key words:** desertification, global warming, crop yield, fresh water

## Introduction

One of the most pressing concerns of the global community today is the increasing frequency of catastrophic natural disasters driven by global warming. These anomalous and destructive events have resulted in extensive damage and significant loss of life. Additionally, as the global population continues to grow, so too does the demand for essential resources such as food, water, housing, energy, and technological goods.

The encroachment upon forested areas and the unsustainable cutting of trees have led to a decline in photosynthesis, which in turn reduces the Earth's ability to regulate solar radiation. This imbalance contributes to rising global temperatures, oxygen depletion, and the emergence of new viral, bacterial, and chronic diseases [1].

In the 21st century, a continued increase in global temperature is anticipated, which will accelerate the melting of Antarctic and Greenland ice sheets, cause a significant rise in ocean levels, and result in the flooding of coastal zones. These changes are expected to trigger profound economic and social disruptions, including crop loss, freshwater scarcity, more frequent flooding, intensified storms, and accelerated coastal erosion [2].

Given that climate change is a global phenomenon, addressing its consequences requires coordinated international efforts. To protect the biosphere and the environment, all nations must take action to mitigate the effects of climate change. Chief among these actions is the rational use of natural resources and the preservation of ecological balance. In this context, forest cover plays a crucial role in climate regulation, stabilization of the oxygen cycle, and the maintenance of biodiversity.

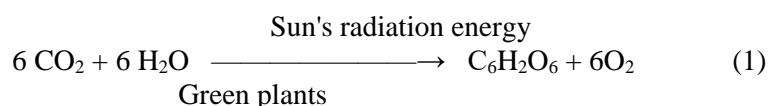
## Study Area and Method

Forests are a vital component of the biosphere, consisting of a complex and dynamic system of trees, shrubs, herbs, animals, birds, and microorganisms that are interdependent and collectively influence both the environment and each other. Forest ecosystems play a critical role in atmospheric processes, geological formations, and the development of essential natural resources, including soil, water, wildlife, minerals, energy, and recreational areas. Furthermore, forests are of significant economic importance, serving as sources of raw materials for various industries. Timber is widely used for construction and energy, while forests also provide food, medicinal products, and materials such as paper, cardboard, furniture, and flooring. Globally, over 15,000 types of products are derived from trees. The rapid growth of the world's population and advances in technology have dramatically increased the demand for forest resources [3].

This study is based on the analysis of historical, informational, and literary sources related to forest ecosystems and their ecological functions.

## Vegetation – The Origin of Life on Earth

In the early history of the planet, Earth's atmosphere contained very little oxygen and was primarily composed of carbon dioxide, methane, and nitrogen compounds. Around three billion years ago, the first life forms appeared in the shallow regions of the hydrosphere, where sunlight and warmth could reach. These conditions resembling those found in modern tropical zones allowed green plants to absorb carbon dioxide and, using chlorophyll and solar energy, synthesize carbohydrates while releasing free oxygen. This process, known as photosynthesis, enables the conversion of inorganic environmental components into organic matter. The general equation for photosynthesis is as follows [4]:



Here, carbon dioxide and water molecules are diluted, and glucose molecules are formed during their combination, after which free oxygen is released.

The first species of the earliest times were the blue-green seaweeds, which transformed solar energy into chemical energy that contributed to the growth and development of the plant and its fruit. Scientists estimate that, annually, more than 10 billion kcal of solar radiation falls per hectare on Earth, which is used by plants for photosynthesis [5]. Each year, due to the effect of solar energy, approximately 83 billion tons of organic substances are formed on Earth. Of these, 53 billion tons are created on land and the rest in seas and oceans. It is noteworthy that plants accumulate only 0.3% of solar energy. As a result of photosynthesis, the quantity of carbon dioxide in the atmosphere was reduced to 0.03%, and the amount of free oxygen increased to 21% or by 1,000 times [4].

According to F. Ramad [6], 2 billion years ago, the first organisms capable of photosynthesis emerged (prokaryotes: blue-green plants, bacteria, viruses). After 0.5 billion years, higher organisms (eukaryotes) appeared. Consequently, 1 billion years ago, the oxygen content in the atmosphere reached 1% of its current level. Phytoplankton increased, and due to the intensity of photosynthesis, a form of oxygen gas atmospheric ozone was created, which blocked the harmful effects of the sun's ultraviolet rays. This contributed to the development of organic life, first in the upper layers of water, then on land.

Millions of years later, various species of plants evolved, becoming the primary source of food for animals and humans [7]. The vegetation on Earth annually assimilates around  $5 \times 10^{10}$  tons of carbon, absorbs  $1.8 \times 10^{11}$  tons of carbon dioxide, decomposes  $1.3 \times 10^{11}$  tons of water, releases  $1.2 \times 10^{11}$  tons of molecular oxygen, and collects  $4 \times 10^{17}$  kcal of solar energy [8].

It is estimated that 50–60% of oxygen is released by land vegetation, with the remainder produced by phytoplankton. One hectare of forest, in one hour, absorbs as much carbon dioxide as 200 people exhale in the same time. Over one year, one hectare of mixed forest absorbs 15 tons of carbon dioxide and releases 13 tons of oxygen.

The amount of oxygen used by humans depends on physiological condition, age, weight, and sex. In medicine, it is known that a person at rest uses 0.35–0.40 liters of oxygen per minute and about 5 liters per minute during physical work. A person needs 500–600 liters of oxygen per day; therefore, the forest area per person should be at least 0.3 hectares [7].

About 600 million years ago, the earliest autotrophic plants emerged; 500 million years ago plants and insects; 350 million years ago angiosperms and mammals. The development of chlorophyll-containing plants on land, along with the increase in oxygen, contributed to soil formation. Later, due to the increased amount of oxygen, a wide variety of flora and fauna, including humans, developed on Earth. The existence of the biosphere before the origin of humans is called biogenesis, while the stage of societal development is referred to as noogenesis.

Currently, there are about 2 million species of plants and animals, including up to 1.5 million animal species. Among plants, angiosperms rank first in number about 300,000 species; mushrooms are second about 100,000 species.

Although trees comprise less than 1% of all plant species, they constitute nearly 90% of the land's phytomass and account for 64% of its productivity [9]. Among animal species, insects rank first with up to 1 million species; mollusks are second with up to 100,000, followed by vertebrates with up to 50,000 species [4].

In the Bible, it is stated that during the seven-day creation of the universe, among many wonders, God created forests on the third day and brought the axe to all barren trees thereby defining the right to use timber. Yet forests are mercilessly destroyed by people.

## **Forest, Its Impact and Importance**

Vegetation cover serves as a vital source of oxygen, food, and energy, making the survival of humans and animals heavily dependent on the state of forest ecosystems. As the global population continues to grow, so does the demand for food, water, housing, energy, household goods, mobile devices, and other resources. The expansion into forested areas and the unsustainable cutting of trees reduce the rate of photosynthesis, leading to increased solar radiation, contributing to global warming, and causing a decline in atmospheric oxygen levels.

**Forest as a Factor in Climate Formation.** The importance of the forest is first revealed in the regulation of air elements (air temperature, humidity, wind speed, etc.), which directly affect human health. For example, in summer, temperatures in treeless areas are relatively 3–5°C higher, which results in an accelerated pulse, overheating of the body, and decreased working capacity. Dry air in areas lacking forest also causes dryness in the mouth, throat, and nose, and reduces the body's anti-infective capabilities. High wind speeds in treeless areas negatively affect breathing, blood circulation, and the nervous system.

Thus, the most comfortable conditions for rest and rejuvenation are created in the forest. Furthermore, the beauty and attractiveness of natural forest landscapes have a positive impact on mental health, mood, working ability, and spiritual well-being.

**The Sanitary-Hygienic Role of the Forest.** In cities, industrial centers, and other settlements, atmospheric air is regularly polluted by harmful chemical contaminants. In such environments, forests play a crucial role in protecting and improving sanitary and hygienic conditions. Tree and plant emissions contain aromatic essential substances phytoncides that can eliminate many microbes and viruses, purifying and improving air quality. As a result, bacteria and microbes are significantly reduced in forests. For example, 1 m<sup>3</sup> of forest air contains up to 500 pathogenic bacteria, while 1 m<sup>3</sup> of city air contains around 36,000. It is estimated that land vegetation releases 175 million tons of aromatic oils annually.

**Forest as a Filter.** In our era, the lower layers of the atmosphere, in addition to carbon dioxide, are increasingly contaminated with harmful chemical and mechanical impurities. Dust reduces the sun's ultraviolet radiation, lowers air transparency, and alters the ionization level. A person breathes about 20 m<sup>3</sup> of air overnight, and if the air is dusty, it can lead to numerous illnesses, such as poisoning, asthma, nasal mucosal atrophy, and erosion. The forest acts as a strong air filter. It is estimated that 1 ha of forest filters 50–70 tons of dust annually. In this regard, specific forest types are especially effective: beech coppices filter about 68 tons per hectare, oak 56 tons, pine 36 tons, and spruce 32 tons [10].

**Forest and Technogenic Pollution.** Today, large-scale technologization has led to the accumulation of harmful chemical substances in nature. The contamination of air, water, and soil with various pollutants has reached levels that threaten life, including forests, in many parts of the world, leading to the desiccation of large forest areas. Experiments have identified plants capable of removing air pollution (detoxification). Oleaster, ash, acacia, oak, plane tree, maple, and willow are particularly resistant to harmful gases, whereas pine is more vulnerable.

**Forest and Noise.** Forests also play an important role in absorbing various kinds of noise, which depends on the composition, structure, frequency, and diversity of tree species. Multi-layered, dense forests

are characterized by high noise absorption. For example, in a forest copse with a high absorption radius (0.8), noise from a source such as a highway is reduced by 30 decibels at a distance of 80–100 meters [11].

**Forest and Yield.** Forests have a significant influence on agricultural crop cultivation. With forest cover, crop yields can increase by 20–25% (Armand, 1964). The importance of forests is clearly illustrated in data showing that each hectare of forest strip protects 30–40 hectares of farmland, increasing grain yields by 2–3 quintals per hectare. From such protected areas, an additional 60–80 centners of crops can be harvested, and within 8–10 years, the costs of forest strip construction are fully compensated. The positive impact of forest strips is especially evident during drought periods. As the saying goes: "The forest produces water, the water produces a harvest, and the harvest produces life."

**Water Management and Protective Functions of Forests in Mountain Regions.** Forests provide natural habitats and essential conditions for life on Earth. In mountainous regions, forests serve as vital protection against various natural disasters. A portion of atmospheric precipitation infiltrates the soil, feeding rivers throughout the year. The higher the seepage rate into the soil, the lower the risk of floods and soil erosion. Thus, forests perform both watershed and protective functions.

In mountain areas, the importance of forests is especially significant, as they possess all the multifunctional roles described above along with additional protective benefits. Forests in mountains regulate river flow. According to statistical observations, high-frequency (>0.8) mountain forests are the main factor facilitating the deep infiltration of precipitation into the soil, thus managing surface runoff, improving water balance, and preventing river desiccation [13]. Most importantly, forests protect populated areas, roads, fields, and soils from dangerous events such as floods, mudflows, landslides, avalanches, and erosion [14].

## Ecosystems of the Biosphere

The word *bios* means life in Greek. The biosphere is a combination of living and non-living substances in dynamic equilibrium, where living organisms transform the environment in accordance with their needs. The history of the biosphere's development spans 2.5–3 billion years. During this time, living organisms have developed under various environmental conditions. For example, some single-celled seaweed and bacteria grow in hot springs at temperatures up to 75–100°C; others, by contrast, survive at -6 to -7°C, and mushroom spores can endure 120–180°C [9]. Thus, the biosphere is the layer of Earth where life exists and develops. It includes the entire hydrosphere, lithosphere, and parts of the atmosphere.

The **hydrosphere** is Earth's watery layer. The World Ocean covers 7/10 of Earth's surface and supports life down to depths of 100–200 meters, where sunlight can reach. Only bacteria can survive at greater depths [2].

The **lithosphere** is the solid layer of the Earth, where life typically exists up to a few tens of centimeters. Some organisms live at depths of 2–3 km on land and 1–2 km beneath the ocean floor. The simplest anaerobic bacteria live in underground aquifers and oil-bearing layers at depths of 3–5 km.

The biosphere ecosystem includes plants, animals, microorganisms, and the non-living components of the environment. The main biomes of the biosphere are land, marine, and freshwater biomes [7].

The upper boundary of the biosphere reaches 6 km in the atmosphere, where only chlorophyll-containing plants exist. Above this, only some arthropods survive, feeding on pollen, spores, and microorganisms carried by the wind [8].

**Atmosphere.** The atmosphere is the gaseous layer surrounding Earth and consists of various gases, water vapor, and dust. It includes the following layers by altitude:

- Troposphere (8–18 km)
- Stratosphere (up to 55–60 km)
- Mesosphere (up to 80–85 km)
- Thermosphere (up to 1,000 km)
- Exosphere (above that)

The **troposphere**, which contains 90% of the atmospheric air mass and 0.5–4% water vapor, extends to 8–10 km at the poles and 16–18 km at the equator. Here, air temperature decreases by 5°C per kilometer of altitude. The troposphere fully transmits short-wavelength solar radiation and absorbs Earth's long-wavelength radiation, which excites the surface layer.

The **stratosphere**, a 40–60 km thick layer above the troposphere, contains dry, rarefied air. In summer, the temperature rises from 0 to 15°C; in winter, from -10 to -5°C [4]. At 20–30 km altitude, this layer contains ozone a form of oxygen that absorbs a large portion of the sun's ultraviolet radiation, which would otherwise destroy living organisms. Thus, the ozone layer is considered Earth's protective shield [5].

The **mesosphere** is 20–25 km thick, with temperatures dropping in summer to  $-80^{\circ}\text{C}$  and in winter to  $-100^{\circ}\text{C}$ . Due to strong turbulence, wind speeds can exceed 50–100 km/h.

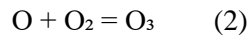
In the **thermosphere**, starting at 80 km altitude, temperature increases by  $5^{\circ}\text{C}$  per kilometer and can reach  $2,000^{\circ}\text{C}$  at 1,000 km. Any object, including meteors, entering at 100–130 km/h burns up as it descends into the mesosphere (around 80 km deep).

The **exosphere** extends for thousands of kilometers, with temperature rising by  $1^{\circ}\text{C}$  per kilometer. Spacecraft fly in this zone, and radio communication is possible here.

Near Earth's surface, dry air consists of 78% nitrogen, 21% oxygen, 0.9% argon, 0.03% carbon dioxide, and 0.1% other gases, with ozone at  $10^{-6}$ . This composition remains constant up to 90–100 km and is called the homosphere. Above 200 km, nitrogen dominates; from 600 km, helium; and from 2,000 km, hydrogen.

The atmosphere absorbs some cosmic rays and most meteorites. Only 48% of solar radiation reaches Earth. Without the atmosphere, the average surface air temperature would be  $23^{\circ}\text{C}$  instead of  $15^{\circ}\text{C}$  [9]. Nearly half of the sun's energy is used for water evaporation, which returns as precipitation.

**Ozone Layer and Its Change.** Ozone is a blue gas whose molecule ( $\text{O}_3$ ) consists of three oxygen atoms. It forms when ultraviolet radiation splits an oxygen molecule, and the resulting atoms bond with other  $\text{O}_2$  molecules [11]:



There is "bad ozone" and "good ozone." Scientists call "bad ozone" the photochemical smog found in the lowest atmospheric layer, the troposphere. At certain concentrations, it is hazardous to human health: it irritates the upper respiratory tract, causes vegetative disorders, pulmonary edema, dizziness, cataracts, etc. This "bad ozone" accounts for only 10% of Earth's ozone; the remaining 90% is "good ozone."

"Good ozone" is found in the stratosphere and protects Earth from harmful ultraviolet radiation. Ozone concentration varies by altitude: 60% is located between 16–32 km, with the highest concentration around 25 km. This forms Earth's protective ozone layer, about 3.5 mm thick, which makes the planet suitable for human life. The ozone absorbs a large portion of ultraviolet radiation, which would otherwise destroy living organisms. Thus, the ozone layer is considered the biosphere's protective shield [5].

Ozone levels in the stratosphere depend on geographic location, altitude, and season. Solar radiation and interactions with oxygen, nitrogen, hydrogen, chlorine, and bromine cause ozone breakdown. A key reason for this is the use of chemical compounds especially Freons ( $\text{CFCl}_3$  and  $\text{CFCl}_2$ ) formerly used in refrigerators and air conditioners.

As a result, the ozone layer has thinned by half in many regions, and in the Arctic during summer and the Antarctic during winter, actual holes have formed. Further ozone layer degradation allows more ultraviolet radiation to penetrate the atmosphere, severely affecting living organisms, climate, and increasing natural disasters.

In 1996, factories producing ozone-depleting substances were closed, resulting in a 34% reduction in the ozone hole by 2014.

According to recent information, the ozone layer is expected to recover by 2030 in the Northern Hemisphere, by 2040 in the Southern Hemisphere, and by 2050 at the Earth's poles. It is also noteworthy that since the 1950s, space has accumulated a large amount of debris around 25,000 objects of varying sizes, from small particles to entire spacecraft. These objects move at speeds of approximately 25,000 km/h, and a collision with any spacecraft could result in a catastrophic event.

## Climate warming factors and changes

Global warming is the process of the rapid increase in the average annual temperatures of Earth's atmosphere. Scientists propose two different explanations for this phenomenon. According to the first version, it is a periodically recurring natural cataclysm linked to solar activity. This activity determines 11-year, 22-year, and 80–90-year cycles of solar intensity. The current global warming is likely associated with an increased rate of solar radiation, which may eventually decrease.

The second version attributes Earth's warming to human-induced (anthropogenic) activity, which traps heat radiation reflected from the Earth's surface due to the accumulation of certain gases in the atmosphere. Notable among these gases are carbon dioxide, methane, nitrogen monoxide, ozone, and freons (halogenated hydrocarbons). These gases allow solar rays to pass through to Earth but trap the heat reflected back from the surface [15].

Between 1880 and 1930, the average annual air temperature increased by  $0.5^{\circ}\text{C}$ . From 1940 onward, the trend alternated between increases and decreases, but since the 1960s, the temperature has risen steadily [16].

Over the past 1.5 centuries, with technological development, the concentration of carbon dioxide (CO<sub>2</sub>) in the atmosphere has increased by one-third, while methane (CH<sub>4</sub>) has increased 2.5 times. Methane is 20–25 times more effective than carbon dioxide at trapping heat.

The rise in methane is linked to pipeline and bog leakage and livestock. Methane is produced by special bacteria in the stomachs of livestock and released from their dung, which is also used as fuel. The 1.5 billion cows on the planet emit 18% of greenhouse gases more than the entire transport sector. This is why eco-activists worldwide promote vegetarian diets, arguing that without livestock, such problems would not exist. One-third of atmospheric methane is generated by livestock [15].

The increase in carbon dioxide is associated with industrial development, and the burning of wood and coal. Each year, humanity burns 4.5 billion tons of coal and 3.2 billion tons of oil, gas, peat, and other fuels. Carbon dioxide emissions rise especially from cars and aircraft. Outdated vehicles and poor-quality fuel are among the main sources of harmful substances.

Due to industrial activity, it is estimated that 27 billion tons of carbon dioxide are released into Earth's atmosphere annually. Its atmospheric concentration has increased by 38%. Of this, 30% is absorbed by the world ocean, 13% by the biosphere and soil, while 57% remains in the atmosphere, contributing to further warming. Since the beginning of the industrial era, the atmosphere has accumulated 770 billion tons of anthropogenic carbon dioxide.

Through photosynthesis, 1 hectare of forest absorbs 5–10 tons of carbon dioxide and releases 10–20 tons of oxygen. The thermal energy of solar radiation falling on 1 hectare of land annually is about 10 billion kcal, 93.8% of which is absorbed by green vegetation [18].

The excessive emission of harmful gases from anthropogenic activities contributes to the expansion of the ozone layer in the atmosphere, a very dangerous phenomenon for living organisms and directly related to global warming. These effects intensified with the advancement of space technology. It is estimated that the launching of space missiles damages and disrupts the ozone layer, leading to increased solar radiation and temperature.

## World Forest Cover

**Forest Cover in the Past.** The oldest known vegetation cover is found in Australia and is estimated to be around 395 million years old. Approximately 370 million years ago, plant life began to take the form of shrubs. Early forests were relatively low, with the tallest trees reaching about 7.5 meters and consisting mainly of primitive ferns. Around 345 million years ago, at the onset of the Stone Age, dense and widespread forests emerged, composed of trees of varying heights and early seed-bearing plants.

By 280 million years ago, under dry climatic conditions, primitive conifers had become widespread. Sequoia trees and flowering seed plants appeared around 225 million years ago. Between 135 and 65 million years ago, the ancestors of today's rubber trees, magnolias, oaks, willows, and maples became dominant.

During the Paleogene period, forests in the Northern Hemisphere began to resemble the modern tropical and temperate forests. Arctic-type flora prevailed in the far north, while tropical vegetation expanded near the equator during the Tertiary period.

In the Neogene period's dry climate, forest coverage declined, and grasslands spread across many regions. Coniferous plants became dominant. The Quaternary period, which began 1.8 million years ago and continues to the present day, has been marked by alternating glacial and interglacial periods, resulting in significant forest reduction [19].

**Forest Cover in the Epoch of Civilization.** Over the past 800,000 years, humans have eliminated around 50% of the world's forest area. These lands have been converted into croplands, pastures, settlements, and other uses. Several hundred years ago, global forest area was approximately 7.2 billion hectares, covering 48% of the Earth's land surface. Today, vegetation covers 12.2 billion hectares, of which 4.1 billion hectares are forests. Only 3.8 billion hectares are covered by trees, while the remainder consists of bushes, marshes, and rocky terrain. 75% of this forest loss occurred in the 20th century, during a period of global demographic explosion. Additionally, 80% of existing forests have been altered by the introduction of cultivated trees [19].

According to FAO estimates (Table 1), in 2015 forests covered 4,000 million hectares of land, or 31% of Earth's total area. Another 1,488 million hectares included sparse forests, bushes, and roadside trees, which are not officially categorized as forests. The world's forests are home to nearly 30,000 species of trees and shrubs, along with thousands of animal and bird species.

In the early 20th century, there were about 2 hectares of forest per person. By 2015, this figure had decreased to only 0.6 hectares per person. The total biomass of living forests is 1,509 billion tons, of which 25% (377 billion tons) consists of roots, leaves, and fruits, and the remaining 1,132 billion tons is timber. Global timber reserves amount to 360 billion cubic meters, with an annual increment (productivity) of 3,200 million m<sup>3</sup> [10].

FAO's regular forest inventories show that forest area has been declining rapidly:

- From 1990 to 2000: 16 million hectares lost annually
- From 2000 to 2010: 13 million hectares lost annually
- From 2010 to 2015: 16.5 million hectares lost in total, or 3.3 million hectares annually

In 2016, 29.7 million hectares of forest were destroyed.

Forest destruction is increasing geometrically each year. Beyond logging, forests are lost due to land-use conversion (to agriculture, towns, roads, etc.). Natural disasters such as landslides and avalanches also destroy forests, and in many cases, tree regrowth does not occur.

According to *National Geographic*, 80,000 m<sup>2</sup> of green cover is damaged annually, causing not only economic losses but also human casualties. For example, forest fires in Indonesia resulted in 100,000 deaths. In 2017, about 100 people died in forest fires in California, Portugal, and Spain. Particularly devastating fires occurred in California in November 2018, where over 70 people died, 1,400 went missing, up to 100 hectares of forest were burned, and around 80,000 homes were destroyed.

It is important to note that during such fires, in addition to human casualties, a significant number of animals and other living beings that inhabit forests also perish.

Wildfires also devastate biodiversity, killing countless forest-dwelling species alongside human populations.

Table 1. Areas of the world forest and their dynamics

Region	Common area, mln ha	Forests of local species, mln ha	Forest, % from the total area	Dynamics of forest areas, mln ha		
				Change of forest area 2010 - 2015		Forest Plant Area 2015
				Total	Annual	
World	3999	1277	31	- 17	- 3,0	290
Africa	624	135	23	- 14,2	- 2,4	16
Asia	593	117	19	- 3,4	0,8	129
Europe	1015	277	34	1,9	0,3	82
North America	751	320	33	0,4	0	43
South America	842	400	49	- 10,1	- 2	15
Oceania	174	27	23	1,5	0,3	4

In addition, fires cause excretion of excessive carbon in the atmosphere, which negatively affects water quality, forest structure, and biodiversity.

With the destruction of forest from the beginning of XXI century, forest cover will be increased by artificial forest (3,3 million hectares) or naturally restored forest (27 million ha a year). From 2000 to 2010, forest area in Asia grew by 2,2 million ha, mainly due to the intensive cultivation of forest in China. Forest areas in Europe have grown annually by 700 thousand ha.

## Forest Cover of Georgia

**Forest Layout and Composition.** Georgia is located in the southwestern Caucasus, where the climate and landscapes are diverse: from wet sea subtropics in the west, to steppe-continental in the south, and constant snow and glaciers in the highlands of the north. Mountain slopes in Georgia were historically covered with dense forests, which produced many varieties of fruits and hosted numerous species of animals

and birds. For this reason, Georgian peasants relied on the forest for sustenance, protection, and livelihood. Thus, the forest industry was established early on in Georgia.

Forest cover begins at the seashore and extends up to 2100–2200 meters, and in some cases, up to 2500 meters above sea level. In 2010, Georgia's total forest fund amounted to 3,007.6 thousand hectares, representing 43.2% of the country's territory, though it is distributed unevenly: 58% in the west and 42% in the east. About 73% of forests are located at elevations above 1,000 meters, and more than 80% are spread over slopes steeper than 20°. Of the state forest fund, 2,770 thousand hectares are covered with forests, and 86 protected areas encompass 600 thousand hectares [20].

Georgia's forests include coniferous and deciduous, evergreen and deciduous trees, shrubs, giant trees (up to 60 meters tall and 2 meters in diameter), lianas, parasitic plants, mushrooms, fruits, berries, and plants used for medicinal and technical raw materials. Many relic and endemic plant species are found here. Of the 400 types of woody plants, 61 are native to Georgia, and 43 are endemic to the Caucasus. In the forest composition, conifers account for 16%, hardwood deciduous trees 68%, softwood deciduous trees 7%, and other species 10%. Notable species include the giant Caucasian fir (70 m tall and 2.5 m in diameter) and the eastern beech (50 m tall and 2 m in diameter), which are considered extraordinary for the temperate climate zone. Chestnut, oak, maple, zelkova, walnut, box-tree, and other valuable timber species are also prominent [21].

In the high mountain valleys and hard-to-reach gorges, untouched forests (566 thousand hectares) still remain. According to World Bank experts, there are few countries in Europe where natural landscapes of such unique beauty are so seamlessly complemented by ancient cultural landscapes. It is noteworthy that Georgia's forests serve as a refuge for pre-Ice Age flora and fauna relic species that link us to ancient geological epochs. The loss of these forests would be a great tragedy not only for Georgia but for all of humanity.

**Forest Resource Potential of Georgia.** Forest resources are very important in terms of the average forest characteristics: age 98 years, height 22 m, diameter 36 cm, Bonita III, frequency 0.54. Timber supplies 1 176 m<sup>3</sup> per hectare, ripe and overripe copse 244 m<sup>3</sup>, coniferous 288 m<sup>3</sup>. Forest's total timber reserves are more than 535 million m<sup>3</sup>. But, 66% of reserves are in the unattainable zone, where the slope incline is greater than 25 °C [22].

In addition to timber, more than 150 forest plant species produce fruits, berries, nuts, and other resources, the utilization of which could make a significant contribution to economic development. More than 110 plant species are used in medicine. Two-thirds of Georgia's 48 medicinal and 200 recreational resorts are located in or surrounded by forests. Their existence in the forest is also aesthetically justified. As a result, ecotourism and resort-recreational farming are well developed in Georgia. Furthermore, the potential for hunting tourism in Georgian forests is also considerable.

## Results of Anthropogenic Impact on Forests

No one disputes the great importance of green forest cover, but the proper attention it deserves is still lacking. The main reason is the enormous increase in demand for forest resources due to population growth and technological advancement. As a result, the extraction and use of forest resources worldwide increase annually. Such an approach leads to forest destruction, particularly in tropical and coniferous (taiga) regions. It is noteworthy that forest exploitation has not only affected vegetation but also led to the reduction of unique species of animals and birds.

The consequences are particularly severe in mountainous areas, where deforestation alters river water regimes, increases catastrophic floods and torrents, and intensifies erosive and landslide processes, soil and rock erosion, and the evolution of snow and glaciers [23].

In addition, trees are often cut not only in forest coppices but also in urban areas and planting strips. This results in a decrease in oxygen production and the loss of water retention and catchment functions, causing the drying up of springs, rivers, and lakes. Areas that are no longer forest-covered begin to desertify, which is accompanied by a decline in food production [24].

Thus, the reduced green cover can no longer effectively absorb and regulate solar thermal energy. This leads to an increase in atmospheric carbon dioxide and intensifies climate warming. Consequently, ecological disasters become more frequent, resulting not only in environmental destruction but also in the loss of human and animal lives.

The accumulated excess of harmful gases resulting from anthropogenic activities returns to Earth in the form of acid rain and radioactive compounds. Sources of acid precipitation (rain, snow, fog) include the

burning of fuel and biomass, metallurgy, motor transport, and other industrial activities. Over the past 100 years, the acidity of precipitation has increased significantly.

Acid precipitation negatively affects ecosystems, as such water harms fish eggs and phytoplankton, thereby reducing aquatic species in reservoirs. Additionally, acid rain causes corrosion of machinery, buildings, and cultural artifacts. Plants are also affected, exhibiting leaf loss and root rot. In the 1990s, damaged forest areas reached 50% in Germany and the Netherlands, 35% in Switzerland, 30% in Austria, and 600,000 hectares in Russia [4].

Thus, the cosmic ecological function of forests is being weakened. It is estimated that the cosmic environmental value provided by forest green cover exceeds the material revenue from forest resource use by 3 to 5 times.

## **Conclusions and Recommendations**

The forest is a complex ecosystem of trees, plants, and living organisms, which, along with water, air, and soil, guarantees the preservation of the cosmic, ecological, economic, and sustainable environment of the Earth's biosphere. The forest absorbs carbon dioxide and releases large amounts of oxygen, and it regulates the microclimate (humidity, temperature, and wind). It is a powerful filter for purifying air and water from harmful impurities and is characterized by antimicrobial, ionizing, and sterilizing properties. By doing so, it creates a healthy and friendly environment that benefits humans and other living organisms. Forests also provide various types of food and medicinal products. Therefore, the forest is a crucial factor in improving environmental sanitation and hygiene conditions with a broad spectrum of biodiversity, earning it the name "green lungs."

In addition, forests protect agricultural lands and populated areas from strong winds. They are also a key factor in regulating water resources, improving groundwater quality, and increasing water retention. In mountainous areas, forests protect communities, roads, and farmlands from floods, mudflows, erosion, landslides, and avalanches. Forests also contribute to increasing agricultural yields.

Forests are of great importance in agriculture, not only for their protective role but also as a source of raw timber, which is used in various industries. With the increase in population and farming activities, the demand for timber continues to grow. As a result, forests are being cut down, and forest areas are reduced by 0.3% annually worldwide. In the last decade, approximately 25,000 plant species and over a thousand animal species have become extinct. This has been caused not only by technological development but also by an exploitative approach toward forests. A portion of society sees nature as a resource to be used for profit even at the cost of environmental degradation. Such attitudes are causing the destruction of forests.

In addition to logging and disease, forests are also damaged by fires, which have become increasingly frequent in various countries due to human negligence and climate warming. It is important to note that fire prevention is much more cost-effective than dealing with the aftermath yet this principle is often neglected. As a result of these factors, the world's diminishing green cover is no longer able to regulate solar thermal energy. Consequently, atmospheric oxygen levels decrease, carbon dioxide levels rise, and the climate heats up rapidly.

According to expert assessments, global warming will continue throughout the 21st century, and Earth's temperature may rise by 2–4°C, which would cause severe damage to ecosystems and the economies of many countries. Thus, while technological progress improves human well-being on one hand, it threatens the future on the other. The processes of self-purification, self-regulation, and self-restoration are weakening not only in individual ecosystems but on a planetary scale.

Today, protecting nature and using its resources rationally is a matter of vital human importance. It is a necessary precondition for the existence of the biosphere. Therefore, all countries must prioritize the protection and expansion of forest cover. The population and local administrations in every settlement must take responsibility for the care and restoration of their forests. Beneficial plant varieties should be selected for reforestation, and selective cuts should be limited to the annual growth increment to ensure natural regeneration. Protective forest strips should be planted in agricultural fields to increase yields. To ensure the rational use of forest resources, production and processing must be conducted using complex, non-waste technologies.

To protect forest biodiversity in the long term, a system of biomonitoring should be established, along with timely forest restoration and effective management. It is necessary to develop long-term programs for the sustainable use of forest resources, aiming to improve both forest productivity and qualitative composition. The comprehensive use of timber including the introduction of advanced processing techniques

and non-waste technologies and the creation of protected areas are crucial for preserving biological and landscape diversity.

Finally, public awareness about nature and its rational use must be raised. Proper education and the fostering of a love for nature among young people can help save the biosphere and the natural environment, ultimately contributing to global ecological balance and economic prosperity.

## References

- [1] Basilashvili Ts. The importance of forest and results of anthropogenic impact on the mountainous areas. Actual problems of Geography. TSU, Tbilisi, 2019, pp. 123-125.
- [2] Basilashvili Ts. Modern challenges of biosphere safety. In: Science and Technologies. No.3 (723), Tbilisi, 2016, pp 36-46, (in Georgian).
- [3] Basilashvili Ts. The role of forests in the development of the biosphere in the context of global warming. In: Science and Technologies, No.1 (721), Tbilisi, 2016, pp 15-23, (in Georgian).
- [4] Qajaia G. Ecological principles of environment protection. Tbilisi, Intelekti, 2008, 272 p.
- [5] Budiko M. Radiation factors modern climate changes. In: News Academy of Sciences of the Soviet Union. No.5, 1965, pp 17-22, (in Russian).
- [6] Ramad F. Foundations of applied ecology. Moscow, Gidrometeoizdat, 1981, (in Russian).
- [7] Dre F. Ecology. Moscow, Atomizdat, 1976, (in Russian).
- [8] Eliava I, Nakhutsrishvili G, Qajaia G. Foundations of Ecology. Tbilisi, 1992, (in Georgian).
- [9] Miqadze I. Ecology. Tbilisi, 2006, (in Georgian).
- [10] Kandelaki T. Forests resources of Georgia. In: Science and Culture. v. II, 2013, pp. 91-109.
- [11] Zhorzholiani T, Gorgadze E. Medical Ecology. Kutaisi, 2008, 372 p., (in Georgian).
- [12] Iashvili N. Soil resources and their rational utilization. Tbilisi, 158 p., (in Georgian).
- [13] Kharashvili G. Water control and antierosion role of mountain forests of Georgia. In: Erosion-debris flows phenomena and some adjacent problems. Tbilisi, 2001, pp 237-241, (in Georgian).
- [14] Basilashvili Ts. Forest Cover – Main protect of various disasters in mountainous areas. “Natural Disasters, in the 21<sup>st</sup> century: Monitoring, Prevention, Mitigation” Tb., 2021, pp. 189-193.
- [15] Tkemaladze G. Biochemical fundamentals of protecting the world from global warming. In: Global warming and agrobiodiversity. Tbilisi, 2015, pp. 32-41, (in Georgian).
- [16] Elizbarashvili E, Tatishvili M, Elizbarashvili M, Meskhia R, Elizbarashvili Sh. Climate change in Georgia under global warming conditions. Tbilisi, Zeon, 2013, 128 p., (in Georgian).
- [17] Buchkovska V, Evstafieva J, Sayenko V. The problem of heat stress in livestock production and global warming. In: Global warming and agrobiodiversity. Tbilisi, 2015, pp. 386-387, (in Russian).
- [18] Aress P. Spring of ecology. Leningrad, Gidrometeoizdat, 1982, (in Russian).
- Armand, 1964 – Armand D. To us and grandchildren. Moscow, Gidrometeoizdat, 1964, (in Russian).
- [19] Les [Forest], [Resource of electronics]. URL: <https://ru.wikipedia.org/wiki/лес>, (in Russian).
- [20] Geography Atlas of Georgia. Tbilisi, Palitra, 2018, 183 p., (in Georgian).
- [21] Gigauri G. In: Forests of Georgia, Tbilisi, 2004, pp 35-65, (in Georgian).
- [23] Basilashvili Ts., Berdzenishvili N. Forest is a factor of environmental safety. Modern Problems of Ecology. Vol. VII, 2020, pp. 60-63, (In Georgian).
- [24] Basilashvili Ts. Forest and problems caused by global warming. In: Global warming and agrobiodiversity. Tbilisi, 2015, pp 75-78, (in Georgian).

## ტყის საფარი - მთავარი მცველი კლიმატის ცვლილებისა და ბიოსფეროს უსაფრთხოებისა

ც. ბასილაშვილი, მ. ჯანელიძე, ხ. ბასილაშვილი

### რეზიუმე

ჩვენს პლანეტაზე მიმდინარე კლიმატის დათბობით გაიზარდა კატასტროფული სტიქიური მოვლენები, რამაც გამოიწვია დიდი ნგრევა და მსხვერპლი. XXI საუკუნეში მოსალოდნელია

კვლავ ტემპერატურის მომატება, რაც უფრო გააქტიურებს ყინულების დნობას, მსოფლიო ოკეანის დონის მკვეთრ აწევას და სანაპიროების დატბორვას. შემცირდება მტკნარი წყლის რესურსები და მოსავლიანობა. გაიზრდება გაუდაზნოება და სხვა ნეგატიური პროცესები. კლიმატის რეგულირების, ჟანგბადის ბალანსის სტაბილიზაციისა და ბიომრავალფეროვნების შენარჩუნების მიზნით, განსაკუთრებული მნიშვნელობა აქვს ტყის საფარს. მაგრამ სადღეისოდ დედამიწაზე ტყეთა ფართობების დაკავება, ხეთა ჭრები და ხანძრები იწვევს ფოტოსინთეზის პროცესის შემცირებას და შედეგად მზის სხივების ჭარბი თბური ენერგია ხდება მიზეზი გლობალური დათბობისა, ჟანგბადის შემცირების, ახალი ვირუსული ბაქტერიული და ქრონიკული დაავადებების გაჩენისა. სადღეისოდ, კლიმატის ცვლილების პროცესის შესარბილებლად, ბიოსფეროსა და გარემოს უსაფრთხოების მიზნით მსოფლიოს ყველა ქვეყანაში განსაკუთრებული ყურადღება უნდა მიექცეს ტყის საფრის დაცვასა და გაფართოებას. ყველამ უნდა იზრუნოს ტყის განახლებაზე და გაშენებაზე. სასოფლო-სამეურნეო მიწებში კი, უნდა გაშენდეს ქარსაცავი ტყის ზოლები, რაც ხელს შეუწყობს მოსავლიანობის გაზრდას.

**საკვანძო სიტყვები:** გაუდაზნოება, გლობალური დათბობა, მოსავალი, მტკნარი წყალი

## **Лесной покров – главный защитник от изменения климата и безопасности биосферы**

**Ц. Басилашвили, М. Джanelidze, Х. Басилашвили**

### **Резюме**

На нашей планете из-за текущего потепления климата, увеличились катастрофические стихийные явления, которые вызвали большие разрушения и жертвы. В XXI веке ожидается опять увеличение температуры, что вызовет активизацию таяния ледников, резкое повышение уровня океана и затопление побережья. Уменьшатся ресурсы пресных вод и урожайности, увеличится опустынивание и другие негативные процессы. Для регулирования климата и в целях сохранения стабильности кислородного баланса и биоразнообразия, особенное значение имеет лесной покров. Но, на сегодняшний день на Земле освоение лесных площадей, вырубка лесов и пожары, вызывают уменьшение процесса фотосинтеза и в результате, насыщенная тепловая энергия солнечных лучей, становится причиной глобального потепления, уменьшение кислорода, появление вирусных бактериальных и хронических заболеваний. На сегодняшний день, для смягчения процесса потепления климата, в целях безопасности биосферы и окружающей среды во всех странах, особенное внимание следует уделить на защиту и расширения лесного покрова. Все должны заботиться об обновлении и разведении леса. На сельскохозяйственных полях нужно развести ветрозащитные лесные полосы, что будет способствовать увеличению урожайности.

**Ключевые слова:** глобальное потепление, опустынивание, пресная вода, урожайность

## **Agroclimatic Challenges in the Mountainous and High-Mountain Areas of Georgia under Climate Change (on the Example of Mtskheta-Mtianeti and Samegrelo-Zemo Svaneti)**

**<sup>1</sup>Maia M. Meladze, <sup>1</sup>Giorgi G. Meladze, <sup>1,2</sup>Mikheil G. Pipia**

<sup>1</sup>*Institute of Hydrometeorology of the Georgian Technical University, Georgia,*

<sup>1,2</sup>*M. Nodia Institute of Geophysics of the I. Javakishvili Tbilisi State University, Georgia,*

<sup>1</sup>*e-mail: [m.meladze@gtu.ge](mailto:m.meladze@gtu.ge)*

### **ABSTRACT**

*Based on the 70-year-long meteorological observations (in 1948-2017) carried out in the areas of the mountainous and high-mountainous areas of Mtskheta-Mtianeti in east Georgia and Samegrelo-Zemo Svaneti in west Georgia, a trend of changing the agroclimatic features (sum of active temperatures ( $>10^{\circ}\text{C}$ ) and atmospheric precipitations (mm)), rise/decline in particular, has been identified under the impact of global warming (as per the designed scenario, at  $1^{\circ}\text{C}$  and  $2^{\circ}\text{C}$  increase in temperature). Under the same scenario, the trends of decreasing atmospheric precipitations and hydrothermal coefficients are also seen. Such a decrease results in more frequent drought. As the equations drafted by considering the above-said future (2020-2050) scenarios ( $1^{\circ}\text{C}$  and  $2^{\circ}\text{C}$  temperature increase), the sums of active temperatures ( $>10^{\circ}\text{C}$ ) and agroclimatic zones with the prospect to grow relevant crops were identified.*

*As per the scenarios developed for global warming, the temperature increase will not have any significant negative impact on the agricultural crops provided it is not higher than the increase forecasted by the scenario. On the contrary, it may be beneficial to grow the agricultural crops at different altitudes from the sea level, by considering vertical zoning, where the  $1^{\circ}\text{C}$  temperature increase will make it possible to grow the agricultural crops 100-200 m higher and 200-300 m higher with the  $2^{\circ}\text{C}$  temperature increase as compared to the present zones. However, proper agrotechnical measures against the negative processes caused by the decreased atmospheric precipitations must be developed.*

**Key words:** *climate change, active temperatures, atmospheric precipitations, agricultural crops*

### **Introduction**

In terms of contemporary global climate warming, the problem of slowing down the ongoing climate change and vulnerability and adaptation to it has become a world-wide issue, which was recognized as the major challenge of the UNO at the beginning of the present century. Consequently, the study of the impact of irregular climate change on the productivity and vulnerability of the agricultural crops and expected transformation of the existing agroclimatic zones is necessary and topical.

Global climate warming started in the 1970-80s and it still continues in the XXI century. As per IPCC, under the influence of global warming, the temperature on earth has increased by  $0.6^{\circ}\text{C}$ . The trend of a temperature increase was confirmed by the studies of the World Meteorological Organization (WMO) and it is an important event for the world, as it influences the ecological balance of the environment established many years ago and the macroclimate as a whole. The global warming may lead to the melting of eternal glaciers, floods, storms, hurricanes, droughts and other natural calamities. As a result, many branches of economy of the world countries, including the agricultural sector, suffer a lot. As the researchers conclude, the present-day frequent natural calamities are caused by both, natural and unforeseen anthropogenic actions. By the end of the XX century, the content of  $\text{CO}_2$  in the atmosphere reached 10%. Unless the exhaust fumes are limited, by 2030-2050, the content of carbon gas may double and the temperature may rise by another  $2-3^{\circ}\text{C}$ . This will lead to the establishment of an absolutely different system of industry and transport and particularly agricultural sector and other branches of economy [1]. Therefore, most world countries must agree to take preventive measures to reduce the emissions of such natural resources as oil, coal, as well as  $\text{CO}_2$  and other greenhouses gases from big factories and vehicles into the air. The said emissions create so called “greenhouse effect” in the atmosphere, with an increased near-earth surface temperature as its major

outcome. Following the above-mentioned, global warming is a problem to solve by the joint action of the word countries [2, 3, 4].

Global warming has affected the territory of Georgia as well as evidenced by the processing and analysis of the data of many-year meteorological observations. As the studies accomplished in Georgia evidence, a temperature increase of 0.2 and 0.5°C is fixed from humid subtropics in the west of Georgia through the high-mountainous region of Kakheti in the east of Georgia, respectively [5, 6, 7]. These temperatures are to be considered for the future, as in terms of the prolonged global warming, after three or five decades, the temperature increase may reach 2°C or more. Therefore, the impact of global warming on the branches of economy of the country, particularly, on the vulnerable agricultural sector, is to be identified in advance. The increased temperature may have a negative impact on the adapted agricultural crops, particularly in the lowland areas (400-600 m above sea level) as more heat will accumulate at such locations. Therefore, without the irrigation measures, satisfactory yield of such vulnerable cultures, as cereal crops, fruits, vegetable, vineyard, etc. will be very difficult to maintain. Following the above-mentioned, it is important to specify the transformation of agro-climatic zones according to various scenarios of the climate change and relevant agro-technical changes are to be incorporated in it.

In terms of global warming, interesting data of meteorological observations are fixed in relation to the glacier melting on the Caucasioni [8] in the high-mountainous zone of Mestia, where a many-year average air temperature increase of 0.1°C is observed what supports the melting of glaciers. Another reason for the reduction of glaciers is an increase in temperature by 0.3 and 0.2°C in the high-mountain zone of east Caucasioni (Jvari Pass, Kazbegi). The given studies, alongside with the increasing trend of sum of active temperatures identified by us, evidence the trend of another kind of (many-year average) temperature increase in terms of global warming, what activates the glacier melting process.

As regards the global warming, the upper limit of the plantation of young birch forest fixed in the high-mountainous zone of Mtskheta-Mtianeti region of east Georgia (on the territory of Kazbegi Municipality) at 2685 m above sea level is noteworthy, while as suggested by the census of 2002, the upper forest limit ended at 2560 m asl. As a result of global warming, the upper limit of the forest is subject to vertical migration [9].

The impact of global warming on the natural environment is immense. For instance, a rise in the near-land air temperature of the crop plantations may be negative in respect of propagation of twice or thrice more new generations of the organisms causing plant diseases. They may appear in the areas where they were not seen before. This will cause problems for agrarian specialists (entomologists, phytopathologists). Therefore, it will be necessary to take relevant efficient measures against them to avoid expected plant diseases reducing the productivity (harvest) by 40-50%. In this connection, we would like to note that in 2017, in Samegrelo-Zemo Svaneti and Imereti regions in west Georgia was seen a massive raid of invasive plant pest brown marmorated stink bug, which was not seen in the region before. The pest badly damaged annual and perennial crops. The agricultural specialists assume that their mass propagation is expected in east Georgia as well and relevant measures were planned against them. Global climate warming is named as the major reason for the propagation of this pest during the vegetation period.

## **Aims and methods**

The goal of the study was, by using the relevant trends, to identify the trend of change of agroclimatic properties (increase/decrease (of the sums of active temperatures (>10°C) and atmospheric precipitations (mm)) under the influence of global warming on the territories of the mountainous and high-mountainous zones of eastern and western regions of Georgia during the vegetation period, which is the major determinant of the plant growth and development and harvest formation and productivity. By using these trends, the dynamics of their change in time could be specified. Another goal of the study was to identify the agroclimatic zones suitable for the satisfactory yield and spread of agricultural crops according to the current (baseline) and future scenarios - in terms of a 1-2°C temperature increase. A mathematical statistical method was used to process and analyze the data of many-year (70-year-long) meteorological observation for Khaishi and Mestia Municipalities of mountainous and high-mountainous Samegrelo-Zemo Svaneti region

in west Georgia and Dusheti and Kazbegi Municipalities of mountainous and high-mountainous Mtskheta-Mtianeti region in east Georgia. Besides, the following materials were used for the same purpose: the meteorological and agro-meteorological databases of the Institute of Hydrometeorology of Georgian Technical University; the data of many-year (1948-2017) baseline (current) meteorological observations of the vegetation period obtained from the National Environmental Agency of Georgia (the sums of average daily air temperatures and atmospheric precipitations); besides, the data of future scenarios (1 and 2°C temperature increase by 2020-2050) were processed, which were obtained by regional climatic model RegCM-4 and social-economic development scenario A1B1 [10].

## Results and discussion

Samegrelo-Zemo Svaneti region in west Georgia is located on the south-eastern slope of the West Caucasioni. The humid subtropical climate in the region is spread from the Black Sea coastline to north-west, up to 500-600 m above sea level, (moderate) mountainous climate dominates up to 1400-1500 m a.s.l., and high-mountainous (continental) climate dominates up to 2500 m a.s.l., Mtskheta-Mtianeti region of east Georgia is located on the southern slope of the Great Caucasioni, stretching from west to north-east. It has dry subtropical climate up to 400-600 m above sea level, as well as moderate mountain climate up to 1400 m a.s.l., and high-mountainous continental climate up to 2500 m a.s.l. As a result of the treatment and analysis of the data of current (baseline) average monthly air daily temperatures in the given regions, the dates of spring and autumn temperature shift above and below 10°C were identified with equations:

$$y = -2.4x + 79 \text{ (in spring)}$$

$$y = 3.2x - 33 \text{ (in autumn)}$$

where  $y$  - is the dates of temperature shift above and below 10°C in spring and autumn;

$x$  - is the sum of average temperature of two months in spring and autumn (in particular, of February and March or March and April in spring and of September and October or October and November in autumn) [11, 12].

In addition, the monthly sums of atmospheric precipitations in the warm period (IV-X) were calculated for different years (Tab. 1).

Table 1. Agroclimatic characteristics of mountainous and high-mountainous regions of Georgia (1948-2017)

Region/ Zone	Meteo- station, (mm) a.s.l.	Data of transition air temperature $t \geq 10^\circ\text{C}$	Data of transition air temperature $t < 10^\circ\text{C}$	Duration of the vegetation period	Sums of active temp. $> 10^\circ\text{C}$ (IV-X)	Sums of active temp. $< 10^\circ\text{C}$ (VI-VIII)	Atmospheric precipitations (mm), (IV-X)	Hydrothermal index (HTC) (IV-X)
Samegrelo- Zemo Svaneti, west Georgia/ mountainous	Khaishi, 730	11.IV	22.X	194	3336	1846	662	2.0
high- mountainous	Mestia, 1441	10.V	28.IX	141	2014	1447	440	2.2
Mckheta- Mtianeti, east Georgia/ mountainous	Dusheti, 922	18.IV	20.X	185	3095	1792	509	1.6
High- mountainous	Kazbegi, 1744	21.V	22.IX	124	1628	1288	476	3.0

The Table shows that in the mountainous zone of Samegrelo-Zemo Svaneti region (west Georgia), the date of the temperature transition above 10°C in spring is observed on 11.IV, while the date of the temperature transition below 10°C in autumn is observed on 22.X. As the scenario suggests, in the given zone, in case of a temperature increase by 1°C, the date of the temperature transition above 10°C in spring is observed on 6.IV and the date of the temperature transition below 10°C in autumn is observed on 28.X (Tab. 2).

Table 2. The dates of air temperature transitions above and below 10°C, duration of the vegetation period (days) and sums of active temperatures (>10°C) in the mountainous and high-mountainous regions of Georgia under the scenarios of the air temperature increase by 1°C and 2°C

Region/ Zone	Meteo- station	t>10°C Starting time	t<10°C Finishing time	duration of vegetation period (day)	ΣT>10°C
Samegrelo-Zemo Svaneti/ mountainous	Scenario, rise of temperature by 1°C				
	Khaishi	6.IV	28.X	205	3525
high-mountainous	Mestia	6.V	3.X	150	2206
Mckheta-Mtianeti/ mountainous	Scenario, rise of temperature by 2°C				
	Dusheti	10.IV	31.X	204	3581
High-mountainous	Kazbegi	12.V	1.X	142	2128

In spring, in case of the scenario, the date of the temperature above 10°C in spring is observed 5 days earlier and the date of the temperature below 10°C in autumn is observed 6 days later as compared to the current (baseline) value (Tab. 1), i.e. the vegetation period is prolonged from 194 days (current, Tab. 1) to 205 days (scenario, Tab. 2), or by 11 days. The vegetation period in the high-mountainous zone of the same region is prolonged by two days less. For instance, in the high-mountainous zone, the date of the temperature above 10°C in spring is observed on 6.V in case of 1°C temperature rise under the scenario (Tab. 2) making a difference of 4 days as compared to the current value (10.V) (Tab. 1), while in autumn, the date of the temperature shift below 10°C is observed on 3.X (scenario, Tab. 2) making a difference of 5 days as compared to the baseline value (28.IX) (Tab. 1). The above-given prolonged days in spring (at the expense of date of the temperature transition above 10°C occurring 4-6 days earlier) and in autumn (at the expense of date of the temperature transition below 10°C occurring 6 days later), in the mountainous and high-mountainous zones allow realizing the agrotechnical measures within relevant terms.

Following the global warming, the sums of active temperatures (>10°C) in the mountainous and high-mountainous zones of the considered regions are given. Such a sum in the mountainous zone is 3336°C (baseline, Tab. 1) and 3525°C in case of a 1°C temperature increase under the scenario (Tab. 2). In the future, the sum of temperatures increased above the baseline value (189°C) will be beneficial (in terms of satisfactory soil moisture) to get rich harvest of cereals (corn, wheat, barley), legumes, vegetable, vineyard, fruit and other crops.

The sum of active temperatures in the high-mountainous zone is 2014°C (baseline, Tab. 1) and is 2206°C in case of a 1°C temperature increase under the scenario (Tab. 2). In the future (2020-2050), the sum of active baseline temperatures is expected to increase by 192°C, what, in the high-mountainous zone will improve the productivity of cereals, vegetable, early fruit varieties, berries, roots for animal forage („Kuuziku”, „ESCO”) and support the development and high yield of pastures and hayfields and sustainable development of forest landscapes.

Mtskheta-Mtianeti region in east Georgia has somewhat different climatic features as compared to Samegrelo-Zemo Svaneti region in east Georgia [13]. Here, as the meteorological observation data in the mountainous zone of Dusheti Municipality suggest, the date of the temperature above 10°C is observed on 18.IV, while the date of the temperature below 10°C is observed on 20.X (baseline, Tab. 2). As per the

scenario of the future, in case of a 2°C rise in temperature (such a rise is considered as in the eastern regions of Georgia, the trend of the temperature increase is more obvious), the date of the temperature above 10°C is observed on 10.IV, while the date of the temperature below 10°C is observed on 31.X (Tab. 2). In other words, in case of the scenario, in spring, the date of the temperature above 10°C occurs 8 days earlier, while in autumn the date of the temperature below 10°C occurs 11 days later (Tab. 2) as compared to the baseline values (Tab. 1). The vegetation period in the mountainous and high-mountainous regions in question is prolonged by 19-18 days (Tab. 1 and 2, respectively). With such extra days, in spring, the vegetation of pasture and hayfield grasses will be possible to start earlier and prepare nomadic cattle to take to the pastures. In autumn, it is possible to produce more and better forage for winter from hayfields and accomplish other agricultural activities. The given zone will also be beneficial to grow and propagate berries.

By considering the global warming, the sum of active temperatures in the mountainous and high-mountainous zones of the given region in case of a 2°C temperature rise under the scenario (2030-2050), is 3581°C in the mountainous zone (Tab. 1) what significantly exceeds (by 486°C) the sum of baseline active temperatures - 3095°C (Tab. 1). The temperature in the high-mountainous zone, in case of a 2°C temperature rise under the scenario, rises similarly (by 500°C) as compared to the sum of baseline active temperatures (1628°C) (Tab. 1).

An increase in the sums of active temperatures in the mountainous and high-mountainous zones of the given region by 500°C on average will be absolutely suitable to develop and ensure satisfactory yield of crops and forest landscapes. As per Tab. 1, following the analysis of the amount of atmospheric precipitations in the above-considered regions, such an amount is actually sufficient to grow crops and develop other forest landscapes in the vegetation period. However, in some droughty years, lack of precipitations may be the case. In such a case, the desirable yield of the crops can be maintained by increasing soil humidity (by irrigation, soil surface tillage, etc.).

The data of the above-mentioned 70-year-long (1948-2017) meteorological observations cover the initial period of global climate warming, the 1970-80s in particular, marked by the onset of the general influence of global warming on a near-surface temperature rise and agroclimatic resources (sums of active temperatures (>10°C) and atmospheric precipitations (mm), etc.) consequently. In order to present these values clearly, the data of 70-year-long observations mentioned above were divided into two 35-year-long periods. The I period covers the years of 1948-1982, and the II period covers the years of 1983-2017 (Tab. 3).

Table 3. Agroclimatic characteristics according to the periods (1948-1982; 1983-2017) of the mountainous and high-mountainous regions of Georgia

Region/ Zone, Meteostation	I and II periods	Data of transition air temperature t>10°C	Data of transition air temperature t<10°C	Duration of the vegetation period	Sums of active temp. >10°C (IV-X)	Sums of active temp. <10°C (VI-VIII)	Atmospheric precipitations (mm), (IV-X)	Hydrothermal index (HTC) (IV-X)
Samegrelo-Zemo Svaneti/ mountainous, Khaishi (Mestia)	1948- 1982	12.IV	21.X	192	3298	1824	664	2.0
	1983- 2017	9.IV	24.X	198	3374	1869	659	1.9
high-mountainous, Mestia	– „ –	11.V	26.IX	138	1945	1411	451	2.3
	– „ –	10.V	30.IX	143	2084	1483	428	2.0

Mckheta-Mtianeti/ mountainous, Dusheti	1948- 1982	20.IV	20.X	183	3049	1751	522	1.7
	1983- 2017	15.IV	21.X	189	3141	1832	495	1.6
High-mountainous, Kazbegi	– „ –	22.V	18.IX	119	1571	1271	516	3.2
	– „ –	21.V	25.IX	127	1684	1305	435	2.9

The analysis of the Table demonstrates that in different municipalities of the region, in the second period, the date of the onset of active air temperatures ( $>10^{\circ}\text{C}$ ) occurs earlier and the date of the temperature below  $10^{\circ}\text{C}$  ends later as compared to the first period. In the same period, the sums of active temperatures are increased and the vegetation period is prolonged. In the second period, the sums of atmospheric precipitations, as well as hydrothermal coefficients (HTC) in the warm period (IV-X) are decreased at all locations. The sums of atmospheric precipitations (mm) in high-mountainous zones (Mestia, Kazbegi) are given for the periods of IV-IX months and VI-VIII months, respectively, as the warm period (with temperatures above  $10^{\circ}\text{C}$ ) in the given months starts late and ends early. In the second period, i.e. for the last 35 years, the amount of precipitations and consequently, the hydrothermal coefficients have decreased. Despite this, if the precipitations do not reduce further, they will be sufficient to grow cereal crops, vegetable and other annual crops, as well as succulent roots for animal forage („Kuuziku”, „ESCO”) and pasture and hayfield grasses with (one-time) irrigation in some years.

The dynamics of the course of the said indices was presented with trends, according to which, the trends of increasing sums of active temperatures ( $>10^{\circ}\text{C}$ ) and decreasing sums of the atmospheric precipitations (mm) were identified in the mountainous and high-mountainous regions of west Georgia and mountainous and high-mountainous regions of east Georgia (Fig. 1, 2).

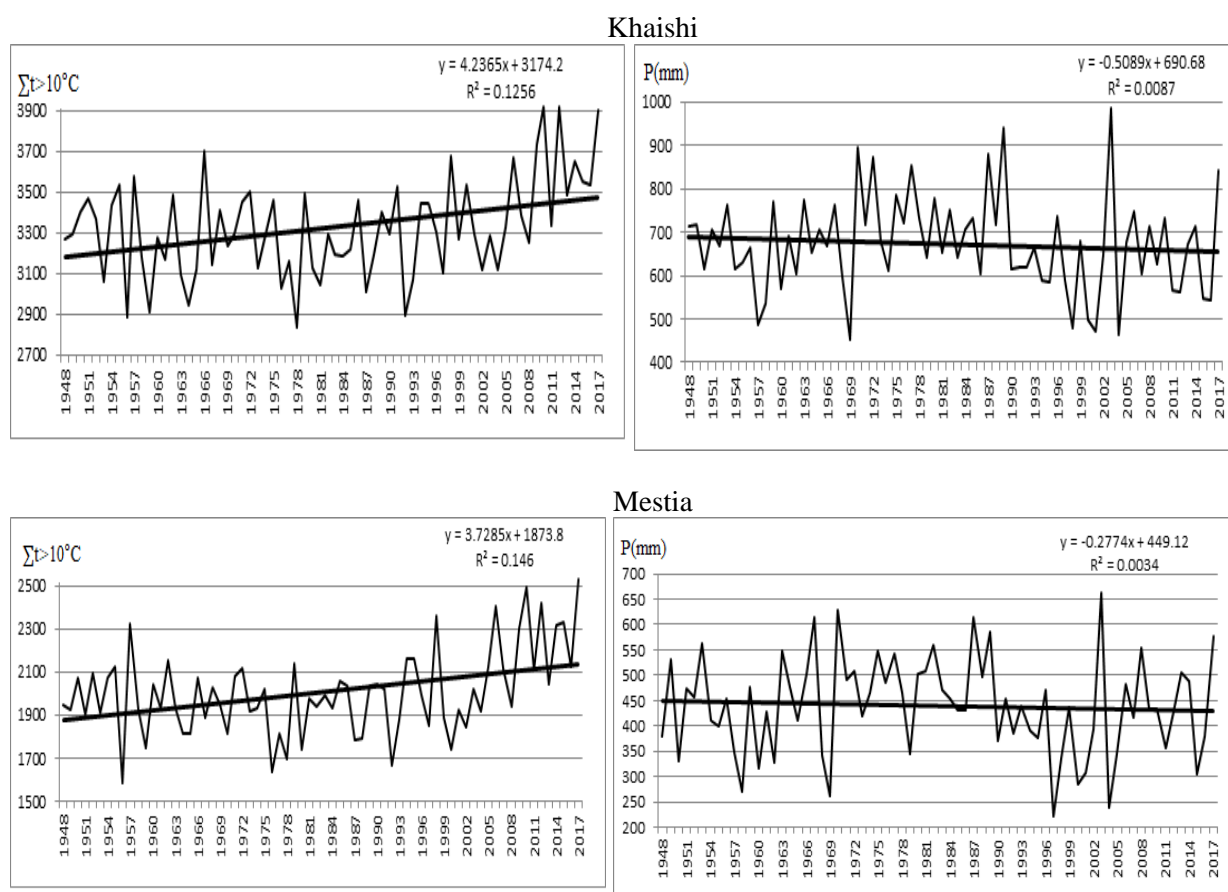
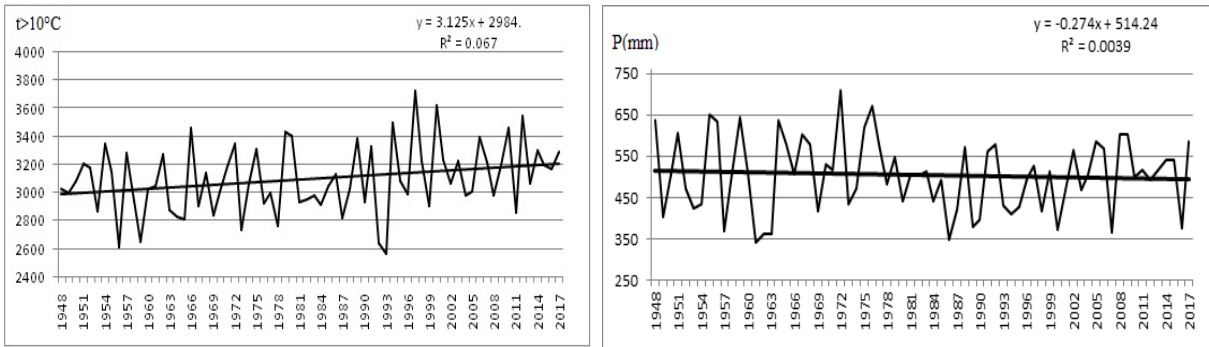


Fig. 1. Dynamics of the sums of active temperatures ( $>10^{\circ}\text{C}$ ) and atmospheric precipitations (mm) in Samegrelo-Zemo Svaneti region of the mountainous and high-mountainous zones of Georgia (1948-2018)

### Dusheti



### Kazbegi

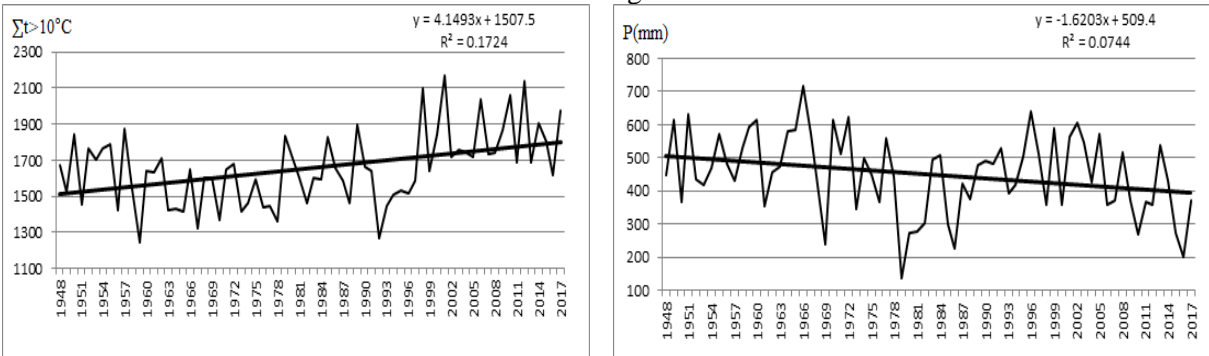


Fig. 2. Dynamics of the sums of active temperatures ( $>10^{\circ}\text{C}$ ) and atmospheric precipitations (mm) in Mckheta-Mtianeti region of the mountainous and high-mountainous zones of Georgia (1948-2018)

The equations of the trends were used to calculate increasing and decreasing trends of the sums of active temperatures ( $>10^{\circ}\text{C}$ ) and atmospheric precipitations (mm) (Tab. 4).

Table 4. The sums of active temperatures ( $>10^{\circ}\text{C}$ ) and atmospheric precipitations (mm) according to trends

Region/ Zone	Meteo- station	Sum of active temperatures ( $>10^{\circ}\text{C}$ )					
		Beginning of the period	End of the period	Increase	Decrease	Average speed in every 10 years	
						Increase	Decrease
Samegrelo-Zemo Svaneti/ Mountainous	Khaishi	3178	3470	292		41.7	
High-mountainous	Mestia	1877	2134	257		36.7	
Mckheta-Mtianeti/ Mountainous	Dusheti	2987	3203	216		30.7	
High-mountainous	Kazbegi	1511	1797	286		40.8	
Samegrelo-Zemo Svaneti/ Mountainous	Khaishi	Sum of atmospheric precipitations (mm)					
		690	655		35		5.0
		449	430		19		2.7
		514	495		19		2.7
High-mountainous	Kazbegi	507	388		119		17.0

As the given Table shows, there is a trend of decreasing atmospheric precipitations (119 mm) in the high-mountainous zone of east Georgia. The average velocity of the given reduction is 17 mm in every 10 years. The increasing and decreasing trends of agroclimatic values in other zones are relatively less.

If, under the influence of global warming, the sum of active temperatures in a similar period continues to increase, after 4 or 5 decades, the sum of current (baseline) temperatures may increase significantly (reaching 300°C or more) in the mountainous and high-mountainous zones of eastern and western regions of Georgia. This may be beneficial to grow crops in the mountainous and high-mountainous zones successfully (in terms of sufficient atmospheric precipitations). It seems that the amount of precipitations decreases in the given zones. Therefore, unless the proper soil moisture is maintained, no satisfactory development or yield of the crops is possible.

In order to identify the agroclimatic zones in the above-said regions, the scenarios consider a 1°C temperature increase in the regions of west Georgia and a 2°C temperature increase in the regions of east Georgia. The dates of average daily air temperature above 10°C, sums of active temperatures and altitude above sea level (m) were used for this purpose. The latter is in direct correlation with the regular change in air temperature depending on the altitude [14]. The given data were processed by using the mathematical statistics method adopted in agrometeorology with close correlations established. Following the obtained reliable associations, relevant regression equations were drafted (Tab. 5). At different times, the equations of the given type were used to identify the sums of active temperatures to identify the relevant zones of crops [15].

Table 5. Regression equations to determine the dates of average daily air temperature transition above 10°C and sums of active temperatures in the mountainous and high-mountainous regions of Georgia

Determination of starting date $t > 10^\circ\text{C}$ and $\sum T$	Current (baseline), mountainous and high mountainous (west Georgia)	Scenario, increase by 1°C, mountainous and high mountainous	Current baseline, mountainous and high mountainous (east Georgia)	scenario, increase by 2°C mountainous and high mountainous
determination of starting date ( $t > 10^\circ\text{C}$ )	$n=0.025h+57$	$n=0.028h+51$	$n=0.029h+55$	$n=0.035h+38$
determination of $\sum T$	$T=-36.53n-0.75h+6537$	$T=-16.711n-1.127h+5496$	$T=-30.923n-0.57h+6085$	$T=-44.25n-0.15h+6742$

In the equations: n - is the number of days from the 1<sup>st</sup> of February to the date of the temperature above >10°C; h - is the altitude above sea level (m); T - is the sum of active temperatures (>10°C).

By using the given equations, the sums of active temperatures by considering the current (baseline) values and future (2020-2050) scenarios (a temperature increase by 1 and 2°C) were identified and the agroclimatic zones of the distribution of crops in the regions were defined [16].

The mountainous area of the region spreads from 500 to 1500 m above sea level of the humid subtropical zone of Samegrelo-Zemo Svaneti region of west Georgia, where two agroclimatic zones (I and II) were identified:

The I agroclimatic zone extends from 500 m to 1000 m altitude above sea level. The sum of baseline active temperatures is 3620-2790°C and is 3800-3110°C under the scenario with a 1°C temperature increase. Juglandaceous plants, fruit and vegetable varieties and other crops grow well in the given zone. Under the future scenario with a 1°C temperature increase, vine varieties (Tsolikauri, Tsitska) may be grown from 700-800 to 1000 m and tea culture may be grown slightly higher, at 600-700 m.

The II agroclimatic zone extends from 1000 m to 1500 m altitude above sea level. The sum of current (baseline) active temperatures is 2790-1960°C and is 3110-2430°C under the scenario. Under the future scenario, the areas with wheat, (winter, spring) barley, oats, potato and vegetable crops at the altitude of 1400-1500 m (baseline) well extend to reach 1600-1750 m altitude and higher, while the area with grain

maize may be extended from 900 m (baseline) to 1200 m s.l., for industrial purposes; the areas with fruits may be extended from 1300 m (baseline) to 1400-1450 m a.s.l., or higher.

Higher mountainous area of the given region, from 1500 to 2500 m altitude, there extends the high-mountainous area of the region, where two agroclimatic zones are identified (III and IV).

The III agroclimatic zone extends from 1500 to 2000 m altitude. The sum of baseline active temperatures in the given zone is somewhat reduced and makes 1960-1130°C on average and 2430-1760°C in case of the scenario. With its heat regime, the region will offer more suitable conditions to grow (winter, spring) wheat, barley, oats, potatoes, berries (blackcurrant, redcurrant, sea-buckthorn, raspberry and haw) as compared to the baseline conditions. The areas with juicy roots as animal forage („Kuuziku”, „ESCO”) and pastures and hayfields will be possible to expand.

The IV zone agroclimatic zone extends from 2000 m to 2500 m altitude above sea level. The sum of baseline active temperatures in the given zone is 1130-300°C. The sum of temperatures is obviously reduced, and it is 630°C (baseline) at the altitude of 2300 m. Growing the given crops (juicy root forage) at the given temperature is not profitable. Under the scenario (a 1°C temperature rise), the sum of active temperatures (>10°C) is 1760-1080°C. At the altitude of 2300 m (under the scenario), the sum of active temperatures is up to 1350°C what, as compared to the baseline temperature, is suitable to grow the above-mentioned root crops as cattle forage and expand pastures and hayfields.

In respect of global warming, the air temperature in Mtskheta-Mtianeti region in east Georgia is increasing more. As it was noted, the temperature is risen by 0.5°C here unlike Samegrelo-Zemo Svaneti region in west Georgia. Therefore, a 2°C temperature increase is considered by the scenario, where 3 agroclimatic zones were identified [17, 18, 19]:

The I agroclimatic zone spreads from 1000 m to 1500 m altitude above sea level in the west and south-east of the region. This zone covers the mountainous areas of Dusheti and Tianeti Municipalities. The sum of current (baseline) active temperatures is 2920-2180°C and is 3360-2500°C under the scenario (a 2°C temperature increase). Wheat (winter, spring), barley, oats, maize (at 1300 m and higher), vine (early and mid ripening varieties), nut, potatoes and vegetable crops can be grown and produced in the given zone. It is desirable to irrigate (once or twice) or loosen the soil in the given zone, particularly in the period of the VI-VIII months.

The II agroclimatic zone belongs to the high-mountainous region, which is located up to 2000 m in the east. The sum of current (baseline) active temperatures is 2180-1450°C and 2500-1660°C under the scenario. Under the future scenario (a 2°C temperature increase), the sum of temperatures, as compared to the sum of baseline temperatures, is almost 300°C more. The sum of the temperature increase will favor the growth of wheat, barley, oats, potatoes, vegetables, berries (blackcurrant and redcurrant), willow-leaved sea-buckthorn and early fruit varieties, as well as juicy roots as animal forage („Kuziku”, „ESCO”) and development and extension of pastures and hayfields.

The III high-mountainous agroclimatic zone spreads from 2000 m to 2500 m altitude above sea level. It covers the upper border of the subalpine zone. In this high-mountainous region, the sum of baseline active temperatures is obviously reduced (to 700°C) making the area non-favorable to grow vegetables or juicy root forage, particularly at 2400-2500 m a.s.l., while at 2300 m, the sum of baseline temperatures is approximately 1000°C. With such a temperature range, growing the said crops or developing pastures and hayfields will be non-profitable. Under the future scenario (a 2°C temperature increase), the sum of active temperatures will be 1150-800°C; however, at the altitude of 2500 m, the temperature of 800°C is not sufficient to grow the above-listed crops, while at the altitude of 2300-2400 m, the sum of temperatures is 1150-1000°C offering better conditions to grow the same crops.

## Conclusion

The results of our studies evidence the impact of global climate warming on Mtskheta-Mtianeti mountainous and high-mountainous regions of east Georgia and Samegrelo-Zemo Svaneti mountainous and high-mountainous regions of west Georgia. It is obviously responsible for the increased sums of active temperatures (>10°C), prolonged vegetation period, decreased atmospheric precipitations (mm) and decreased hydrothermal coefficient (HTC) causing droughts.

The increase of the sum of active temperatures above the current (baseline) value in the mountainous (3525°C) and high-mountainous (2206°C) areas of Samegrelo-Zemo Svaneti in the west is 189°C and 192°C, respectively. The vegetation period in the mountainous and high-mountainous areas has increased by 11 and 9 days, respectively. An increase in the sum of active temperatures in the mountainous (3581°C) and high-mountainous (2128°C) areas of Mtskheta-Mtianeti in the east is 486°C and 500°C, respectively, and the vegetation period has increased by 19 and 18 days, respectively.

The mountainous zone of Samegrelo-Zemo Svaneti region in west Georgia spreads above the humid subtropical zone of the region, 500 to 1500 m above sea level, where two agroclimatic zones were identified, and the high-mountainous zone of the same region spreads from 1500 to 2500 m above sea level, with two agroclimatic zones. Three agroclimatic zones were identified in Mtskheta-Mtianeti region in east Georgia. The I mountainous zone spreads from 1000 to 1500 m altitude, the II high-mountainous zone spreads up to 2000 m altitude, and the III high-mountainous zone spreads from 2000 to 2500 m altitude.

The future scenarios (2020-2050), or 1 or 2°C temperature rise in terms of global warming will not have a significant influence on the agricultural crops in the zones of the study regions unless the temperature in the process of global warming is higher than that envisaged by the scenario. Just on the contrary, it may be suitable to grow agricultural crops at different altitudes above sea level, where in the future, in case of 1°C temperature rise, growing the agricultural crops will be possible 100-200 m higher and 200-300 m higher in case of 2°C temperature rise as compared to the present-day zones.

In the considered region, in the zones designated to grow the above-listed crops, where high-mountainous villages of Mestia Municipality (e.g. Ushguli (2200 m asl)), villages of Dusheti Municipality (Khone (2150 m a.s.l.), Roshka (2050 m a.s.l.)), villages of Kazbegi Municipality (Juta (2200 m asl)) and other villages (Akhieli, Shatili, at relatively lower altitudes) are located, the agricultural specialists and agricultural farmers, together with the local residents, with the future perspective, will be able to grow the crops profitable for them and to produce high-quality products with them to be used by the residents of the above-listed villages. If necessary, they will even realize some of the products. This will promote the employment and establishment of the local residents what will support the reduction of depopulation in the mountainous and high-mountainous zones of the country. As a result, the social-economic conditions will improve. These activities are supported by the Law of Georgia „On the Development of High Mountainous Regions” adopted by the Government of Georgia on July 16, 2016 as well. In particular, the goal of the Law is to ensure the wellbeing of the residents in the high-mountainous regions of Georgia, support employment and improve the quality of life and social-economic conditions. In line with this major Law, the results of the study conducted by us for high-mountainous regions given in the present work are worthwhile. It should be noted that the given regions with their natural location (relief and orographic conditions, diversified forest landscape, etc.) are interesting and attractive. They have good prospects to develop tourism and recreation activities in summer, autumn and winter seasons. On the territory of Mestia (located at 1500 m above sea level and higher), ski mountaineering is very popular sports in autumn and winter seasons, while sporting activities organized in Gudauri Ski Resort (at 2200 m above sea level and higher) are also very important.

Following the global warming, certain mitigation and adaptation measures against some negative events are recommended to use in the agrarian sector at present and in the future. Growing selective crops, which are resistant to higher temperatures and droughts, is a good choice. Besides, it is important to make terraces over the mountain and high-mountain slopes (with >10° gradient) to reduce intense evaporation of water runoff and water from soil; soil surface cultivation and loosening to reduce water evaporation from the soil is another efficient measure. Besides, efficient use of modern irrigation and drip irrigation and other methods will be beneficial.

## References

- [1] Workbook on climate change impact assessment in agriculture. Preparad by Rodar E. Riwero Vega. Camaguey meteorological center, 2008, p. 110.
- [2] Mavi H.S., Graeme J. Agrometeorology: principles and applications of climate studies in agriculture. Binghamton, NY, USA, 2004, p. 364.
- [3] Hubbard G. Agriculture climatology. Climate center the university of Nebraska, vol.1, №2, 2007, p. 134.

- [4] Human development report, 2007-2008. Fighting climate change human solidarity divided word. published for the United development program (UNDP), 2008, p. 98.
- [5] Tavartkiladze K. Begalishvili N., Tsintsadze T., Kikava A. Influence of global warming on the near-surface air temperature field in Georgia. Bulletin of The Georgian National Academy of Sciences, vol. 6(3), 2012, pp. 55-60.
- [6] Meladze G., Meladze M. Agroclimatic resources of eastern regions of Georgia. publ. "Universal", Tbilisi, 2010, p. 293, (in Georgian).
- [7] Meladze G., Meladze M. Agroclimatic resources of western regions of Georgia. publ. "Universal", Tbilisi, 2012, p. 435, (in Georgian).
- [8] Tielidze L. Glaciers catalog of Georgia. Tbilisi, 2016, p. 116, (in Georgian).
- [9] Togonidze N. Climate change and anthropogenic impact on subalpine birch forest. Modern problems of geography and anthropology. Proceedings of International conference, 2015, pp.144-148, (in Georgian).
- [10] The Third National Communication Climate Change of Georgia, UNDP, 2015, p. 287, (in Georgian).
- [11] Meladze G., Meladze M. Global warming: tendency of change the agroclimatic features of Samegrelo-Zemo Svaneti. Transactions of the Institute of Hydrometeorology, Georgian Technical University, vol. 127, 2019, pp.46-52, (in Georgian).
- [12] Climate of Georgia. 3.Samegrelo-Zemo Svaneti. Transactions of the Institute of Hydrometeorology, vol. 113, 2010, (in Georgian).
- [13] Climate of Georgia. 9. Mtskheta-Mtianeti, Agroclimatic resources. Transactions of the Institute of Hydrometeorology, Georgian Technical University, vol. 134, 2023, 165 p., (in Georgian).
- [14] Mumladze D., Gagua G., Lomidze N. Georgian mountain zones. Climatic, landscape and ecological assessment. Collected papers new series №4 (83), Proceedings of the conference dedicated to the 100<sup>th</sup> birthday anniversary of professor Levan Maruashvili, 2012, pp.126-137, (in Georgian).
- [15] Meladze M., Meladze G. Climate change: agroclimatic zoning of grape varieties in Eastern Georgia (on the example of Mtskheta-Mtianeti). Pressing problems in hydrometeorology and ecology dedicated to the 100<sup>th</sup> anniversary of the Georgian Technical University, vol. 135, 2024, pp. 44-49.
- [16] Meladze M., Meladze G. Transformation of agroclimatic zones of Samegrelo-Zemo Svaneti in conditions of global warming. Scientific conference: Actual problems of Geography, 2019, pp. 96-102.
- [17] Meladze M., Meladze G. Agro-ecological zoning of Mtskheta-Mtianeti region in the conditions of global warming. International Scientific Conference - Modern Problems of Ecology, Proceedings -vol. VI, 2018, (in Georgian).
- [18] Meladze M., Meladze G. Impact of climate change on agro-climatic characteristics and zones of Mtskheta-Mtianeti region. Proceedings of International Scientific Conference „Natural Disasters in the 21st Century: Monitoring, Prevention, Mitigation”, Iv. Javakhishvili Tbilisi State University, 2021, pp.38-41.
- [19] Meladze M., Mamasakhlisashvili L., Ujmajuridze L., Migliaro D., Domanda C., Rustioni L. Neglected cultivars for the Mtskheta-Mtianeti region (East Georgia): Ampelography, phenology, and agro-climatology. Journal of Grapevine Research - Vitis, vol. 62, N2, 2023, pp.75-84.

## **აგროკლიმატური გამოწვევები საქართველოს მთიან და მაღალმთიან ტერიტორიებზე კლიმატის ცვლილების პირობებში (მცხეთა-მთიანეთის და სამეგრელო-ზემო სვანეთის მაგალითზე)**

**მ. მელაძე, გ. მელაძე, მ. ფიფია**

**რეზიუმე**

საქართველოს აღმოსავლეთ მცხეთა-მთიანეთის და დასავლეთ სამეგრელო - ზემო სვანეთის მთიანი და მაღალმთიანი რეგიონების ტერიტორიებზე ჩატარებული 70 წლიანი (1948-2017) მეტეოროლოგიური დაკვირვებების საფუძველზე, გამოვლენილია გლობალური დათბობის გავლენით აგროკლიმატური მახასიათებლების (აქტიურ ტემპერატურათა (>10°C) და

ატმოსფერული ნალექების (მმ) ჯამების) ცვლილების ტენდენცია - მატება/კლება (სცენარით, ტემპერატურის 1 და 2°C-ით მატებისას).

საკვლევ ტერიტორიებზე აღნიშნული სცენარების მიხედვით, გამოვლენილია ატმოსფერული ნალექების და ჰიდროთერმული კოეფიციენტების კლების ტენდენციები, რაც გვალვების განმეორადობის გახშირების მიზეზია.

ზემოაღნიშნული მომავლის (2020-2050) სცენარების (1 და 2°C-ით მატება) გათვალისწინებით შედგენილი განტოლებებით, განისაზღვრა აქტიურ ტემპერატურათა ჯამები (>10°C) და გამოიყო აგროკლიმატური ზონები, შესაბამისი კულტურების გავრცელების პერსპექტივით. სადაც, 1°C-ით მატებისას აგროკულტურების გავრცელება შესაძლებელი იქნება 100-200 მ-ით, ხოლო 2°C-ით მატებისას 200-300 მ-ით უფრო მაღლა, არსებულ ზონებთან შედარებით. თუმცა, გასათვალისწინებელია შემცირებული ატმოსფერული ნალექებით გამოწვეული ნეგატიური პროცესების მიმართ შესაბამისი აგროტექნიკური ღონისძიებების შემუშავება.

**საკვანძო სიტყვები:** კლიმატის ცვლილება, აქტიური ტემპერატურა, ატმოსფერული ნალექები, აგროკულტურა

## **Агроклиматические вызовы в горных и высокогорных регионах Грузии в условиях изменения климата (на примере Мцхета-Мтианети и Самегрело-Земо Сванети)**

**М.Меладзе, Г.Меладзе, М.Пициа**

### **Резюме**

На основе 70-летних (1948-2017) метеорологических наблюдений, проводимых в горных и высокогорных регионах Восточной Мцхета-Мтианети и Западной Самегрело-Земо Сванети Грузии, выявлена тенденция изменения агроклиматических характеристик (суммы активных температур (>10°C) и атмосферных осадков (мм)) под влиянием глобального потепления - повышение/снижение (сценарий с повышением температуры на 1 и 2°C).

По указанным сценариям на территориях исследований выявлены тенденции снижения атмосферных осадков и гидротермических коэффициентов, что является причиной повторяемости засух.

С использованием уравнений, разработанных с учетом выше указанных сценариев будущего (2020-2050 гг.) (повышение температуры на 1 и 2°C), определены суммы активных температур (>10°C) и выделены агроклиматические зоны с учетом перспектив распространения соответствующих сельскохозяйственных культур. Где при повышении температуры на 1°C можно распространение сельскохозяйственных культур на 100-200 м выше, а при повышении температуры на 2°C - на 200-300 м выше по сравнению с существующими зонами. Однако необходимо рассмотреть вопрос разработки соответствующих агротехнических мероприятий по устранению негативных процессов, вызванных уменьшением количества атмосферных осадков.

**Ключевые слова:** изменение климата, активная температура, атмосферные осадки, сельскохозяйственная культура

# Wavelet Coherence Analysis of Magnetic Declination During Quiet and Disturbed Geomagnetic Activity

Oleg A. Kharshiladze, Luka K. Tsulukidze, Mariam J. Martiashvili

M. Nodia Institute of Geophysics of the I. Javakishvili Tbilisi State University, Georgia  
e-mail: [luka.tsulukidze617@ens.tsu.edu.ge](mailto:luka.tsulukidze617@ens.tsu.edu.ge)

## ABSTRACT

*This study investigates characteristics of magnetic declination (D) at the mid-latitude Dusheti Geophysical Observatory and its coupling to solar wind during both quiet and disturbed periods, with a specific focus on the intense storm of May 11, 2024. We analyze one-minute resolution geomagnetic and solar wind data from July 2023 to July 2024. Using power spectral density (PSD) and continuous wavelet transform (CWT), we characterize the spectral behavior of declination. The analysis confirms the persistent presence of diurnal (24h) and semidiurnal (12h) periodicities, characteristic of the quiet time, also a period of 8h, while demonstrating significant spectral broadening during the geomagnetic storm. We then employ wavelet coherence analysis to quantify the coupling between declination and the IMF magnitude (B), its southward component (Bz), and the solar wind velocity (v). The results reveal distinct coupling mechanisms: coherence with B is dependent on storm intensity, being strong only during the intense May 11 storm. In contrast, coherence with Bz is robust and significant during both intense (May 11) and moderate (April 19) storms, highlighting its fundamental role in driving disturbances in geomagnetic data regardless of storm intensity. This work demonstrates the effectiveness of wavelet coherence for evaluating solar wind magnetosphere coupling at different frequencies.*

**Key words:** Magnetic declination, Magnetic storm, Solar wind, Interplanetary magnetic field, Wavelet transform, Wavelet coherence.

## Introduction

The geomagnetic field is a complex phenomenon characterized by a non-uniform spatial structure and a wide spectrum of temporal variations. Its origins are twofold, with sources located both deep within the planet and in the near-Earth space environment. The primary contributor is the geodynamo, a process driven by the rotation and convection of the Earth's liquid, conductive outer core [1]. This internal source generates the main magnetic field and its slowly evolving secular variations, which occur over timescales of years to millennia.

Complementing the main field are external sources situated in the ionosphere and magnetosphere. These regions contain complex and dynamic systems of electrical currents that are shaped by the Earth's intrinsic magnetic field. The interaction between these currents and the solar wind—a stream of charged particles flowing from the Sun—produces a variety of magnetic effects observed on the ground [2]. These effects range from regular daily variations to sporadic and intense disturbances, with timescales spanning from seconds to several days.

The Earth's magnetic field vector is described by several components, including magnetic declination (D). As the angle between magnetic and geographic north, declination is particularly sensitive to magnetospheric state changes and fluctuates significantly during magnetic storms, making it a valuable parameter for this study [4].

The most significant manifestation of the Sun-Earth connection is the magnetic storm, a global disturbance of the magnetosphere that serves as a key indicator of space weather. These storms are primarily caused by energetic solar events that intensify the solar wind, leading to a strong interaction with the Earth's magnetosphere [3]. The resulting deformation of the magnetic field induces powerful currents in the upper atmosphere, which are observed on the ground as magnetic storms. The intensity of this activity is often quantified using indices such as the Kp [5], Ae, and Dst [6].

The impact of geomagnetic disturbances is not uniform across the globe; it is strongly dependent on latitude [7]. In the auroral zones, near the magnetic poles, storms are most frequent and intense, causing sharp deviations in the magnetic field. At mid-latitudes, where the Dusheti Geophysical Observatory (DGG) is

located, the effects are less severe but still significant. In contrast, the equatorial regions are generally more stable due to the horizontal orientation of the magnetic field lines.

While magnetic declination is traditionally understood as a slowly varying and predictable quantity for a given location, magnetic storms are rapid, intense, and unpredictable phenomena. A fundamental question arises from this contrast: can the intense, short-term processes of a magnetic storm influence the behavior of magnetic declination, and is there a quantifiable connection between them?

This study aims to investigate this relationship by analyzing high-resolution magnetic declination data from the Dusheti Geophysical Observatory. We focus on its spectral characteristics during both geomagnetically quiet periods and the intense magnetic storm of May 11, 2024. Using wavelet transform analysis and power spectral density (PSD), we will examine the frequency and energy distribution of declination variations. Furthermore, we will employ wavelet coherence analysis to evaluate the correlation between declination and key solar wind parameters and interplanetary magnetic field (IMF) data, trying to understand the nature of magnetospheric coupling during both calm and storm conditions.

## Data and methods

To fully characterize the geomagnetic field at a specific location, it is described by a vector, which can be broken down into several standard components. The vector is defined by its orthogonal coordinates: the northward component (X), the eastward component (Y), and the vertical component (Z), directed towards the Earth's center. From these, other critical parameters can be derived, including the total intensity (F), the horizontal component (H), the inclination (J), and the declination (D). These are calculated as follows:

$$D = \arctan\left(\frac{x}{y}\right), \quad F = \sqrt{H^2 + Z^2}$$

$$J = \arctan\left(\frac{Z}{H}\right), \quad H = \sqrt{X^2 + Y^2}$$

In this study, our primary focus is on magnetic declination (D), which is a highly informative parameter. It is exceptionally sensitive to the state of the magnetosphere, and its variations clearly reflect even subtle magnetic activity [4]. During geomagnetically quiet periods, declination exhibits slow, predictable changes. However, during magnetic storms, it is characterized by large-amplitude, chaotic fluctuations, providing a clear signal of the disturbance. The geomagnetic data for this research were obtained from the Dusheti Geophysical Observatory (TBS Geographic Latitude: 42.09° Geographic Longitude: 44.70° The dataset spans from July 2023 to July 2024 and consists of one-minute resolution recordings of the H, Z and D. Any gaps present in the time series were filled using linear interpolation to ensure a continuous dataset for spectral analysis.

To investigate the relationship between ground-based magnetic field variations and extraterrestrial drivers, we utilized high-resolution solar wind and Interplanetary Magnetic Field (IMF) data. This data was acquired from the NASA/GSFC OMNIWeb data repository [8]. The selected parameters are: B - The magnitude of the Interplanetary Magnetic Field,  $B_z$  - The z component of the IMF in Geocentric Solar Magnetospheric (GSM) coordinates, V - The bulk flow velocity of the solar wind. These parameters were also obtained at a one-minute time resolution to match the geomagnetic data. Similar to the TBS data, any gaps in the OMNIWeb time series were filled using linear interpolation.

## Wavelet transform

The continuous wavelet transform (CWT) decomposes a time series  $x(t)$  into time–frequency space by convolving it with scaled and shifted versions of a chosen mother wavelet  $\psi(t)$ . Unlike the Fourier transform, which assumes stationarity, the CWT adapts its time–frequency resolution to capture both slow and rapid variations—a key advantage for non-stationary signals such as geomagnetic records during storms. Mathematically, the CWT is defined as:

$$W(a, b) = \frac{1}{\sqrt{|a|}} \int_{-\infty}^{\infty} x(t) \psi\left(\frac{t-b}{a}\right) dt,$$

where  $a$  is the scale (inversely related to frequency),  $b$  is the translation (time shift), and the overbar denotes complex conjugation. The resulting wavelet coefficients  $W(a,b)$  describe how well the wavelet at a given scale and time matches the signal. Because the wavelet's width adapts with scale, high-frequency (small-scale) features are localized in time while low-frequency (large-scale) features are resolved with finer frequency precision—ideal for capturing both the slow secular variation and rapid storm-time fluctuations of  $D$  [9].

### Wavelet coherence

To quantify the degree of linear coupling between two non-stationary time series (e.g., magnetic declination  $D$  and solar wind parameter  $B_z$ ), we compute the wavelet coherence:

$$R^2(a, b) = \frac{|S\{W_x(a, b)W_y^*(a, b)\}|^2}{S\{|W_x(a, b)|^2\}S\{|W_y^*(a, b)|^2\}}$$

where  $W_x$  is a wavelet transform of the time series and  $W_y^*$  is complex conjugate of wavelet transform of second time series.  $S\{\cdot\}$  denotes smoothing in both the time ( $b$ ) and scale ( $a$ ) dimensions. Commonly,  $S$  is implemented via convolution with a separable Gaussian (or boxcar) kernel in time and a similar window in scale [10].

Likewise, the cross-wavelet spectrum that underpins the coherence is itself smoothed before you extract phase:

$$\phi(a, b) = \tan^{-1} \frac{\text{Im}\{W_x W_y^*\}}{\text{Re}\{W_x W_y^*\}}$$

revealing lead–lag relationships at each scale and time [10].

### Power spectral density

The power spectral density (PSD)[11] estimates the distribution of signal power across frequency. For a discretely sampled time series  $x_n$  of length  $N$  a common unbiased PSD estimator is:

$$PS(f_k) = \frac{\Delta t}{N} \left| \sum_{n=0}^{N-1} x_n e^{-\frac{2\pi i k n}{N}} \right|^2$$

This parameter has been used to estimate dominant frequency for magnetit declination

### Results

Analysis of the power spectral density (PSD) of the one-minute declination time series reveals two prominent peaks at periods of approximately 24 h and 12 h. Specifically, the PSD shows a dominant spectral line at 1 cycle per day and a secondary line at 2 cycles per day, with both peaks standing well above the background noise level.

Wavelet power spectra repeats these findings: across the entire July 2023–July 2024 interval, the continuous wavelet transform of  $D$  exhibits persistent, high-energy bands at the diurnal (24 h) and semidiurnal (12 h) scales. These bands persist through both geomagnetically quiet and storm intervals, indicating that the underlying mechanism is not storm-specific but a regular, solar-driven modulation of the ionosphere.

The appearance of 24 h and 12 h periodicities in magnetic declination is a classic signature of the solar quiet (Sq) current system: daytime solar ultraviolet radiation increases ionospheric conductivity, driving global current vortices that peak once per day, while the semidiurnal tides in ionospheric density generate the second harmonic [12], PSD and CWT also showcase dominant periodicity at 8 hours, which needs further investigation.

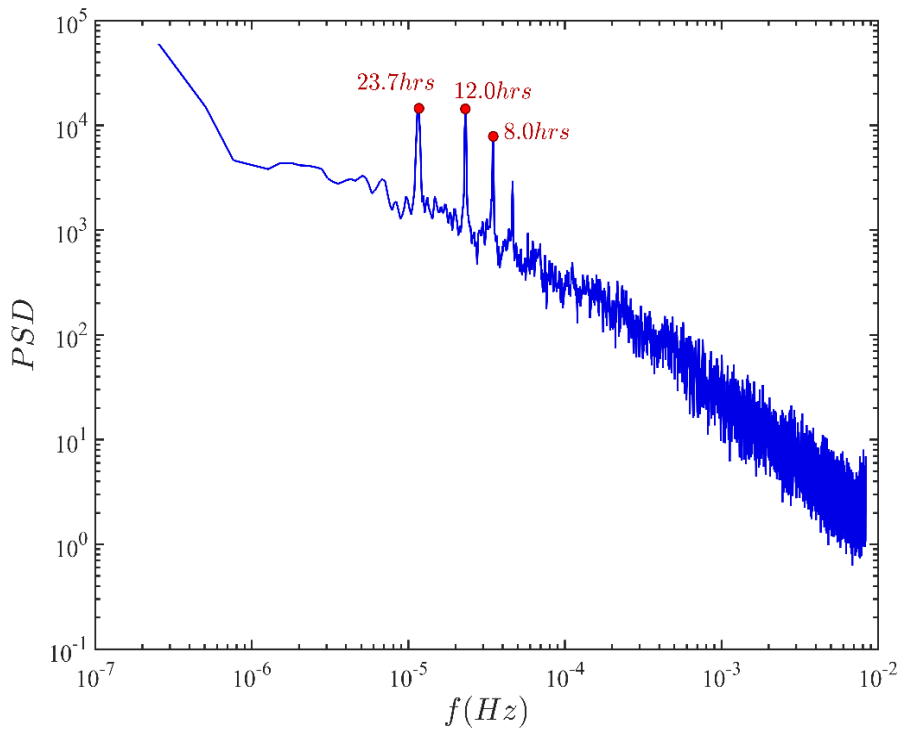


Fig. 1 PSD of magnetic declination D.

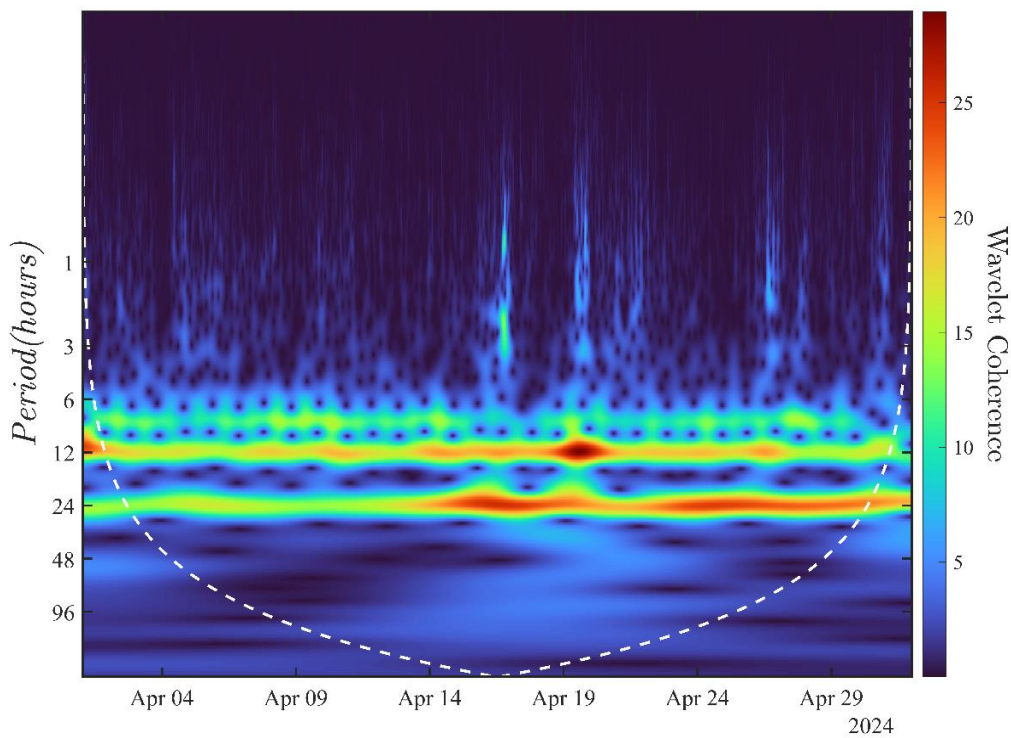


Fig. 2 Wavelet Transform of declination - D from April 1 to May 1 (storm at April 19).

During the intense geomagnetic storm of May 11, 2024, the wavelet spectrum shows a significant change. While the 24-hour peak remains dominant, the spectrum broadens, with a marked increase in wavelet power across a wide range of shorter periods. This indicates the superposition of multi-frequency processes during the storm, causing the declination signal to become more complex and noise-like compared to its structured, quiet-time behavior.

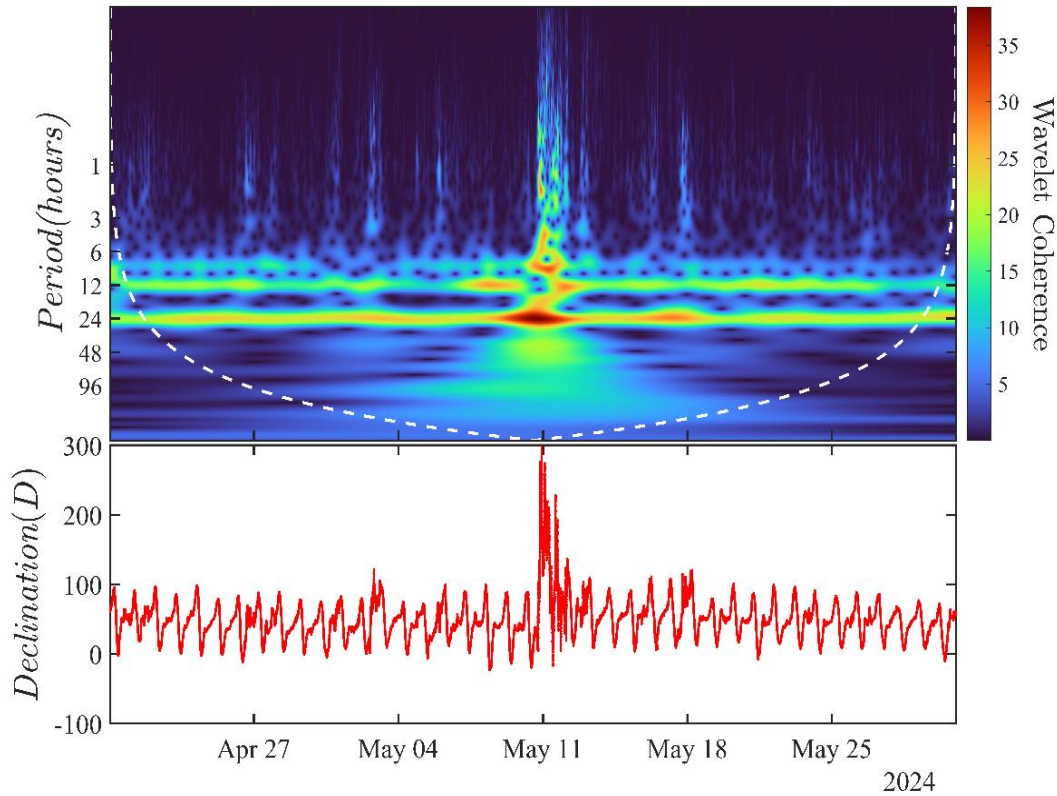


Fig. 3 Wavelet transform of Declination - D during April 20 - May 30 (storm on May 11).

### Wavelet coherence

The coupling between the solar wind and the magnetosphere is a complex, multi-frequency process. To investigate this coupling, we performed a wavelet coherence analysis between the declination ( $D$ ) and key solar wind parameters during the study period, with a focus on the May 2024 storm intervals.

A persistent coherence is observed at long periods (greater than 64 hours) throughout the entire time series. This long-period coherence should be interpreted with some caution due to the wavelet transform's lower time resolution at these scales; however, its persistence is notable. More dynamically, during the major storm on May 11, a distinct region of strong coherence emerges across a broad band of shorter periods (approximately 2-16 hours). A similar, though less intense, region of coherence is also visible at periods of 32-64 hours during the weaker storm event around May 19.

The north-south component of the IMF ( $B_z$ ) is a primary driver of magnetic storms, with a southward orientation (negative  $B_z$ ) ensuring magnetic reconnection [13]. Unlike the IMF magnitude, the coherence between  $D$  and  $B_z$  is significant regardless of storm intensity. A strong coherence is observed during the major storm on May 11, but it is particularly wide and sustained in the 32-128 hour period range during the less intense storm of April 19. The presence of strong coherence during events of differing magnitudes highlights the fundamental role of southward  $B_z$  in driving ground-level disturbances; this coupling mechanism appears robust and less dependent on the overall storm intensity.

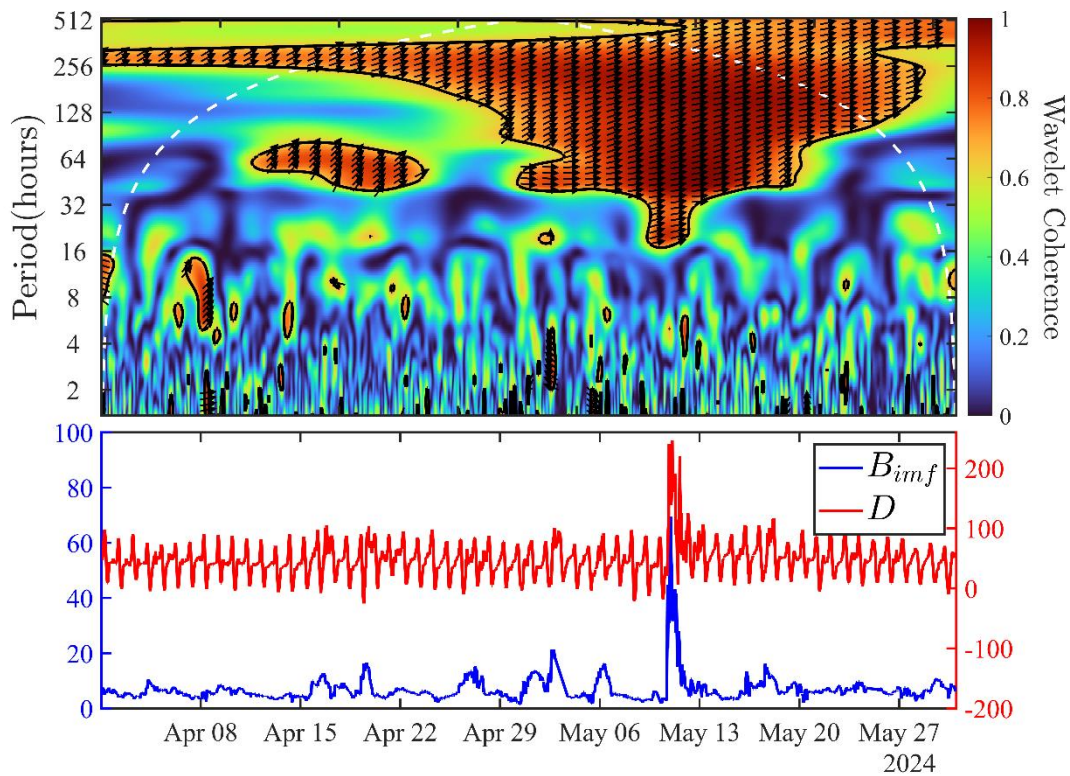


Fig. 4. Wavelet coherence of  $B_{imf}$  and  $D$ .

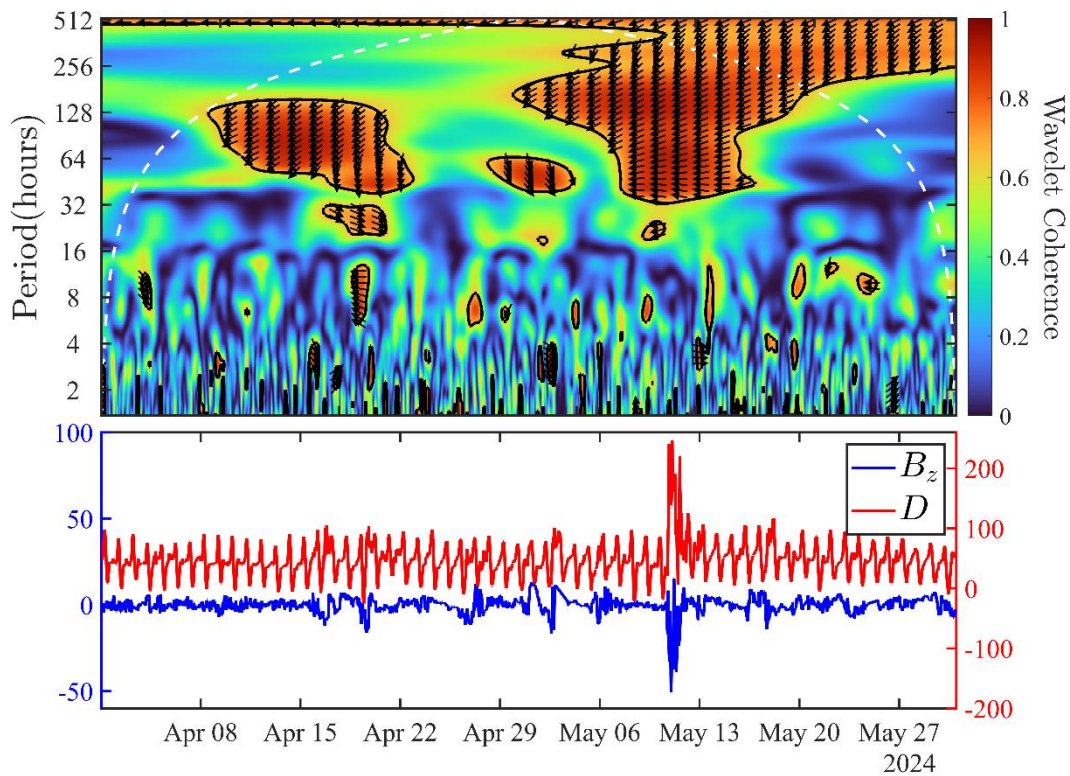


Fig. 5. Wavelet coherence of  $B_z$  and  $D$ .

The impact of a high-speed solar wind stream is a well-known trigger for geomagnetic storms. The coherence analysis between  $D$  and solar wind velocity shows a persistent low-frequency coherence, similar to the other parameters. However, specifically during the major storm of May 11, a distinct island of coherence appears in the 16-32 hour period range. This feature is notably absent during the less intense storm of April

19, which may suggest that solar wind velocity variations in this specific period range played a more significant role in driving the magnetospheric response during the more intense May 11 storm.

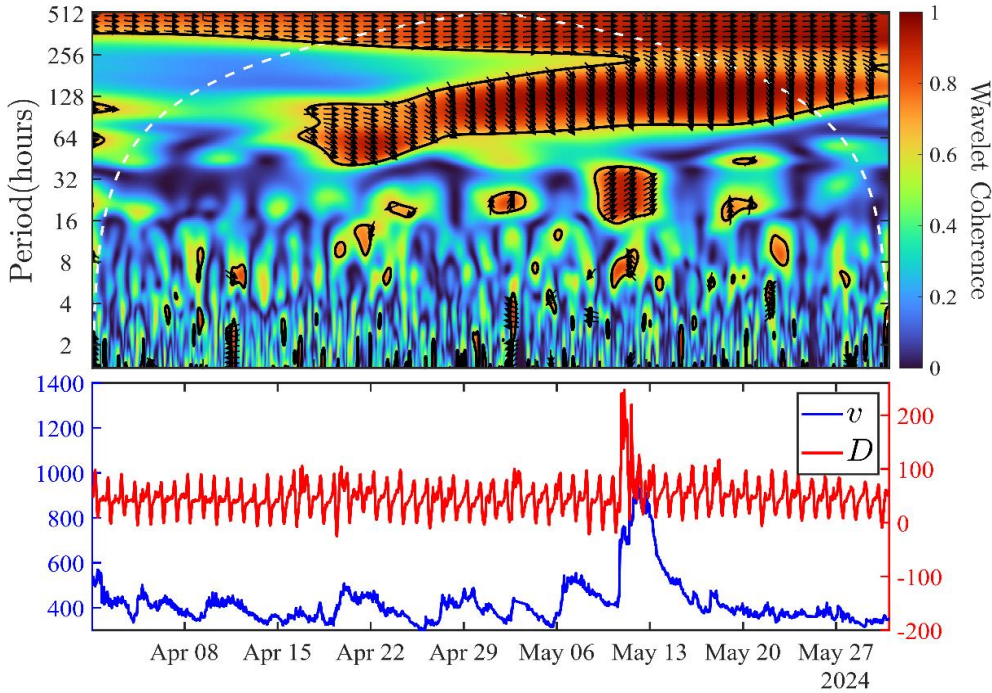


Fig. 6. Wavelet Coherence between flow speed and D.

## Conclusion

In this paper, we presented a detailed analysis of magnetic declination variations recorded at the Dusheti Geophysical Observatory and their coherence with key solar wind parameters. By employing spectral and wavelet-based techniques, we aimed to investigate the nature of magnetospheric coupling during both quiet time and geomagnetic storms.

First, the spectral analysis of the declination data consistently revealed dominant 24-hour and 12-hour periodicities. These are the well-established signatures of the solar quiet (Sq) current system, confirming the baseline solar-driven behavior at the observatory. 8-hour periodicity was also detected. During the intense May 11, 2024 magnetic storm, the wavelet spectrum showed that these primary cycles were superimposed with a broad spectrum of higher-frequency fluctuations, quantitatively illustrating the transition from a structured signal to a more complex, noise-like state characteristic of storm-time dynamics.

The core of our study focused on the wavelet coherence between declination and solar wind drivers. The results exposed nuanced differences in the coupling mechanisms:

A strong, broad-band coherence with declination was observed only during the most intense storm (May 11), suggesting that coupling related to the overall field magnitude is most effective during highly energetic events.

**IMF Southward Component (Bz):** In contrast, strong coherence with Bz was significant during both the intense May 11 storm and a less intense event on April 19. This demonstrates that the coupling driven by the southward IMF component—the primary engine for magnetic reconnection—is a fundamental process that operates efficiently regardless of the overall storm intensity.

**Solar Wind Velocity (v):** Coherence with solar wind speed revealed a unique signature in the 16-32 hour period band exclusively during the major May 11 storm, implying that dynamic pressure changes associated with high-speed streams may excite a distinct magnetospheric response during the most extreme events.

In summary, this work successfully demonstrates that magnetic declination at a single mid-latitude observatory can serve as a sensitive probe of solar wind-magnetosphere coupling. The use of wavelet

coherence, in particular, proved to be a powerful tool for distinguishing between the impacts of different solar wind parameters, revealing that while southward Bz provides a fundamental and consistent driver, the roles of IMF magnitude and solar wind velocity can be highly dependent on the specific characteristics and intensity of a geomagnetic storm.

## Acknowledgements

The authors wish to thank Tamaz Matiashvili for providing the Dusheti magnetometer data and for sharing his expertise and assistance throughout this work.

O.Kharshiladze was supported by Shota Rustaveli National Scientific Foundation Grant No. FR-22-18445.

## References

- [1] Merrill R. T., McElhinny M. W., McFadden P. L. The Earth's magnetic field: its history, origin and planetary perspective. Academic Press, 1998.
- [2] Kivelson M. G., Russell C.T. Introduction to Space Physics. Cambridge University Press, 1995.
- [3] Gonzalez W.D., Joselyn J.A., Kamide Y., Kroehl H.W., Rostoker G., Tsurutani B.T., Vasyliunas V. M. What is a geomagnetic storm? Journal of Geophysical Research: Space Physics, 99(A4), 5771-5792, 1994.
- [4] Campbell W.H. Introduction to Geomagnetic Fields. Cambridge University Press, 2023.
- [5] Matzka J., Stolle C., Yamazaki Y., Bronkalla O., Morschhauser A. The geomagnetic Kp index and derived indices of geomagnetic activity. Space Weather, 19(5), e2020SW002641, 2021.
- [6] Sugiura M., Kamei, T. Equatorial Dst index 1957-1986. IAGA Bulletin No. 40. World Data Center C2 for Geomagnetism, 1991.
- [7] Akasofu S.I. The latitudinal profile of the Dst index. Journal of Geophysical Research: Space Physics, 116(A12), 2011.
- [8] King J.H., Papitashvili N.E. Omni, combined solar wind plasma moments and interplane-tary magnetic field (IMF) time-shifted to the nose of the Earth's bow shock, plus geomagnetic indices, 1 min data. NASA Space Physics Data Facility, 2020.
- [9] Torrence C. Compo, G.P. A Practical Guide to Wavelet Analysis. Bulletin of the American Meteorological Society, 79, 61-78, 1998.
- [10] Grinsted A., Moore J.C., Jevrejeva S. Application of the cross wavelet transform and wavelet coherence to geophysical time series. Nonlinear Processes in Geophysics, 11, pp. 561-566, 2004.
- [11] Percival D. B., Walden, A.T. Spectral Analysis for Physical Applications. Cambridge University Press, 1993.
- [12] Chapman S., Bartels J. Geomagnetism. Oxford University Press, 1940.
- [13] Russell C.T. Space physics: An introduction. Cambridge University Press, 2016.

# მაგნიტური მიხრილობის ვეივლეტ კოჰერენტული ანალიზი გეომაგნიტური აქტივობის მშვიდ და შეშფოთებების პერიოდებში

ო. ხარშილაძე, ლ.წულუკიძე, მ. მარტიაშვილი

## რეზიუმე

ამ კვლევაში განხილულია დუშეთის გეომაგნიტურ ობსერვატორიაში გაზომილი მაგნიტური მიხრილობის (D) მახასიათებლები და მისი ურთიერთქმედება მზის ქართან გეომაგნიტური აქტივობის მშვიდ და შეშფოთებების პერიოდებში, განსაკუთრებული აქცენტით 2024 წლის 11

მაისის ინტენსიურ შტორმზე. ჩვენ გამოვიკვლიეთ მონაცემები ერთი წუთის რეზოლუციით 2023 წლის ივლისიდან 2024 წლის ივლისამდე. სპექტრალური სიმკვრივის და უწყვეტი ვეივლეტ გარდაქმნის გამოყენებით გამოვიკვლიეთ დომინანტი სიხშირეები. ანალიზი ადასტურებს დღიურ (24 სთ) და (12 სთ) პერიოდების არსებობას მშვიდ პერიოდებში, ასევე გამოკვეთილია 8 საათიანი პერიოდი და აჩვენებს სპექტრის მნიშვნელოვან გაფართოებას შტორმის დროს. ამის შემდეგ გამოვიყენეთ ვეივლეტ კოჰერენტული ანალიზი, რათა შეგვეფასებინა D-ის და IMF-ის მოდულის (B), მისი z კომპონენტის (Bz) და მზის ქარის სიჩქარის (v) კავშირი. შედეგები აჩვენებს განსხვავებულ მექანიზმებს: B-თან კოჰერენტულობა დამოკიდებულია შტორმის ინტენსივობაზე და მეტია მძლავრი 11 მაისის შტორმის დროს, ხოლო Bz-თან შეინიშნება მნიშვნელოვანი კოჰერენტობა როგორც ძლიერ (11 მაისი), ისე შედარებით მსუბუქი (19 აპრილი) შტორმების დროს, რაც ადასტურებს Bz-ის მნიშვნელობას მიუხედავად გეომაგნიტური შტორმების ინტენსივობისა. ეს კვლევა ადასტურებს ვეივლეტ კოჰერენტობის ეფექტურობას მზის ქარისა და მაგნიტოსფეროს კავშირის შესაფასებლად.

**საკვანძო სიტყვები:** მაგნიტური მიხრილობა, მაგნიტური შტორმი, პლანეტათშორისი მაგნიტური ველი, ვეივლეტ ანალიზი, ვეივლეტ კოჰერენტობა

## **Вейвлет когерентный анализ магнитного склонения в периоды спокойной и возмущённой геомагнитной активности**

**О. Харшиладзе, Л. Цулукидзе, М. Мартиашвили**

### **Резюме**

В данном исследовании изучаются особенности магнитного склонения (D) на геофизической обсерватории г. Душети, расположенной на средних широтах, и его связь с солнечным ветром в периоды спокойной и возмущённой геомагнитной активности, с особым акцентом на мощную бурю 11 мая 2024 г. Анализируются данные с разрешением одна минута по геомагнитным параметрам и параметрам солнечного ветра за период с июля 2023 г. по июль 2024 г. С помощью оценки спектральной плотности мощности (PSD) и непрерывного вейвлет-преобразования (CWT) характеризуется спектральное поведение склонения. Анализ подтверждает стабильное присутствие суточной (24 ч) и полусуточной (12 ч) периодичностей, характерных для спокойных периодов, а также периодичности 8 ч, одновременно демонстрируя значительное расширение спектра во время геомагнитной бури. Далее применяется анализ вейвлет-когерентности для количественной оценки связи между склонением и величиной межпланетного магнитного поля (B), его южным компонентом (Bz) и скоростью солнечного ветра (v). Результаты показывают различные механизмы связи: когерентность с величиной B зависит от интенсивности бури и проявляется значительно лишь во время мощной бури 11 мая. Напротив, когерентность с Bz является устойчивой и значимой как во время мощной бури (11 мая), так и умеренной (19 апреля), что подчёркивает её фундаментальную роль в формировании возмущений геомагнитных данных независимо от силы бури. Работа демонстрирует эффективность вейвлет-когерентного анализа для оценки связи солнечного ветра и магнитосферы на разных частотах.

**Ключевые слова:** Магнитное склонение, магнитная буря, солнечный ветер, межпланетное магнитное поле, вейвлет-преобразование, вейвлетная когерентность.

## Energy Spectrum of the March 1989 Forbush Decrease

<sup>1</sup>Eteri M. Alania, <sup>1</sup>Tengiz B. Bochorishvili, <sup>1</sup>Revaz G. Aslamazashvili, <sup>1</sup>Teimuraz S. Bakradze, <sup>1</sup>Nugzar Ya. Glonti, <sup>1</sup>Tereza G. Erkomaishvili, <sup>2</sup>Anatoly V. Belov, <sup>2</sup>Victor G. Yanke, <sup>2</sup>Raisa T. Gushchina, <sup>2</sup>Evguenia A. Eroshenko, <sup>3</sup>Anna Wawrzynczak-Szaban, <sup>4</sup>George K. Vanishvili

<sup>1</sup> M. Nodia Institute of Geophysics, Ivane Javakishvili Tbilisi State University, Georgia.

<sup>2</sup>Institute of Terrestrial Magnetism, Ionosphere and Radio Wave Propagation, Russian Academy of Sciences, Troitsk, Russia

<sup>3</sup>Institute of Computer Science, University of Podlasie, Siedlce, Poland.

<sup>4</sup>Sokhumi State University, Georgia.

e-mail: g.vanishvili@sou.edu.ge

### ABSTRACT

*Energy Spectrum of the Primary Cosmic Rays based on the experimental data of the World Wide Network of the Neutron Component of the Galactic Cosmic Rays, during the Huge Forbush Decrease of the March 1989 was calculated.*

**Key words:** cosmic rays, Forbush effect, energy spectrum.

## Electromagnetic properties of the heliosphere

The discovery of cosmic rays more than 113 years ago opened new horizons for further understanding and studying of the laws of the mega-universe and astrophysics. The World Wide Network of neutron monitors and meson telescopes located on the Earth's surface is a fairly effective and highly economical tool, which, first of all, requires knowledge of the physical processes occurring in the Earth's magnetosphere and atmosphere.

Scott Edward Forbush from the Carnegie Institution (Washington, DC, USA) in the 1930s, observing the intensity of cosmic rays with four identical ionization chambers located in Huancaya (Peru), Christ Church (New Zealand), Godhaven (Greenland), and Cheltenham (USA), discovered three types of temporal variations of primary cosmic radiation, which appear on completely different time scales: a) an increase in the intensity of cosmic rays caused by solar flares lasting minutes and hours, b) the Forbush decrease of cosmic rays, the so-called Forbush decay, which lasts for hours and days, and which was later called the Forbush effect, and c) large-scale (11-year) changes in cosmic ray intensity [1].

The Forbush decrease is one of the two largest [2] and most significant transient changes observed in cosmic ray intensity, the other being the increase in cosmic ray intensity caused by a solar flare. Typically, cosmic ray intensity during a [8]. Forbush decrease reaches a minimum value of the observed cosmic rays intensity for a few hours, and then begins a gradual recovery to its previous value, often slowly, over several days. Sometimes, but rarely, a second decrease occurs even before the first recovery is complete. Often, but not always, a Forbush decrease occurs after a cosmic ray increase caused by a solar flare. Also, Forbush decreases in cosmic ray intensity are often, but not always, associated with geomagnetic storms. Geomagnetic storms, in their turn, are usually associated with shock waves propagating through interplanetary space [2].

The majority of works devoted to the study of cosmic ray intensity Forbush effects have adopted the idea that cosmic ray Forbush effects represent a certain reflection of the geometric structure and physical parameters of shock waves and magnetic clouds arising from chromospheric flares on the Sun and variations in cosmic ray intensity. The existence of plasma clouds coming from the Sun to the Earth was not known for a long time before the discovery of the solar wind [3,4]. To explain geomagnetic storms, the idea of the existence of magnetic fields frozen in the plasma, according to which its propagation should occur along the lines of force of the solar magnetic field [5], was later proposed. This idea was later developed by various authors, and the reason for the Forbush effect in the intensity of cosmic rays was mainly believed to be the

scattering of charged cosmic particles by the magnetic field of the plasma cloud, which should have a turbulent character [6] and the shape of a smooth loop [7], or even the shape of a magnetic tongue [8].

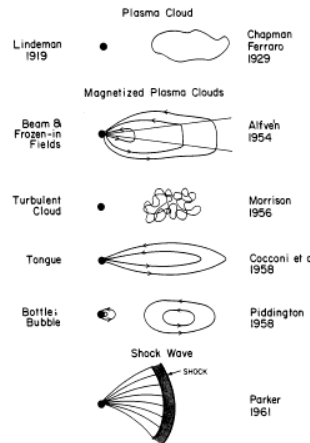


Fig. 1. Various possible configurations of Interplanetary Structures considered to be responsible for Forbush Decreases of Cosmic rays.

Fig. 1 shows the development of the basic ideas about the structure of turbulent magnetic phenomena, before the introduction of the concept of a shock wave [9,10] and the strict definition of the properties of a magnetic cloud. The concept of a magnetic cloud [11 -14] was introduced to describe such structures of the solar wind, which have an enhanced flow of magnetic field intensity. Which rapidly changes its direction at a large angle under conditions of low plasma temperature. Most of such structures have been observed after the passage of shock waves. It is now believed that magnetic clouds represent a certain variety of eruptions, its specific type, in interplanetary space [11,15] Fig. 2 [15,16].

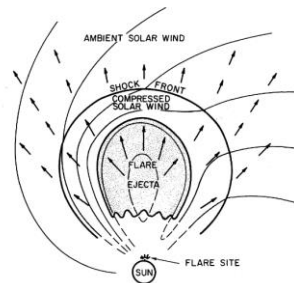


Fig. 2. Magnetic Clouds

A large series of recently published papers has focused on the contribution of magnetic clouds to the decline in cosmic ray intensity. In some works [11], the decrease in cosmic ray intensity was attributed to turbulent magnetic fields between the shock wave and the associated magnetic cloud. The correctness of such ideas is supported by the observation that the beginning of the decrease in cosmic ray intensity coincides with the moment of passage of the shock wave and the decrease process continues after the magnetic cloud, and that magnetic clouds without shock waves are associated with a small or insignificant decrease in cosmic ray intensity [11, 17].

Before entering the Earth's magnetosphere and atmosphere, cosmic rays of galactic origin pass through an area of space that is constantly under the influence of all solar activity, called the heliosphere (its boundaries are quite close to the dimensions of interplanetary space). Therefore, the study of cosmic ray variations requires an analysis of the physical processes that take place within the heliosphere, and, of course, on the Sun. Therefore, before moving on to the study of the Forbush effects, let us briefly review the physical processes taking place in the heliosphere and on the Sun.

It can also be noted that the solar wind, whose influence is characterized by the [8]. modulation of galactic cosmic rays, is gradually becoming the subject of heliosphere studies. [18, 19].

On the other hand, the use of information obtained by artificial Earth satellites and various space vehicles is statistically unjustified due to the small number of their localization sites. And Forbush effects, especially grandiose ones, such as those of July 1959 [20], August 1972, March 1989 and March 1991, reflect more completely and on a global scale the physical processes occurring inside the heliosphere. Therefore, experimental and model studies of Forbush effects are the only powerful tool that allows us to understand on a global scale the physical processes that took place in the heliosphere during the course of a particular Forbush effect.

## Characteristics of solar activity and solar wind

The most obvious manifestation of the solar activity cycle [21] is the number of sunspots and the area of sunspots. Therefore, the term sunspot cycle is always used synonymously with the solar cycle. The duration of the period varies somewhat from one cycle to the next, but on average it is 11 seconds. The beginning of a new cycle is taken to be the moment when the number of sunspots is minimal [21].

In order to follow the development of the solar activity cycle, it is most convenient to observe how the number of sunspots that form on the Sun changes over time. The temperature of sunspots is, on average, 200–300 degrees lower than that of the surrounding photosphere [22], so they appear as black spots on a white background.

A universal indicator of solar activity is the Wolff number R. It is calculated by the formula:  $R = K(10g + f)$ , where f is the number of individual spots, g is the number of groups of spots, and K is a correction factor that is selected individually to take into account the characteristics of the instrument, the environment, and the person [21, 24]. The factor 10 is somewhat arbitrary. It is believed that the effect of a group of spots is much more effective, about 10 times, (for example, on the Earth's magnetic field), than that of individual spots [25].

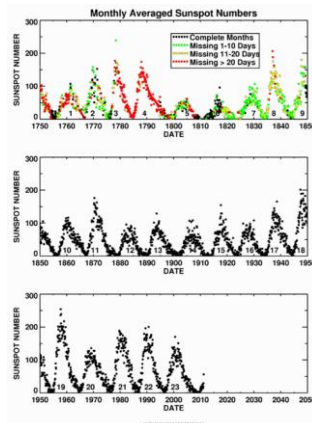


Fig. 3. Daily values of the sunspot Wolff number

Based on the analysis of daily values of the sunspot Wolff number (Fig. 3), it has been established that the cycle periods are less than 11 years long, among which the 28-day changes in the sunspot Wolff number are very important. They are caused by the rotation of the Sun around its axis, as they are associated with the helio-longitudinal asymmetry of solar activity [21,24]. Solar activity is accompanied by corresponding changes in the intensity of cosmic rays. An excellent example of this is the 27-day variations in cosmic rays intensity [26, 27, 28].

There are also periodicities with a duration longer than 11 years. The most important of these is the 22-year periodicity, called the Halley cycle. It is associated with the reversal of the Sun's magnetic poles. It should be noted that the 11-year cycle is not exactly periodic, but rather quasi-periodic [24].

The so-called flares observed on the visible disk of the Sun are the result of a sudden (transient) release of energy from the Sun's core into the Sun's atmosphere (mainly the chromosphere and corona). Solar flares cause, first of all, localized and temporary heating (thermal flares), and then the acceleration of electrons, protons, and premature heavy ions (particle flares). The temperature in the chromosphere reaches 104 K (chromospheric low-temperature flares). The temperature in the corona reaches 107 K (coronal or high-

temperature flares). The energy of the ejected particles varies from 20 GEV to 1 TEV. The energy released in the largest flare is  $10^{32}$  ergs [21,24,25]

Solar flares produce transient electromagnetic radiation, in a very wide energy range, from hard X-rays to radio radiation of wavelengths of several kilometers ( $10^{-9} - 10^6$  cm), the radiation is mostly thermal in nature [21, 24].

Flares are closely associated with active regions: the majority are observed in young and mature active regions; large flares, in particular, occur in regions with large vortices, complex magnetic field configurations, and large field gradients [25, 29].

The most efficient event occurring in solar active regions is the conversion of a significant amount of energy ( $10^{32} - 10^{33}$  ergs) in a relatively short time ( $2 \cdot 10^3$  seconds) [29]. Such an event can be called a solar storm [29]. The optical manifestation of a solar storm is a sudden increase in the brightness of the Balmer series  $H_{\alpha}$  line. This specific event is called a solar flare [29]. It is also often observed as intense X-ray, ultraviolet, and radio emission. During some flares, the brightness of the continuous spectrum increases over the entire region of the flare, even in the visible region of the spectrum. Solar storms also cause various dynamic processes in the solar atmosphere. Shock waves are generated, which then propagate in the solar wind plasma. Some of them overcome the Sun's gravity and extend beyond the Earth's orbit [29].

Five types of radio emission (I–V) are known [29]. The most remarkable and long-lasting type of radio emission is type IV. This emission usually lasts for several hours after the optical flare. It is believed that this type of radio emission contains both synchronous and plasma emission. Wild [30] has shown that this emission sometimes originates from the active region [29].

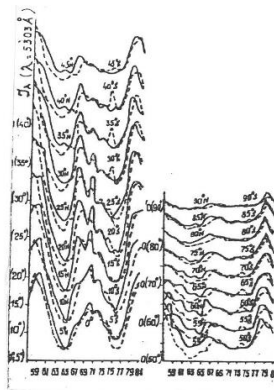


Fig. 4. Coronal green line for each  $5^\circ$  zone of the northern and southern solar hemispheres [31].

Fig. 4 shows the time course of the coronal green line for each  $5^\circ$  zone of the northern and southern solar hemispheres [31]. During the period 1957–1981, this allows us to identify heliogenomic features of the the 10<sup>th</sup> and 21<sup>st</sup> cycles in different hemispheres, which are also characteristic of other indices. For example, such as the double peak of the 20th cycle maximum, the “slippage” of activity to lower latitudes as the cycle progresses, and the predominantly high activity in the northern hemisphere. In addition, it is also possible to observe some of the characteristic features of the cyclic changes in solar activity that are characteristic only for this index and are indicated [32] at high latitudes ( $<45^\circ$ ) In the absence of a minimum in 1969-1971 (in these areas the line brightness increases 1- 4 years before the magnetic activity minimum at low latitudes), the areas of increased brightness of the coronal green line slowly, over 4-6 years, shift towards the poles, and disappear during the maximum of the spots. If we consider that the change in the magnetic cycle of the poloidal field can be traced according to the change in coronal activity, then this delay indicates an increase in the poloidal component at high latitudes, at a time when it is minimal at low latitudes. i.e. the poloidal field is maximal when the toroidal one has a minimum of activity [33]. The fields in the northern and southern hemispheres are often quite similar, and the inversion does not occur simultaneously. Obviously, if the assumption that the solar activity data we use (the area of the spots  $S$  and the intensity of the coronal green line  $I_{\lambda}$ ) reflect the changes in the various components of the solar magnetic field over a 22-year cycle is justified, then this relationship is most clearly confirmed by the figure, which shows the changes in  $S$  and  $I_{\lambda}$  during the course of the field inversion for both hemispheres of the Sun [31].

The analysis of the changes in the area of sunspots and coronal activity in different hemispheres and the change in the sign of the solar total magnetic field, carried out for the 19<sup>th</sup>-21<sup>st</sup> solar activity cycles, allows us to draw the following conclusions: 1) the change in the sign of the solar total magnetic field observed on the solar disk is reflected in the change in the intensity distribution of the coronal green line; 2) the inversion,

starting in one of the hemispheres of the Sun, leads to the achievement of the maximum intensity in the coronal green line radiation. In addition, it should be noted that the correspondence between these phenomena is observed only if the coronal radiation is considered in the entire hemisphere, and not in its separate latitudinal zone [31].

### **Investigation of the Forbush effect of March 11-25, 1989**

The classification of the Forbush effect [ 34 – 37 ] showed that the change in the energy spectrum of the Forbush effect over time obeys certain regularities. It is interesting to single out a case when the energy spectrum of the Forbush effect is soft during the period of the cosmic ray intensity minimum (  $\gamma = 1.2 - 1.5$  ), and then, over time, hardens and becomes hard at the end of the Forbush effect (  $\gamma = 0.2 - 0.4$  ). Such a change in the energy spectrum of the Forbush effect was described in the works of M.V. Alania and his co-authors [34 – 42] , and also in the doctoral dissertation of M.V. Alania. [43]. In particular, these works show that the time broadening of the energy spectrum of the Forbush effect should be related to the emergence of new, large-scale magnetic inhomogeneities in interplanetary space as a result of the interaction of the shock wave and the background solar wind.

These large-scale magnetic inhomogeneities cause an increase in the magnetic field strength fluctuations of interplanetary space, in the frequency range  $f = 10^5 - 10^6$  Hz, which is accompanied by an increase in the power spectral density (PSD) of the fluctuations of the magnetic field inhomogeneities in interplanetary space,  $v$ , which in turn leads to a decrease in the power spectral density of the energy spectrum of the isotropic intensity variations of cosmic rays,  $\gamma$ .

Naturally, the question arises whether the energy dependence of the energy spectrum of cosmic ray variations,  $\gamma$ , also occurs in Forbush effects, as this has been shown for the energy spectrum of 11-year cosmic ray variations [ 44 – 52]. For this purpose, several Forbush effects should be studied, and as an example, we will consider the Forbush effect of March 11-35, 1989, in detail.

### **Heliospheric and magnetospheric events in March 1989**

The first and most energetic series of solar activity cycle 22 began with the appearance of an active area near the eastern limb of the Sun, AR 5395 [2]. From 6 March 1989, a moving active area, AR 5395, appeared on the visible disk of the Sun. Even before this area became visible, it was possible to observe how the upward activity spread from the limb. The corresponding sunspot area itself was rotating inside the Sun. By 6 March 1989, it was located at  $34^\circ$  of the northern heliolatitude, which is a very high heliolatitude for such a large sunspot group [53]. The sunspot configuration was very complex, with well-defined spots of opposite polarity located close to each other. There were several notable energetic solar events as the center of activity moved across the solar disk. This included an event on March 6, during which the GOES X-ray monitor indicator went off scale; it was rated as an X15-class X-ray event. On March 9, X4 and 4B (strong X-ray and optical emission at the same time) events were observed. On March 10, an X4.6 and 3B class event occurred, which is believed to have triggered the geomagnetic storm of March 13, which had the largest aa (24-hour aa index) in the last 120 years. According to the criterion of X-ray emission productivity observed to date, the active region AR 5395 was the most productive of the active regions observed in the last 15 years [54].

On March 13, 1989, at 09:30 UTC, the global network of cosmic ray stations around the Earth recorded a grandiose Forbush effect, the second largest in amplitude (27.20%) after the Forbush effect of August 1972. It began with the arrival of an interplanetary shock wave [2].

The change in the number of sunspots clearly indicates the fact that since September 1986, an 11-year cycle of solar activity began. Usually, by this time, the intensity of cosmic rays has reached another peak, and has begun to decrease further, and by March 1989 it had decreased to 90%. According to neutron monitors (located on the Earth's surface). The active area AR 5395 began to rotate on the visible disk of the Sun since March 6, 1989. It was a very active area, and was accompanied by several bright flares. During the two weeks during which the process of crossing the visible disk of the Sun by the active area AR 5395 continued, the onset of a geomagnetic storm was recorded five times at different times, with its sudden onset, which, as a rule, is expressed, in each individual case, i.e. at all five times, the fact of the arrival of a shock wave propagating in interplanetary space to Earth has been recorded. Such cases occurred at the following moments in time:

1) March 8, 17:55 UTC; 2) March 13, 01:27 UTC; 3) March 13, 07:43 UTC,  $\sim 450 \gamma$ ; 4) March 16, 05:34 UTC; 5) March 19, 04:23 UTC; [ 55 ]. In addition, there is also a signal of a large shock wave reaching the Earth (  $\sim 450 \gamma$  ), at one of the geomagnetic stations, March 13, 07:43 UTC.

## Investigation of the Forbush Effect of March 11-25, 1989 (continued)

Fig. 5 shows the change in the intensity of cosmic rays during the Forbush Effect of March 1989. This figure shows that the minimum of the intensity of cosmic rays is observed at different times at different stations, which is obviously associated with the numerous flares on the Sun that occurred on March 9-10. The energy spectrum of cosmic rays, based on the data of all stable and well-functioning neutron monitors of the World Wide Web, is shown in Fig. 6. Analysis of the results obtained shows that during the period of decrease in the intensity of cosmic rays, on March 13-14, the energy spectrum is relatively soft. In the following period. This case can be considered as one of the good examples of the Forbush effects, when convection intensively removes low-energy particles, and at the same time, due to the reflective properties of the shock wave or magnetic cloud, it is difficult for mainly low-energy particles to penetrate into the inner region of the magnetic cloud or shock wave. In both cases, the energy spectrum of the isotropic intensity variations of cosmic rays should be relatively soft, which is clearly seen from the given figure.

From March 15 to March 24, the energy spectrum of the isotropic intensity variations of cosmic rays is relatively rigid, which indicates that as a result of the interaction of the shock wave and the background solar wind, a structure of interplanetary magnetic field strength fluctuations was formed, when the density characteristic of the energy spectrum of these fluctuations is index  $\nu = 1.5$ , almost up to a frequency of  $f = 10^6$  Hz.

In order to determine whether there is a dependence of the cosmic ray energy spectrum characteristic  $\gamma$  on the magnetic hardness  $R$  of cosmic ray particles, the neutron monitors of the World Wide Web were divided into two groups:

- 1) the first group includes neutron monitors of the World Wide Web in the cutoff threshold range from 0 to 7 GV;
- 2) the second group includes neutron monitors of the World Wide Web in the cutoff threshold range above 7 GV.

The change in the energy spectrum characteristic  $\gamma$  of the Forbush effects of cosmic rays with time is given in Fig. 7 and Fig. 8 respectively. These figures show that the energy spectrum of the Forbush effects of cosmic rays according to the data of the first group (low energies) stations is softer than that of the second group (high energies). This is especially clearly observed for the period from March 13 to 16. Therefore, there is actually a tendency, even during the Forbush effect, for the energy dependence of the energy spectrum characteristic of the isotropic intensity variations of cosmic rays,  $\gamma$ . The latter once again confirms the proposition [120] that the characteristic  $\gamma$  of the energy spectrum of isotropic intensity variations of cosmic rays well describes the dynamical-structural change (change in  $\gamma$ ) that occurs in fluctuations of the interplanetary magnetic field strength.

Therefore, the change in the energy spectrum characteristic of cosmic ray Forbush effects,  $\gamma$ , with time, allows us to study the integral changes in the interplanetary magnetic field strength fluctuations after solar flares, which are mainly sources of interplanetary shock waves and magnetic clouds.

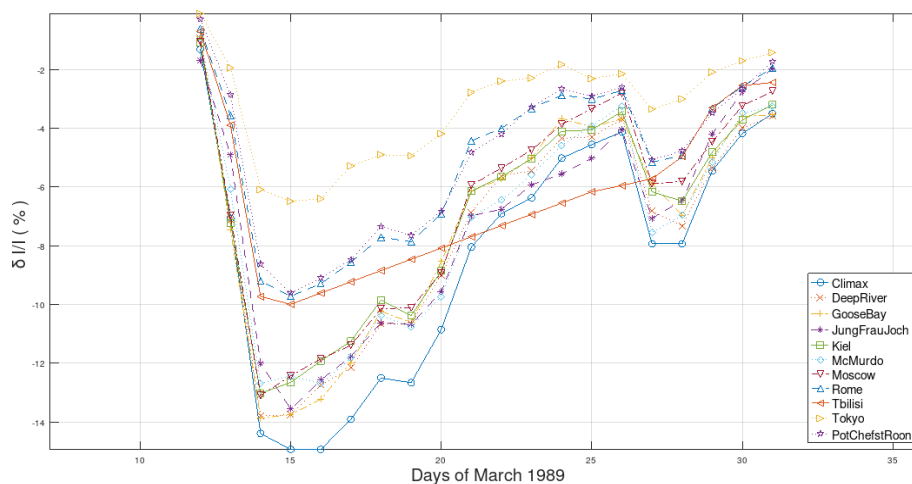


Fig. 5. Cosmic Rays Intensity Changes during March 1989 Forbush-Decrease

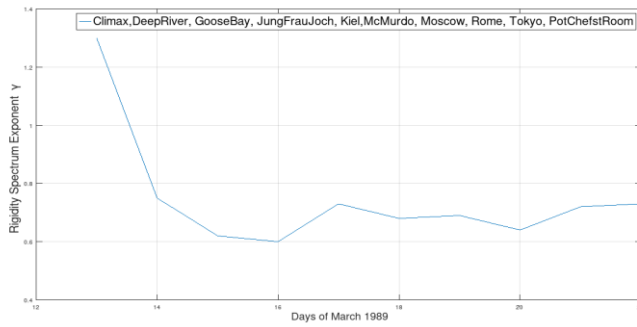


Fig. 6. The energy spectrum of cosmic rays, based on the data of all stable and well-functioning neutron monitors of the World Wide Web

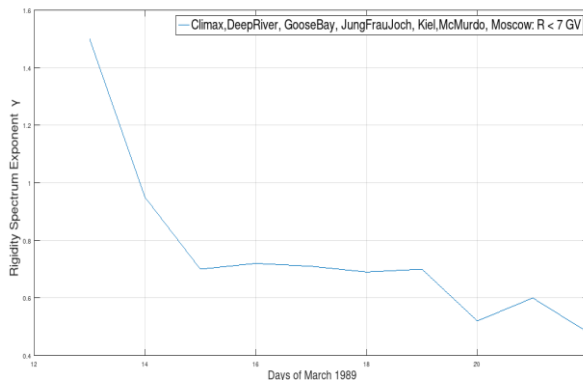


Fig. 7. Energy spectrum of the Forbush effects of cosmic rays according to the data of the first group (low energies)

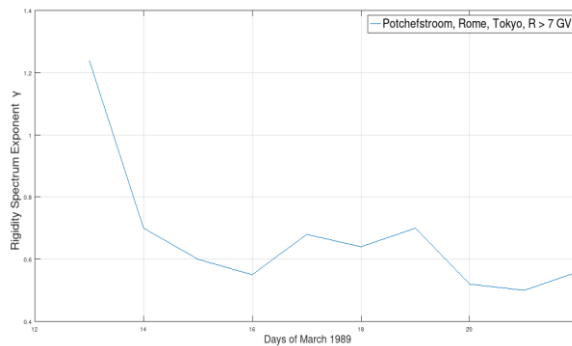


Fig. 8. Energy spectrum of the Forbush effects of cosmic rays according to the data of the first group (high energies)

## Conclusion

The energy spectrum of the Forbush effects of cosmic rays according to the data of the Neutron Monitor data with the lower CutOff Rigidity is softer than that of the second group Neutron Monitor Data with the higher CutOff Rigidity

## References

- [1] Vankarasin D., and Badruddin. Cosmic ray intensity variations in the 3-dimensional heliosphere. *Space Science Reviews*, 52m, 1990, pp. 121-194.
- [2] Vankatesan D., Decker R.B., Krimgis S.M., Matthews T., Sarris E.T. The great Forbush-Decrease of March 1989 and the interplanetary energetic particle environment. 21-st ICRC, 6-19 January, 1990, Adelaida, Australia, conference papers, vol., 6, SH 7.1-16, 1990, pp. 247-249.
- [3] Lindeman F.A. London, Edinburg, and Dublin Phylosophical Magazine and Journal of Science, Series 6, Vol. 37, Iss. 221, 1919. <https://www.tandfonline.com/doi/full/10.1080/14786440508635912>
- [4] Chapman S., Ferraro V.C.A. Solar streams of corpuscles their geometry, absorption of light and penetration. *Monthly notices Roy Astron. Society* 89, 470, 1929.
- [5] Ajfven H. *Tellus*, 6, 232, 1954.
- [6] Morrison P. Solar-connection variations of cosmic rays. *Phys. Rev.*, 95, 646, 1954.
- [7] Paddington J.H. *Phys. Rev.* 112, 589, 1958.
- [8] Cocconi G., Gold T., Greisen K., Hayakawa., Morisson J.P. Cosmic ray flare effect. *Nuvo Cimento*, 8, 161, 1958.
- [9] Parker E. N., *Interplanetary Dynamical Processes*. InterScience Publishers John& Willey Sons, NY, 1963.
- [10] Burlaga, L. F. E. *Magnetic Clouds. Physics of the Inner Heliosphere II. Particles, Waves and Turbulence. Series: Physics and Chemistry in Space*, Springer, Berlin, Heidelberg, 1991.
- [11] Cane H. V. Cosmic ray decreases and magnetic clouds. *American Geophysical Union Journal of Geophysical Research* J. Vol. 98 (A3), 1993, pp. 3509-3512. <https://doi.org/10.1029/92ja02479>
- [12] Zang G., Burlaga L.F. Magnetic clouds, geomagnetic disturbances, and cosmic decreases. *Journal of Geophysical Research*, 93, 1988, pp. 2511–2518.
- [13] Badruddin R., Yadav S., Yadav N.R., Agrawal S.P. Influence of magnetic clouds on cosmic ray intensity variations. *Proc. of the 19-th ICRC, SH 5.1-12 NASA Conf. Publ.*, 5, 258, 1985.
- [14] Badruddin, Venkatesan D., Zhu B.Y. Study and effect of magnetic clouds on the transient modulation of cosmic-ray intensity. *Solar Physics*, vol. 134, July 1991, pp. 203-209.
- [15] Cane H.V. The structure and the evolution of the interplanetary shocks and the relevance for particle acceleration. *Nuclear Physics, B, Proc. Suppl.*, 39A, 1995, pp. 35-44.
- [16] Hund Hausen A.J. Interplanetary shock waves and the structure of solar wind: ph. 393-417, *Solar Wind, The Proc. of a conf sponsored by the NASA and held on March 21-26, 1971*.
- [17] Lockwood J. A., Webber W. R., Debrunner H. Forbush decreases and interplanetary magnetic field disturbances: Association with magnetic clouds. *Journal of Geophysical Research*, Vol. 96, Iss. A7, July 1991, pp. 11587-11604. DOI: 10.1029/91JA01012
- [18] Thomson D.J., Maclennan C.G., Lanzerotti L.J. Propagation of solar oscillations through the interplanetary medium. *Nature*, vol. 376, 1995, pp. 139- 144.
- [19] Ladbury R. Search and discovery: is the answer blowing in the solar wind? *Physics Today*, 17, September 1995.
- [20] Shea M.A., Smart D.F. History of solar proton observations. *Nuclear Physics, B, (Proc Suppl.)*, 39 A, 1995, pp. 16 – 25.
- [21] Smith H.J., Smith E.V.P. *Solar flares*. The Mc Millan Company, New York, Collier-MacMillan Limited London, 1963, p. 30.
- [22] Gibson E. *The quiet Sun*. NASA, Washington, 1973, p. 408.
- [23] *Introduction to solar-terrestrial relations*. Edited by Ortner and MaseLand -D Reidel Publishing Company, Dordrect Holland, 1965.
- [24] Brusek A., Durrant C.J. *Faunhofer Institut, Freiburg. Illustrated Glossary for Solar and Solar-Terrestrial Physics*, D. Reidel Publishing Company, Dordrech-Holland/ Boston USA, 1978.
- [25] Vitinskiy YU. V., Kopetskiy M., Kuklin G. V. *Statistika pyatnoobrazovatel'noy deyatel'nosti Solntsa*. M., Nauka, 1986, (in Russian).
- [26] Alaniya M.V., Shatashvili L.Kh. *Kvaziperiodicheskiye variatsii intensivnosti kosmicheskikh luchey*. Metsniyereba, Tbilisi, 1974, (in Russian).
- [27] Naskidashvili B.D., Shatashvili L.Kh. *Kvaziperiodicheskiye variatsii intensivnosti i anizotropii kosmicheskikh luchey*. Metsniyereba, Tbilisi, 1981, (in Russian).
- [28] Nachkebiya N.A., Rogava O.G., Shatashvili L.Kh. *Kvaziperiodicheskiye variatsii kosmicheskikh luchey i solnechno-zemnyye svyazi*. Metsniyereba, Tbilisi, 1981, (in Russian).
- [29] Akasofy S-I., Chapman S. *Solar-Terrestrial Physics*, Oxford, 1972, p. 199.

- [30] Wild J.P., Observation of the magnetic structure of type IV solar radio outburst. *Solar Physics* 9, 1969, pp. 260-264.
- [31] Alaniya M.V., Dorman L.I., Aslamazashvili R.G., Gushchina R.T., Dzhapiashvili T.V. *Modulyatsiya galakticheskikh kosmicheskikh luchey solnechnym vetrom*. Metsniyereba, Tbilisi, 1987, str. 18, (in Russian).
- [32] Trellis M. Contribution s l'etude la couronne. *Solaire Ann D'Astrophysique*, Supp. 5, 1957, pp. 3-80.
- [33] Babcock H.D. *Astrophys. J.* 130, 1959, pp. 364-365.
- [34] Alania M.V., Despotashvili M.A. On the features of Forbush - decreases of cosmic ray intensity. 12-th ECRS Nottingham England, 1990, SH – 37 <https://adsabs.harvard.edu/full/1995ICRC.4..860A>
- [35] Despotashvili M.A. Osobennosti effekta Forbusha i anomal'nykh izmeneniy intensivnosti kosmicheskikh luchey. *Dissertatsiya na soiskaniye uchennoy stepeni kandidata fiziko-matematicheskikh nauk*, Tbilisi, 1990, (in Russian).
- [36] Alaniya M.V., Despotashvili M.A., Nachkebiya N.A. Klassifikatsiya effektov Forbusha kosmicheskikh luchey na osnove osobennostey energeticheskogo spektra variatsiy. *Izvestiya Akademii Nauk, Seriya Fizicheskaya*, t. 59, №4, 1995, (in Russian).
- [37] Alania M.V., Despotashvili M.A., Kudela K., Langer R., Iskra K., Nachkebia N.A., Slivka M., Soliwodska-Swider E. The feature or the relationship of cosmic ray Forbush-decreases and solar wind parameter's fluctuations. 24-th ICRC, Roma, Italy, vol 4, August 28-September 8, 1995, pp. 860 – 863.
- [38] Alaniya M.V., Bochorishvili T.B., Despotashvili M.A., Nachkebiya N.A. Ozhidayemyye raspredeleniya plotnosti kosmicheskikh luchey vo vremya effekta Forbusha. *Solnechno-zemnyye svyazi i kosmicheskkiye luchi*. *Trudy IG AN GSSR, Metsniyereba*, t. 52, 1985, str. 51, (in Russian).
- [39] Alaniya M.V., Bakradze T.S., Bochikashvili D.P., Dzhapiashvili T.V., Despotashvili M.A., Rogava O. G., Tkemaladze V. S. Effekty Forbusha na pod'yome solnechnoy aktivnosti v 1988-1989 gg. po dannym Tbilisskogo kompleksa i mirovoy seti stantsiy kosmicheskikh luchey. V simpozium, KAPG, Samarkand, 1989, s. 279, (in Russian).
- [40] Alaniya M.V., Despotashvili M.A., Nachkebiya N.A. Izmeneniye energeticheskogo spektra Forbush-ponizheniy intensivnosti kosmicheskikh luchey v razlichnykh 11-letnykh tsiklakh solnechnoy aktivnosti. V simpozium, KAPG, Samarkand, 1989, s. 291, (in Russian).
- [41] Alania M.V., Bakradze T.S., Bochorishvili T.B., Bochikashvili D.P., Despotashvili M.A., Nachkebia N.A. Theoretical and experimental investigation of cosmic ray Forbush-effects. 19 –th ICRC, La Jolla, USA, v. 5, 1985, p. 285.
- [42] Alania M.V., Bakradze T.S., Bochorishvili T.B., Bochikashvili D.P., Despotashvili M.A., Nachkebia N.A. The features of temporal change of cosmic ray energy spectrum during Forbush-effects. 10 –th ECRS, Bordeaux, France, SH – 6, 1986.
- [43] Alaniya M.V. Anizotropnaya diffuziya kosmicheskikh luchey v okolozemnom i mezhplanetnom prostranstve. *Doktorskaya dissertatsiya*, Tbilisi, 1980, (in Russian).
- [44] Alania M.V., Aslamazashvili R.G., Bochorishvili T.B., Gushchina R. T., Dorman L.I., Iskra K. *Physics of outer Heliosphere*, Editors Grdzielsky S., Page D.E. Pergamon 199, 1990.
- [45] Alania M.V., Aslamazashvili R.G., Bochorishvili T.B., Dorman L.I., Iskra K. Proc. 19-th ICRC, La Jolla, v4., 1985, pp 465-568.
- [46] Iskra K., Alania M.V., Aslamazashvili R.G., Bochorishvili T.B., Dorman L.I., Gushchina R.T. The features of the temporal changes of 11-year variations of cosmic ray intensity. Proc. 20-th ICRC vol. 3, Moscow, 1987.
- [47] Alania M.V., Aslamazashvili R.G., Bochorishvili T.B., Dorman L.I., Iskra K. On the nature of 11-year energy spectrum changes of cosmic ray variations. SH 6.1-17 Proc. 21-st ICRC, Adelaida, 1990, pp. 48-51.
- [48] Alania M.V., Iskra K. Features of the solar wind large-scale structure in the different periods of solar activity based on the variations of cosmic rays. *Advanced Space Researches*, vol. 16, No 9, COSPAR, 1995, pp. 241 – 244.
- [49] Alania M.V., Aslamazashvili R.G., Bochorishvili T.B., Vanishvili G.K., Lomtadze Z.G. Iskra K. Proc. 23 -rd ICRC, Calgary, vol. 3, 559, 1993.
- [50] Alania M.V., Aslamazashvili R.G., Vanishvili G.K., Iskra K. Large Scale structure changes of the interplanetary magnetic field fluctuations and the mechanism of 11-year cosmic rays modulation. 14 European Cosmic Rays Symposium, Balatonfured, Hungary, August 28 – September 3, 1994.
- [51] Alania M.V., Aslamazashvili R.G., Bochorishvili T.B., Gushchina R. T., Dorman L.I., Iskra K., Vanishvili G.K. The modeling study of cosmic ray long-period modulation. Proc 24-th ICRC, Roma, vol. 3, 1995, p. 751.

- [52] Alaniya M. V., Aslamazashvili., Vanishvili G. K., Iskra K. Kobilinski Z. O mekhanizme 11-letney variatsii kosmicheskikh luchey i krupno-masshtabnaya struktura solnechnogo vetra. Izvestiya Akademii Nauk, Seriya Fizicheskaya, t. 59, № 4, 1995, (in Russian).
- [53] Abbott M.S., et al. Region 5395 of March 1989. Edited by W. Cliffswallow, Tech memo 1529, National Oceanic and Atmospheric Administration, Environmental research Lab, and Space Environmental Lab., Boulder, Colorado, 1993.
- [54] Feinman J., Hundhausen A.J. Coronal mass ejection and major solar flares: the great active center of March 1989. Journal of Geophysical Research, vol. 99, No. A5, May, 1, 1994, pp. 8451 – 8464.
- [55] Solar Geophysical Data, April 1989.

## 1989 წლის მარტის ფორბუმ ეფექტის ენერგეტიკული სპექტრი

ე. ალანია, თ. ბოჭორიშვილი, რ. ასლამაზაშვილი, თ. ბაქრაძე, ნ. ლლონტი, თ. ერქომაიშვილი, ა. ბელოვი, ვ. იანკე, რ. გუმჩინა, ე. ეროშენკო, ა. ვავრზინჩაკ-საბანი, გ. ვანიშვილი

### რეზიუმე

კოსმოსური სხივების ფორბუმ ეფექტის ენერგეტიკული სპექტრი, დაბალი მოჭრის ზრურბლის მქონე ნეიტრონული მონიტორების მონაცემების მიხედვით არის რბილი, ვიდრე მაღალი მოჭრის ზღურბლის მქონე ნეიტრონული მონიტორებიდან მიღებული მონაცემების შემთხვევაში.

საკვანძო სიტყვები: კოსმოსური სხივები, ფორბუმის ეფექტი, ენერგიის სპექტრი.

## Энергетический спектр Форбуш-эффекта в марте 1989 года

Э. Алания, Т. Бочоришвили, Р. Асламазашвили, Т. Бакрадзе, Н. Глонти, Т. Еркомаишвили, А. Белов, В. Янке, Р. Гущина, Е. Ерошенко, А. Вавжинчак-Сабан, Г. Ванишвили

### Резюме

Энергетический Спектр Форбуш-эффекта космических лучей, согласно данным, полученных от станций нейтронных мониторов мировой сети, с низким уровнем жёсткости магнитного обрезания является более мягким, чем в случае нейтронных мониторов, с высоким уровнем обрезания жёсткости.

Ключевые слова: космические лучи, эффект Форбуша, энергетический спектр.

## **7<sup>th</sup> Eurasian Conference “RISK-2025” and Newly Created Journal “International Journal of Sustainability and Risk Control”**

**Vugar A. Aliyev**

*AMIR Technical Services Company*

*e-mail: profvugaraliyev@gmail.com*

### **ABSTRACT**

*Information by Prof. V. Aliyev about the 7th Eurasian Conference “RISK-2025” to be held on October 21-23, 2025 in Baku (Azerbaijan), as well as the newly created journal “International Journal of Sustainability and Risk Control” and its first issue which was published at the end of June 2025, is presented.*

**Key words:** *natural and man-made risks; risk analysis, forecast and control; taking risks into account when planning sustainable economic development and improving the safety of environmental objects.*

### **Introduction**

On July 1, 2025, at the M. Nodia Institute of Geophysics of I. Javakhishvili Tbilisi State University hosted another city seminar, where an information report was heard on the upcoming 7th Eurasian Conference “**RISK-2025**” (<https://www.eurasianrisk2025.com>, with the publication of reports in a journal indexed in Scopus) to be held on October 21-23, 2025 in Baku (Azerbaijan), as well as the newly created international journal “**International Journal of Sustainability and Risk Control**” (<https://ijsrc.com>) and its first issue (<https://ijsrc.com/index.php/ijsrc/issue/view/1>), which was presented by professor Vugar Aliyev, General Chairman of the “**RISK-2025**” Conference, General Director and Founder of “AMIR Technical Services Company”, the main organizer and sponsor of the conference, as well as the editor-in-chief of the above-mentioned new journal.

### **About Journal**

“International Journal of Sustainability and Risk Control” is a specialized scientific publication dedicated to current issues in sustainable development and risk management. The journal brings together research from various fields, including ecology, economics, social sciences, and engineering, providing an interdisciplinary approach to addressing global challenges. Publications in the journal help scientists, practitioners, and policy makers develop strategies to reduce risk and ensure long-term sustainability.

Publisher: AMIR Technical Services LLC, Baku, AZ1022, R. Behbudov str., 93, Azerbaijan  
<https://ijsrc.com>; e-mail: [journal\\_mail@ijsrc.com](mailto:journal_mail@ijsrc.com); e-ISSN: 3104-8358; p-ISSN: 3104-834X.

The first issue of the journal (June 2025) published 9 articles [1-9].

### **Key topics**

Technical, technological, transportation and climate risks; seismic risks and earthquake engineering; critical infrastructure protection, vulnerability and resilience building; risk-oriented design and operation of

infrastructure systems; risk-oriented multi criteria decision making for sustainable and resilient infrastructure systems; impact scenario analysis of infrastructure risks induced by natural, technological and intentional hazards; resilient and environmentally sustainable country/regional/city and sector strategies; infrastructure systems interdependencies; infrastructure investment; human factor in the sustainability paradigm; riskbased methodologies for the design and operation of (critical and strategic) infrastructures; interdisciplinary research based on MABICS technologies and infranetics; Application of artificial intelligence to the tasks of analysis and synthesis of technogenic and anthropogenic risks.

Priority is given to descriptions of case studies.

## Editorial Board

### Editor-in-Chief



**Aliyev, Vugar** (Azerbaijan)  
Doctor of Sci., Professor,  
Director of the AMIR Technical  
Services Company, e-mail:  
prof.vugar.aliyev@gmail.com

### Managing Editor



**Bochkova, Alexandra** (Russia)  
Faculty for Business Informatics  
and Integrated Systems  
Management, NRNU MEPhI,  
Russian Federation 31,  
Kashirskoye shosse, Moscow,  
115409, e-mail: aabochkova@gmail.com

### Deputy Editors



**Amiranashvili, Avtandil** (Georgia)  
Prof. Dr., Institute of Geophysics,  
Tbilisi State University, GEORGIA  
e-mail: avtandilamiranashvili@gmail.com



**Arcieri, Marco** (India)  
Dr. of Sci, President of the  
International Commission on Irrigation  
and Drainage, INDIA  
e-mail: m.arcieri@cid.org



**Azizov, Rufat** (Azerbaijan)  
Assoc. Prof., Rector, Azerbaijan  
State Oil and Industry University,  
AZERBAIJAN  
e-mail: info@asoil.edu.az



**Bochkov, Alexander** (Russia)  
Doctor of Sci., Scientific  
Secretary, JSC NIIS, Bldg 1, 5  
Orlikov Pereulok, Moscow,  
107078, Russia  
e-mail: a.bochkov@gmail.com



**Dimitrov, Boyan** (USA)  
Dr. of Math. Sci., Associate Professor  
of Mathematics (Probability and  
Statistics), Kettering, President,  
Gnedenko Forum,  
e-mail: dimitrob@gmail.com



**Kelman, Ilan** (United Kingdom)  
Professor, Department of Risk and Disaster  
Reduction, University College London,  
UNITED KINGDOM,  
e-mail: i.kelman@ucl.ac.uk



**Kuo, Way** (Hong Kong)  
Dr. of Sci, Prof., Senior Fellow  
Institute for Advanced Study, City  
University, HONG KONG, Emeritus  
President and University  
Distinguished Professor, City  
University of Hong Kong, e-mail: way@cityu.edu.hk



**Nikitina, Elena** (Russia)  
Dr., Nobel Prize winner as a part of  
expert group for Intergovernmental  
Panel on Climate Change Assessment  
Report 2007; Head of Section Global  
Economic Problems, Institute of World  
Economy and International Relations RAS, RUSSIA,  
e-mail: elenankitina@bk.ru



**Rouainia, Mounira** (Algeria)  
Prof. – Department of  
Petrochemicals, University of 20  
August 1955 Skikda, ALGERIA  
e-mail: rouainia\_m@yahoo.fr



**Şahin, Ahmet Duran** (Türkiye)  
Prof. Dr., Department of  
Meteorological Engineering, Istanbul  
Technical University, TÜRKIYE  
e-mail: sahind@itu.edu.tr



**Sinh, Bach Tan** (Vietnam)  
Dr., Institute of Policy and  
Management, Hanoi Vietnam  
national University, VIETNAM  
e-mail: sinhbt@gmail.com



**Stewart, Mark** (Australia)  
Prof. Dr., Center for Built  
Infrastructure Resilience,  
University of Technology Sydney,  
AUSTRALIA  
e-mail: Mark.Stewart@uts.edu.au



**Timashev, Sviatoslav** (Russia)  
Doctor of Sci., Professor,  
Laureate of the Nobel Peace Prize  
(2007). Ural Federal University;  
Science and Engineering Center  
"Reliability and Safety of Large  
Systems and Machines" Ural

Branch of Russian Academy of Sciences,  
Ekaterinburg, RUSSIA,  
e-mail: timashevs@gmail.com

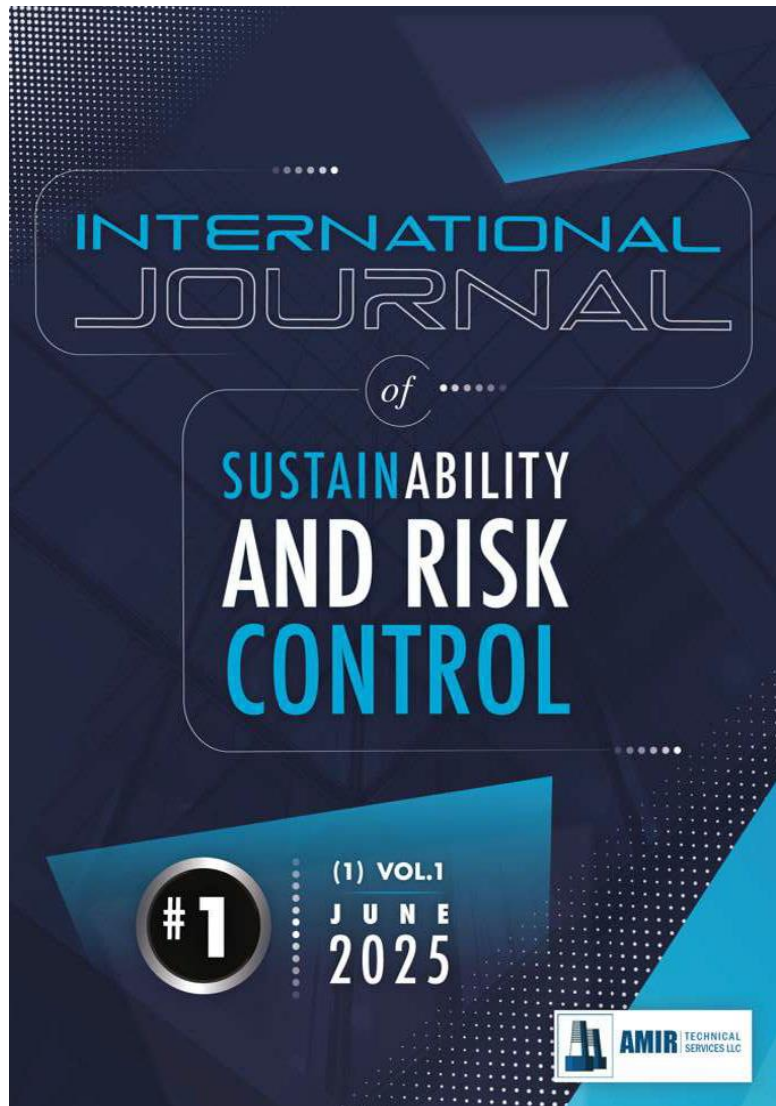


**Zio, Enrico** (Italy)  
Ph.D. in nuclear engineering  
from Politecnico di Milano (1996)  
and in probabilistic risk  
assessment at MIT (1998). Full  
professor at the Centre for  
research on Risk and Crises

(CRC) of Ecole de Mines, Paris, PSL University,  
France and at Politecnico di Milano, Italy, where  
he is also President of the Alumni Association and  
Vice-President of the Foundation. Member of the  
Academic Committee of the International Coalition  
of Intelligent Manufacturing, ICIM (2025). Member  
of the Board Committee of the International Joint  
Research Center for Resilient Infrastructure (ICRI)  
2021-2026, e-mail: Enrico.Zio@polimi.it

## Photos from Seminar





## References

- [1] Aliyev V., Pkhovelishvili M., Archvadze N., Gasitashvili Z. Hybrid risk review. Int. Journal of Sustainability and Risk Control, Baku, Azerbaijan, Vol.1, No 1(1), June 2025, pp. 12-23.
- [2] Kolev N., Dimitrov B. Bivariate Kaminsky's functional equations and their probability solutions generated by line integral approach: a new modeling tool for risks under dependencies. Int. Journal of Sustainability and Risk Control, Baku, Azerbaijan, Vol.1, No 1(1), June 2025, pp. 24-32.
- [3] Bochkov A. Rethinking sustainable development. Int. Journal of Sustainability and Risk Control, Baku, Azerbaijan, Vol.1, No 1(1), June 2025, pp. 33-46.
- [4] Akimov V., Olga Derendiaeva O. Developing an indicator system for integrated monitoring of sustainable development in the Russian arctic based on the DPSIR framework. Int. Journal of Sustainability and Risk Control, Baku, Azerbaijan, Vol.1, No 1(1), June 2025, pp. 47-54.
- [5] Pozhilova N. Disclosure of non-financial information: experience of international organizations and third countries. Int. Journal of Sustainability and Risk Control, Baku, Azerbaijan, Vol.1, No 1(1), June 2025, pp. 55-58.
- [6] Nikonorova I., Ilyin V., Ilyina A., Andrey Nikitin A. Springs as an alternative to reducing georisks of water scarcity (using the example of the northeastern part of the east European plain - the Chuvash republic). Int. Journal of Sustainability and Risk Control, Baku, Azerbaijan, Vol.1, No 1(1), June 2025, pp. 59-64.
- [7] Mulev S., Romanevich K., Taratinsky G. Identification of seismic surface development and geodynamic risk forecast in coal and ore mines. Int. Journal of Sustainability and Risk Control, Baku, Azerbaijan, Vol.1, No 1(1), June 2025, pp. 65-68.
- [8] Timashev S. Infranetics – the umbrella science of governing the second nature. Part 1. Int. Journal of Sustainability and Risk Control, Baku, Azerbaijan, Vol.1, No 1(1), June 2025, pp. 69-90.
- [9] Nikitina E. Sustainability through adaptation to climate risks: regional perspective. Int. Journal of Sustainability and Risk Control, Baku, Azerbaijan, Vol.1, No 1(1), June 2025, pp. 91-97.

*მეცნიერების სიახლეები*

## **მე-7 ევრაზიული კონფერენცია „RISK-2025“ და ახლადშექმნილი ჟურნალი „მდგრადობისა და რისკების კონტროლის საერთაშორისო ჟურნალი“**

**ვ. ალიევი**

**რეზიუმე**

წარმოდგენილია პროფესორ ვ. ალიევის ინფორმაცია 2025 წლის 21-23 ოქტომბერს ბაქოში (აზერბაიჯანი) გასამართი მე-7 ევრაზიული კონფერენციის „RISK-2025“-ის, ასევე ახლადშექმნილი ჟურნალის „მდგრადობისა და რისკების კონტროლის საერთაშორისო ჟურნალი“ და მისი პირველი ნომრის შესახებ, რომელიც 2025 წლის ივნისის ბოლოს გამოიცა.

**საკვანძო სიტყვები:** ბუნებრივი და ადამიანის მიერ შექმნილი რისკები; რისკების ანალიზი, პროგნოზირება და კონტროლი; მდგრადი ეკონომიკური განვითარების დაგეგმვისას რისკების გათვალისწინება და გარემოსდაცვითი ობიექტების უსაფრთხოების გაუმჯობესება.

## **7-я Евразийская конференция „RISK-2025“ и новый журнал “Международный журнал устойчивого развития и контроля рисков”**

**В. Алиев**

### **Резюме**

Представлена информация профессора В. Алиева о 7-й Евразийской конференции „RISK-2025“, которая состоится 21-23 октября 2025 года в Баку (Азербайджан), а также о недавно созданном журнале “Международный журнал устойчивого развития и контроля рисков” и его первом номере, вышедшем в свет в конце июня 2025 года.

**Ключевые слова:** природные и техногенные риски; анализ, прогноз и контроль рисков; учет рисков при планировании устойчивого развития экономики и повышения безопасности объектов окружающей среды.

## Information for contributors

Papers intended for the Journal should be submitted in two copies to the Editor-in-Chief. Papers from countries that have a member on the Editorial Board should normally be submitted through that member. The address will be found on the inside front cover.

1. Papers should be written in the concise form. Occasionally long papers, particularly those of a review nature (not exceeding 16 printed pages), will be accepted. Short reports should be written in the most concise form not exceeding 6 printed pages. It is desirable to submit a copy of paper on a diskette.
2. A brief, concise abstract in English is required at the beginning of all papers in Russian and in Georgian at the end of them.
3. Line drawings should include all relevant details. All lettering, graph lines and points on graphs should be sufficiently large and bold to permit reproduction when the diagram has been reduced to a size suitable for inclusion in the Journal.
4. Each figure must be provided with an adequate caption.
5. Figure Captions and table headings should be provided on a separate sheet.
6. Page should be 20 x 28 cm. Large or long tables should be typed on continuing sheets.
7. References should be given in the standard form to be found in this Journal.
8. All copy (including tables, references and figure captions) must be double spaced with wide margins, and all pages must be numbered consecutively.
9. Both System of units in GGS and SI are permitted in manuscript
10. Each manuscript should include the components, which should be presented in the order following as follows:  
Title, name, affiliation and complete postal address of each author and dateline.  
The text should be divided into sections, each with a separate heading or numbered consecutively.  
Acknowledgements. Appendix. Reference.
11. The editors will supply the date of receipt of the manuscript.

## CONTENTS - სარჩევი

N. Tsereteli, L. Ghomidze, N. Tugushi - Temporal Evolution of Microseismicity in Response to Reservoir Operation at the Enguri Dam (Georgia) ნ. წერეთელი, ლ.ღომიძე, ნ. ტულუში - ენგურის კაშხლის (საქართველო) მიმდებარე ტერიტორიაზე მიკროსეისმური აქტივობის დროითი ცვლილება წყალსაცავის ექსპლუატაციის გავლენის ფონზე	5 – 20
D. Odilavadze, T. Chelidze, O. Yavolovskaya - A Three-Dimensional Representation of the Piles Radio Image on the Radargram for the Completed Construction დ. ოდილავაძე, თ. ჭელიძე, ო. იავოლოვსკაია - რადაროგრამაზე ხიმინჯის რადიოსახის სამგანზომილებიანი წარმოდგენა დასრულებული ნაგებობისთვის	21 – 26
D. Odilavadze, T. Chelidze, O. Yavolovskaya - Preliminary Archaeogeophysical Survey of the Construction Site in the Vicinity of the Narikala Citadel დ. ოდილავაძე, თ. ჭელიძე, ო. იავოლოვსკაია - ნარიყალას ციტადელის მიმდებარე ტერიტორიაზე სამშენებლო მოედნის წინასწარი არქეოგეოფიზიკური კვლევა	27 – 35
G. Kobzev, T. Chelidze, G. Melikadze, T. Jimshehadze, T. Kiria, A. Tchankvetadze, Z. Maghradze, N. Gogvadze - Water Level Phase Shift Relative to Gravity into Georgian Wells გ. კობზევი, თ. ჭელიძე, გ. მელიქაძე, თ. ჯიმშელაძე, თ. ქირია, ა. ჭანკვეტაძე, ზ. მაღრაძე, ნ. გოგვაძე - საქართველოს ჭაბურღილებში წყლის დონის ფაზური წანაცვლება გრავიტაციასთან მიმართებაში	36 – 39
A. Surmava, V. Kukhalashvili, N.Gigauri, L. Intskirveli, L. Gverdtsiteli - Numerical Modeling of Kutaisi City Atmospheric Air Pollution with PM2.5 Particles in Winter During Ground Level Calm and Background Eastern Wind in the Free Atmosphere ა. სურმავა, ნ. გიგაური, ვ. კუხალაშვილი, ლ. ინჭვირველი, ლ. გვერდწითელი - ქ.ქუთაისის ატმოსფერული ჰაერის PM2.5 -ნაწილაკებით დაბინძურების რიცხვითი მოდელირება ზამთარში მიწისპირა შტილისა და თავისუფალ ატმოსფეროში ფონური აღმოსავლეთის ქარის დროს	40 – 49
A. Amiranashvili, L. Brocca, T. Chelidze, D. Svanadze, T. Tsamalashvili, N. Varamashvili - Statistical Analysis of Annual and Semi-Annual Sum of Atmospheric Precipitation Data for 59 Municipalities (11 Regions) of Georgia with Landslide Hazard Zones from 2015 to 2024 ა. ამირანაშვილი, ლ. ბროკა, თ. ჭელიძე, დ. სვანაძე, თ. წამალაშვილი, ნ. ვარამაშვილი - ატმოსფერული ნალექების წლიური და ნახევარწლიური ჯამის სტატისტიკური ანალიზი საქართველოს 59 მუნიციპალიტეტის ზონების მქონე მუნიციპალიტეტისთვის (11 რეგიონი) 2015 - 2024 წწ.	50 – 63
Ts. Basilashvili, M. Janelidze, K. Basilashvili - Forest Cover – the Primary Guardian Against Climate Change and Biosphere Security ც. ბასილაშვილი, მ. ჯანელიძე, ხ. ბასილაშვილი - ტყის საფარი - მთავარი მცველი კლიმატის ცვლილებისა და ბიოსფეროს უსაფრთხოების	64 – 74
M. Meladze, G. Meladze, M. Pipia - Agroclimatic Challenges in the Mountainous and High-Mountain Areas of Georgia under Climate Change (on the Example of Mtskheta-Mtianeti and Samegrelo-Zemo Svaneti) მ. მელაძე, გ. მელაძე, მ. ფიფია - აგროკლიმატური გამოწვევები საქართველოს მთიან და მაღალმთიან ტერიტორიებზე კლიმატის ცვლილების პირობებში (მცხეთა-მთიანეთის და სამეგრელო-ზემო სვანეთის მაგალითზე)	75 – 86
O. Kharshiladze, L. Tsulukidze, M. Martiashvili - Wavelet Coherence Analysis of Magnetic Declination During Quiet and Disturbed Geomagnetic Activity ო. ხარშილაძე, ლ.წულუკიძე, მ. მარტიაშვილი - მაგნიტური მიხრილობის ვივლენტ კოჰერენტული ანალიზი გეომაგნიტური აქტივობის მშვიდ და შეშფოთებების პერიოდებში	87 – 95
E. Alania, T. Bochorishvili, R. Aslamazashvili, T. Bakradze, N. Glonti, T. Erkomaishvili, A. Belov, V. Yanke, R. Gushchina, E. Eroshenko, A. Wawrzynczak-Szaban, G. Vanishvili - Energy Spectrum of the March 1989 Forbush Decrease ე. ალანია, თ. ბოჭორიშვილი, რ. ასლამაზაშვილი, თ. ბაქრაძე, ნ. ღლონტი, თ. ერქომაიშვილი, ა. ბელოვი, ვ. იანკე, რ. გუშჩინა, ე. ეროშენკო, ა. ვაერზინჩაკ-საბანი, გ. ვანიშვილი - 1989 წლის მარტის ფორბუშ ეფექტის ენერგეტიკული სპექტრი	96 – 105
V. Aliyev - Science News. 7th Eurasian Conference “RISK-2025” and Newly Created Journal “International Journal of Sustainability and Risk Control” ვ. ალიევი - მეცნიერების სიახლეები. მე-7 ევრაზიული კონფერენცია „RISK-2025“ და ახლადშექმნილი ჟურნალი „მდგრადობისა და რისკების კონტროლის საერთაშორისო ჟურნალი“	106 – 111
Information for contributors ავტორთა საყურადღებო	112 – 112

საქართველოს გეოფიზიკური საზოგადოების ჟურნალი  
მყარი დედამიწის, ატმოსფეროს, ოკეანისა და კოსმოსური პლაზმის ფიზიკა

*ტომი 28, № 1*

ჟურნალი იბეჭდება საქართველოს გეოფიზიკური საზოგადოების პრეზიდიუმის დადგენილების  
საფუძველზე

ტირაჟი 20 ცალი

**JOURNAL OF THE GEORGIAN GEOPHYSICAL SOCIETY**

*Physics of Solid Earth, Atmosphere, Ocean and Space Plasma*

*Vol. 28, № 1*

Printed by the decision of the Georgian Geophysical Society Board

Circulation 20 copies

**ЖУРНАЛ ГРУЗИНСКОГО ГЕОФИЗИЧЕСКОГО ОБЩЕСТВА**

**Физика Твердой Земли, Атмосферы, Океана и Космической Плазмы**

*Том 28, № 1*

Журнал печатается по постановлению президиума Грузинского геофизического общества

Тираж 20 экз

**Tbilisi-თბილისი-Тбилиси**  
**2025**